Template Induction of Supramolecular Structure: Synthesis and Characterisation of the Mesoporous Molecular Sieve, MCM-41.

Karen Jean Edler

July 1997

Amorphous silica - a radiolarian and a silica sphere.
Photograph by Roger Heady, EMU, ANU. (used with permission)

A thesis submitted for the degree of Doctor of Philosophy
of The Australian National University

Declaration

This dissertation is an account of research undertaken primarily in the Research School of Chemistry at the Australian National University, under the supervision of Professor John W. White. Additional experiments were performed at the ISIS Pulsed Neutron Source at the Rutherford Appleton Laboratory, Chilton, UK, the Intense Pulsed Neutron Source at Argonne National Laboratories, Illinios, USA, the Cold Neutron Research Facility at the National Institute of Standards and Technology, Washington D.C., USA and the Australian National Beamline Facility at the Photon Factory Synchrotron, Tsukuba, Japan.

All of the sample preparation required for this thesis was carried out by the candidate, except in cases where it was not possible for her to do so, in which case, detailed experimental instructions, written by the candidate, were supplied to those who carried out the work. Sample sets prepared in this fashion by Gordon Lockhart while the candidate was visiting overseas facilities for data collection purposes, are those listed in Appendix 1, Table A1.1, labelled GP, R, J, LOQ heated ordinary and LOQ heated acid. All characterisation and analysis, except where noted in the text and where indicated below, were also performed by the candidate. Gas adsorption isotherm data collection was performed by Gordon Lockhart and Dr Peter Branton, but all subsequent analysis was done by the candidate. Due to insufficient funding the overseas experiments listed below were carried out on the candidate's behalf as noted. For the shear experiments discussed in Chapter 4, section 4.3.3, one third of the data on the shear behaviour of silicate-surfactant gels was collected at the ISIS facility by Dr Philip Reynolds and Dr Tony Brown. Small angle neutron scattering contrast variation data on five samples total, on two separate occasions, was collected at the ISIS facility by Dr Jonathon Watson and Dr Tony Brown. All data processing and analysis in those cases was done by the candidate. Similarly, for the quasielastic neutron scattering experiments on hydrogen adsorbed in MCM-41 discussed in Chapter 6, section 6.7 carried out at the Argonne National Laboratories, data collection and initial data processing was carried out by Dr Philip Reynolds. For the quasielastic neutron scattering experiments on methane, Dr. Frans Trouw continued data collection and initial data reduction after the candidate returned to Australia, as funding was insufficient for her to remain to complete the experiment. Data collection and initial processing of the synchrotron X-ray patterns collected at the Australian National Beamline in Japan, were done by Dr David Cookson, and Wilfred Fullagar. All subsequent data processing was done by the candidate. All other data collection and analysis reported herein was done by the candidate. Other contributions to this work, by way of technical support and advice are acknowledged on the following pages.

None of the work presented in this thesis has been submitted to any other institution for any degree.

Karen J. Edler
11 July 1997

Abstract

The pure silicate mesoporous material, MCM-41 having hexagonally packed cylindrical channels with a centre to centre distance of *ca.* 45 Å may be synthesised from a preparation containing only sodium silicate solution, a surfactant template molecule, water, and some acid. The preparation was optimised initially both for heated and unheated syntheses. The effects of aging in the gel, heating time and stirring were investigated. MCM-41 materials which were stable to calcination were prepared in an ambient temperature synthesis, with stability proportional to aging time in the gel. Heated preparations proved to have highest long range order after 3 days at 100˚C in unstirred systems.

The effect of pH during synthesis was then investigated. Preparations titrated against 1 M acid to maintain a constant pH during the whole of the synthesis developed much higher long-range order, as determined by the number and intensity of the observed X-ray diffraction peaks. A small counterion effect, dependant upon the type of acid used was noted. The most highly ordered materials were prepared from preparations titrated with sulphuric acid to maintain a pH of 10 during the synthesis. Heated preparations were more ordered than those carried out at ambient temperatures, although the addition of acid also promoted order in unheated syntheses.

From these highly ordered materials X-ray diffraction patterns containing up to seven peaks were obtained using synchrotron radiation. These peaks could all be indexed to a hexagonal lattice. The intensity envelope for these peaks was modelled by the expected envelope for an array of cylinders. The data could not be fitted by a model containing only one cylinder, but required two concentric cylinders of different scattering length density. This indicates the presence of three regions in the MCM-41 framework. Firstly, a denser, continuous wall structure about 6 Å wide filling the regions between pores. Secondly, each pore is lined with a less dense silica region about 12 Å thick. The empty holes down the centre of each channel in this material have a radius of about 7 Å. The average bulk MCM-41 density calculated from the X-ray results and gas adsorption measurements was found to be low, around 0.83(5) g cm^{-3}, with the denser part of the wall being 0.99 g cm^{-3} and the less dense lining of the pores 0.87 g cm^{-3}.

This low density model with porous walls is supported by results from neutron diffraction, inelastic and quasielastic neutron scattering measurements on hydrogen adsorbed in the pores of MCM-41, and by small angle neutron scattering using contrast variation on MCM-41 materials at all stages of preparation. Other possible interpretations of the data are presented and discussed.

The behaviour of methane adsorbed in the channels of MCM-41 was also observed by quasielastic neutron scattering. Considerable alteration in the phase behaviour from that of bulk methane was observed. The melting point was depressed from 91 K in bulk methane to between 45 and 60 K for the confined methane in this system, and a liquid phase was still present in the pores at 180 K, around 70 K above the normal boiling point of the bulk material.

Acknowledgments

Firstly, I wish to thank my supervisor, Professor John White for allowing me to work with him and his research group. His infectious enthusiasm, creativity and encouragement have made the last three years interesting and memorable. I also wish to acknowledge the invaluable co-supervisory role of Dr Philip Reynolds, whose down-to-earth advice provided an essential balance and who was always available for questions.

Two other members of the research group who deserve special mention are Trevor Dowling, and Gordon Lockhart. Trevor ensured the smooth running of that vital piece of equipment, the small angle X-ray camera, and his technical expertise in creating the heating cell and other useful items was much appreciated. Likewise, the assistance of Gordon, often in rushed situations, in the synthesis of some of the materials studied for this thesis permitted a much more extensive investigation than would otherwise have been possible. His collection of most of the nitrogen and methane isotherm data is also gratefully acknowledged. The assistance of Dean Gilkes with computer related matters and of Heather Jauncey for all administrative concerns big and small, particularly organisation of the overseas trips were also invaluable.

The assistance of research scientists at overseas institutions must also be noted. The aid of Dr. Frans Trouw at IPNS in the collection and reduction of quasielastic neutron scattering data was deeply appreciated. Dr. Tania Slawecki at CNRF, NIST must be thanked for her enthusiasm, vegetarian cooking and all her help with the shear cell experiments on the NG-3SANS beamline. Dr. B. Hammouda is also thanked for assistance with those experiments. Dr. Richard Heenan and Dr. Steve King at ISIS, RAL gave willing and cheerful support for the small angle neutron scattering experiments on LOQ and Dr. P. Thiyagarajan did likewise for experiments at IPNS on SAD, the small angle neutron scattering machine at ANL.

Some of the work reported in this thesis has benefited from the use of the Intense Pulsed Neutron Source at Argonne National Laboratory which is funded by the U.S. Department of Energy, BES-Materials Science, under Contract W-31-109-ENG-38. Some of the other material is based upon activities supported by the National Foundation under Agreement No. DMR-9423101. I acknowledge the support of the National Institute of Standards and Technology, U.S. Department of Commerce, in providing the neutron research facilities used in some of this work. Travel grants through the Australian Government ISTAC/ANSTO Access to Major Facilities Program are gratefully acknowledged.

Closer to home, my adviser Dr. Ray Withers is to be thanked for taking the transmission electron micrographs included in this thesis. I also wish to thank Dr. Julieanne Dougherty and Dr. John Thompson for taking the scanning electron micrographs included herein. The assistance of Dr. Tim Senden with AFM experiments is acknowledged, even though the results were not as useful we had hoped. He is also to be thanked for synthesising the surfactant used in the Langmuir trough experiment and for many stimulating discussions. Discussions with Dr Paul Saville on many things, but

especially the interpretation of the Langmuir trough data were deeply appreciated. The assistance of Dr Peter Branton with the collection and analysis of some of the nitrogen isotherms is also recognised. The hard work and dedicated assistance of all those who carried out experiments at overseas facilities on my behalf, when the funding situation would not allow me to be there in person, is gratefully acknowledged. These people were Dr. Tony Brown, Dr. Philip Reynolds, Dr. Jonathan Watson, Dr. David Cookson and Wilfred Fullagar.

All of the many and varied occupants of Room 2; Richard Durand, Elliot Gilbert, Wilfred Fullagar, Graeme Lindsell, Ian Jamie, Phillippe Espeau, Jonathon Watson, Peter Branton, and Gavin Kirton, will be long remembered for their diverting conversation, and as a source of amusement, encouragement and comradeship over the past few years. Paul Saville and Julieanne Dougherty are, in particular, to be thanked for their friendship and willingness to share their experience and wisdom. Their encouragement and sense of perspective helped to maintain sanity, or at least some semblance thereof, throughout this process of education.

The last few acknowledgments and heartfelt thanks are for those who have influenced me most over the past three and a half years. Firstly to David Clarke, for encouraging me to leave the safe haven of Sydney University for a strange new lab at the RSC. Secondly, to my parents and brothers for supporting that decision, and assisting with all the mundane aspects of every residential relocation. Their continued love and support will always be valued.

The penultimate thanks go to Sandra Nissen, for her friendship and assistance from the moment I moved in to Fenner Hall until the present. For dragging me along to choir, and then to coffee and onto the committee, and for all the email and morning teas, for her understanding of all hassles, big and small - thank you.

Finally, to Cameron, for patience, philosophy, proof reading and a monopoly on the computer, for collecting me from or delivering me to the airport at early hours of the morning, for teaching me an appreciation of good red wine, twentieth century music, and flambe-ing the Cointreau. For his encouragement and support, careerwise and personally, he has my abiding thanks and love.

Publications

1. K.J. Edler and J.W. White, *J. Chem. Soc., Chem. Commun.,* **1995**, 155-156.
   Room Temperature Synthesis of Molecular Sieve MCM-41.

2. K.J. Edler, J. Dougherty, R. Durand, L. Iton, G. Kirton, G. Lockhart, Z. Wang, R.L. Withers, J. W. White, *Colloids Surfaces, A*, **1995**, *102*, 213-230.
   Small Angle X-ray Scattering from MCM-41 and its Synthesis Gels: Optimisation of the Synthesis Parameters.

3. K.J. Edler, P.A. Reynolds, F. Trouw, J.W. White, *Chem. Phys. Lett.,* **1996** *249*, 438-443.
   Methane Dynamics in the 36 Å Mesopores of MCM-41 Studied by Neutron Scattering

4. K.J. Edler, P.A. Reynolds, J.W. White, D. Cookson, *J. Chem. Soc., Faraday Trans.*, **1997**, *93*(1), 199-202.
   Diffuse Wall Structure and Narrow Mesopores in Highly Crystalline MCM-41 Materials Studied by X-Ray Diffraction.

5. K.J. Edler, P.A. Reynolds, P.J. Branton, F. Trouw, J.W. White, *J. Chem. Soc., Faraday Trans.,* **1997**, *93*(8), 1667-1674.
   The Structure and Dynamics of Hydrogen Adsorption in Mesoporous MCM-41.

6. K.J. Edler and J.W. White, *Chem. Mater.,* **1997**, *9*(5), 1226-1233.
   Further Improvements in the Long Range Order of MCM-41 Materials.

7. K.J. Edler, P.A. Reynolds and J.W. White, *J. Phys. Chem.* submitted, **1997**.
   Small Angle Neutron Scattering Studies on the Mesoporous Molecular Sieve, MCM-41.

8. K.J. Edler and J.W. White, *manuscript in preparation,* **1997**.
   Hydrothermal Stability of Pure Silica MCM-41 Materials.

9. K.J. Edler, P.A. Reynolds, A. Brown, T. Slawecki and J.W. White, *manuscript in preparation*, **1997**.
   Shear Induced Ordering in Surfactant/Silicate/Salt Gels.

Table of Contents

Chapter 1:

Introduction

"The most important thing is not to stop questioning. Curiosity has its own reason for existing. One cannot help but be in awe when he contemplates the mysteries of eternity, of life, of the marvellous structure of reality."

Albert Einstein

Porous materials have long been of interest in industrial fields as catalytic supports and adsorbents. Many different types of porous materials have been used in these applications, ranging from activated carbons, to zeolites. More specifically, silica based systems such as clays, silica gels and zeolites have been used in many catalytic processes and adsorption and separation applications. ZSM-5 is used as a catalyst for conversion of natural gas to motor fuel.[1] Zeolites A and X are used in detergents to soften water by removal of calcium and magnesium ions via ion exchange.[1] Porous silica gels have been used in filtration, chromatography, thermal/acoustic insulation, and as desiccants.[2] These, however, each have a range of practical use dictated by the size, shape and selectivity of the pores in the material and each has a distinct manner of preparation to produce the required pore structure. The molecular sieve MCM-41 forms a part of this spectrum of porous, silicate materials. A short comparison with some of these other materials follows.

Silicates are built up from $[SiO_4]^{2-}$ tetrahedra. Each tetrahedron is connected to other tetrahedra to form a three dimensional network. They may share from one, up to all four of the oxygen atoms with adjacent tetrahedra. Tetrahedra connected by two atoms form a chain; by three atoms, a sheet; and by four atoms, a three dimensional network.[3] Materials in which all four oxygen atoms in all tetrahedra are shared with other tetrahedra form dense structures such as quartz and cristobalite. In amorphous silica, which is less dense, there is a random packing of tetrahedra in a non-periodic structure in which at least two corners in each tetrahedron are shared. The Si-O-Si angles in these structures may vary, but the silicon-oxygen bond length is constant at around 0.162 nm.[3]

1.1 Porous Silicates

Porous silica is generally discussed as a subsection of the larger group of porous aluminosilicate materials. These may be one of two general types. The crystalline form, zeolites, or the less ordered porous silicates and aluminosilicates which include silica gels, and pillared clays. Both contain pores within the bulk material which may host other molecules, allowing interactions with the surface or with other molecules trapped within the structure to take place.

Zeolites are crystalline aluminosilicates where the channel structure may be one or two dimensional. The channels in these materials are part of the crystal lattice of the material, and so are highly monodisperse and have fixed directionality within the crystal. They have a pore size range[1] between about 4 and 7 Å, since the size and shape of these holes is determined by the stability of large rings made up of alternating silicon and oxygen atoms. The widest aperture in conventional aluminosilicate zeolites is a ring of 12 tetrahedral atoms and is 7.4 Å in diameter.[4,5] The uniformity of the channels in zeolitic systems means they are extremely selective adsorbents for small molecules of particular molecular geometries and sizes,[1,6,7] and so make highly selective catalytic supports, and adsorbents. However the narrow range of pore sizes available and the relatively small cross section of those pores restricts the size of molecules which may escape from or enter the pores to access catalytic or adsorption sites. This limits their use in applications involving larger organic molecules. Crystalline materials with larger pores (8-14.5 Å) have been prepared in aluminophosphate systems,[8-10] and are found in the natural ferroaluminophosphate, cacoxenite (14 Å),[11] but again, these materials are apparently limited by the size of void which may be accommodated in a crystalline system.

Porous silica gels are generally prepared via sol-gel methods, in which molecular or colloidal silicate species are dispersed in a solvent, and then form a gel which may lose solvent as the condensation of the silica proceeds. The silica walls in these materials are amorphous, showing no long-range order. The pores in these materials are a result of the process of gelation, which depends upon the reaction conditions (*eg.* temperature, pH), and the solvents and reagents used.[2] Other porous materials include modified layered materials, such as pillared smectite clays and layered double hydroxides, as well as porous glasses. Generally these materials have larger pores than zeolites, but the distribution of pore sizes is also larger, and the pores exist as a disordered network throughout the solid. This lack of uniformity is reflected in a corresponding lack of selectivity in adsorption and catalysis applications. They provide relatively high surface area, inert supports for catalysts, and can be prepared at various densities. Aerogel materials prepared by supercritical drying of wet gels may have densities as low as 0.003 g cm^{-3} with porosities of 98%[12] and surface areas of more than 1000 m^2 g^{-1}.[2] They are used as Cherenkov detectors in particle physics applications and as window and bulk insulation. It has been suggested aerogels could be used as gas filters or that metal-loaded aerogels could be used as catalyst beds in the petroleum industry.[12] The distribution of pore sizes in these materials is *ca*. 10-500 Å. In xerogels, which are air-dried gels with a surface area of 500-900 m^2 g^{-1}, the pore diameters can range from 10-200 Å within the one sample.[2]

The pillaring of layered silicates, such as montmorillonite, hectorite and saponite with intercalates, such as polyoxocations of aluminium, zirconium and chromium, results in materials with Lewis acid sites, provided by coordinately unsaturated metal ions on the pillars.[13] These materials therefore have novel catalytic properties and void volumes which are mostly within the nanoporous range (1.0-10 nm). Layered double hydroxides may be pillared with Keggin and other polyoxometallate ions, or metallo macrocyclic anions. Applications of these pillared materials focus on use as shape-selective heterogeneous catalysts for petroleum cracking, and for use in the treatment of polluted ground waters and industrial effluent.[13] Porous silica glasses, made by etching phase-separated borosilicate glasses prepared from high temperature melts,[2] have been used to measure the effects of confined spaces upon the collective behaviour of molecules adsorbed in the pores,[14] and to provide experimental observations whereby theories of molecular adsorption may be tested. Applications such as these would benefit from a simplified analysis if a material with a monodisperse pore size distribution was used.

1.2 MCM-41

The mesoporous molecular sieve, MCM-41 shares characteristics of both types of porous silica. The wall structure of this material appears to be amorphous, with densities close to those of colloidal silica.[15] In X-ray diffraction patterns, no sharp Bragg peaks are seen at angles corresponding to the silicon-oxygen distances observed in crystalline silicates. Instead, a broad hump of scattering is observed, more characteristic of a glass or amorphous silica system.[16,17]

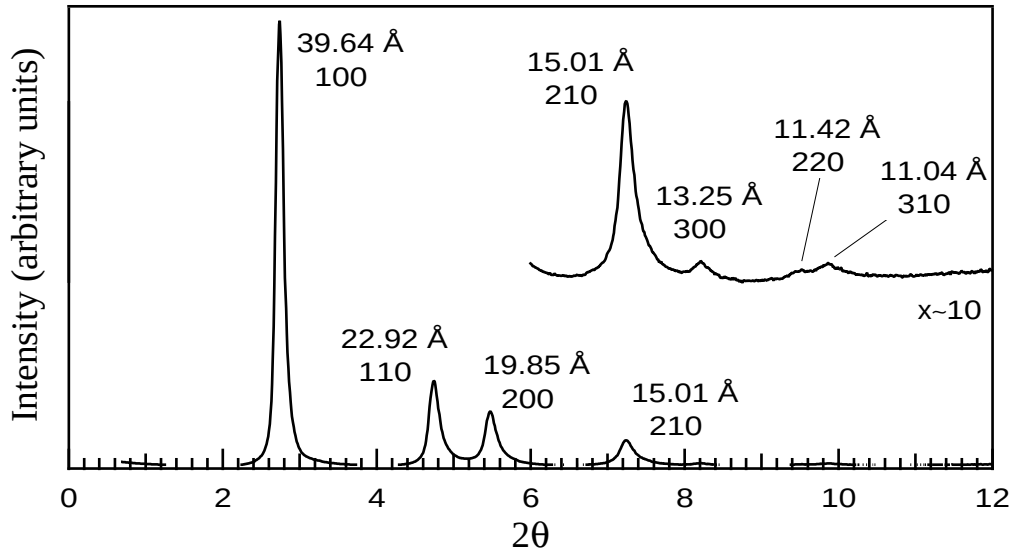

Figure 1.1 *Powder diffraction pattern, showing the intensity versus the scattering angle, 2θ, for a pure silica MCM-41 material. The inset is the pattern for the last four peaks multiplied by a factor of ten so that they could be shown on the same scale as the first three peaks. The peaks are indexed on a hexagonal lattice in two dimensions, and the d-spacing for each peak are given.*

The pore system of MCM-41 within this amorphous framework is, however, very well ordered. The long, cylindrical channels in this material are in a hexagonally close

packed arrangement, which is sufficiently organised for a diffraction pattern to arise from the arrangement of these pores. The pores are large (15-100 Å[18]), in the mesopore range (which is defined as between 20 - 500 Å[19]) which is two to three times those found in crystalline zeolitic systems, and so the repeat distance between channels is much greater than the distances between diffracting layers in crystals.

The X-ray diffraction pattern derives from this large channel repeat distance, rather than any crystalline order in the atoms comprising the walls, and is therefore seen at low angles. The inherent disorder in such an amorphous system may be seen in the rapid decrease in diffraction peak intensity as higher orders of diffraction, at larger angles, are reached. An indexed diffraction pattern of a well-ordered MCM-41 material taken at a high intensity synchrotron X-ray source is shown in Figure 1.1 above. Further discussion of the diffraction methods and instrumentation may be found in Chapter 3.

1.3 Templated Systems

Zeolitic materials, with their pores incorporated in a crystalline framework, may occur naturally, but are more often made synthetically by hydrothermal processes. The synthetic methods usually involve the addition of silicate monomers or polymers to pre-existing "seed" crystals,[20] or a nucleation process around an organic template molecule.[21] The presence of a molecular template determines to some extent the size and shape of the pore created in the zeolite, but it forms part of the crystal lattice of the growing zeolite, and so is encapsulated only in certain sites in the crystal. Some zeolites form in the absence of these template molecules, and whether the template has a structure-directing, or merely a space-filling role is dependant upon the particular zeolite and template molecule concerned.[21,22]

There are several competing pathways proposed for the mechanism of zeolite synthesis, which allow for the presence of the template molecule in the condensing silica framework. In all of these however, the driving force for the observed ordering is the condensation of the silica framework. The liquid-phase-ion-transport mechanism[23-25] proposes the formation of composite species in solution, made up of the template molecule surrounded by a loose shell of silica polyanions and water molecules. The structure of these nuclei has been described as clathrate-like,[26] but is probably not sufficiently ordered so as to resemble crystal fragments. Secondary building units comprised of silicon-oxygen rings of various sizes and connectivities, as seen in the structures of fully formed zeolites, have been proposed as one pathway for structure development.[20,27] There is some debate over whether such structures in fact exist in solution, and their role in zeolite nucleation.[28] Knight[29] has described such secondary building units as "red herrings", preferring to describe the process as the displacement of the ordered sheath of water molecules present around a template molecule by small silicate oligomers. These less ordered oligomers are held in place long enough to allow condensation into partially ordered structures around the template, which then continue condensation with further oligomers in order to nucleate the zeolite.

In the liquid-phase-ion-transport mechanism, these zeolite nuclei both agglomerate during the synthesis process, and draw further silicate species from the reaction solution, or from any precipitated silica gel in the system to assemble the crystalline silica/organic lattice. The solid-hydrogel-reconstruction model[30,31] instead suggests that the template molecule is precipitated along with amorphous silica into a silica gel phase. Within this gel, local re-ordering around each template molecule occurs, with atoms diffusing into place on the crystal lattice. Composite models have also been put forward, in which the zeolite nuclei form in solution and then adhere to the gel phase where further crystal growth occurs.[32-34]

In MCM-41 syntheses, by contrast, the template role is taken not by a *single* molecule but by an *array* of molecules, self-organised into a liquid crystalline phase. The liquid crystal template mechanism differs from that of zeolite formation in that it is not the silicate condensation which is the dominant factor in the formation of the structure. Instead it is the organisation of the surfactant molecules into micellar phases which defines the structure.[18] In support of this mechanism it has been found that in regions of the phase diagram where a surfactant does not form liquid crystal phases, *ie.* for very high temperatures,[35,36] or at concentrations below the critical micelle concentration[5,37] (cmc), addition of silicate does not result in mesoscale structures. At high temperatures porous materials such as ZSM-48, which are templated around a single surfactant molecule are formed, rather than structures based on liquid crystal arrays.[35]

The species first used in mesophase syntheses were quaternary amine surfactants. These are known to form a variety of liquid crystal phases in water by virtue of the interaction of their hydrophilic headgroups and hydrophobic hydrocarbon tails with the polar water phase.[38,39] The surfactant phase which forms in an aqueous solution is dependant upon the surfactant concentration and its counterion. It may be determined by the packing parameter v/al where v is the volume of the hydrocarbon chain, a the headgroup area and l the maximum effective chain length (somewhat less than the fully extended molecular length of the chain, typically l=1.5+1.265n Å where n is the number of carbon atoms in the chain or one less).[40-42] For cylindrical micelles $1/3<v/al<1/2$, whereas for spherical micelles $v/al<1/3$. The parameter, a, is known to be sensitive to the surfactant counterion. The packing parameter is essentially a measure of the curvature of the structure formed. Generally, at the lowest concentrations, the surfactant will exist as monomers in solution. With increasing surfactant concentration (for the same counterion) it becomes more energetically favourable to form micelles, which initially are spherical. Spherical micelles contain the largest area per headgroup for any of the surfactant micelle phases. Increasing concentration further raises the aggregation number in the micelle, reduces the area per headgroup, and may result in elongation of the micelle to form a rod in solution. Still further increases in surfactant concentration leads to agglomeration of the micelles, whether spherical or cylindrical, into a close packed phases, which, in the case of rod-like micelles is a hexagonal phase. The next level of concentration gives a cubic phase in which there is one continuous bilayer of surfactant separating two distinct water regions in which the surfactant forms a cubic gyroid minimal surface. The final phase transition is to a lamellar phase, composed of bilayers of surfactant, separated by a water phase. This phase has the least curvature and the smallest area per surfactant headgroup. Figure 1.2 illustrates the

surfactant liquid crystal phases and shows a phase diagram for pure cetyltrimethylammonium bromide, the surfactant used as the template molecule in this work.

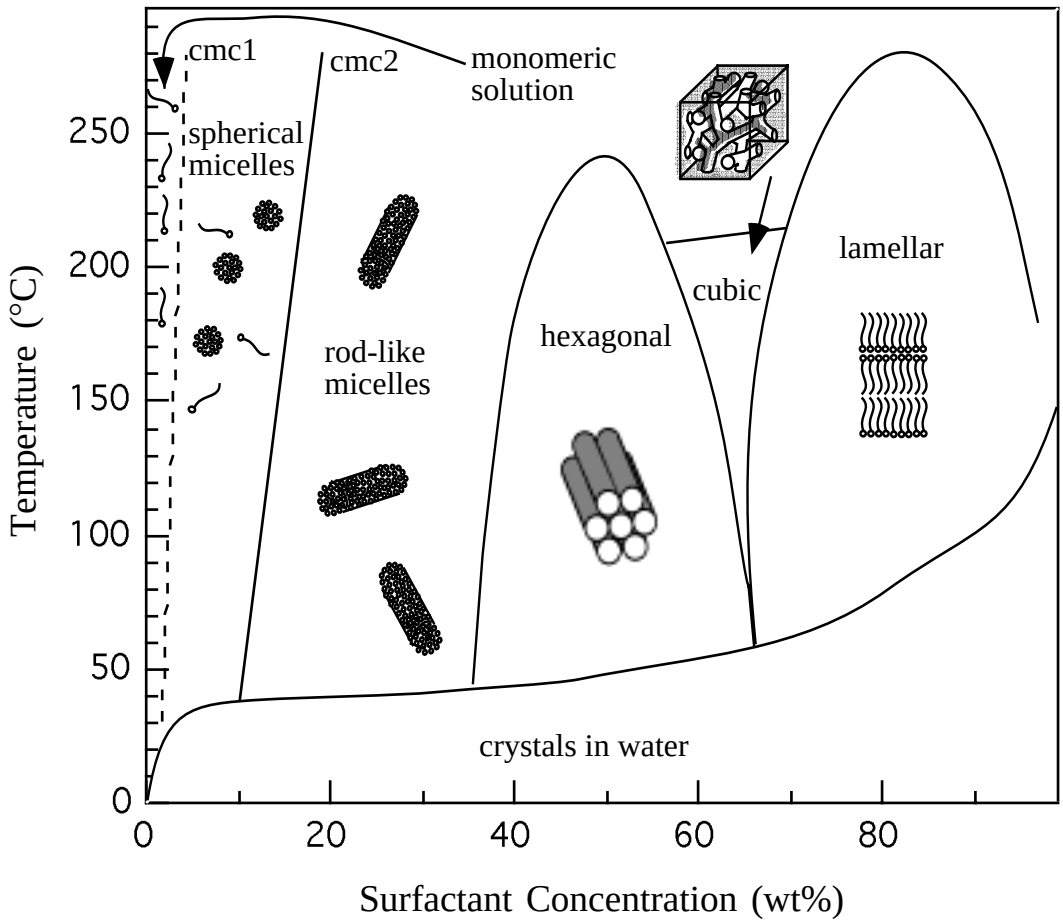

Figure 1.2 *A phase diagram*[43] *and schematics of the corresponding surfactant liquid crystal phases for the surfactant used as template in this work. Cmc1 is the critical micelle concentration for the formation of spherical micelles, which has been exaggerated to higher concentrations for the purposes of the illustration. Cmc2 is the critical micelle concentration for the formation of rod-like micelles.*

The MCM-41 material discussed in this work has the same overall structure as the surfactant hexagonal liquid crystal phase. Considerable work has also been carried out on silica/surfactant systems which mimic the other concentrated surfactant liquid crystal phases.[44] Lamellar phases were synthesised by Bull *et al.*[45] and by Dubois *et al.*,[46] who used a double chain surfactant. The lamellar silica/surfactant phase has also been observed as a precursor phase to the formation of the hexagonal phase.[47] The cubic phase was also reported by Beck *et al.*[18] and interconversions between the hexagonal and cubic phase have been observed.[48] More complex systems with multiwalled surfactant vesicles have also formed templates for the formation of patterned spheres,[49,50] and other structures strongly suggestive of silica frameworks formed by diatoms.[51,52] Combinations of the mesoporous system with other structure directing systems has given discrete, large mesoporous silica spheres, grown in an oil-water emulsion[53] and ordered macroporous fibres of mesoporous silica templated around a thread of co-aligned multicellular filaments of *Bacillus subtilis*.[54] The surfactants used

to create mesophase silicates have covered the full range of micelle forming species; cationic, anionic[55] and neutral molecules[56,57] have been used.

1.4 The Synthesis of MCM-41

MCM-41 was first reported by researchers from Mobil Oil in 1992.[18,58-61] They reported the formation of the hexagonal phase mesoporous material under a wide range of synthetic conditions. They used temperatures for the hydrothermal synthesis ranging from 25˚C to 175˚C[61] for periods from 5 minutes to 14 days, at initial pH values of 1-14.[60] Quaternary ammonium surfactants with chain lengths ranging from 8 carbon atoms to 16 were used, and other organic molecules, such as mesitylene, were used to swell the surfactant phases to allow templating of larger pores.[18] A variety of silica sources, from monomeric to highly condensed, and a corresponding variety of alumina sources were investigated.

Since this early work, other authors have commonly used tetraethylothosilicate (TEOS) as the silica source, and the n-C_{16} quaternary ammonium chloride or hydroxide surfactant, although there have also been many other reagents reported in the literature. Notably, a highly ordered hexagonal MCM-41 material has recently been reported by Khushalani *et al.*[62] which was prepared using TEOS and a cetylpyridinium chloride surfactant. Generally it has been found that increasing the degree of condensation of the silica source favours hexagonal phase formation while increasing the initial pH of the synthesis gel favours the lamellar phase.[63] Various post-synthesis treatments have also been applied to increase the long-range order and stability of this material. These include continued heating at 100˚C in a water solution with a range of pH values,[48,64] or impregnating with 20% nitric acid at room temperature overnight.[65]

In this work, a relatively simple system was chosen, in order to reduce the number of possible variables. The set of reagents selected (see Chapter 2), and their concentrations (based on a preparation initially published by Beck *et al.*[18]) were taken as standard, and optimisation and investigation of the synthesis restricted to that context only. The factors investigated were: heating/aging time in the gel, the presence or absence of stirring, the pH of the preparation during synthesis, and the effect of the type of acid used to maintain a selected pH. The effect of these factors throughout the synthesis process was examined as well as the structure and stability of the final products.

1.5 Mechanism of MCM-41 Formation

The molecular interaction between an inorganic material and a surfactant headgroup can be understood using conventional reaction schemes. Six different possible molecular reaction pathways[57,66,67] which use the principle of liquid crystal templating have been identified: S^+I^-, S^-I^+, $S^+X^-I^+$, $S^-X^+I^-$, S–I and S˚I˚, where S is the surfactant, I is the inorganic phase, and X is a mediating ion. S–I indicates systems where the inorganic precursor is covalently bonded to the template throughout synthesis, an approach which has been used for some transition metal oxide analogues of MCM-41.[68-70] The pathway applicable to a particular synthesis will be dictated by the reagents and synthetic

conditions and can influence the physical and chemical properties of the product. In this work, the S^+I^- reaction mechanism is used since the pH used (7 to 12) ensures negatively charged silicate ions, although mesoporous silicates may also be formed via $S^\circ I^\circ$ (pH ≈ 7) and $S^+X^-I^+$ (pH ≈ 2) pathways.[43,55] The way in which these silica-surfactant composites form the mesophase structures, and the stage in the reaction where the silica-surfactant molecular interactions become important are, however, not yet fully understood.

The mechanism suggested by the inventors of MCM-41 and related phases for their formation is the liquid crystal templating (LCT) mechanism.[18] This proposes that the structure of the channel systems in these mesoporous materials is determined by the surfactant aggregation behaviour, rather than the condensation of the silica around the template molecule, as occurs for zeolites. Exactly how the silica and surfactant interact in the system is still, however, under debate. Beck *et al.*[18] proposed two alternate mechanisms in which the surfactant might self-assemble into the observed silica-surfactant composite structures.

The first mechanism (Figure 1.3(a)) posited the existence of a hexagonally ordered, concentrated surfactant phase, prior to the addition of the silicate to the system. Upon silicate addition, the anions entered the water regions between adjacent micelles in this pre-existing phase and condensed in these interstitial sites without greatly perturbing the surfactant structure. The second mechanism (Figure 1.3(b)) required only that some surfactant micelles be present in the solution prior to the addition of the silicate anions. It was not necessary that the surfactant already exist in the hexagonal liquid crystal phase observed in the final product. In this case, upon the addition of silica to the system, silicate anions coated the surface of the surfactant micelles by some form of ion-exchange with the surfactant counterion. These silica encased micelles then self-ordered to form the hexagonal phase observed in the final product, and condensation of the silicate occurred to freeze in this structure.

Much work was then carried out to distinguish these mechanisms. In the form of the preparation frequently used to obtain hexagonal phase composite silica-surfactant material, the concentration of the surfactant used (10-26 wt%) is far below the concentration where the hexagonal phase would normally form, even at room temperature. Addition of the silicate anion to the system appears to move the phases which occur normally for the templating surfactant to lower concentrations,[43] despite the fact that the cmc would usually increase for increasing counterion radius and pH. The cmc would however be expected to decrease with increases in the valency of the counterions and the ionic strength of the solution.[65] Evidence from small angle neutron scattering,[71,72] X-ray scattering,[73] scanning and transmission electron microscopy[74] and ^2H, ^{29}Si[75] and ^{14}N[37] nmr also show that no hexagonal phase surfactant structures exist prior to the addition of the silicate, favouring the second mechanism suggested above. It has also been shown that varying the silicate concentration at constant surfactant concentration will result in the formation of hexagonal, lamellar and cubic phases, implying a prominent structure directing role for the inorganic silicate anions in this system.[44]

There are, however a few examples in the literature where very high concentrations of surfactant have been used to create a surfactant liquid crystal phase,[43,76] into which monomeric silicate anions were then introduced. Condensation of the silica in these phases led to the formation of monolithic rigid silica-surfactant composites with structures the same as those of the original surfactant phase. This approach however, appears only to work with very high concentration surfactant systems under conditions where the silicate condensation and consequent release of small molecules do not greatly perturb the existing surfactant structure.

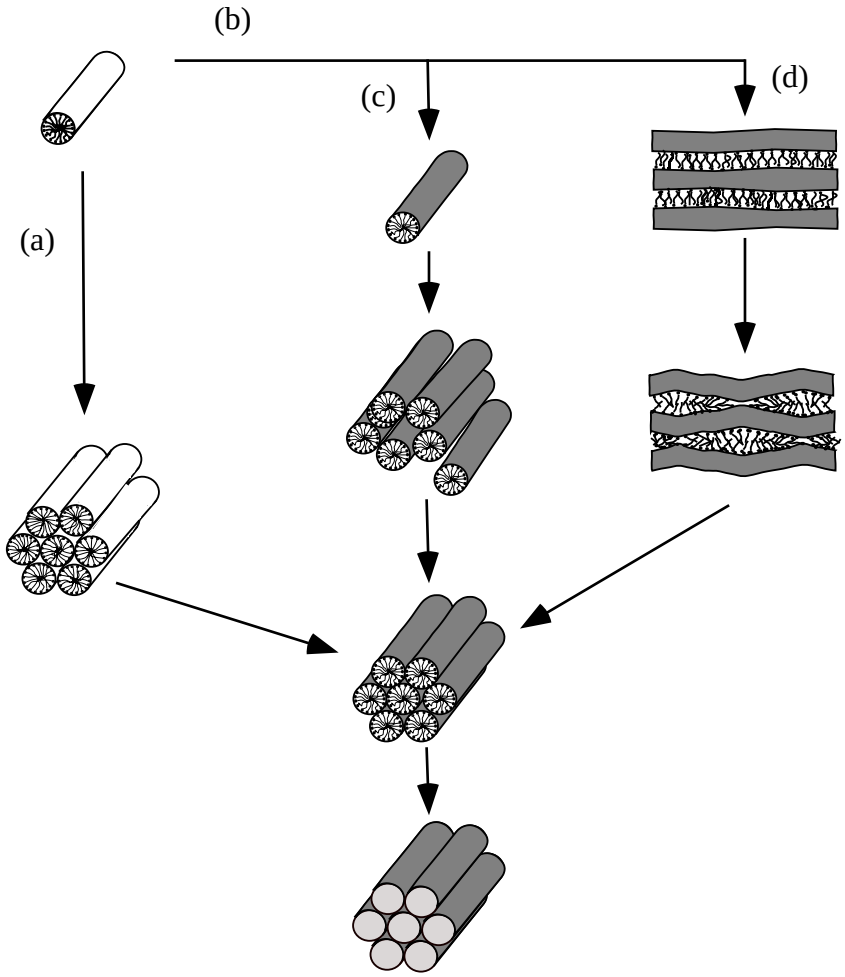

Figure 1.3 *Schematic showing various suggested mechanisms for the formation of MCM-41 as referred to in the text. The change in micelle colour from white to grey indicates the coating of the micelle headgroups with silicate oligomers which results in either (a) an unperturbed cast of the pre-existing surfactant liquid crystal phase, (b) the formation of silica coated surfactant species which form either (c) micelles which then agglomerate to form ordered and disordered arrays or (d) a lamellar phase when converts into the final hexagonal phase material. The final step, calcination results in an array of hollow, hexagonally packed tubes.*

In preparations using lower surfactant concentrations, two further refinements of the second micellar-assembly mechanism have been suggested. Several groups have observed the formation of a lamellar silica-surfactant phase in the early stages of preparations which subsequently formed hexagonal phase MCM-41.[37,47,63,77] This observation, led them to propose a "charge density matching" reaction scheme,[37,63]

(Figure 1.3(c)) in which surfactant monomers or micelles in solution become coated with silica oligomers, which act as multidentate ligands for the headgroups of the surfactant. The charge on these oligomers will probably cause the surfactant micelle to alter shape during the ion-exchange process. The screening of the electrostatic double-layer repulsion among the aggregates, by the silicate coating, then induces self-assembly of the ordered mesophases. The mesophase formed, by analogy with the surfactant packing parameter discussed in section 1.2 above, will be that with the least curvature which is consistent with the surfactant, pH and silicate concentration. These two processes - the coating of the micelle and the self-assembly of the mesophase occur on a similar time scale. With the subsequent condensation of the silicate, the inorganic charge density decreases, and lower surfactant charge densities are needed to stabilise the structure, and so the headgroup area per surfactant molecule increases. This increase in headgroup area drives a phase change, for example from lamellar to hexagonal, which is possible since the incompletely condensed silicate walls are still sufficiently flexible to under go the thinning which this entails. In this model, the wall thickness is determined by the double-layer potential - silica is only accumulated at the interface to the extent necessary for charge compensation. This results in wall thicknesses of 10-11 Å for lamellar phases, and 8-9 Å for hexagonal phases, as observed.[47] Post-synthesis treatment in water at 100˚C with pH = 7-10 of various silica-surfactant phases, made with different surfactants, also show phase changes consistent with changes in charge density due to increasing silica condensation and wall reconstruction.[48] A detailed scheme based on the free energy of the various interactions contributing to the synthesis process in this reaction scheme has been proposed.[47,55,63]

Other workers however, do not observe the formation of a lamellar phase as a precursor to hexagonal phase formation.[78-80] In fact, at room temperature in one preparation where a lamellar phase is initially present, the subsequent formation of the hexagonal phase does not occur as a direct transformation but proceeds via the dissolution of the lamellar phase followed by crystallisation of the hexagonal phase.[81] Evidence from transmission electron microscopy, which shows hexagonal phase MCM-41 where a significant proportion of the crystal edges meet at 120˚, led Cheng *et al*.[74] to propose a different pathway (Figure 1.3(d)). In this mechanism, the silicate anion first reacts with the pre-existing surfactant micelle, enabling formation of rods of silicated surfactant species. These then self-assemble directly into the hexagonal phase, via the formation of small hexagonal clusters. These clusters are enormous molecular groups which have faces that may grow at different rates, due to inhomogeneities in concentration in the surrounding synthesis gel. Adjacent faces are however more likely to be in the same solution environment, allowing the 120˚ angle between the neighbouring edges of the resultant crystal to be preserved. This mechanism allows for the formation of both perfect and imperfect crystal shapes, depending on the homogeneity of the reaction medium. Formation of the hexagonal phase via a lamellar phase is unlikely to produce 120˚ angles between crystal faces. The formation of a wide range of macroscopic morphologies made up from mesoporous silica in a silica/surfactant system seen using scanning electron microscopy has also been explained by an accretion of silicated micelles mechanism.[52] It is suggested that the growth patterns observed are characteristic of a system which is far from equilibrium and not necessarily described by a free energy function.

Packing arguments have also been put forwards for this direct assembly of silicated rods mechanism.[82] They suggest that it is difficult to see how a transformation from a lamellar phase to a multidimensional phase like the cubic phase would occur. All of the mesophases can, however, be considered as various forms of packing of silicated rods - the lamellar phase being caused by packing rods directly on top of each other, and the cubic by intertwined rods. Other evidence for the direct formation of hexagonal phase material from silicated rod structures is given by transmission electron microscopy. Micrographs show areas of randomly oriented tubes of the same dimensions as those in hexagonally packed areas within the same MCM-41 crystal. In this case, imperfect packing of the silica-coated rod-like micelles leads to the formation of the randomly oriented phase.[78] Also, work done using cryo-TEM at very early stages of the MCM-41 preparation has detected clusters of highly elongated, partially silicated micelles with dimensions similar to the correlation lengths seen in small angle X-ray scattering from the same solution.[73] As the reaction proceeds, silica covers more of each micelle and penetrates into them, causing the decrease in intermicellar distance from *ca*. 50 Å to that observed in hexagonal phase MCM-41, *ca*. 40 Å. The formation of these micelles from the pre-existing spherical surfactant micelles in solution is explained using curvature arguments, as were used above. The headgroup repulsion between surfactant molecules is decreased by the presence of silica anions, which increases the curvature of the micelle by decreasing the headgroup area, and promotes formation of longer micelles, which then form clusters.

In this mechanism the driving force for the reaction is both the energetically favourable organic-inorganic interactions and entropic gain from binding of the silicate anions to the micelles, which displaces a layer of ordered water surrounding the micelle. It has been predicted that organic species which do not cause the organisation of water will not act as templates in this system.[35] *In situ* ^{14}N nmr has shown no evidence of hexagonal surfactant phases in the synthesis media during MCM-41 formation. Rather, the results were consistent with randomly ordered rod-like micelles coated with a silica sheath which did not perturb the motion of the nitrogen containing surfactant headgroups.[78] This result also favours the direct formation of the hexagonal phase from these silicated micelles. Work on the catalytic effect of the surfactant micelles upon silica condensation also suggests the direct assembly of silicated rod-like micelles into the hexagonal phase when monomeric silica at ambient temperatures is used in the preparation. It was, however, also acknowledged that the precise mechanism might strongly depend upon the silica source or reaction conditions (particularly temperature).[5]

As an interesting comparison, the mechanism of formation of the other hexagonally ordered mesoporous silicate is noted. This material is formed by the intercalation of a surfactant into the layered polysilicate kanemite and is called FSM-16 (from Folded Sheet Mechanism, where the number refers to the length of the carbon chain used in the intercalating surfactant).[83] Kanemite consists of single layered silica sheets of linked silica tetrahedra with hydrated sodium ions in the interlayers.[84] The first step in FSM-16 formation is the ion-exchange of a cationic surfactant ion for the Na^+ between the layers. The second step is the folding and condensation of the silicate into a three-

dimensional silicate framework through an interlayer cross-linking process.[85] There may be some breaking up of the layers of kanemite at this stage with local reordering of the silica tetrahedra within the layer occurring.[86] The synthetic conditions for formation of FSM-16 are milder than those for MCM-41, occurring at 70˚C and requiring only low surfactant concentrations (3.2 wt%). The silicate walls are more condensed in these materials than in MCM-41 and they retain the particle morphology of the initial polysilicate, indicating substantial differences from the LCT materials.[86] Much greater disorder has been seen in the packing of channels in FSM-16, by electron microscopy, than in MCM-41 materials. It has been suggested that FSM-16 may contain pores which are not straight or long, but are likely to be interconnected in a three dimensional network.[86] No cubic phase has been synthesised from these materials. However, the mechanism is still driven by the aggregation of surfactant ions which is induced by the higher concentration of ions between the silicate layers. This is similar to the lamellar $\rightarrow$ hexagonal phase mechanism described above.

One report has been made concerning the heterogenous nucleation of MCM-41. In that work, the presence of colloidal particles was shown to promote the formation of hexagonal phase mesopores in a system which otherwise produced amorphous silica.[87] When colloidal silica was used, the colloidal particles formed sites for initial aggregation of silica-surfactant composites. The particle then slowly dissolved and was converted into well ordered, hexagonal phase material, growing in towards the centre of the particle. The presence of more colloidal material induced greater long range order in the product. When colloidal titania which did not dissolve during the reaction, was used, well ordered mesoporous silicates again nucleated on the surface. This ordering is probably due to the adsorption of the surfactant species on the particle surface and probably shares some features with the mechanisms of formation of thin films of MCM-41 on mica,[88] and at the air-water interface.[89,90]

In the present work, aging experiments and *in situ* heating experiments on synthesis gels were carried, out in order to determine the evolution of the formation of MCM-41 in the particular system under study. Investigation of the silica-surfactant species, under conditions where micelles were not present, was done using monomolecular films of surfactant on a Langmuir trough. The ability of the silica-surfactant hexagonal phase to align under shear or to decompose into silica coated rod-like micelles which would align was also investigated. Some conclusions concerning the mechanism of hexagonal phase MCM-41 formation were drawn from this work, described in Chapter 4.

1.6 Applications of MCM-41

Applications of MCM-41 largely turn on its large, monodisperse and adjustable pore sizes, and its high surface areas and pore volumes. In its aluminosilicate form it has been shown to be mildly acidic,[91] and its hydrophobicity can be altered by changing the Si/Al ratio. Materials containing more silica are more hydrophobic.[92,93] It is relatively thermally stable, however in the presence of moisture may undergo hydrolysis causing breakdown of the pore structure on time scales of 6 to 18 months (see Chapter 4).

Many suggestions have been made for possible uses of MCM-41.[18,61,65] Catalytic processes such as the processing of high distillates of crude oils into more valuable products,[60] and the synthesis of large molecules are frequently mentioned. The MCM-41 materials in this case would be either substituted with various catalytically active transition metal oxides, either in whole or in part, or else would act as inert, high surface area supports for catalytic entities bound to the walls of the channels. Some shape-selection may possibly arise from the shape of the pores by analogy with zeolites. It has been shown that the narrow pore size distribution of these materials promotes catalytic activity for the production of dimethylacetals, over materials with broader pore size distributions.[94]

Aluminosilicate MCM-41 materials have been shown to be moderately good catalysts for the cracking of large organic molecules to smaller ones. The activity generally increases with increasing aluminium content.[91] Comparisons with commercial fluid catalytic cracking catalysts has shown that AlMCM-41, for a given conversion, gives higher amounts of gaseous products, indicating more severe cracking, and yields more olefins and lower amounts of branched hydrocarbons.[95] Many patents and papers mention the catalytic use of AlMCM-41 for acid catalysis, and TiMCM-41 and VMCM-41 for liquid redox catalysis, and these have been reviewed.[65,95] These conclude that the improvement observed over conventional catalysts is often due to higher surface areas and increased accessibility of active sites, although much work still is required on regeneration, and behaviour under realistic working conditions before industrial usage will be feasible.[95]

Some workers have reported incorporation of catalysts such as 2,4,6-triphenylpyrylium[96] (for isomerisation of *cis*-stilbene) and $[Pt_{15}(CO)_{30}]^{2-}$ (in FSM-16 channels for catalysis in the water gas shift reaction)[97] via ship-in-a-bottle syntheses inside mesoporous silica channels. Molecules of titanocene dichloride have been diffused into the MCM-41 pores and grafted to the walls via reactions with the pendant silanol groups. These were then converted to isolated titania species by calcination, with the resulting materials proving to have a very high turnover frequency for the epoxidation of alkenes.[98] Many other molecules especially organometallics have been directly adsorbed into the MCM-41 pores and anchored, by various methods of grafting, to the walls.[96,99-104] These often prove to have good catalytic activity for various reactions including the production of highly isotactic polypropene,[100] the conversion of low-density polyethylene into hydrocarbon feedstocks,[105] alkene oxidation[101,103] and the formation of fine chemicals which involve bulky reactants or products.[94,104] Catalytic activity has also been observed for aluminosilicate MCM-41 ion-exchanged

with sodium and caesium cations.[106] Organically modified MCM-41 materials with possible catalytic applications have also been directly prepared in one-step syntheses by neutral templating routes which allow the template to be removed by washing rather than by calcination.[107]

The channels of MCM-41 have also been used to create nanosized metal clusters of platinum by various methods,[108,109] NiMo oxides,[110] caesium-lanthanum oxides[111] and Fe_2O_3[112] by incipient wetness techniques. The materials containing platinum nanocrystals were shown to be good catalysts for the oxidation of CO, with samples prepared using the incipient wetness method showing the best performance.[108] They also show high catalytic activity for the hydrogenolysis of ethane,[109] and of branched alkanes.[113] The NiMo impregnated material showed good performance as a catalyst for cracking vacuum gasoil under mild operating conditions.[110] Iron (II) impregnated MCM-41 materials loaded with palladium amine clusters showed some activity in an oxygen-rich environment for breakdown of NO_x and hydrocarbons present in exhaust gases.[114]

The use of nanoscale fabrication technology within the large pores of these materials has also been suggested, in order to form many other types of composite material. These include the formation of quantum wires through the polymerisation of conducting polymers, or metal complexes encapsulated in the silicate frameworks. Previously quantum wires have been formed by molecular beam epitaxy and atomic layer epitaxy but it is difficult to make structures below diameters of about 100 Å using these methods. Wu and Bein[115,116] have already shown that it is possible to polymerise monomers for conducting polymers, such as polyaniline, within the MCM-41 channels, resulting in conducting filaments lining the mesopores.[117] They have also produced conducting carbon wires inside MCM-41 channels by pyrolysing polyacrylonitrile polymerised inside the pores. Previous work with zeolites had resulted in filaments too small to carry charge, but inside the larger MCM-41 channels, interchain and transverse interactions are permitted, allowing significant conductivity to be observed.[118] Other workers report the polymerisation of styrene,[119] methyl methacrylate, and vinyl acetate[120] within the silica based mesopores. Properties of the encapsulated polymers were different to those in the bulk. Specifically the glass transition temperature was reduced and the molecular weight was inversely dependant on pore size. Ko and Ryoo[121] have manufactured platinum wires within the pore system of MCM-41 by repeated soaking in $Pt(NH_3)_4(NO_3)_2$ solutions, followed by drying and reduction to metallic platinum. These wires were used to image individual channels via transmission electron microscopy.

Separation and adsorption applications such as protein separations and the selective adsorption of large organic molecules from waste water are also frequently proposed. Pure silica zeolite analogues exhibit a high efficiency in selectively adsorbing organic pollutants from waste waters. Increased pore sizes might extend this usage of pure silica frameworks, to filter out larger molecules such as polychlorinated biphenyls or herbicide and pesticide molecules in drinking water.[122] MCM-41 with its monodisperse, ordered pores which may be varied in size, has been put forward as a model mesoporous adsorbent for the testing of theories of adsorption of small

molecules such as nitrogen, argon, oxygen and water in porous systems.[123-127] MCM-41 materials with varied pore sizes have been used to test models for the diffusion of glucose and glucitol in water.[128]

The steep rise in adsorption at certain value of P/P_0, caused by the sudden filling of mesopores with water vapour, in a pure silica MCM-41 has been shown to be function of the pore size. This effect is reproducible, and reversible and the MCM-41 substrate is stable over several cycles. This has led to the suggestion that such mesoporous materials be used in the design and fabrication of humidity sensors.[93]

The structuring observed in these mesoporous materials is of a length scale where quantum confinement of the electronic states, related to the pore size, could be expected, and so porous metal oxides made in this fashion should also posses altered electronic properties. Porous materials made from semiconducting metal oxides may be able to be used as sensors, if their electronic surface states react to the adsorption of the substance to be detected.[66] Use of porous transition-metal oxide systems for applications in non-linear optics, such as molecular sieves for electronic and optical applications,[65] and as thermal or acoustic insulation have also been suggested.[68]

In the early literature, including patents, MCM-41 has been put forward as having possible uses in drug delivery systems,[61] and as even being able to encapsulate proteins in ultra-large pore materials. Confining such difficult to crystallise molecules in a rigid lattice may create an ordering matrix to allow structure determination by X-ray diffraction.[129] The large number of pendant hydroxyl groups lining the inside surface of MCM-41 also suggests the possibility of anchoring enzymes to the interior surfaces. These enzymes would then be situated in precisely defined chemical environments, and could be used for the commercial production of biological molecules.[130] Surfactant templating techniques have been used to create porous calcium oxide (aragonite) and calcium phosphate structures similar to those found in the skeletons of marine algae.[131,132] This points to the possibility of considerable application of such techniques in the field of biomineralisation, to create artificial bone, or shell or to mimic the structure of natural organic-inorganic composites optimised for a particular task.

Since many of these applications utilise the high surface area and relative stability of MCM-41 materials, it becomes important to have a detailed knowledge of the structure of the material in order that its properties may be optimised for various applications. Uses such as the testing of theoretical models of adsorption require a good model of the molecular potentials which make up the wall surfaces. The optimisation of binding of catalytically active complexes, or the formation of molecular wires or nanosize particles of other materials within the channels will benefit greatly from a molecular level structure. Work on the structure and wall characteristics of pure silica MCM-41 is reported in Chapters 5 and 5. Data from a number of techniques, small angle X-ray and neutron scattering, quasielastic neutron scattering from molecules adsorbed in the MCM-41 channels, gas adsorption isotherms, and X-ray and neutron diffraction have been combined to determine a detailed model of the wall structure of these materials.

1.7 References

1. E.M. Flanigen, *Pure & Appl. Chem.,* **1980**, *52,* 2191-2211.
2. C.J. Brinker and G.W. Scherer, *Sol-Gel Science. The Physics and Chemistry of Sol-Gel Processing*, Academic Press, San Diego, **1990**.
3. H.E. Bergna in *The Colloid Chemistry of Silica*; Advances in Chemistry Series, (Ed. H.E. Bergna), American Chemical Society, Washington D.C., **1994**, *Vol. 243*, 1-47.
4. D.H. Olson, *J. Phys. Chem.,* **1970**, *74,* 2758-2764.
5. C.-F. Cheng, Z. Luan and J. Klinowski, *Langmuir,* **1995**, *11,* 2815-2819.
6. S.L. Suib, *Chem. Rev.,* **1993**, *93*(2), 803-826.
7. W.O. Haag in *Zeolites and Related Microporous Materials: State of the Art 1994*; Studies in Surface Science and Catalysis, (Eds. J. Weitkamp, H.G. Karge, H. Pfeifer and W. Hölderich), Elsevier Science B.V., **1994**, *Vol. 84*, 1375-1394.
8. R.M. Dessau, J.L. Schlenker and J.B. Higgins, *Zeolites,* **1990**, *10,* 522-524.
9. M.E. Davis, C. Saldarriaga, C. Montes, J. Garces and C. Crowder, *Nature,* **1988**, *331,* 698-699.
10. R.H. Jones, J.M. Thomas, J. Chen, R. Xu, Q. Huo, S. Li, Z. Ma and A.M. Chippindale, *J. Solid State Chem.,* **1993**, *102,* 204-208.
11. P.B. Moore and J. Shen, *Nature,* **1983**, *306,* 356-358.
12. L.W. Hrubesh, *Chem. & Ind.,* **1990**, *17 December,* 824-827.
13. T.J. Pinnavaia in *Materials Chemistry: An Emerging Discipline*; Advances in Chemistry Series, (Eds. L.V. Interrante, L.A. Carper and A.B. Ellis), ACS, Washington D.C., **1995**, *Vol. 245*, 283-300.
14. P.E. Sokol, R.T. Azuah, M.R. Gibbs and S.M. Bennington, *J. Low Temp. Phys.,* **1996**, *103*(1/2), 23-33.
15. T. Dabadie, A. Ayral, C. Guizard, L. Cot and P. Lacan, *J. Mater. Chem.,* **1996**, *6*(11), 1789-1794.
16. H.F. Poulsen, J. Neuefeind, H.-B. Neumann, J.R. Schneider and M.D. Zeidler, *J. Non-Cryst. Solids,* **1995**, *188,* 63-74.
17. A.C. Wright, *J. Non-Cryst. Solids,* **1994**, *179,* 84-115.
18. J.S. Beck, J.C. Vartuli, W.J. Roth, M.E. Leonowicz, C.T. Kresge, K.D. Schmitt, C.T.-W. Chu, D.H. Olson, E.W. Sheppard, S.B. McCullen, J.B. Higgins and J.L. Schlenker, *J. Am. Chem. Soc.,* **1992**, *114,* 10834-10843.
19. D.H. Everett, *Pure Appl. Chem.,* **1972**, *31,* 578.
20. E.J.P. Feijen, J.A. Martens and P.A. Jacobs in *Zeolites and Related Microporous Materials: State of the Art 1994*; Studies in Surface Science and Catalysis, (Eds. J. Weitkamp, H.G. Karge, H. Pfeifer and W. Hölderich), Elsevier Science B.V., **1994**, *Vol. 84*, 3-20.
21. S.L. Burkett and M.E. Davis, *Chem. Mater.,* **1995**, *7*(5), 920-928.
22. M.E. Davis and R.F. Lobo, *Chem. Mater.,* **1992**, *4,* 756.
23. S.P. Zhdanov in *Molecular Sieve Zeolites - 1*; Advanced in Chemistry Series, (Eds. E.M. Flanigen and L.B. Sand), ACS, Washington D.C., **1971**, *Vol. 101*, 20-43.
24. G.T. Kerr, *J. Phys. Chem.,* **1966**, 1047.
25. R.M. Barrer, J.W. Baynham and F.W. Bultide, *J. Chem. Soc.,* **1959**, 195.
26. M. Wiebcke and D. Hoebbel, *J. Chem. Soc., Dalton Trans.,* **1992**, 2451-2455.

27. R.M. Barrer, *Hydrothermal Chemistry in Zeolites*, Academic Press, London, **1982**.
28. J.J. Keijsper and M.F.M. Post in *Zeolite Synthesis*; ACS Symposium Series, (Eds. M.L. Occelli and M.E. Robson), ACS, Washington D.C., **1989**, *Vol. 398*, 28-48.
29. C.T.G. Knight, *Zeolites,* **1990**, *10,* 140-144.
30. B.D. McNicol, G.T. Pott, K.R. Loos and N. Mulder in *Molecular Sieves*; Advances in Chemistry Series, (Eds. W.M. Meier and J.B. Uytterhoeven), ACS, Washington D.C., **1973**, *Vol. 121*, 152-161.
31. W.H. Dokter, H.F. van Garderen, T.P.M. Beelen, R.A. van Santen and W. Bras, *Angew. Chem. Int. Ed. Engl.,* **1995**, *34*(1), 73-75.
32. A. Culfaz and L.B. Sand in *Molecular Sieves*; Advances in Chemistry Series, (Eds. W.M. Meier and J.B. Uytterhoeven), ACS, Washington D.C., **1973**, *Vol. 121*, 140-151.
33. F. DiRenzo, F. Remoue, P. Massiani, F. Fajula, F. Figueras and T. Des Courières in *Molecular Sieves - Synthesis of Microporous Material*; (Eds. M.L. Occelli and H.E. Robson), Van Nostrand Reinhold, New York, **1992**, *Vol. 1*, 115-128.
34. J.C. Jansen, C.W.R. Engelen and H. van Bekkum in *Zeolite Synthesis*; (Eds. M.L. Occelli and H.E. Robson), ACS, Washington D.C., **1989**, *Vol. 398*, 257-273.
35. M.E. Davis, C.-Y. Chen, S.L. Burkett and R.F. Lobo in *Mat. Res. Soc. Symp. Proc. "Better Ceramics Through Chemistry VI"*; "Better Ceramics Through Chemistry IV", (Eds. C.J.B. A. K. Cheetham M. L. Mecartney and C. Sanchez), Materials Research Society, Pittsburg, PA, **1994**, *Vol. 346*, 831-842.
36. J.S. Beck, J.C. Vartuli, G.J. Kennedy, C.T. Kresge, W.J. Roth and S.E. Schramm, *Chem. Mater.,* **1994**, *6,* 1816-1821.
37. A. Firouzi, D. Kumar, L.M. Bull, T. Besier, P. Sieger, Q. Huo, S.A. Walker, J.A. Zasadzinski, C. Glinka, J. Nicol, D. Margolese, G.D. Stucky and B.F. Chmelka, *Science,* **1995**, *267*, 1138-1143.
38. Y. Chevalier and T. Zemb, *Rep. Prog. Phys.,* **1990**, *53,* 279-371.
39. G.J.T. Tiddy, *Physics Reports,* **1980**, *57*(1), 1-46.
40. J.N. Israelachvili, *Surfactants in Solution*, Plenum, New York, **1987**.
41. J.N. Israelachvili, D.J. Mitchell and B.W. Ninham, *J. Chem. Soc., Faraday Trans. 2,* **1976**, *72,* 1527.
42. J.N. Israelachvili in *Physics of Amphiphiles: Micelles, Vesicles and Microemulsions*; (Ed. X.C. Corso), Soc. Italiana di Fisica, Bologna, **1985**, 24-58.
43. N.K. Raman, M.T. Anderson and C.J. Brinker, *Chem. Mater.,* **1996**, *8*(8), 1682-1701.
44. J.C. Vartuli, K.D. Schmitt, C.T. Kresge, W.J. Roth, M.E. Leonowicz, S.B. McCullen, S.D. Hellring, J.S. Beck, J.L. Schlenker, D.H. Olson and E.W. Sheppard, *Chem. Mater.,* **1994**, *1994*(6), 2317-2326.
45. L.M. Bull, D. Kumar, S.P. Millar, T. Besier, M. Janicke, G.D. Stucky and B.F. Chmelka in *Zeolites and Related Microporous Materials: State of the Art 1994.*; Stud. Surf. Sci. Catal., (Eds. J. Weitkamp, H.G. Karge, H. Pfeifer and W. Hölderich), Elsevier Science B.V., **1994**, *Vol. 84A*, 429-434.

46. M. Dubois, T. Gulik-Krzywicki and B. Cabane, *Langmuir,* **1993**, *9*(3), 673-680.
47. A. Monnier, F. Schüth, Q. Huo, D. Kumar, D. Margolese, R.S. Maxwell, G.D. Stucky, M. Krishnamurty, P. Petroff, A. Firouzi, M. Janicke and B.F. Chmelka, *Science,* **1993**, *261*, 1299-1303.
48. Q. Huo, D.I. Margolese and G.D. Stucky, *Chem. Mater.,* **1996**, *8*(5), 1147-1160.
49. P.T. Tanev and T.J. Pinnavaia, *Science,* **1996**, *271,* 1267-1269.
50. A. Chenite, Y. Le Page, V.R. Karra and A. Sayari, *J. Chem. Soc., Chem. Commun.,* **1996**, 413-414.
51. S. Schacht, Q. Huo, I.G. Voigt-Martin, G.D. Stucky and F. Schüth, *Science,* **1996**, *273*, 768-771.
52. H. Yang, N. Coombs and G.A. Ozin, *Nature,* **1997**, *386,* 692-695.
53. Q. Huo, J. Feng, F. Schüth and G.D. Stucky, *Chem. Mater.,* **1997**, *9*(1), 14-17.
54. S.A. Davis, S.L. Burkett, N.H. Mendelson and S. Mann, *Nature,* **1997**, *385,* 420-423.
55. Q. Huo, D.I. Margolese, U. Ciesla, D.G. Demuth, P. Feng, T.E. Gier, P. Sieger, A. Firouzi, B.F. Chmelka, F. Schüth and G.D. Stucky, *Chem. Mater.,* **1994**, *6,* 1176-1191.
56. S.A. Bagshaw, E. Prouzet and T.J. Pinnavaia, *Science,* **1995**, *269*, 1242-1244.
57. P.T. Tanev and T.J. Pinnavaia, *Science,* **1995**, *267,* 865-867.
58. J.S. Beck, C.T.-W. Chu, I.D. Johnson, C.T. Kresge, M.E. Leonowicz, W.J. Roth and J.C. Vartuli, *US Patent, No. 5,108, 725,* **1992**.
59. C.T. Kresge, M.E. Leonowicz, W.J. Roth, J.C. Vartuli and J.S. Beck, *Nature,* **1992**, *359*, 710-712.
60. C.T. Kresge, M.E. Leonowicz, W.J. Roth and J.C. Vartuli, *US Patent, No. 5,102,643,* **1992**.
61. C.T. Kresge, M.E. Leonowicz, W.J. Roth and J.C. Vartuli, *US Patent No. 5,098,684,* **1992**.
62. D. Khushalani, A. Kuperman, N. Coombs and G.A. Ozin, *Chem. Mater.,* **1996**, *8*(8), 2188-2193.
63. G.D. Stucky, A. Monnier, F. Schüth, Q. Huo, D. Margolese, D. Kumar, M. Krishnamurty, P. Petroff, A. Firouzi, M. Janicke and B.F. Chmelka, *Mol. Cryst. Liq. Cryst.,* **1994**, *240,* 187-200.
64. D. Khushalani, A. Kuperman, G.A. Ozin, K. Tanaka, J. Garcés, M.M. Olken and N. Coombs, *Adv. Mater.,* **1995**, *7*(10), 842-846.
65. X.S. Zhao, G.Q. Lu and G.J. Millar, *Ind. Eng. Chem. Res.,* **1996**, *35*(7), 2075-2090.
66. P. Behrens, *Angew. Chem. Int. Ed. Engl.,* **1996**, *35*(5), 515-518.
67. Q. Huo, D.I. Margolese, U. Ciesa, P. Feng, T.E. Gier, P. Sieger, R. Leon, P.M. Petroff, F. Schüth and G.D. Stucky, *Nature,* **1994**, *368,* 317-321.
68. D.M. Antonelli and J.Y. Ying, *Chem. Mater.,* **1996**, *8*(4), 874-881.
69. D.M. Antonelli and J.Y. Ying, *Angew. Chem. Intl. Ed. Engl.,* **1996**, *35*(4), 426-430.
70. D.M. Antonelli, A. Nakahira and J.Y. Ying, *Inorg. Chem.,* **1996**, *35*(11), 3126-3136.
71. C.J. Glinka, J.M. Nicol, G.D. Stucky, E. Ramli, D. Margolese, Q. Huo, J.B. Higgins and M.E. Leonowicz, *J. Porous Materials,* **1996**, *3,* 93-98.

72. L. Auvray, A. Ayral, T. Dabadie, L. Cot, C. Guizard and J.D.F. Ramsay, *Faraday Discuss.,* **1995**, *101,* 235-247.
73. O. Regev, *Langmuir,* **1996**, *12*(20), 4940-4944.
74. C.-F. Cheng, H. He, W. Zhou and J. Klinowski, *Chem. Phys. Lett.,* **1995**, *244,* 117-120.
75. W. Kolodziejski, A. Corma, M.-T. Navarro and J. Pérez-Pariente, *Solid State Nuclear Magnetic Resonance,* **1993**, *2,* 253-259.
76. G.S. Attard, J.C. Glyde and C.G. Göltner, *Nature,* **1995**, *378*, 366-368.
77. A. Steel, S.W. Carr and M.W. Anderson, *J. Chem. Soc., Chem Commun.,* **1994**, 1571-1572.
78. C.Y. Chen, S.L. Burkett, H.-X. Li and M.E. Davis, *Microporous Mater.,* **1993**, *2,* 22.
79. S. O'Brien, R.J. Francis, S.J. Price, D. O'Hare, S. Clark, N. Okazaki and K. Kuroda, *J. Chem. Soc., Chem. Commun.,* **1995**, 2423-2424.
80. A. Ortlam, J. Rathousky, G. Schulz-Ekloff and A. Zukal, *Microporous Mater.,* **1996**, *6*(4), 171-180.
81. A. Matijasic, A.-C. Voegtlin, J. Patarin, J.L. Guth and L. Huve, *J. Chem. Soc., Chem. Commun.,* **1996**, 1123-1124.
82. J.C. Vartuli, K.D. Schmitt, C.T. Kresge, W.J. Roth, M.E. Leonowicz, S.B. McCullen, S.D. Hellring, J.S. Beck, J.L. Schlenker, D.H. Olson and E.W. Sheppard in *Zeolites and Related Microporous Materials: State of the Art 1994.*; Stud. Surf. Sci. Catal., (Eds. J. Weitkamp, H.G. Karge, H. Pfeifer and W. Hölderich), Elsevier Science B.V., **1994**, *Vol. 84A*, 53-60.
83. S. Inagaki, Y. Fukushima and K. Kuroda in *Zeolites and Related Microporous Materials: State of the Art 1994.*; Stud. Surf. Sci. Catal., (Eds. J. Weitkamp, H.G. Karge, H. Pfeifer and W. Hölderich), Elsevier Science B.V., **1994**, *Vol. 84A*, 125-132.
84. K. Kuroda, *J. Porous Mater.,* **1996**, *3,* 107-114.
85. S. Inagaki, A. Koiwai, N. Suzuki, Y. Fukushima and K. Kuroda, *Bull. Chem. Soc. Jpn.,* **1996**, *69*(5), 1449-1457.
86. C.-Y. Chen, S.-Q. Xiao and M.E. Davis, *Microporous Mater.,* **1995**, *4*(1), 1-20.
87. J. Liu, A.Y. Kim, J.W. Virden and B.C. Bunker, *Langmuir,* **1995**, *11*(3), 689-692.
88. H. Yang, A. Kuperman, N. Coombs, S. Mamiche-Afara and G.A. Ozin, *Nature,* **1996**, *379,* 703-705.
89. H. Yang, N. Coombs, I. Sokolov and G.A. Ozin, *Nature,* **1996**, *381,* 589-592.
90. I.A. Aksay, M. Trau, S. Manne, I. Honma, N. Yao, L. Zhou, P. Fenter, P.M. Eisenberger and S.M. Gruner, *Science,* **1996**, *273,* 892-898.
91. R. Mokaya, W. Jones, Z. Luan, M.D. Alba and J. Klinowski, *Catal. Lett.,* **1996**, *37,* 113-120.
92. P.L. Llewellyn, F. Schüth, Y. Grillet, F. Rouquerol and K.K. Unger, *Langmuir,* **1995**, *11,* 574-577.
93. S. Komarneni, R. Pidugu and V.C. Menon, *J. Porous Mater.,* **1996**, *3,* 99-106.
94. M.J. Climent, A. Corma, S. Iborra, M.C. Navarro and J. Primo, *J. Catal.,* **1996**, *161,* 783-789.
95. A. Sayari, *Chem. Mater.,* **1996**, *8*(8), 1840-1852.

96. A. Corma, V. Fornés, H. García, M.A. Miranda and M.J. Sabater, *J. Am. Chem. Soc.,* **1994**, *116*(21), 9767-9768.
97. T. Yamamoto, T. Shido, S. Inagaki, Y. Fukushima and M. Ichikawa, *J. Am. Chem. Soc.,* **1996**, *118*(24), 5810-5811.
98. T. Maschmeyer, F. Rey, G. Sankar and J.M. Thomas, *Nature,* **1995**, *378,* 159-162.
99. S. O'Brien, J. Tudor, S. Barlow, M.J. Drewitt, S. Heyes and D. O'Hare, *J. Chem. Soc., Chem. Commun.,* **1997**, 641-642.
100. J. Tudor and D. O'Hare, *J. Chem. Soc., Chem. Commun.,* **1997**, 603-604.
101. C.-J. Liu, S.-G. Li, W.-Q. Pang and C.-M. Che, *J. Chem. Soc., Chem. Commun.,* **1997**, 65-66.
102. P. Sutra and D. Brunel, *J. Chem. Soc., Chem. Commun.,* **1996**, 2485-2486.
103. R. Burch, N. Cruise, D. Gleeson and S.C. Tsang, *J. Chem. Soc., Chem. Commun.,* **1996**, 951-952.
104. I.V. Kozhevnikov, A. Sinnema, R.J.J. Jansen, K. Pamin and H. van Bekkum, *Catal. Letts.,* **1995**, *30,* 241-252.
105. J. Aguado, D.P. Serrano, M.D. Romero and J.M. Escola, *J. Chem. Soc., Chem. Commun.,* **1996**, 725-726.
106. K.R. Kloetstra and H. van Bekkum, *J. Chem. Soc., Chem. Commun.,* **1995**, 1005-1006.
107. D.J. Macquarrie, *J. Chem. Soc., Chem. Commun.,* **1996**, 1961-1962.
108. U. Junges, W. Jacobs, I. Voigt-Martin, B. Krutzsch and F. Schüth, *J. Chem. Soc., Chem. Commum.,* **1995**, 2283-2284.
109. R. Ryoo, C.H. Ko, J.M. Kim and R. Howe, *Catal. Lett.,* **1996**, *37,* 29-33.
110. A. Corma, A. Martínez, V. Martínez-Soria and J.B. Montón, *J. Catal.,* **1995**, *153,* 25-31.
111. K.R. Kloetstra, M. van Laren and H. van Bekkum, *J. Chem. Soc., Faraday Trans.,* **1997**, *93*(6), 1211-1220.
112. T. Abe, Y. Tachibana, T. Uematsu and M. Iwamoto, *J. Chem. Soc., Chem. Commun.,* **1995**, 1617-1618.
113. T. Inui, J.-B. Kim and M. Seno, *Catal. Lett.,* **1994**, *29,* 271-279.
114. P.P. Paul, M.A. Miller, M.J. Heimrich and S.T. Schwab in *Microporous and Macroporous Materials*; Mat. Res. Soc. Symp. Proc., (Eds. R.F. Lobo, J.S. Beck, S.L. Suib, D.R. Corbin, M.E. Davis, L.E. Iton and S.I. Zones), MRS, Pittsburgh, **1995**, *Vol. 431*, 117-122.
115. C.-G. Wu and T. Bein in *Zeolites and Related Microporous Materials: State of the Art 1994.*; Stud. Surf. Sci. Catal., (Eds. J. Weitkamp, H.G. Karge, H. Pfeifer and W. Hölderich), Elsevier Science B.V., **1994**, *Vol. 84A*, 243-250.
116. C.-G. Wu and T. Bein, *Chem. Mater.,* **1994**, *6,* 1109-1112.
117. C.-G. Wu and T. Bein, *Science,* **1994**, *264*, 1757-1759.
118. C.-G. Wu and T. Bein, *Science,* **1994**, *266*, 1013-1015.
119. H.L. Frisch and J.E. Mark, *Chem. Mater.,* **1996**, *8*(8), 1735-1738.
120. P.L. Llewellyn, U. Ciesla, R. Stadler, F. Schüth and K.K. Unger in *Zeolites and Related Microporous Materials: State of the Art 1994.*; Stud. Surf. Sci. Catal., (Eds. J. Weitkamp, H.G. Karge, H. Pfeifer and W. Hölderich), Elsevier Science B.V., **1994**, *Vol. 84A*, 2013-2020.
121. C.H. Ko and R. Ryoo, *J. Chem. Soc., Chem. Commun.,* **1996**, 2467-2468.

122. P. Behrens, *Adv. Mater.,* **1993**, *5*(2), 127-132.
123. O. Franke, G. Schulz-Ekloff, J. Rathousky, J. Stárek and A. Zukal, *J. Chem. Soc., Chem. Commun.,* **1993**, 724-725.
124. P.J. Branton, P.G. Hall and K.S.W. Sing, *J. Chem. Soc., Chem Commun.,* **1993**, 1257-1258.
125. P.J. Branton, P.G. Hall, K.S.W. Sing, H. Reichert, F. Schüth and K.K. Unger, *J. Chem. Soc., Faraday Trans.,* **1994**, *90*(19), 2965-2967.
126. P.J. Branton, PhD Thesis, University of Exeter, **1994**.
127. R. Schmidt, M. Stöcker, E. Hansen, D. Akporiaye and O.H. Ellestad, *Microporous Mater.,* **1995**, *3*(4/5), 443-448.
128. R. Netrabukkana, K. Lourvanij and G.L. Rorrer, *Ind. Eng. Chem. Res.,* **1996**, *35*(2), 458-464.
129. Z. Blum and S.T. Hyde, *Acta Chemica Scandinavica,* **1994**, *48,* 88-90.
130. J.M. Thomas, *Nature,* **1994**, *368*, 289-290.
131. D. Walsh and S. Mann, *Nature,* **1995**, *377*, 320-323.
132. D. Walsh and S. Mann, *Chem. Mater.,* **1996**, *8*(8), 1944-1953.

Chapter 2:

Synthesis of MCM-41

"Good questions outrank easy answers."

Paul A. Samuelson

The principle of surfactant liquid crystal templating has been applied to many different systems, to create mesophase structures with very different characteristics. Some of these are referred to below. In this work however, the emphasis is on the simpler, pure silica hexagonal phase templated by a single surfactant species.

2.1 Introduction

The synthesis of the hexagonal mesoporous silicate known as MCM-41 is possible via a number of methods. The initial paper by Beck *et al.*[1] cites a number of representative syntheses, using silica sources ranging from colloidal silica to tetraethyl orthosilicate (TEOS), alkyltrimethylammonium templates with varying carbon chain lengths, and counterions and other ingredients such as alumina, to affect the wall properties and mesitylene, to alter pore size. Other workers have investigated the addition of catalytically active elements such as vanadium,[2-4] titanium,[5-11] zirconium,[12] iron,[13] manganese,[14] chromium,[15] nickel[16,17] and tin.[18,19] Gallosilicate[20-22] and borosilicate[23-26] MCM-41 materials have also been prepared. The use of surfactant templating methods has been expanded to create porous materials from other oxides including transition metals, such as niobium,[27,28] tungsten,[29] vanadium,[29,30] zirconium[31-33] and tantalum[34] which contain no silica at all. Mesostructured aluminophosphates[35,36] and tin sulphides[37] have also been made. Similar mesoporous materials, designated FSM-16, can also be formed from the surfactant-modified layered polysilicate clay kanemite.[38-42] These materials have similar pore sizes and hexagonal structure to that of MCM-41 and debate continues over whether the FSM-16 derived from kanemite and MCM-41 are the same material.[43]

The initial aim of the synthetic work described here was to discover the mechanism of MCM-41 formation. Later, the aim also became to optimise the preparation method, so as to create materials with the highest possible long range order, in order to investigate

the structure of the MCM-41 formed. A pure silica version of MCM-41 was used, in an attempt to reduce the number of variables in the system. Also, although versions of the preparation of MCM-41 in acidic media have been published by other workers[44-49] this work has been restricted to an alkaline preparation, also for the sake of simplicity.

2.2 Materials

The simplest form of the MCM-41 preparation requires only four ingredients: a silicate source, a template molecule, some acid, to increase the rate of silica condensation, and water. In this work the silica source used was sodium silicate solution (Aldrich, ~14% NaOH, ~27% SiO_2, density = 1.390 g cm^{-3}) a dissolved form of silica comprised of oligomeric and monomeric species.[50-52] Sodium silicate solution was used as the silica source as it was a convenient, pre-dissolved form of silica which preliminary work[53] had shown to give MCM-41 structures. The template molecule was cetyltrimethylammonium bromide (CTAB, $C_{16}H_{33}N(CH_3)_3$ Br, Fluka, 98%), a surfactant with well known aggregation behaviour.[54,55] The acid used was sulfuric acid (H_2SO_4,Univar, Analytical Reagent, 98%). These chemicals were used without further purification. Water was purified by a Millepore filtration system to a resistivity of 18 M• cm.

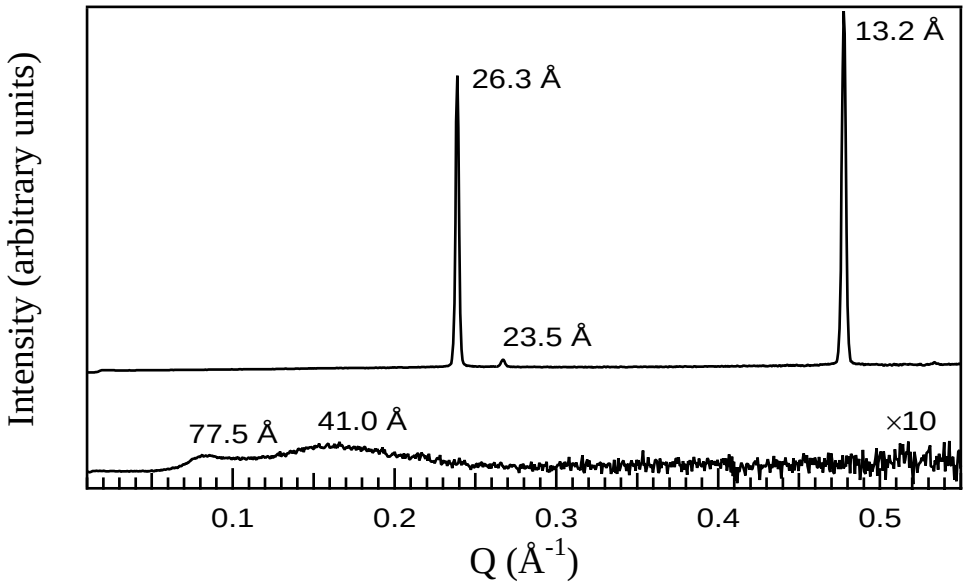

Figure 2.1 *Diffraction pattern from pure crystalline CTAB (top), and from a 28 wt% CTAB in water solution at 27•C (bottom). The solution pattern has been multiplied by a factor of 10. Intensities are on an arbitrary, but consistent scale.*

A small angle diffraction pattern for pure, solid CTAB is shown in Figure 2.1, as intensity versus momentum transfer, Q where $Q = 4\bullet/\lambda \sin\theta$, λ is the wavelength of the radiation used (in this case λ = 1.54 Å) and θ is half of the scattering angle (see Chapter 3 for further details concerning small angle scattering). The pattern for a water solution of 28 wt% CTAB at 27•C is also shown. This CTAB concentration corresponds to the hexagonal phase concentration regime for this surfactant at this temperature,[54] however the double peak visible in that pattern suggests the presence of two phases in the

solution. From the *d*-spacings, there is probably a rod-like micelle phase present as well as the hexagonal phase.[55] The CTAB concentration used in the MCM-41 preparations in this work, 11.5 wt%, is within the rod-like micelle region of the phase diagram at 27•C, but in the spherical micelle region at temperatures above 50•C.[54]

In order to increase the long range order of the MCM-41 materials, a number of preparations were treated with additional acid (1 M in water) as the synthesis progressed. The acids used in these syntheses were acetic acid (CH_3COOH, BDH, Analar), sulphuric acid (Univar, analytical reagent grade, 98%), hydrochloric acid (HCl, Univar, analytical reagent grade, 36%) and ammonium bromide (NH_4Br, BDH, laboratory reagent grade, 99%). One preparation was titrated with equivalent amounts of sodium acetate ($Na\ CH_3CO_2$, Univar, analytical reagent grade, 99.0%) to observe the effects of the acetate ion on the synthesis.

In the Langmuir trough work discussed in Chapter 4, an insoluble surfactant $(C_{18}H_{37})_2N(CH_3)_2\ Br$ was prepared by Dr Tim Senden, and used as received. Surfactant solutions were prepared in distilled chloroform (Univar, analytical reagent grade, 99.8%).

In the neutron scattering work discussed in Chapter 5, D_2O (AEC Canada, 99% and Cambridge Isotope Laboratories, 99.9%) was partially substituted for the water in the synthesis gels. In other experiments potassium bromide (KBr, Aldrich, FTIR grade 99+%) was used to alter the behaviour of the gels under shear. Nitrogen, hydrogen and methane used for gas adsorption isotherms and quasielastic neutron scattering experiments were 99.99%, 99.95% and 99.99% pure, respectively.

2.3 Preparative Method

The synthetic method used in this work was essentially that of Beck *et al.*[1] Outlines of typical preparations for the three reactions studied; unheated, heated and acid-titrated, are provided here. Further synthetic details are discussed in Chapter 4, and quantities of reagents for all preparations are given in Table A1.1 in the Appendix. Other preparative information can be found in Chapter 4, Tables 4.9 and 4.10. Compositions of preparations made for shear experiments can be found in the Appendix at Table A1.2.

For each preparation, two solutions were initially prepared. A solution of 16.4 g of CTAB in 49.2 g water was made by heating to 75•C to dissolve the CTAB. An acidic sodium silicate solution was also prepared, by diluting 19.0 g of sodium silicate with 40.6 g of water and adding 1.2 g of sulfuric acid with rapid stirring. The hot CTAB solution was then added into this at room temperature, and the resulting gel stirred for a further 15 minutes, during which time it cooled to ambient temperature. 20.0 g of water was then added and stirring continued for 30 minutes. Unheated MCM-41 preparations were set aside at this point in sealed containers, and allowed to age in the synthesis gel for various periods. These were then filtered, washed, dried and calcined in the same manner as described below, for heated samples.

Otherwise, this mixture was then heated to 100•C in an autoclave for three days. This heating time was found to give materials with the greatest long range order.[56] The reaction gel was usually not stirred during heating. For the larger preparations a teflon-lined Berghoff autoclave with a capacity of *ca.* 250 ml was used. This had a teflon coated thermocouple to monitor the solution temperature directly, and an internal magnetic stirring mechanism. This autoclave had a delay time of about 30 minutes in reaching the set temperature of 100•C and often overshot the set temperature on initial heating by up to 20•C for around 30 minutes. For smaller preparations, (25-30 ml) a set of five small autoclaves made at the RSC were used. These were heated in an oven maintained at 100•C, so the solution temperature could not be directly monitored in this case. Some later preparations, following the method of Ryoo and Kim,[57] were titrated with various dilute acids in order to further improve the long range order of the MCM-41 product. These are referred to as the 'acid-titrated' preparations. In these preparations, three times during heating, at 24 hour intervals, the autoclave was cooled to a comfortable handling temperature, opened and titrated with one molar acid, to return the whole gel system to a predetermined pH. Each titration required about one hour from the beginning of initial cooling of the autoclave. This procedure and its effects are discussed in greater detail in Chapter 4. Preparations which were not treated with acid are referred to as the 'ordinary' syntheses.

After heating, the materials were filtered while still warm and washed with 70•C Millepore filtered water to remove any unincorporated CTAB. The material was dried in an oven at 100•C for up to one hour and stored in glass vials sealed with a screw cap, usually in the dark, although no special precautions were taken to exclude light or atmospheric moisture from these materials.

2.4 Removal of Template

The organic template molecule, CTAB, was removed from the silicate lattice by one of two techniques, calcination or washing. Calcination is the burning out of the template under conditions which do not greatly affect the integrity of silicate structure. This has the advantage of ensuring the removal of all carbonaceous material, but also causes a significant shrinkage in the MCM-41 lattice parameter which is discussed further in Chapter 4. In an attempt to avoid this, template removal by washing was also considered, although in this work, complete template removal by this method was never achieved. The development of the acid-titrated preparation reduced the need for mild methods of template removal, as calcination had a much smaller effect on the lattice parameter of acid-treated samples.

Other investigators have reported calcination at temperatures up to 540•C under oxygen.[1,58,59] The temperature used for calcination does not appear to affect the quality of the product greatly. A shrinkage of up to 25% in the lattice constant has been observed occur on calcination,[60] depending on the synthesis conditions, although pore collapse occurs only after heating to temperatures of 900•C in dry air.[59] Washing out of the template by boiling in HCl/ethanol mixtures has also been reported as effective for template removal and as causing less lattice shrinkage than the burning out methods.[59,61] Template removal by washing in acidic ethanol has been shown to be

more successful in mesoporous silicates made via neutral templating routes than by ionic templating.[62] There is however, debate as to whether some template remains in the structure after such treatments.[63] Ionic template recovery has also been reported. That technique requires the use of exchange ions or ion pairs which replace the charged template molecules during the extraction process.[61] Template removal by supercritical extraction or oxygen plasma treatment has also been suggested.[60]

Calcination was performed in either a tube furnace or a muffle furnace. In the small tube furnace the product was dried and then slowly heated under a stream of pure nitrogen, over a period of several hours to 350•C. The sample was maintained at this temperature for one day and then calcined further at 350•C under a stream of dry air for four days. Samples calcined in the muffle furnace or a larger tube furnace were heated to 500•C over about 30 minutes and were maintained at this temperature overnight. The large tube furnace allowed a stream of dry air to be passed over the samples during calcination, but the muffle furnace did not. Calcined samples were also stored in sealed glass vials. Calcination at higher temperatures for shorter times appeared to be most successful in eliminating the template, judged by the final, pure white colour of the product, but did not appear to significantly affect the stability (see Tables 4.9 and 4.10 below) or the pore size of the product.

Table 2.1 *Surfactant/silica ratios for samples from acid treated and ordinary preparations after washing, calculated by gravimetric calcination.*

Sample	Treatment	Surfactant/Silica wt/wt	N/Si mol/mol
Acid Titrated Prep 1.1	as prepared	2.68	0.442
1.2	1 wash	1.13	0.186
1.3	2 washes	1.04	0.171
1.4	3 washes	0.93	0.153
1.5	calcined	0	0
Ordinary Prep 2.1	as prepared	2.12	0.349
2.2	1 wash	1.51	0.254
2.3	2 washes	1.35	0.223
2.5	3 washes	1.27	0.209
2.5	calcined	0	0

An attempt was also made to remove the template by a succession of washings in water. In one experiment two bulk samples, one from an ordinary preparation and one from an acetic acid titrated preparation were separated into four parts. Each was washed by being mixed in 13.3 g of water per gram of unwashed MCM-41 at room temperature

overnight, then heated in an oven at 100•C for 10-15 minutes before the supernatant water was removed with a pipette. This was repeated up to three times for each sample. On the final wash each sample was filtered while still warm, then dried in the oven for two hours. Gravimetric calcination of small amounts of these washed samples showed that successive washings did reduce the CTAB to silica ratio (shown in Table 2.1), however significant amounts of template remained in these samples. Chen *et al*.[64] have previously reported the N/Si ratio in as-synthesised MCM-41 to be 0.294 for a pure silica sample synthesised in a preparation which initially contained 14 wt% CTAB.[64] The preparations discussed here initially contained 11.5 wt% CTAB.

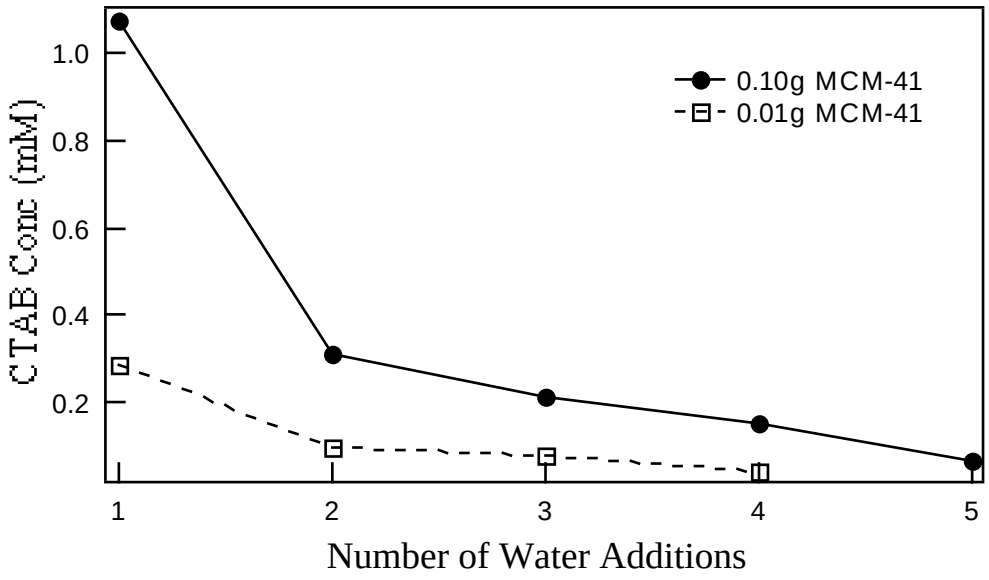

Figure 2.2 *CTAB concentration from conductivity measurements made 24 hours after the addition of water in successive 20 g aliquots to 0.0990 g and 0.0100 g MCM-41 samples.*

A similar washing experiment was carried out on an uncalcined ordinary MCM-41 specimen (Argonne Prep 2). In this case the 0.0990 g of uncalcined MCM-41 was successively washed with 20 g water and the conductivity of this suspension monitored from the addition of the water until 2-3 hours after the addition. The water was removed after 24 hours, the sample dried in the oven, the water replaced with an equal mass and the conductivity followed for the first couple of hours. This was repeated 5 times. A similar experiment was performed using only 0.01 g of the same uncalcined MCM-41 in 18 g of water. The conductivity of the water removed from both experiments after standing overnight is shown in Figure 2.2 above and the change in conductivity of the water upon addition in each case is shown in Figure 2.3 below.

Figure 2.2 and 2.3 show that the most CTAB is removed by the first wash, although the rising trend in conductivity for subsequent washes indicates that the surfactant is still diffusing out from within the structure. An equilibrium state, with the surfactant partitioned between the MCM-41 structure and the solution, was therefore never reached on the time scale of these measurements. A change in the behaviour of the MCM-41 particles as the surfactant was washed out was noted. The particles began to be suspended in the solution and eventually to float on the surface of the solution after

about the third washing of the samples. This indicates that the overall density of the re-hydrated, washed particles must be slightly less than that of the solution, so some air must be trapped in the structure.

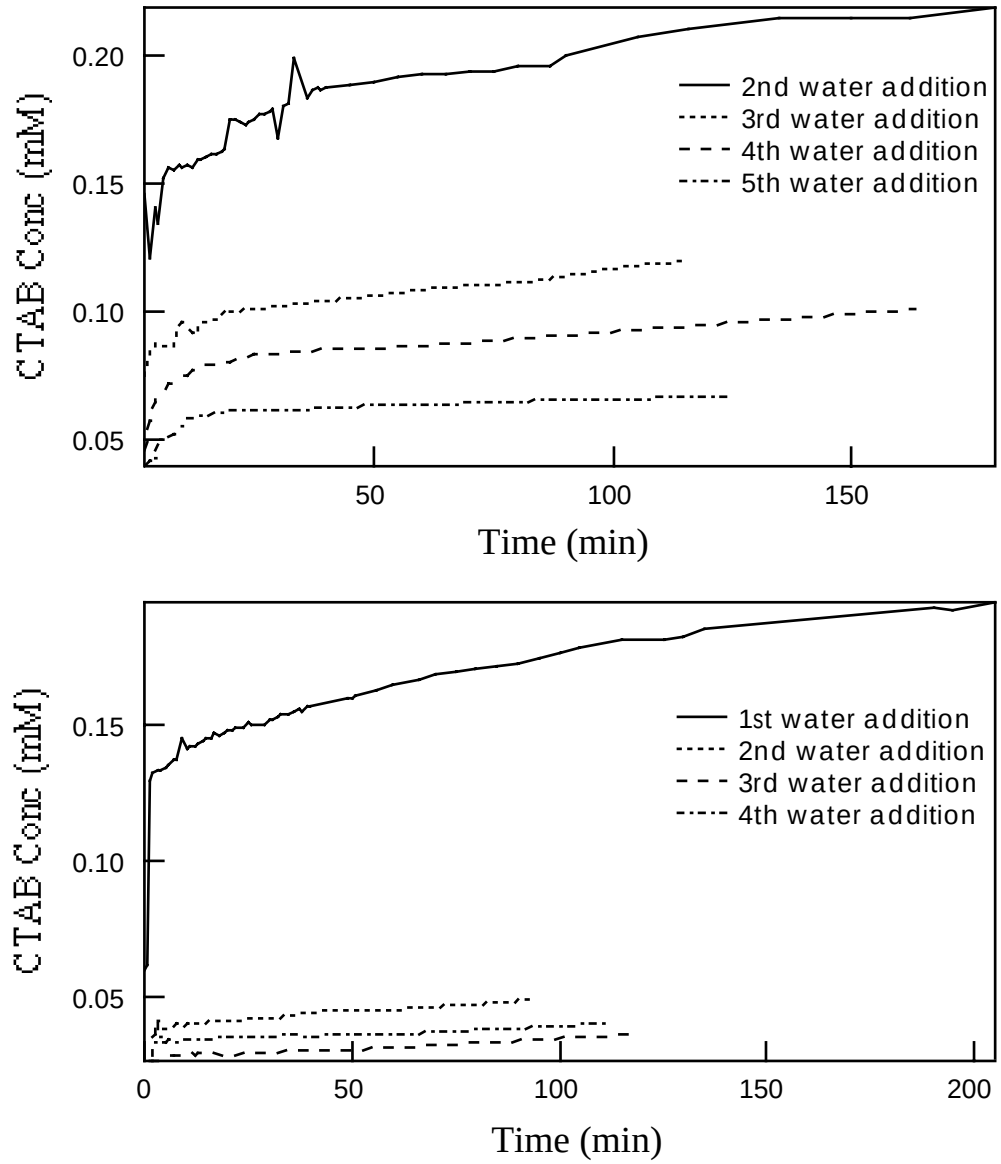

Figure 2.3 *CTAB concentration as a function of time for successive water washings. The top graph is for 0.0990 g of uncalcined MCM-41 in 20 g water (the first water addition cannot be put on the same graph as the CTAB concentrations are too large) and the bottom graph is for 0.0100 g uncalcined MCM-41 in 18 g water.*

The conductivity data indicate that although washing with water successfully removed some CTAB from the MCM-41 structure, there was still a significant amount of template trapped inside even after five successive washings. Calcination was therefore used to remove the template from all further samples discussed in this work.

2.5 Physical Description of MCM-41 Materials

The MCM-41 materials produced by this method were white powders. The density of the unpacked powder for a material from an acid-titrated preparation was 0.098(5) g cm^{-3}. The uncalcined materials tended to be coarser and slightly sticky owing to the hydroscopic nature of the CTAB template. Calcined materials varied from a light brown in colour to pure white, depending on the method of calcination. The smaller tube furnace with its lower calcination temperature often produced darker specimens, however the colour did not noticeably affect other properties of the material. Samples produced using the acid-titration method had a much finer texture and were more friable than those produced using the initial method outlined above.

The grain size of these materials as determined by optical microscopy is around 3-10 µm for materials from ordinary preparations and 2-5 µm for acid-titrated materials, although both types of MCM-41 also contain many larger, aggregated particles. Scanning electron micrographs of the acid-titrated materials show particles of between 5 and 10 µm across with smooth surfaces. Micrographs of the ordinary preparation materials show much larger, rougher masses of coiled, intertwined tubes. These are discussed in greater detail in Chapter 4.

2.6 References

1. J.S. Beck, J.C. Vartuli, W.J. Roth, M.E. Leonowicz, C.T. Kresge, K.D. Schmitt, C.T.-W. Chu, D.H. Olson, E.W. Sheppard, S.B. McCullen, J.B. Higgins and J.L. Schlenker, *J. Am. Chem. Soc.,* **1992**, *114*, 10834-10843.
2. D.H. Park, C.-F. Cheng, H. He and J. Klinowski, *J. Mater. Chem.,* **1997**, *7*(1), 159-162.
3. K.M. Reddy, I. Moudrakovski and A. Sayari, *J. Chem. Soc., Chem. Commun.,* **1994**, 1059-1060.
4. J.S. Reddy and A. Sayari, *J. Chem. Soc., Chem. Commun.,* **1995**, 2231-2232.
5. T. Blasco, A. Corma, M.T. Navarro and J. Pérez Pariente, *J. Catal.*, **1995**, *156*, 65-74.
6. M.D. Alba, Z. Luan and J. Klinowski, *J. Phys. Chem.,* **1996**, *100*(6), 2178-2182.
7. A. Corma, M.T. Navarro and J.P. Pérez-Pariente, *J. Chem. Soc., Chem. Commun.,* **1994**, 147-148.
8. A. Corma, M. Iglesais and F. Sánchez, *Catal. Lett.,* **1996**, *39*(3/4), 153-156.
9. O. Franke, J. Rathousky, G. Schulz-Ekloff, J. Stárek and A. Zukal in *Zeolites and Related Microporous Materials: State of the Art 1994.*; Stud. Surf. Sci. Catal., (Eds. J. Weitkamp, H.G. Karge, H. Pfeifer and W. Hölderich), Elsevier Science B.V., **1994**, *Vol. 84*, 77-84.
10. S. Gontier and A. Tuel, *Zeolites,* **1995**, *15*, 601-610.
11. P.T. Tanev, M. Chibwe and T.J. Pinnavaia, *Nature,* **1994**, *368*, 321-323.
12. A. Tuel, S. Gontier and R. Teissier, *J. Chem. Soc., Chem. Commun.,* **1996**, 651-652.
13. Z.Y. Yuan, S.Q. Liu, T.H. Chen, J.Z. Wang and H.X. Li, *J. Chem. Soc., Chem. Commun.,* **1995**, 973-974.

14. D. Zhao and D. Goldfarb, *J. Chem. Soc., Chem. Commun.,* **1995**, 875-876.
15. N. Ulagappan and C.N.R. Rao, *J. Chem. Soc., Chem. Commun.,* **1996**, 1047-1048.
16. M. Hartmann, A. Pöppl and L. Kevan, *J. Phys. Chem.*, **1996**, *100*(23), 9906-9910.
17. M. Hartmann, A. Pöppl and L. Kevan, *J. Phys. Chem.*, **1995**, *99*(49), 17494-17496.
18. T.M. Abdel-Fattah and T.J. Pinnavaia, *J. Chem. Soc., Chem. Commun.,* **1996**, 665-666.
19. T.K. Das, K. Chaudhari, A.J. Chandwadkar and S. Sivasanker, *J. Chem. Soc., Chem. Commun.,* **1995**, 2495-2496.
20. C.-F. Cheng, H. He, W. Zhou, J. Klinowski, J.A.S. Gonçalves and L.F. Gladden, *J. Phys. Chem.,* **1996**, *100,* 390-396.
21. C.F. Cheng and J. Klinowski, *J. Chem. Soc., Faraday Trans.,* **1996**, *92*(2), 289-292.
22. C.-F. Cheng, M.D. Alba and J. Klinowski, *Chem. Phys. Lett.,* **1996**, *250*(3/4), 328-334.
23. S. Liu, H. He, Z. Luan and J. Klinowski, *J. Chem. Soc., Faraday Trans.,* **1996**, *92*(11), 2011-2015.
24. U. Oberhagemann, I. Kinski, I. Dierdorf and M.H. Gies, *J. Non-Crystalline Solids,* **1996**, *197,* 145-153.
25. D.T. On, P.N. Joshi and S. Kaliaguine, *J. Phys. Chem.*, **1996**, *100*(16), 6743-6748.
26. A. Sayari, I. Moudrakovski, C. Danumah, C.I. Ratcliffe, J.A. Ripmeester and K.F. Preston, *J. Phys. Chem.*, **1995**, *99*, 16373-16379.
27. D.M. Antonelli and J.Y. Ying, *Angew. Chem. Intl. Ed. Engl.*, **1996**, *35*(4), 426-430.
28. D.M. Antonelli, A. Nakahira and J.Y. Ying, *Inorg. Chem.,* **1996**, *35*(11), 3126-3136.
29. G.G. Janauer, A. Dobley, J. Guo, P. Zavalij and M.S. Whittingham, *Chem. Mater.*, **1996**, *8*(8), 2096-2101.
30. V. Luca, D.J. MacLachlan, J.M. Hook and R. Withers, *Chem. Mater.*, **1995**, *7,* 2220-2223.
31. M.J. Hudson and J.A. Knowles, *J. Mater. Chem.,* **1996**, *6*(1), 89-95.
32. J.A. Knowles and M.J. Hudson, *J. Chem. Soc., Chem. Commun.,* **1995**, 2083-2084.
33. G. Larsen, E. Lotero, M. Nabity, L.M. Petkovic and D.S. Shobe, *J. Catal.,* **1996**, *164*, 246-248.
34. D.M. Antonelli and J.Y. Ying, *Chem. Mater.,* **1996**, *8*(4), 874-881.
35. A. Sayari, V.R. Karra, J.S. Reddy and I.L. Moudrakovski, *J. Chem. Soc., Chem. Commun.,* **1996**, 411-412.
36. A. Sayari, I. Moudrakovski, J.S. Reddy, C.I. Ratcliffe, J.A. Ripmeester and K.F. Preston, *Chem. Mater.,* **1996**, *8*(8), 2080-2088.
37. J. Li, H. Kessler and L. Delmotte, *J. Chem. Soc., Faraday Trans.*, **1997**, *93*(4), 665-668.
38. S. Inagaki, Y. Fukushima and K. Kuroda in *Zeolites and Related Microporous Materials: State of the Art 1994.*; Stud. Surf. Sci. Catal., (Eds. J. Weitkamp,

H.G. Karge, H. Pfeifer and W. Hölderich), Elsevier Science B.V., **1994**, *Vol. 84A*, 125-132.
39. S. Inagaki, Y. Fukushima and K. Kuroda, *J. Chem. Soc., Chem. Commun.*, **1993**, 680-682.
40. S. Inagaki, A. Koiwai, N. Suzuki, Y. Fukushima and K. Kuroda, *Bull. Chem. Soc. Jpn.*, **1996**, *69*(5), 1449-1457.
41. S. Inagaki, Y. Sakamoto, Y. Fukushima and O. Terasaki, *Chem. Mater.*, **1996**, *8*(8), 2089-2095.
42. K. Kuroda, *J. Porous Mater.*, **1996**, *3*, 107-114.
43. C.-Y. Chen, S.-Q. Xiao and M.E. Davis, *Microporous Mater.*, **1995**, *4*(1), 1-20.
44. Q. Huo, D.I. Margolese, U. Ciesa, P. Feng, T.E. Gier, P. Sieger, R. Leon, P.M. Petroff, F. Schüth and G.D. Stucky, *Nature*, **1994**, *368*, 317-321.
45. Q. Huo, D.I. Margolese, U. Ciesla, D.G. Demuth, P. Feng, T.E. Gier, P. Sieger, A. Firouzi, B.F. Chmelka, F. Schüth and G.D. Stucky, *Chem. Mater.*, **1994**, *6*, 1176-1191.
46. Q. Huo, R. Leon, P.M. Petroff and G.D. Stucky, *Science*, **1995**, *268*, 1324-1244.
47. Q. Huo, D.I. Margolese and G.D. Stucky, *Chem. Mater.*, **1996**, *8*(5), 1147-1160.
48. A. Monnier, F. Schüth, Q. Huo, D. Kumar, D. Margolese, R.S. Maxwell, G.D. Stucky, M. Krishnamurty, P. Petroff, A. Firouzi, M. Janicke and B.F. Chmelka, *Science*, **1993**, *261*, 1299-1303.
49. E. Terrés, S.S. Ramirez, J.M. Dominguez, A. Montoya, J. Navarrete and M. Gómez-Cisneros in *Microporous and Macroporous Materials*; Mat. Res. Soc. Symp. Proc., (Eds. R.F. Lobo, J.S. Beck, S.L. Suib, D.R. Corbin, M.E. Davis, L.E. Iton and S.I. Zones), MRS, Pittsburgh, **1995**, *Vol. 431*, 111-116.
50. R.K. Iler, *The Chemistry of Silica. Solubility, Polymerization, Colloid and Surface Properties, and Biochemistry*, John Wiley & Sons, New York, **1979**.
51. P.W.J.G. Wijnen, T.P.M. Beelen and R.A. van Santen in *The Colloid Chemistry of Silica*; Advances in Chemistry Series, (Eds. H.E. Bergna), ACS, Washington, **1994**, *Vol. 234*, 517-531.
52. G.D. Stucky, A. Monnier, F. Schüth, Q. Huo, D. Margolese, D. Kumar, M. Krishnamurty, P. Petroff, A. Firouzi, M. Janicke and B.F. Chmelka, *Mol. Cryst. Liq. Cryst.*, **1994**, *240*, 187-200.
53. J. Dougherty and Z.Y. Wang, Personal Communication, **1993**.
54. F. Reiss-Husson and V. Luzzati, *J. Phys. Chem.*, **1964**, *68*(12), 3504-3511.
55. P.F. Husson, H. Mustacchi and V. Luzzati, *Acta. Cryst.*, **1960**, *13*, 668-677.
56. K.J. Edler, J. Dougherty, R. Durand, L. Iton, G. Kirton, G. Lockhart, Z. Wang, R. Withers and J.W. White, *Colloids Surfaces A*, **1995**, *102*, 213-230.
57. R. Ryoo and J.M. Kim, *J. Chem. Soc., Chem. Commun.*, **1995**, 711-712.
58. C.T. Kresge, M.E. Leonowicz, W.J. Roth, J.C. Vartuli and J.S. Beck, *Nature*, **1992**, *359*, 710-712.
59. C.-Y. Chen, H.-X. Li and M.E. Davis, *Microporous Mater.*, **1993**, *2*, 17.
60. X.S. Zhao, G.Q. Lu and G.J. Millar, *Ind. Eng. Chem. Res.*, **1996**, *35*(7), 2075-2090.
61. R. Schmidt, D. Akporiaye, M. Stöcker and O.H. Ellestad in *Zeolites and Related Microporous Materials: State of the Art 1994.*; Stud. Surf. Sci. Catal., (Eds. J.

Weitkamp, H.G. Karge, H. Pfeifer and W. Hölderich), Elsevier Science B.V., **1994**, *Vol. 84*, 61-68.
62. P.T. Tanev and T.J. Pinnavaia, *Chem. Mater.*, **1996**, *8*(8), 2068-2079.
63. A. Tuel and S. Gontier, *Chem. Mater.*, **1996**, *8*, 114-122.
64. C.Y. Chen, S.L. Burkett, H.-X. Li and M.E. Davis, *Microporous Mater.*, **1993**, *2*, 22.

Chapter 3:

Characterisation Techniques & Theory

"There are no such things as applied sciences, only applications of science."
Louis Pasteur, Address, 11 September 1872.

The work reported in this thesis concerns, not only the synthesis of mesoporous MCM-41 materials, but also their characterisation and analysis by a number of techniques. The methods used most frequently were small angle X-ray and neutron scattering. These procedures, especially when used in conjunction, are very powerful, giving much structural information in a critical size range. Other techniques used included gas adsorption isotherm analysis, quasielastic neutron scattering, X-ray and neutron diffraction, and transmission and scanning electron microscopy. The Langmuir trough was also used for some studies.

The most commonly used methods for characterising MCM-41 are X-ray diffraction,[1,2] gas isotherms,[3] transmission electron microscopy[4-6] and nmr.[7-9] Of these methods, the first two give information about bulk properties of MCM-41 and identify long range characteristics. Gas adsorption isotherms are often used to estimate average pore volumes and characterise MCM-41 surface behaviour,[10,11] while X-ray diffraction is usually used to provide confirmation that the MCM-41 phase has been synthesised[12-15] or to observe structure evolution over time.[16-19] Only a few workers have taken the diffraction work further with modelling.[1,20] Small angle X-ray scattering is not often used.[6,21,22] The first three commonly used techniques investigate the silica framework only. Transmission electron microscopy is generally used to show localised order,[2,23] and to investigate pore dimensions by direct imaging.[24-26] MCM-41 materials doped with boron have been developed to improve TEM imaging of this material.[27-29] Some modelling of channel arrangement has been based on these images.[30] This technique has also been extended to investigate channel structure by filling individual pores with platinum to allow direct imaging of the spatial behaviour of one channel.[31]

The last technique, nmr, the only one which looks at molecular level interactions both within the silicate framework and between the silicate and the template, has been used

in several ways. ^{29}Si and ^{27}Al magic angle spinning (MAS) nmr allow observation of the degree of silicate polymerisation,[2,16,32] and ^{13}C, ^{14}N and ^{1}H nmr have been employed to look at the surfactant behaviour during syntheses.[33] Solid state ^{13}C nmr has given additional structural information about surfactant molecules within silicate mesophases.[2,34] ^{1}H nmr has also been used to characterise molecules such as water residing in the MCM-41 channels.[35-37] This method has been developed to allow calculation of channel dimensions from such measurements.[38,39] MCM-41 materials doped with various transition metals have been investigated with electron paramagnetic resonance,[40-42] which also gives information on chemical interactions on a molecular scale.

Other techniques which have been used to characterise MCM-41 include IR[43] and FTIR, to investigate surface siloxyl groups,[44] and, when combined with temperature programmed ammonia desorption, to allow the number and strength of acid sites in Al substituted materials to be determined.[2,45] Temperature programmed desorption has also been applied to calculate pore volumes.[46] Thermogravimetric analysis has been used to investigate MCM-41 stability and silica/surfactant ratios in dried, unheated synthesis gels[47] and dried as-synthesised samples.[33] These showed that the MCM-41 samples contain around 50 wt% surfactant, and 10 wt% water, with the remaining mass being silica.[33] Various forms of catalytic testing have also been done.[45,48-50] Rheological studies of the surfactant template have been carried out.[51] High temperature calorimetry studies measured the enthalpy of MCM-41 relative to that of quartz, while a Raman study suggested the presence of 3-fold siloxane rings in the wall structure.[52] Some small angle neutron scattering work has also been reported by Firouzi *et al.*[47] who merely give one pattern and by Glinka *et al.*[53] who carried out a more detailed analysis, to investigate the formation mechanism of MCM-41. Scanning electron microscopy is becoming a more common characterisation technique, as templated materials with macroscale structure are developed.[54]

Results of these characterisation techniques, where relevant, are discussed throughout this work, in the context of the experimental results reported.

3.1 Size

The choice of characterisation techniques for this work was largely governed by considerations of size. 'Meso' is a Greek prefix meaning 'in between', which is used to refer to objects in the size range 20-500 Å.[55] The interesting features of MCM-41 materials, the channels, are in the mesoscale size range. Structures in this size range can be awkward to access, being neither at an atomic nor a microscopic scale. The material, being mostly amorphous silica, has few X-ray diffraction peaks which are resolvable under normal, high angle X-ray diffraction conditions. The wide angle diffraction pattern shows only a broad feature at around 20-40° 2θ (for λ = 1.8963(1) Å) in highly ordered MCM-41 samples, and a narrower distribution of 10-20° 2θ (for λ = 1.0052(8) Å) in less well ordered samples. Such a distribution is characteristic of the distribution of Si-O bond lengths in amorphous silica.[56,57] At small angles, which may not be within the range of ordinary settings for conventional wide angle cameras,

up to five peaks may be seen. These diffraction patterns result from the hollow channel array which has a repeat distance of *ca.* 40 Å. This distance however, falls in the centre of the detection range for most small angle scattering cameras, making small angle diffraction and scattering an ideal technique for the study of MCM-41. Small angle scattering also had the advantage that sample preparation did not require any alteration of the sample state. Wet or dried samples could be investigated, and facilities were available for observation of *in situ* heating or shearing of the samples. The time necessary for a SAS pattern to be taken was short enough that successive shots allowed limited kinetic data to be obtained. Contrast variation techniques, used in small angle neutron scattering, also allowed some chemical information, in that size range, to be determined.

Small angle diffraction does not, however, allow determination of pore diameters without modelling. It gives only the distance between pore centres. Complementary analysis techniques are therefore needed. Gas adsorption techniques are useful in determining pore characteristics such as surface area and energies of adsorption in the mesoscale region. There is some debate over whether the assumptions made in the Kelvin equation (see section 3.4.1, equation 3.13 below) are legitimate for small mesopores,[3,58] but pore volumes determined using this method are often reported in the literature.[1,51,59] Quasielastic neutron scattering measurements on adsorption sites for various gases have also been used in this work to characterise pore wall structures. Atomic scale interactions were also investigated by studying the formation of silicate-surfactant films on the Langmuir trough.

Diffraction techniques do not give a good impression of the amount of amorphous material which co-exists with the ordered channel arrays. Transmission electron microscopy can provide information on thin, dried samples in the mesoscale size range and has been used in this work to give an indication of the overall order in the sample. Scanning electron microscopy covers a slightly larger size range (0.1 - 10 microns) and, although the channels in MCM-41 can not be detected using this technique, it allows direct observation of the crystallite morphology. All of the above techniques have been used in conjunction, in this work to investigate the formation and the structure of MCM-41.

3.2 Small Angle Scattering

Small angle scattering (SAS) was used in two ways - as a diffraction technique, since the Bragg peaks for the size range of interest happen to fall within the limits of the small angle region - but, also using the more traditional small angle scattering methods of fitting the fall off from the region of the straight-through X-ray beam, with the scattering function from particles of different shapes and densities. Diffraction techniques are discussed in greater detail in section 3.3 below. Quantities in bold type in the discussions which follow are defined to be vector quantities.

3.2.1 Small Angle Scattering Theory

A detailed treatment of the theory of SAS is readily available in many textbooks,[60-63] so only a brief explanation of the background, relevant to the experiments discussed here will be given. Small angle scattering measures the elastic scattering of X-rays or neutrons, that is, when the radiation incident on a sample undergoes a change of direction, but not of energy. Such scattering is shown in Figure 3.1 where **s** and $\mathbf{s_0}$ are unit vectors of the incident and scattered radiation respectively, both with wavelength, λ.

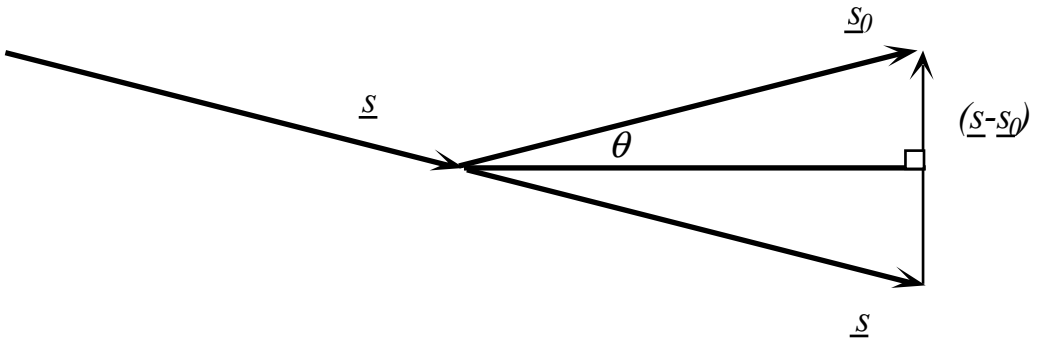

Figure 3.1 *Scattering of incident radiation from a point object.*

For elastic scattering, the amplitude of the radiation scattered by an object differs only in phase from that of the incident radiation. Phase, ϕ depends upon the position of the wave in space and is defined as $2\pi/\lambda$ times the difference between the optical path length of the wave and an arbitrary reference wave, **r**. The path difference therefore is $-\mathbf{r}(\mathbf{s}-\mathbf{s_0})$, and so the phase becomes $\phi = (-2\pi/\lambda)\mathbf{r}.(\mathbf{s}-\mathbf{s_0})$. The scattering vector, **Q**, is then defined to be:

$$\boldsymbol{Q} = \frac{2\pi}{\lambda}(\boldsymbol{s} - \boldsymbol{s_0}) \quad \text{where } |\boldsymbol{Q}| = Q = \frac{4\pi}{\lambda}\sin\theta \qquad \textbf{(3.1)}$$

where 2θ is the scattering angle. The quantity Q is often referred to as momentum transfer, however it has units of reciprocal length, not those of momentum. The momentum transfer however is simply related to Q by a factor of m/ , so Q may be described as the momentum transfer in units of .

Interatomic distances are small on the size scale of the small angle scattering experiment, and so are not generally observed in SAS patterns. It is therefore more convenient to consider an assembly of individual scattering objects, for example micelles or particles. Such an object has a factor, P(**Q**) which describes interparticle scattering and a structure factor, S(**Q**) which describes intraparticle scattering, if it is assumed that there is no correlation between particle orientation and interparticle motion**.** The intensity of radiation scattered from N such objects in a volume, V is:

$$I(\boldsymbol{Q}) = \Psi P(\boldsymbol{Q}) S(\boldsymbol{Q}) \qquad \textbf{(3.2)}$$

where $\Psi = N/V$, the number density of individual scattering particles in the sample. Each of these individual scatterers will interact with radiation depending on the constituent atoms of that sample. The interaction with X-rays will be dependent upon the number of electrons around each atom, and the interaction with neutrons upon the number of particles in the nuclei of the atoms making up the scattering material. This interaction is quantified in terms of a scattering length for each atom, which differs for X-rays and neutrons. Table 3.1 shows the X-ray and neutron scattering lengths for the elements of interest in this work. The scattering length density of the whole scattering particle is then defined as:

$$\rho_n(\boldsymbol{r}) = \frac{b_i d N_A}{M_W} \qquad \textbf{(3.3a)} \text{ for neutrons}$$

$$\rho_x(\boldsymbol{r}) = \frac{n d N_A b_x}{M_W} \qquad \textbf{(3.3b)} \text{ for X-rays}$$

where d is the physical density of the material, b_i is the neutron scattering length for a particular nucleus, n is the number of electrons per molecular unit of scatterer, and b_x is the scattering length per electron (2.8×10^{-13} cm). For both X-rays and neutrons, the scattering length has coherent and incoherent parts. The incoherent part, in the case of neutron scattering is related to neutron, and nuclear spin and is isotropic. It forms a constant background in the coherent SANS scattering patterns and is particularly significant for some nuclei, most importantly ^{1}H (see Table 3.1). For X-rays, the incoherent scattering is small at small angles and so can usually be ignored.

Table 3.1 *X-ray and neutron scattering lengths for selected elements.*[64,65] *Except in the case of hydrogen and deuterium, the values are averages over the natural abundance of all isotopes of the element.*

Atom	X-ray scattering length at Q = 0 / 10^{-14} m	Neutron scattering length / 10^{-14} m	Neutron coherent cross-section / 10^{-28} m^2	Neutron incoherent cross-section / 10^{-28} m^2
^{1}H	0.281	-0.37423	1.7599	79.91
^{2}D	0.281	0.6674	5.597	2.04
C	1.686	0.66484	5.554	0.001
N	1.967	0.936	11.01	0.49
O	2.249	0.5805	4.235	0.000
Na	3.092	0.363	1.66	1.62
Si	3.935	0.4149	0.015	2.163
S	4.497	0.2847	1.0186	0.007
K	5.340	0.371	1.73	0.25
Br	9.80	0.679	5.79	0.10

The intraparticle scattering factor, $S(\mathbf{Q})$ is equal to $\langle|F(\mathbf{Q})|^2\rangle$, where $F(\mathbf{Q})$ is the Fourier transform of the particle density distribution shown in equation 3.4 below. That is, it is

the form factor directly related to the shape of the particle, and to the contrast $\Delta\rho$ between the scattering length density of the particle $\rho(\mathbf{r})$, and the surrounding medium, ρ_s. The use of contrast in neutron experiments is discussed further below.

$$F(\boldsymbol{Q}) = \int_V \Delta\rho \exp(i\boldsymbol{Q}.\boldsymbol{r}) d^3\boldsymbol{r} \qquad \textbf{(3.4)}$$

3.2.1.1 The Guinier Approximation

The Guinier approximation provides a method of extracting information from the very low Q parts of the scattering curve.[61] It results from making an expansion of the exponential in equations 3.2 and 3.4 in a power series, with terms in **Q.r**. For centrosymmetric particles, with a radius of gyration, R_g, and a uniform scattering length density, the term in **r** vanishes, and for $Q.R_g << 1$, the interparticle scattering factor P(Q) becomes:

$$P(Q) = I(0)\exp\left|\frac{-Q^2R_g^2}{3}\right| \quad \text{where } R_g^2 = \frac{1}{\Delta\rho V}\int_V \boldsymbol{r}^2(\rho-\rho_S)d^3r \qquad \textbf{(3.5)}$$

$$\text{and } I(0) = (\Delta\rho V)^2$$

I(0) can therefore be determined by extrapolation from a ln(I) versus Q^2 plot, using only those points which obey the Guinier approximation, *ie.* those at Q values such that $Q.R_g<1$. Unfortunately, however, this approximation is not valid for the particles studied in this work. From other methods, described below, the MCM-41 particles have coherence lengths of the order of 1000 Å, even in the least ordered systems, and particle sizes which are larger still. The lowest Q value available was *ca.* 0.006 $Å^{-1}$ which corresponds to a *d*-spacing of around 1000 Å. At this Q value however, the Guinier approximation is only valid for particles with a radius of gyration below 160 Å. An alternative method discussed in the next section was therefore used to analyse the SAS data.

3.2.1.2 Porod's Law

Porod's law[62] is a power law describing the behaviour of I(Q) at higher Q than the Guinier region. It characterises the scattered intensity of a system where two scattering length densities are separated by a sharp boundary, and the length scale of curvature fluctuation in the boundary is large compared with $2\pi/Q$.

$$P(Q) = \frac{2\pi(\rho-\rho_s)^2 S}{Q^4} \qquad \textbf{(3.6)}$$

S is the total area of surface boundary. From equations 3.2 and 3.6, a plot of ln(I) versus ln(Q) will generate a curve where, at the largest Q values, all shapes of particle will give a cross-section which decreases as Q^{-4}. At lower values of Q there will be regions of nearly constant slope which have been interpreted variously as indicators of

particle shape,[63] or as the fractal dimension of the object at low Q and the fractal dimension of the surface structure at intermediate Q.[64] Deviations from Q^{-4}, even at high Q values, are often seen in practice, since the boundaries in question are not perfectly sharp and the scattering length densities within the phases contain local fluctuations.[66-70] From equation 3.6, it can be seen that the intensity on any point of a scattering curve which obeys power law behaviour will be proportional to the square of the contrast, $\Delta\rho$. It is therefore possible, in systems which show power law scattering, to carry out contrast variation experiments as described in the next section.

3.2.1.3 Contrast Variation in Neutron Scattering

The intensity, I(Q), of the scattering from a system is thus related to the square of the contrast, $\Delta\rho$. The contrast is the difference in scattering length density between the particle and the medium. In a system where particles with scattering length density, ρ, are suspended in aqueous solution with scattering length density, ρ_s the contrast can be made to vary, by varying the composition of that solution. This is the basis of the contrast variation method frequently used in small angle neutron scattering.

The scattering length density for neutrons, ρ_n is given by:

$$\rho_n = \frac{dN_A \quad b_i}{M_W} \qquad \textbf{(3.3a)}$$

where $\sum b_i$ is the summation of the scattering lengths of all nuclei in the scattering medium, d is the density of the medium, N_A is Avogadro's number, and M_W is the molecular weight of the scatterer. The variation of scattering length density with changes in isotopic composition leads to the ability to change the contrast of a solution without significantly varying other properties of the sample.

The contrast variation method of small angle neutron scattering often relies on the differences between the scattering length densities of H_2O (-0.562×10^{10} cm^{-2}) and D_2O (6.34×10^{10} cm^{-2}).[71] As these are of opposite sign, it is possible to create solutions having intermediate scattering length densities by mixing H_2O and D_2O in various proportions. Particles in a solution which have a uniform scattering length density which is the same as that of the surrounding solution will not contribute to the scattering in a SANS experiment and are said to be contrast matched (*ie.* I(Q) = 0). Figure 3.2, below, illustrates this concept. We measure the scattering from a series of samples containing fractions of H_2O and D_2O, which bracket an unknown scattering length density for particles in a solution. The point of zero scattering, the contrast match or null point, for that sample can thus be determined, and therefore its scattering length density. From equation 3.5 or 3.6, above, it can be seen that a plot of $\sqrt{I}$ versus $[D_2O]$ will be linear, crossing the concentration axis at a D_2O concentration corresponding to a scattering length density equal to the average scattering length density of the particles in solution.

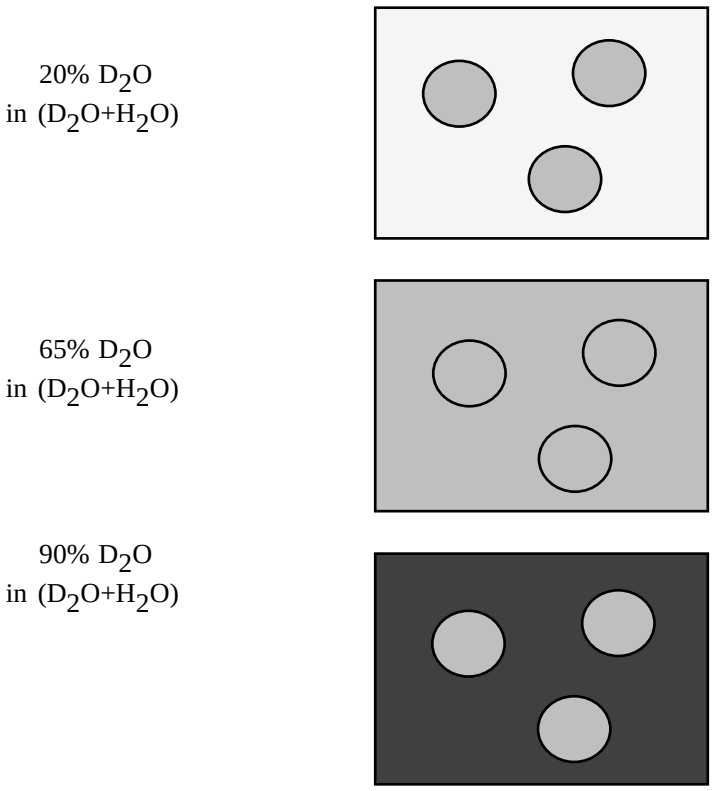

Figure 3.2 *The concept of contrast matching. The concentration of D_2O in the solvent is given on the left, and the contrast relative to that of the suspended silica particles is shown on the right.*

Table 3.2 *Scattering length densities for all components used in the MCM-41 preparations studied.*

Material	Neutron Scattering Length Density / $\times 10^{10}$ cm^{-2}
CTAB	-0.244†
SiO_2	3.48[71]
H_2SO_4	2.101†
NaOH	1.826†
CH_3COOH	1.046†
H_2O	-0.562[71]
D_2O	6.34[71]
KBr	1.461†

Note: † calculated from the atomic scattering lengths[72] and densities of the materials.[72]

In the case of MCM-41 the surfactant template has quite a different scattering length density to the silica. The surfactant is mostly hydrogenous and so its scattering length density in the crystalline state is small and negative, -0.244×10^{10} cm^{-2}, while that of amorphous silica is 3.48×10^{10} cm^{-2}.[71] This difference in contrast will mean that

different parts of the surfactant/silicate composite structure will be contrast matched at different concentrations of H_2O/D_2O. It is therefore possible to draw conclusions about the distribution of surfactant and silica in the composite particles. The scattering length densities for all components of the MCM-41 preparations are given in Table 3.2 for reference purposes.

3.2.2 Instrumentation and Sample Containment

The samples were characterised using the small angle X-ray scattering (SAXS) camera in the Research School of Chemistry at the Australian National University.[73] The machine is made up of an Elliott GX-13 X-ray generator which creates Cu $K\alpha_1$ and $K\alpha_2$ X-rays by impinging electrons from a heated tungsten filament on a rotating copper anode. X-rays created pass through a Huxley-Holmes camera, 980 mm in length, and the scattered X-rays are sensed by a Gabriel detector. This is a linear position sensitive detector consisting of a gold plated wire under high potential in a P10 gas (90% argon, 10% methane) atmosphere. A schematic for the SAXS camera is shown in Figure 3.3.

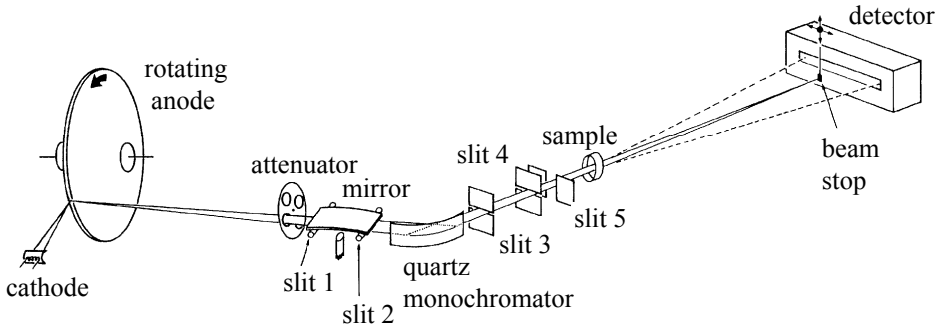

Figure 3.3 *Schematic diagram of the small angle X-ray scattering camera at the Research School of Chemistry, ANU.*[73]

The SAXS patterns presented in this work were taken using X-rays of wavelength 1.54 Å and are shown as plots of intensity against the momentum transfer, Q. All samples for X-ray pattern determination were run in Lindemann glass (lithium borate) X-ray capillary tubes. Dry powder samples were run in 0.7 mm or 1.0 mm diameter capillaries and wet gel samples were generally run in 1.5 mm capillaries owing to the difficulties involved in filling smaller capillaries with the stiff gel. Samples for *in situ* heating experiments, despite being wet synthesis gels, were run in 1.0 mm capillaries. All capillaries were sealed with Torr-Seal™ high vacuum glue. The sample was not usually in contact with the seal. *In situ* heating experiments on the SAXS camera were carried out using the capillary heater designed and built by Trevor Dowling at the RSC. The coiled Nichrome resistance heater was used in the range of 70-100˚C to heat nitrogen gas and controlled at the set temperature by an Omega CN76000 temperature controller to an accuracy of ±1.0˚C although as much as 30 minutes was required to reach the set temperature. The heated gas was blown down the length of the capillary, with pressure controlled by a gas rotameter.

The small angle neutron scattering experiments were carried out on the LOQ small angle scattering instrument at ISIS at the Rutherford Appleton Laboratory, UK;[74,75] on the SAD instrument at IPNS, at Argonne National Laboratory, Chicago, USA;[76] and on the NG3SANS instrument at the CNRF, NIST, Washington, USA.[77,78] LOQ and SAD are both time-of-flight instruments on pulsed spallation neutron sources. At these spallation sources, neutrons are generated by the impact of protons on a tantalum or uranium target producing a pulse of neutrons. The time-of-flight between the neutron generation at the target and the arrival of each neutron at a detector is measured, and from this the neutron velocity and thus wavelength may be calculated. Rotating blade "choppers" and frame overlap mirrors shape each pulse, preventing fast neutrons from the next pulse, or slow neutrons from the previous pulse interfering with those of the current pulse. The interaction of the neutrons with the sample gives a scattering pattern measured in counts versus time-of-flight which is then converted to momentum transfer, Q. A schematic of LOQ is shown in Figure 3.4.

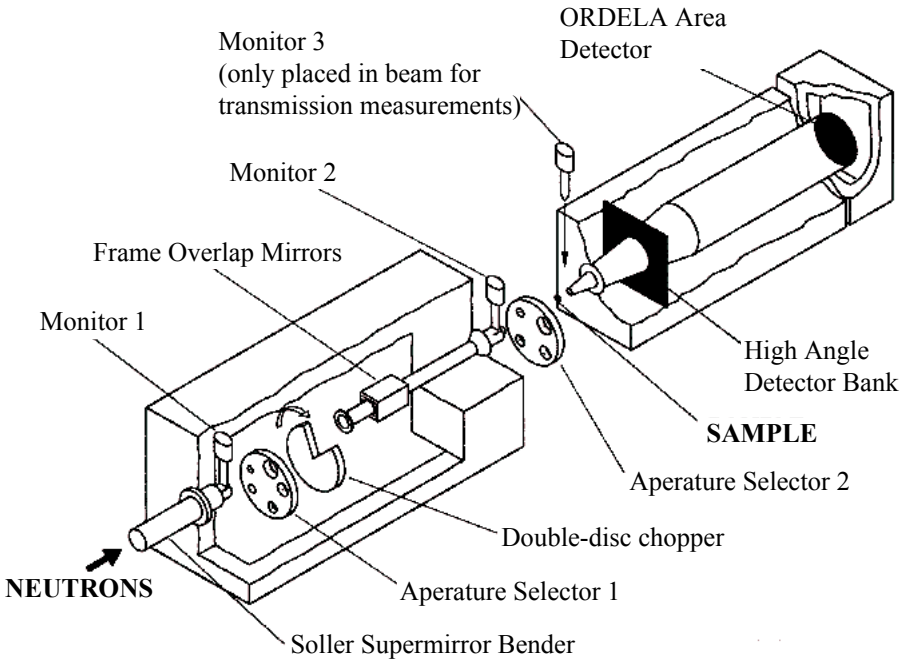

Figure 3.4 *Schematic of the LOQ time-of-flight small angle neutron scattering machine at ISIS, RAL, UK, used with permission.*[79]

The NIST small angle scattering machine, NG3SANS is on a reactor source which generates a continuous neutron beam. In this machine a particular wavelength (6 Å for the experiments reported here) is selected by a monochromating crystal. The scattering pattern is determined as a function of counts at a particular angle, for neutrons of that energy only. Both reactor and spallation sources use a moderator to control the energy spectrum of the neutrons, reducing the energy of "hot" neutrons by passing them through a liquid methane filled area, prior to entry into the neutron guides for each machine. Figure 3.5 shows a schematic of the NIST, NG3SANS machine. The samples were contained in flat quartz cells, 1 mm sample thickness, sealed with teflon stoppers. All static SANS measurements were performed at 25˚C.

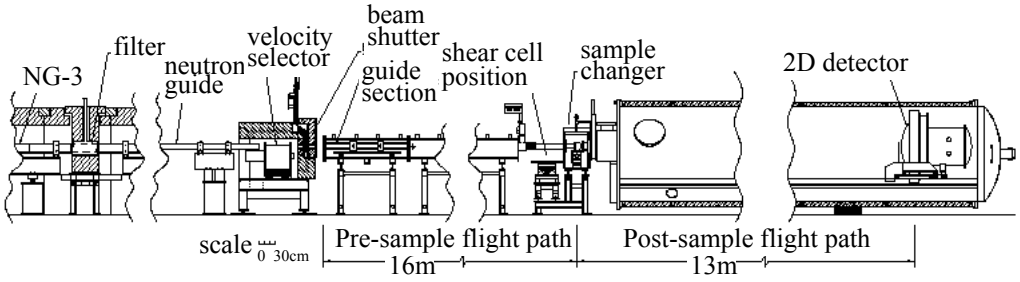

Figure 3.5 *Schematic of the NG3SANS small angle neutron scattering machine at NIST, USA, used with permission.*[80]

Measurements of the MCM-41 synthesis gels under shear were also made at ISIS on the LOQ instrument, and at NIST on the NG3SANS instrument. In both cases a quartz shear cell in a Couette geometry was used. The gap between the inner (static) cylinder and the outer (rotating) cylinder was 0.5 mm in both cases. The shear cells were run at temperatures between 25 and 40˚C, by using a water bath to pump thermostatted water through the inner cylinder, excepting in the region of the neutron window.

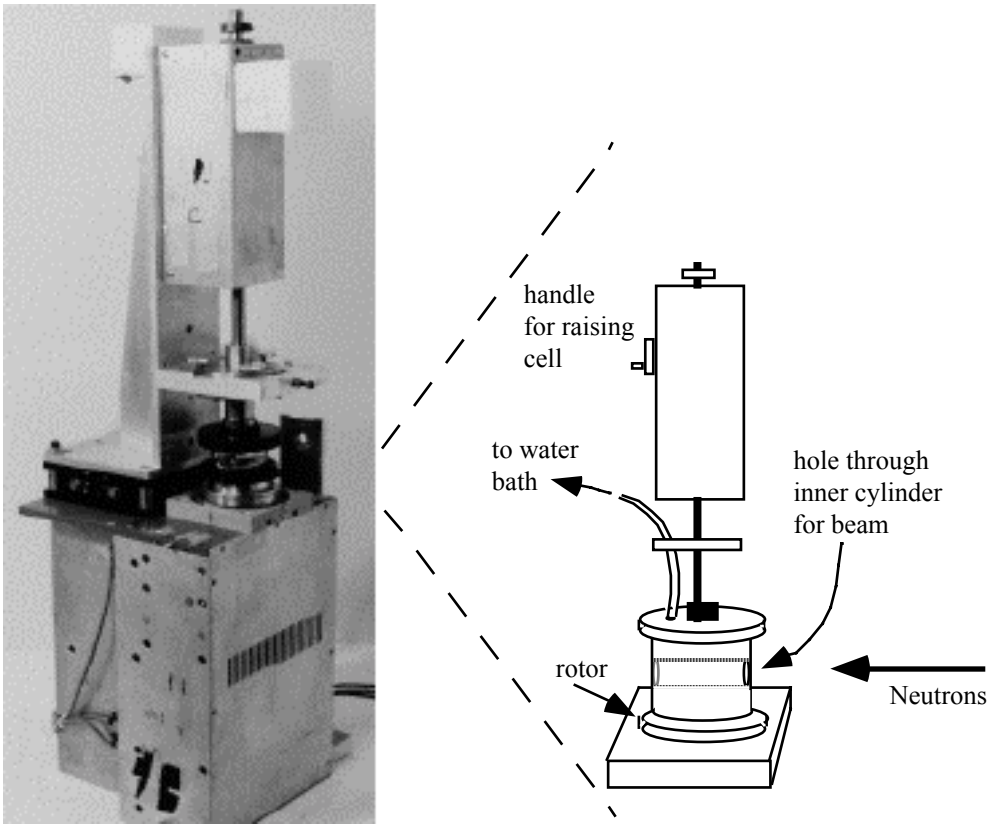

Figure 3.6 *Photograph (used with permission) and schematic of the Couette shear cell at ISIS, RAL, for use on the small angle neutron scattering instrument, LOQ. The clear cylinder near the middle of the picture is the cell. It is composed of an inner stationary cylinder which is temperature controlled by a water circulator/heater system and an outer rotating cylinder. The neutron beam passes through the centre of the cylinders, perpendicular to the plane of the rotation.*[81]

Shear rates used varied from one revolution per minute (0.02 s^{-1}) up to 10 000 s^{-1} on the LOQ shear cell and from 78 to 3112 s^{-1} on the NIST shear cell. Figure 3.6 shows a

photograph of the LOQ shear cell. Solutions used in the shear cell contained 89.7 wt% D_2O, to give the greatest available contrast (it is not possible to achieve a higher concentration of D_2O in a MCM-41 synthesis gel, as the sodium silicate solution contains a significant amount of H_2O).

3.3 Synchrotron X-ray Powder Diffraction

Powder diffraction was carried out using both neutrons and X-rays. The theory is the same for both so it is discussed only once. However, as the purpose of the two experiments were very different, the instrumentation and sample containment are discussed separately.

3.3.1 Powder Diffraction Theory

Again, a more detailed account of X-ray diffraction may be found in many textbooks.[82] A brief overview relevant to the work discussed in this thesis is given here. X-ray diffraction is dependent upon the fact that X-rays have a wavelength comparable to that of the regular atomic spacing in crystals. Diffraction arises from interference between X rays scattered by being passed through a solid containing regular arrays of atoms. Where the X-rays waves are scattered so that their amplitudes are in phase, the intensity is enhanced, where the amplitudes are out of phase they cancel. The waves are in phase and undergo constructive interference when the path-length difference (AB+BC in Figure 3.7) is an integral number of wavelengths.

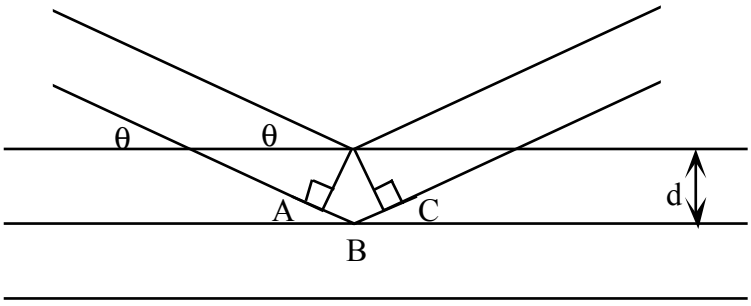

Figure 3.7 *Bragg diffraction from a series of planes.*

This is also expressed in the Bragg equation below, where λ is the wavelength of the X-rays.

$$n\lambda = 2d\sin\theta \qquad \textbf{(3.7)}$$

In a crystal, a set of crystallographic planes hkl can be defined as the set of parallel equidistant planes, one of which passes through the origin, and the next nearest makes intercepts of a/h, b/k, and c/l on the three crystallographic axes. a, b, and c are the dimensions of the smallest repeat unit of the crystal (the unit cell). hkl are called the Miller indices. The spacing between diffracting planes is called the *d*-spacing. In a hexagonal system such as MCM-41 it is a measure of the centre-to-centre distance (2/√3

times the *d*-spacing for a hexagonal system) between the hexagonally arranged channels in the MCM-41 matrix.

In powder diffraction, the sample is made up of many randomly oriented microcrystallites and so all reflections, from every possible orientation of the crystal, will be present in the diffraction pattern. For a system with two dimensional hexagonal symmetry, such as MCM-41 (although the diffraction in this case is from layers of ordered channels rather than atoms) the unit cell dimensions a, b are equal, and one of the cell angles is equal to 90˚ while the other angle is 120˚. The angles at which the hk planes diffract is given by:[82]

$$\frac{1}{d^2} = \frac{4}{3}\left| \frac{h^2 + hk + k^2}{a^2} \right| \qquad \textbf{(3.8)}$$

In MCM-41 there is no repeat unit in the c axis and so only reflections from the hk planes, in two dimensions, are seen.

X-ray peaks although usually most intense at the Bragg angles, are not delta functions. Broadening of the peak is caused by several factors; instrumental resolutions, crystal imperfections, small crystal size and overall sample size. Since most of these factors are roughly constant in MCM-41 patterns, and the resolution functions of the X-ray machines used are known to be much smaller than the peak widths, the peak widths can be used to obtain an estimate of the crystal size. The Scherrer equation[82] predicts:

$$B(2\theta) = \frac{0.94\lambda}{L\cos\theta} \qquad \textbf{(3.9)}$$

where B(2θ) is the full width in radians subtended by the half maximum intensity width of the powder pattern peak, λ is the wavelength of the radiation, L is the edge dimension of the crystal (assuming cubic crystals) and θ is half the scattering angle. Although this equation was derived for cubic crystals, it gives quite a good approximation, if for each hkl reflection, the value of L is interpreted as an average crystal dimension perpendicular to the reflecting planes.[82]

3.3.2 Instrumentation and Sample Containment

MCM-41 samples mounted in 1.0 mm diameter Lindemann tubes were examined by X-ray diffraction on the Australian National Beamline Facility at the Photon Factory synchrotron, Tsukuba, Japan. The "Big Diff" instrument on Beamline 20a is a powder diffractometer equipped with image plate detection[83] (Figure 3.8). In this diagram, synchrotron radiation enters from the left, is monochromated in the circular apparatus in the centre of the figure and passed through to the diffractometer, the large circular drum on the right. The diagram also shows a number of beamstops and slit controllers. Samples are housed in the large (*ca*. 2.5 m diameter) stainless steel cylinder which is evacuable. Image plates are mounted 1 m away from the sample, on the circumference of the cylinder. After exposure, the image plates are removed from the cylinder,

scanned and digitally converted into intensity versus angle data. The wavelength of the synchrotron radiation is tuneable so that it can be optimised for collection of data at specific lattice spacing ranges. The samples required exposures of *ca.* 5 minutes at $\lambda = 1.8963(1)$ Å (one pattern, taken earlier, used $\lambda = 1.54$ Å).

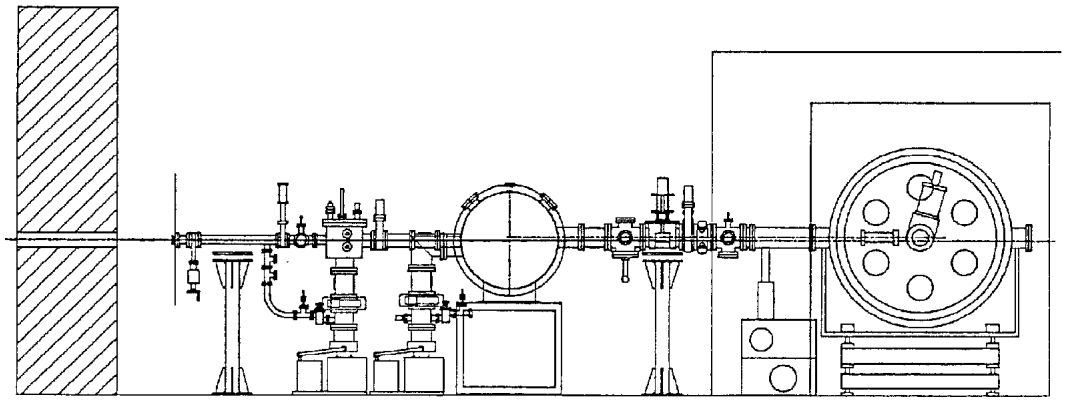

Figure 3.8 *Schematic of the layout of the Australian National Beamline Facility on Beamline 20a at Tsukuba, Japan, used with permission.*[84]

3.4 Gas Adsorption Isotherms

The interaction of gases with MCM-41 is of interest for several reasons. Firstly, the characteristic MCM-41 nitrogen adsorption isotherm[3,11,39] and high surface areas[1] were used to confirm synthesis of this material. Secondly, methane and hydrogen isotherms were run to assist in the quasielastic neutron scattering gas adsorption studies, and finally, nitrogen and hydrogen isotherms were analysed to provide thermodynamic information on the MCM-41 surface. The theory described below is given in outline only. More detailed accounts may be found in Adamson,[85] and Gregg and Sing.[86]

3.4.1 Adsorption Isotherm Theory

Adsorption of gases on solid surfaces can take place as physisorption, in which there is no change in the molecule adsorbed or the adsorbing surface beyond some physical re-arrangement of molecules, or as chemisorption in which a reaction significantly modifying the electronic properties of the surface and/or the adsorbate occurs. The two may be distinguished by the energy released during the adsorption, which is much larger for chemisorption. In this work, using unreactive gases, at low temperatures on a silica substrate, only physisorption was observed, and so the discussion which follows is limited to this type of adsorption.

Adsorption isotherms were initially categorised into five types by Brunauer,[87] which indicate different adsorption behaviours due to surface characteristics. These classifications have been adopted by IUPAC,[88] with the addition of one extra category. Figure 3.9 shows the five typical adsorption isotherms as plots of amount adsorbed in mmol g^{-1} versus P/P_0 where P is the pressure of the adsorbate and P_0 is the vapour pressure of the adsorbate at the temperature at which adsorption is occurring. Type I is a Langmuir type isotherm, having a monotonic approach to a limiting adsorption which

often corresponds to one monolayer. Type II corresponds to reversible, unrestricted monolayer-multilayer adsorption on a surface and is very common for physical adsorption. The point where the almost linear middle portion of the isotherm begins is called the "B" point and is often taken to indicate the stage at which monolayer coverage is complete and multilayer adsorption about to begin. Type III is rare and occurs in cases where the heat of adsorption is equal to, or less than, the heat of liquefaction of the adsorbate. Types IV and V are examples of capillary condensation phenomena indicating a porous solid. These isotherms level off before the saturation vapour pressure is reached and may show hysteresis. Nitrogen isotherms on MCM-41 are typical of Type IV isotherms and Type IV is typical of mesoporous adsorbents generally. The sharpness of the steps in Type VI isotherms depends upon the system and the temperature. They represent stepwise multilayer adsorption on a uniform non-porous surface and the step height represents the monolayer capacity for each adsorbed layer.

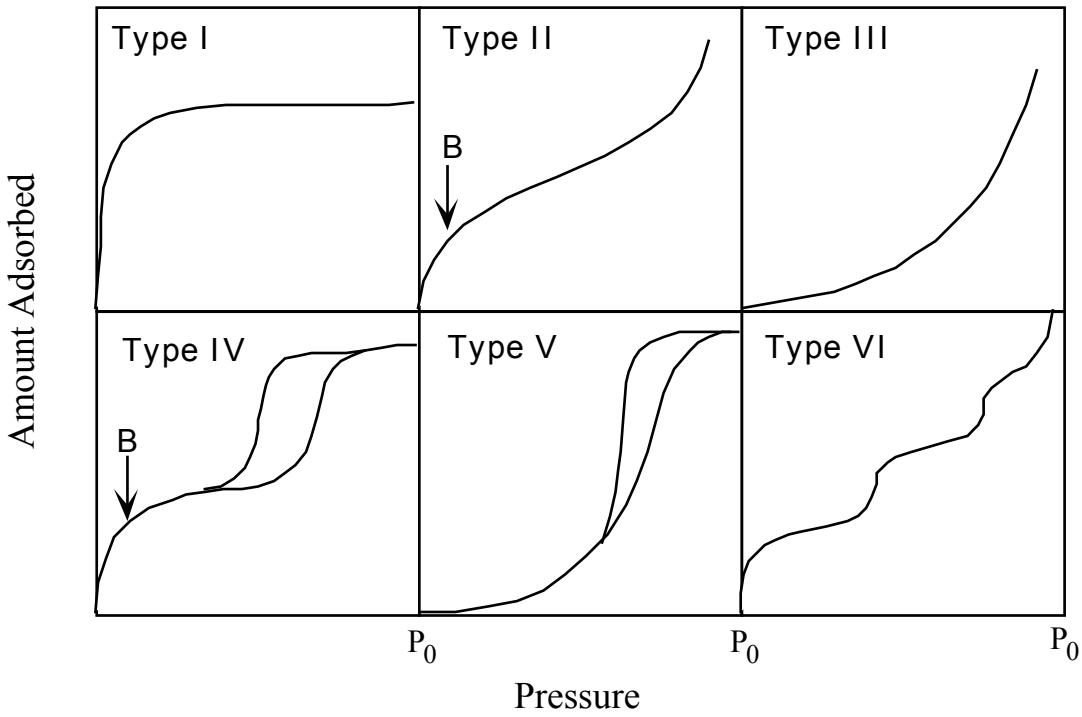

Figure 3.9 *The six types of gas adsorption isotherm as categorised by Brunauer, and adopted by IUPAC.*[85,88]

The analysis of isotherms of Type II and IV, which are typical of multilayer adsorption, is accomplished by use of the BET equation. The derivation of this equation is based on a detailed balancing of forward and reverse adsorption rates and by assuming that the heat of adsorption is the same for all adsorbed layers, except the first one which may have some special value. The heat of adsorption for successive layers is assumed to be equal to the heat of condensation of the liquid adsorbate. The resulting equation is often written in the form:

$$\frac{x}{n(1-x)} = \frac{1}{cn_m} + \frac{(c-1)x}{cn_m} \qquad \textbf{(3.10)}$$

where n is the amount adsorbed, n_m is the moles of gas per gram of solid adsorbed at the monolayer point (known as the monolayer capacity), x is the relative pressure, also written as P/P_0, and c is a constant related to the difference between the heat of adsorption for the first monolayers and that of all successive monolayers. n_m and c can be evaluated from the slope (s) and intercept (i) of the straight line best fitting a plot of x/n(1-x) versus x. For MCM-41 materials, such BET plots are typically linear over the range $0.05 < P/P_0 < 0.3$. At higher P/P_0 values, the capillary condensation requires different theory for analysis. One example is shown in Figure 3.10. From this n_m may be calculated using $n_m = 1/(s+i)$. The surface area of the solid, S, may then be calculated from $S = n_m N A_m 10^{-20}$ where S is the specific surface area, N is Avogadro's number and A_m is the area of the adsorbate molecule. The values of A_m used in this work are 16.2 Å^2 for nitrogen,[86] 10.3 Å^2 for hydrogen[89] and 14.2 Å^2 for methane.[90] For a system of hexagonally close-packed cylinders with an internal diameter between 28-35 Å and walls 10 Å thick, the limiting surface area can be calculated to be 990 - 880 $m^2 g^{-1}$ (neglecting external surface area). MCM-41 materials typically have specific surface areas of around 1000 $m^2 g^{-1}$, indicating that they are largely composed of such channels, although there is some contribution from the external surface area of the particles in real systems.

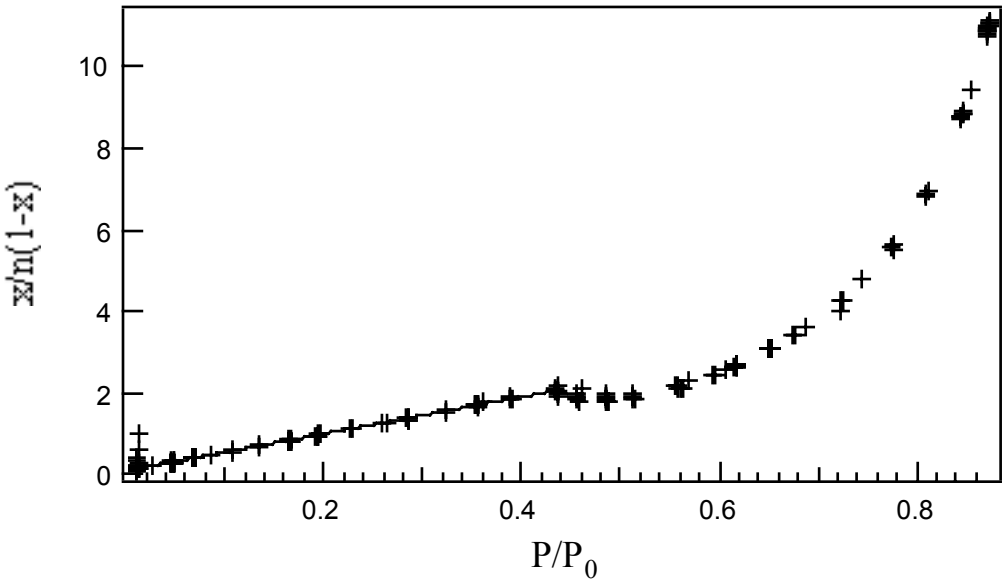

Figure 3.10 *BET plot for nitrogen adsorption on acetic acid titrated MCM-41 at 77 K, showing the curve (crosses) over the whole pressure range for the isotherm. The fitted part of the data is indicated by a solid line.*

From adsorption data taken over several temperatures, the isosteric heat of adsorption, q^{st} can be calculated from equation 3.11:

$$q^{st} = RT^2 \left| \frac{\partial \ln x}{\partial T} \right|_{\theta} \qquad \textbf{(3.11)}$$

In this equation, R is the gas constant, T is temperature and θ is the fraction of the surface covered (*ie.* $\theta = n/n_m$). If the isotherms are recorded over a small temperature range, a plot of ln x versus T for a particular n may appear linear. It may therefore be assumed that q^{st} is independent of temperature over small temperature ranges,[91] so that equation 3.11 may be integrated to give:

$$q^{st} = \frac{RT_1T_2}{T_2 - T_1} \ln \left| \frac{P_2}{P_1} \right|_{n} \qquad \textbf{(3.12)}$$

where P_1 and P_2 are the equilibrium pressures at temperatures T_1 and T_2 respectively. Values of q^{st} may be calculated from isotherms measured at only two temperatures provided the temperature range is small enough to justify the assumption that q^{st} is independent of temperature.[91] For values of θ above a monolayer, values of q^{st} close to that of the enthalpy of vaporisation of the adsorbate indicate that physisorption only is taking place. Much higher values would indicate chemisorption. For less than monolayer coverages, variation in the value of q^{st} at different coverages may distinguish between a homogeneous and heterogeneous surface. Plots of q^{st} versus θ can give information about adsorption sites, surface heterogeneity[92] and adsorbate interactions.

In porous systems with Type IV isotherms, the sharp rise in the isotherm around $P/P_0 = 0.4$ is due to capillary condensation in the pores. If the adsorbent is represented as a bundle of various-sized capillaries, the pore radius distribution may be calculated from the desorption branch of the isotherm, using the Kelvin equation for cylindrical pores open at one end;

$$\ln(x) = \left| \frac{-2\gamma V_1}{RT} \right| \left(\frac{1}{r^k} \right) \cos\phi \qquad \textbf{(3.13)}$$

In this equation, r^k is the radius of the capillary from which liquid begins to evaporate at the relative pressure, x, γ is the surface tension, V_1 is the molar volume of the liquid adsorbate and ϕ is the contact angle between the liquid and the capillary wall (usually taken to be zero, so that $\cos(\phi) = 1$). The Kelvin radius is the radius of the capillary plus the thickness, t, of the adsorbed layer remaining on the pore wall after desorption. That is, the actual radius of the capillary is $r = r^k - t$. The thickness, t, is taken to be $t = (n/n_m)\sigma$ where n is the amount adsorbed at relative pressure P/P_0, n_m is the monolayer capacity, and σ is the effective thickness for each layer (3.45 Å for N_2 at 77 K[91]).

Comparison plots between an unknown material and a non-porous material with similar surface characteristics can show the existence of micropores in the unknown.[93] Adsorption values in normalised units (mmol m^{-2}) at the same P/P_0 value for the unknown are plotted against those for the non-porous substrate, with a non-zero intercept on the unknown adsorption axis indicating the presence of micropores. The method is merely a comparison between the shapes of the two isotherms - if they are identical over the entire pressure range measured the plot will be merely a straight line passing through the origin. The slope of the line is equal to the ratio of the surface area for the two adsorbents. Adsorption data for MCM-41 were compared to the standard nitrogen isotherm at 77 K for hydroxylated silica.[86] A comparison plot for a sulphuric acid titrated sample (X3.6) is shown in Figure 3.11.

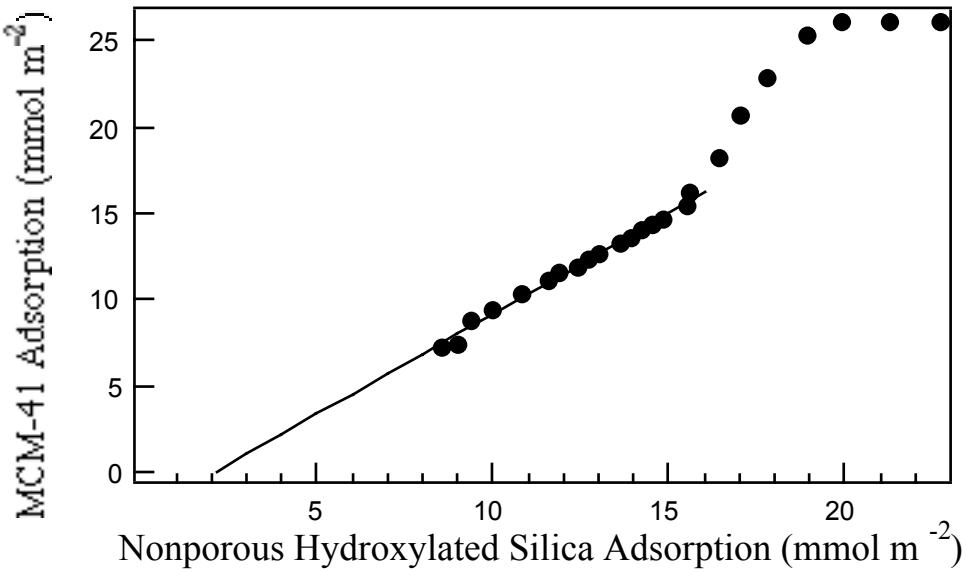

Figure 3.11 *Comparison plot for adsorption data from nitrogen at 77 K adsorbed on a sulphuric acid titrated MCM-41 sample. The intercept on the y-axis is at -2.4829 mmol m^{-2}. The circles are the experimental data, while the line is the fit to the linear region.*

3.4.2 Instrumentation and Sample Preparation

Gas adsorption isotherm data were measured with a Sartorius microbalance at 77 K. The calcined samples had been heated *in situ* to ca 250˚C under a vacuum of better than 10^{-4} torr for at least 12 hours before isotherms were measured. Both sample and counterweight were held at 77 K to avoid differences in buoyancy due to the density of nitrogen gas, as this had been found to be a significant problem for the very low surface area uncalcined samples. A schematic of the adsorption apparatus is shown in Figure 3.12. To ensure equilibrium adsorption, the pressure above the sample and its mass were monitored at 10 second intervals after each gas admission using an analogue to digital card in an IBM compatible computer and the results continuously displayed. Further gas was admitted to the system after the rise in pressure levelled out for each previous admission.

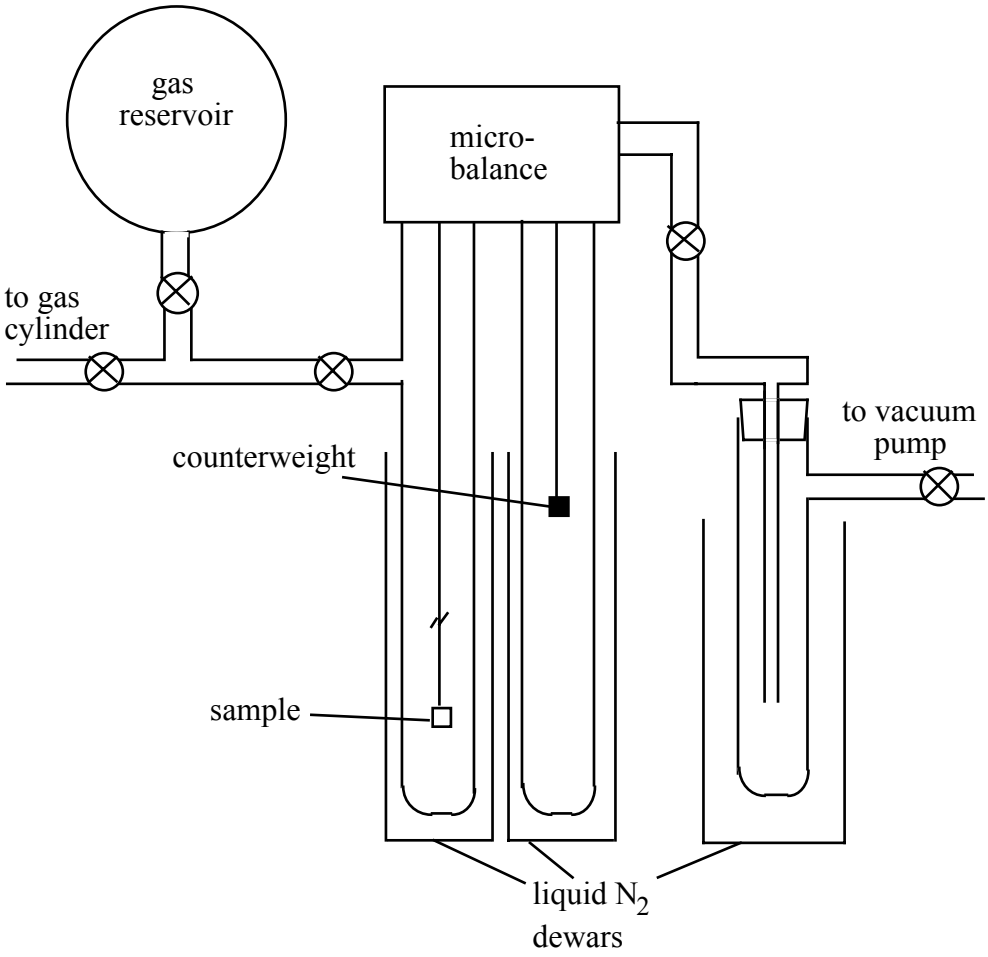

Figure 3.12 *Schematic diagram of the gas adsorption apparatus used at the RSC. The sample and counterweight hang by fine glass wires from the microbalance, which is connected to an IBM compatible PC for data collection.*

3.5 Quasielastic & Inelastic Neutron Scattering

Quasielastic neutron scattering (QENS) and inelastic neutron scattering are used here to gain information on the motions of molecules of hydrogen and methane adsorbed into MCM-41 over various temperature ranges. This allows conclusions to be drawn concerning the structure and motion of these molecules as adsorbates. But also, since these molecules are so well characterised as pure materials,[94-99] they can be used as probes to investigate the properties of the MCM-41 framework.

3.5.1 Theory

A brief overview of some of the theory behind quasielastic and inelastic neutron scattering is given here. A much more detailed account can be found in many textbooks.[65,100,101] Thermal neutrons have energies comparable to molecular energy levels and wavelengths which are of the order of interatomic spacings in solid phases. This makes them a good probe of molecular dynamics.
Inelastic scattering occurs when the scattered neutron undergoes an exchange of energy and momentum with the sample, which causes both the direction and magnitude of the

neutron's wavevector to change. QENS refers to inelastic scattering in which the energy change is small, and originates from interactions with nuclei diffusing or reorientating over time scales of 10^{-10}-10^{-12} s. The energy transfer involved can be up to 1 meV (8.06 cm^{-1}) and results in a broadening of the narrow elastic line associated with neutrons which are scattered with no energy transfer. The term "inelastic scattering" is usually used to refer to higher energy transfers, up to 1 eV and higher, resulting from interactions with molecular vibrations, crystal lattice phonons, and electronic excitations.

Inelastic neutron scattering has both coherent and incoherent components. In coherent scattering, from the 'average' crystal, the neutron wave interacts with the whole sample as a unit so that scattered waves from different nuclei interfere. Coherent scattering therefore gives information on the relative spacings between atoms, and inelastic coherent scattering thus gives information on collective motions of atoms, such as vibrations in a crystal lattice. In incoherent scattering, from the variations within the crystal, (often isotropic) the neutron wave interacts independently with each nucleus in the sample so that scattered waves form different nuclei do not interfere. Rather, intensities from waves scattered from each nucleus are additive. This means that incoherent scattering may be from the same atom, at different positions and different times. This results in Doppler broadening of the incident energy distribution from which information about atomic diffusion and the range and type of motion may be deduced.

The QENS and inelastic scattering measurements reported in this work are of inelastic incoherent scattering, and measure $S_{inc}(\mathbf{Q},\omega)$, where S is the incoherent, inelastic scattering function, $\mathbf{Q}$ is the momentum transfer (as defined in section 3.2 above) and ω is the energy transfer (see equation 3.14 below). Hydrogen has a large incoherent cross-section compared to both the coherent and incoherent cross-sections of other elements (see Table 3.1, the cross-section, $\sigma = 4\pi b^2$ where b is the scattering length). Thus QENS and inelastic scattering are used here as a probe of the hydrogen motions in the methane molecules, and of dihydrogen interactions with the MCM-41 pore walls.

For inelastic scattering from molecules with internal degrees of freedom (which are assumed to be decoupled from the translational degrees of freedom), the scattering cross-section results from a sum of the scattering function for each internal energy level, over all of the internal excitations of the molecule.[96] Often the molecule may be treated as a rigid body, but for sufficiently high energy transfers, vibrational modes will also be excited. The inelastic scattering seen in the measurements of gas adsorbed on MCM-41 shows a broad continuum of intensity to the highest energy transfers measured. Such continuous spectra arise from the nature of the molecular form factors and from translational recoil in the scattering collision which broadens the rotational transitions[102,103] as well as the vibrational modes which may also start to become excited at the highest energy transfers. In the hydrogen data, peaks are also seen at energies which correspond to the $J = 0 \rightarrow 1$ rotational transitions (see Chapter 5). The energies of the rotational levels for hydrogen are given by $E_{rot} = J(J+1)B$ where $B = 7.35$ meV.[96]

In a quasielastic experiment, $S_{inc}(\mathbf{Q},\omega)$ can be separated into a purely elastic component, $S^{el}_{inc}(\mathbf{Q},\infty)\delta(\omega)$ superimposed upon the quasielastic component $S^{q}_{inc}(\mathbf{Q},\omega)$.

$$S_{inc}(\boldsymbol{Q},\omega) = S^{el}_{inc}(\boldsymbol{Q},0)\delta(\omega) + S^{q}_{inc}(\boldsymbol{Q},\omega) \qquad \textbf{(3.15)}$$

The quasielastic component is the time Fourier transform of a time dependent term and which therefore possesses a non-vanishing broadening that gives information on the characteristic times of the nuclear motion. The coefficient of the delta function is the space-Fourier transform of the final distribution of scattering nuclei averaged over all possible positions (since all positions are equivalent). It has the dimensions of a structure factor and is called the elastic incoherent structure factor (EISF). The EISF can be calculated experimentally from the ratio:

$$EISF = \frac{I^{el}(Q)}{I^{el}(Q) + I^{q}(Q)} \qquad \textbf{(3.16)}$$

where I^{el} is the integrated intensity of the elastic part and I^{q} is the integrated intensity of the quasielastic part of the data. They are found by fitting the observed peak shapes to a delta function and a Lorentzian peak shape, which is assumed for the wider quasielastic contribution. The EISF is the fraction of total quasielastic intensity contained in the purely elastic peak.

Instrumental resolution therefore becomes important in these experiments. The finite resolution of real machines means that the delta function will not appear as an infinitely sharp line, but has an energy width characteristic of the instrument. This width determines the time scales over which motions are observable. Motions which are too rapid cause peak broadenings which are negligible in comparison to that of the instrumental resolution and so are not visible, whereas motions which are too slow cause considerable broadening which tends to a flat background underlying the spectra (see Figure 3.13). As broadening is a function of temperature, it is therefore possible to watch molecular motions being activated, as mobility increases with temperature.

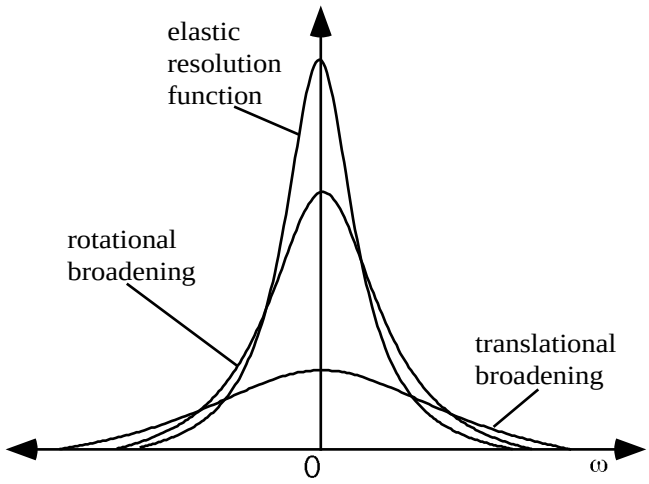

Figure 3.13 *Components of a quasielastic scattering peak due to different types of motion occurring on different time scales within the same system.*

$S_{inc}(\mathbf{Q},\omega)$ for quasielastic scattering is the result of single particle motions. Thus, by assuming that coupling between the various degrees of freedom can be ignored, it can be written as the convolution of the lattice motions, rotational motions and vibrational motions for a molecular solid, or translational, rotational and vibrational motions for a liquid. That is:

$$S_{inc}(\boldsymbol{Q},\omega) = S_{inc}^{T}(\boldsymbol{Q},\omega) \otimes S_{inc}^{R}(\boldsymbol{Q},\omega) \otimes S_{inc}^{V}(\boldsymbol{Q},\omega) \qquad \textbf{(3.17)}$$

where the superscripts T, R, and V correspond to contributions from translational, rotational and vibrational components respectively. In the quasielastic region, vibrations contribute only through a Debye-Waller factor, $\exp(-\langle u^2\rangle Q^2)$ where $\langle u^2\rangle$ is the mean square amplitude for the vibrational motion, however they are also visible as peaks in the higher energy inelastic scattering regime.

Rotational motions have been described by a number of different models ranging from isotropic rotational diffusion for molecules with no preferred orientation in space, to jump diffusion through any number of possible sites on a circle or sphere. For isotropic rotational diffusion, the incoherent structure factor is:

$$S_{inc}^{R} = \frac{1}{\pi} \sum_{m=1}^{\infty} (2m+1) j_m^2(QR) \frac{m(m+1)D_R}{[m(m+1)D_R]^2 + \omega^2} \qquad \textbf{(3.18)}$$

where D_R is the isotropic rotational diffusion constant, R is the radius of the sphere, $j_m(x)$ is the spherical Bessel function of order m. This type of motion produces broadening of the quasielastic Lorentzian widths which are oscillatory in Q and therefore bounded. Dihydrogen in the solid state is a prime example of free rotation.[100] The isotropic rotational diffusion model has also been used to model the motion of methane in the zeolites ZSM-5[104] and NaY.[105] In solid methane, tunnelling of the methane hydrogens between sites on the surface of a sphere is observed as discrete peaks on either side of the quasielastic peak.[100,106] These tunnelling peaks were not observed in the methane adsorbed on MCM-41 investigated in this work.

Translational motions, modelled as continuous diffusion via a random walk give a scattering law:

$$S_{inc}^{T}(Q,\omega) = \frac{1}{\pi} \cdot \frac{DQ^2}{\omega^2 + (DQ^2)^2} \qquad \textbf{(3.19)}$$

where D is the translational diffusion constant $D = \langle l^2\rangle/6\tau$ in which l is the step length taken in time τ. The energy spectrum of the scattered neutrons is a Lorentzian, with a half width at half maximum which increases with the momentum transfer according to a DQ^2 law. This allows a direct determination of the diffusion constant at small Q values and small energy transfers. That is, under conditions of weak interparticle interactions where the continuous stochastic motion description is obeyed, which is also the limit for jump translational diffusion models.

3.5.2 Instrumentation and Sample Preparation

Prior to the neutron scattering experiments involving methane adsorption, the MCM-41 sample was outgassed at 250˚C with pumping to 10^{-5} torr for about 12 hours. It was then heated for three hours at 350˚C at 10^{-5} torr, before being transferred into the aluminium sample container under an atmosphere of pure helium. This was then mounted in a displex cryostat capable of reaching 15 K. A few measurements were also made in a cryostat at 1.5 K. The sample, from an ordinary MCM-41 preparation, weighed 0.725 g. It was filled with methane at 760 torr, sample temperature 140 K, that is, well above the condensation temperature of liquid methane and 6.68 mmol g^{-1} of methane was taken up.

Prior to any hydrogen adsorption experiments, the material was outgassed under a pressure of 10^{-4} torr at 350˚C for two days, to remove any residual water in the mesopores. A small quantity of residual hydroxyl groups arising from incomplete siloxyl condensations in the synthesis remain as the only hydrogenous material in the substrate. To remove these the calcined MCM-41 material, prepared using an acid-titrated synthesis, was soaked in D_2O to exchange the hydrogen for deuterium. Although the experiment involved doping this deuterium exchanged material with hydrogen gas, further exchange of the deuterium was unlikely because the low temperature experimental conditions and lack of catalytic material ensured stability of the dihydrogen molecules both to spin conversion (so that spin equilibrium was never reached) and exchange. The sample, weighing 1.10(5) g, was transferred to an aluminium sample can mounted in a cryostat capable of reaching 1.5 K. Hydrogen gas was admitted to the sample in volumetrically determined amounts, with an accuracy of *ca.* 2% in volumes, and 2 torr in pressure, which is 0.2% of the highest pressures used.

The quasielastic neutron scattering spectrometer, QENS, at the Intense Pulsed Neutron Source, Argonne National Laboratory was used for the inelastic neutron scattering experiments.[107] This time-of-flight spectrometer has an energy resolution of about 0.08 meV, and possesses counter banks at scattering angles of 40, 90, and 130˚. A schematic of this type of instrument is shown in Figure 3.14.

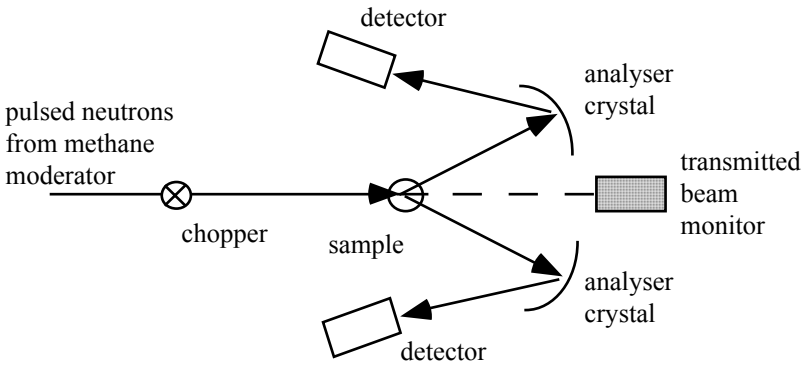

Figure 3.14 *Schematic of a typical time-of-flight neutron spectrometer.*

In the methane experiment there were clear changes in the elastic scattering intensity and the momentum transfer (Q) dependence of the quasielastic broadening with

temperature between 15 and 180 K. Quasielastic neutron scattering experiments on the outgassed MCM-41 at a number of temperatures, were also carried out to ensure that any inelastic scattering from the siloxyl groups was accounted for and also to define the elastic resolution function of the instrument. The resolution was found to be about 80 microelectron volts over a momentum transfer, Q, range of $0.3 < Q < 2.6$ Å^{-1}. The resolution of the instrument did not allow clear observation of excitations below *ca.* 100 microelectron volts and no conclusions were made on the existence of tunnelling. Data from bulk methane were taken with the same apparatus in a subsequent experiment as a control.

In the hydrogen experiment, a series of spectra at 1.9 K were taken with hydrogen loadings of 0, 9.5, 12.1, 21.5, 34.5 and 40.3 mmol g^{-1} on the MCM-41. At higher temperatures, spectra were obtained at 9.8 K (34.5 mmol g^{-1}), 13.3 K (37.7 mmol g^{-1}), 14.7 K (33.1, 40.3 mmol g^{-1}), and 21 K (23.1 mmol g^{-1}).

3.6 Neutron Powder Diffraction

The theory of neutron powder diffraction is identical to that of X-ray powder diffraction and has been discussed in detail in Section 3.3 above. The instrumentation and sample preparation for the neutron work is described below.

The neutron powder diffractometer HIPD[108] at the Intense Pulsed Neutron Source, Argonne National Laboratory with 30˚ and 90˚ scattering angle counter banks was used for the elastic neutron scattering experiments to discover the structure of hydrogen adsorbed in MCM-41. To optimise short wavevector diffraction results on this machine, resolution has been compromised to obtain high intensity at a given wavelength. The counter bank at 30˚ was at a comparatively low scattering angle for this type of instrument. Thus this diffractometer is capable of reaching to longer *d*-spacings than more conventional neutron powder diffractometers. Powder diffraction patterns were measured at 4.2 K, with good statistics since subtractions were necessary, at 0, 19.3, 27.2, 34.8 and 50.4 mmol g^{-1}. The latter sample was produced by loading to 50.4 mmol g^{-1} at 21 K and cooling over 30 mins to 4.2 K. This enabled the excess, unadsorbed hydrogen to first liquefy, and then crystallise, producing a completely loaded sample with the excess as crystalline solid hydrogen. Although it depends on the temperature, full filling of the space within this sample of MCM-41, by hydrogen, was about 40 mmol g^{-1}.

A point about the diffraction concerns the use of H_2 rather than D_2. Apart from concerns about isotopic effects changing the system properties marginally, it would seem that the lack of incoherent background in D_2 would be a significant advantage. However the deuterium scattering length is virtually the same as that of silicon and oxygen at about 6 pm, while the proton is -3.8 pm. This large difference between H and Si or O potentially, and in fact does, produces large changes in contrast at different fillings, while D_2 filling would just tend to gradually obscure void scattering. This consideration favours H_2 over D_2. Ideally both experiments should be performed, but

neither is obviously preferable in a high-flux experiments such as this, where incoherent effects are more easily subtracted.

3.7 Langmuir Trough

The Langmuir trough is a convenient method for studying the behaviour of thin, usually monomolecular, films of molecules.[85,109,110] In this work it is used primarily as a dilution method to investigate the limiting behaviour of silicate ions aggregating at a surfactant headgroup in two dimensions, without the additional complication of the three dimensional solution chemistry of micelle formation. It observes the silica-surfactant complex in a much simplified state, and it was hoped therefore to draw some conclusions concerning the formation of this likely MCM-41 precursor species.

3.7.1 Theory

To form a monomolecular film of an insoluble surfactant on a liquid surface, it must generally be spread from a low concentration solution, where the solvent is one which will spread on the liquid surface, rather than forming a lens at the interface. The spreading solvent will carry the molecule of interest with it as it spreads, ensuring a relatively even distribution of the insoluble species. This solvent must also evaporate readily, leaving only the molecule of interest behind. Generally one liquid will spread on the surface of the other if it has a low surface tension compared to that of the liquid at the surface.[85] Chloroform was chosen for these experiments since it spreads well on water (spreading coefficient 23 mN m^{-1} at 20˚C),[110] evaporates readily and dissolves the quaternary ammonium surfactants used in the study.

The quantities measured in a Langmuir trough experiment are the amount of the material per unit area - a known quantity calculated from the amount of solution spread, and the trough area - and the film pressure (Π, in mN m^{-1}). The film pressure is defined as the difference between the surface tension of the clean surface and that of the film-covered surface.[85] In this work the film pressure was measured by the Wilhelmy plate method,[85,109] with the plate being made of 10.0 mm wide filter paper (Whatman's Chr 1) to ensure a zero-contact angle between the plate and the meniscus, once the plate is wetted.[111] The change in force acting on the plate as the film is compressed is measured by the an electronic microbalance and recorded digitally. Since only the change in force is measured, the length of the filter paper plate is unimportant, as it is constant. The width of the plate is assumed to be negligible.[111] This method is sensitive to temperature changes and so the trough must be thermostatted to ensure these do not cause errors in the measured Π. Measurements on the films are therefore expressed as Π-A plots where A may be the real area occupied by the film on the trough or expressed as area per molecule in the film.

Various types of monolayer give different types of Π-A curves which are described as gaseous, liquid or solid films.[85] Examples of the isotherm expected from each are shown in Figure 3.15. Gaseous films are those where the area per molecule is large compared with the actual molecular areas, so that it obeys the equation of state of a two

dimensional perfect gas. These films can be expanded indefinitely without phase change. Solid films are those of low compressibility with almost linear Π-A plots. They are quite rigid and appear to consist of close-packed molecules, but may become liquid-like upon expansion. Liquid films are of two types, liquid expanded and liquid condensed. Both show some degree of cooperative interaction and the Π-A plots extrapolate to zero pressure at large areas per molecule. Liquid expanded films have higher compressibility than solid films and may show a first-order transition to gaseous films at low pressure, and, upon compression, a point of reasonably sharp change to a film of much higher compressibility, called an intermediate film. Liquid expanded films are typical of long chain compounds having highly polar groups such as amides and alcohols. Further compression of an intermediate film results in a liquid condensed film, with linear Π-A behaviour but relatively low compressibility. Such films have been described as films with close-packed heads which are re-arranged upon compression or as semi-solid films where the water between polar headgroups is squeezed out until a solid film is obtained. Limiting areas per molecule in these films are found by fitting a straight line to the solid-like part of the curve and extrapolating it down to the area axis.

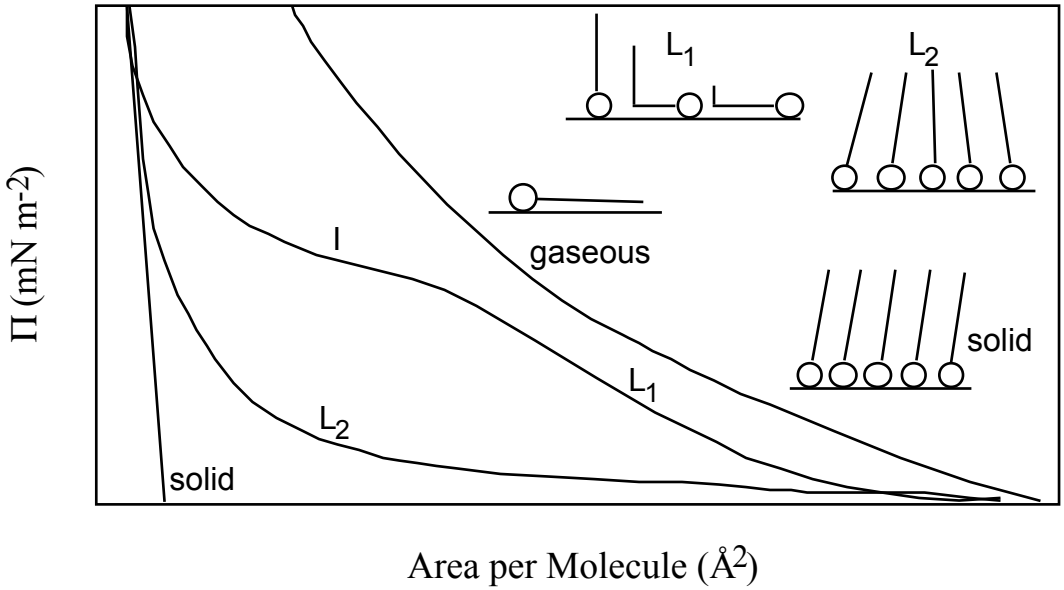

Figure 3.15 *Isotherms typical of each type of monomolecular film, and suggested molecular conformations for each. The polar headgroup is indicated as a circle.*

Solutions of soluble surfactants may also be studied on the Langmuir trough. In this case the surfactant is dissolved in the sub-phase and a proportion of the dissolved molecules assemble at the air-water interface.[112] This film, which forms due to the favourable free energy of freeing the surfactant hydrocarbon chains from the water phase, is called the surface excess. It is defined as the difference between the number of moles of surfactant in the surface region and in the bulk solution.[85] Isotherms from the surface excess were measured in the same way as isotherms from a monomolecular film, however the actual surface excess present was not evaluated in this work. Much work has previously been carried out on the structure of the surface excess of CTAB under a range of experimental conditions.[113-115]

3.7.2 Instrumentation and Sample Preparation

The Langmuir trough used in this work was a NIMA 601A Langmuir trough with a surface area of 600 cm^2 (20 cm wide by 30 cm long) and thermostatted to 20±1˚C. A Wilhelmy plate for surface pressure measurement was used for these measurements, with a clean paper plate used for each compression experiment. Isotherms were typically run in a continuous compression mode at compression rates of 20-100 cm^2 min^{-1} to a fixed pressure or area, and then run on a constant area or constant pressure mode while following the film behaviour over time. Care with solvent purity and general cleanliness was necessary to exclude even low levels of impurities. The spreading solvent, chloroform was distilled in glass to remove traces of grease and all glassware was cleaned with an ionic detergent and rinsed with large quantities of fresh, Millepore filtered water, with a resistivity of 1.8×10^5 Ω m.

Prior to film spreading, a similar volume of solvent to that which would be used to spread the film was spread on the water surface and compressed to ensure no isotherm from impurities had formed. The surfactant $(C_{18}H_{37})_2N(CH_3)_2$ Br, synthesised by Dr Tim Senden was used as received. It was chosen since it has a similar headgroup to that of CTAB, and is insoluble in water so that it would form a monolayer film when spread on the water surface. The solutions spread typically had a concentration of 0.996 mg ml^{-1}. Sodium silicate solution was either used as received or diluted with fresh Millepore water immediately before use. It was injected under the Langmuir trough barriers on the side away from the film, and allowed to diffuse towards the compressed surfactant film. This will cause a slight change in the pH of the substrate, which may also affect the film behaviour. Given the relative volumes of the substrate and the added sodium silicate solution, any change will, however, be small. Studies of CTAB surface excess in solutions below the critical micelle concentration (0.8-0.9mM)[116,117] and its behaviour in the presence of silicate solutions were also investigated using these methods.

3.8 Electron Microscopy

Scanning electron microscopy (SEM) was performed using a JEOL JSM6400 microscope, a Cambridge S360 microscope or a Hitachi S4500 field emission scanning electron microscope (FESEM). Samples were prepared by depositing the wet gel or, in the case of the calcined materials, either as a slurry in water onto a SEM stub and allowing it to dry in a desiccator before gold coating or by brushing small amounts of powder onto conductive silver tape before coating. Transmission electron microscopy was carried out on a JEOL 120 CX microscope. The samples were prepared by crushing under methanol and dispersed on a holey carbon film mounted on a copper grid. Both of these methods were used to image the MCM-41 powders. The scanning electron micrographs included in this thesis were taken by Dr Julieanne Dougherty and Dr John Thompson, and the transmission electron micrographs by Dr Ray Withers, all from the RSC.

3.9 References

1. J.S. Beck, J.C. Vartuli, W.J. Roth, M.E. Leonowicz, C.T. Kresge, K.D. Schmitt, C.T.-W. Chu, D.H. Olson, E.W. Sheppard, S.B. McCullen, J.B. Higgins and J.L. Schlenker, *J. Am. Chem. Soc.,* **1992**, *114,* 10834-10843.
2. C.-Y. Chen, H.-X. Li and M.E. Davis, *Microporous Mater.,* **1993**, *2,* 17.
3. P.J. Branton, P.G. Hall and K.S.W. Sing, *J. Chem. Soc., Chem Commun.,* **1993**, 1257-1258.
4. Q. Huo, J. Feng, F. Schüth and G.D. Stucky, *Chem. Mater.,* **1997**, *9*(1), 14-17.
5. K.R. Kloetstra, H.W. Zandbergen and H. van Bekkum, *Catal. Lett.,* **1995**, *33,* 157-163.
6. O. Regev, *Langmuir,* **1996**, *12*(20), 4940-4944.
7. W. Kolodziejski, A. Corma, M.-T. Navarro and J. Pérez-Pariente, *Solid State Nuclear Magnetic Resonance,* **1993**, *2,* 253-259.
8. C.-F. Cheng, Z. Luan and J. Klinowski, *Langmuir,* **1995**, *11,* 2815-2819.
9. Q. Huo, D.I. Margolese and G.D. Stucky, *Chem. Mater.,* **1996**, *8*(5), 1147-1160.
10. H.Y. Zhu, X.S. Zhao, G.Q. Lu and D.D. Do, *Langmuir,* **1996**, *12*(26), 6513-6517.
11. P.J. Branton, P.G. Hall, K.S.W. Sing, H. Reichert, F. Schüth and K.K. Unger, *J. Chem. Soc., Faraday Trans.,* **1994**, *90*(19), 2965-2967.
12. F.H.P. Silva and H.O. Pastore, *J. Chem. Soc., Chem. Commun.,* **1996**, 833-834.
13. M. Ogawa, *J. Chem. Soc., Chem. Commun.,* **1996**, 1149-1150.
14. P.T. Tanev and T.J. Pinnavaia, *Science,* **1995**, *267,* 865-867.
15. C.-G. Wu and T. Bein, *J. Chem. Soc., Chem. Commun.,* **1996**, 925-926.
16. L.M. Bull, D. Kumar, S.P. Millar, T. Besier, M. Janicke, G.D. Stucky and B.F. Chmelka in *Zeolites and Related Microporous Materials: State of the Art 1994.*; Stud. Surf. Sci. Catal., (Eds. J. Weitkamp, H.G. Karge, H. Pfeifer and W. Hölderich), Elsevier Science B.V., **1994**, *Vol. 84A*, 429-434.
17. S. O'Brien, R.J. Francis, S.J. Price, D. O'Hare, S. Clark, N. Okazaki and K. Kuroda, *J. Chem. Soc., Chem. Commun.,* **1995**, 2423-2424.
18. A. Matijasic, A.-C. Voegtlin, J. Patarin, J.L. Guth and L. Huve, *J. Chem. Soc., Chem. Commun.,* **1996**, 1123-1124.
19. N. Ulagappan, B. Neeraj, V.N. Raju and C.N.R. Rao, *J. Chem. Soc., Chem. Commun.,* **1996**, 2243-2244.
20. G.D. Stucky, A. Monnier, F. Schüth, Q. Huo, D. Margolese, D. Kumar, M. Krishnamurty, P. Petroff, A. Firouzi, M. Janicke and B.F. Chmelka, *Mol. Cryst. Liq. Cryst.,* **1994**, *240,* 187-200.
21. T. Dabadie, A. Ayral, C. Guizard, L. Cot and P. Lacan, *J. Mater. Chem.,* **1996**, *6*(11), 1789-1794.
22. L. Auvray, A. Ayral, T. Dabadie, L. Cot, C. Guizard and J.D.F. Ramsay, *Faraday Discuss.,* **1995**, *101,* 235-247.
23. C.T. Kresge, M.E. Leonowicz, W.J. Roth, J.C. Vartuli and J.S. Beck, *Nature,* **1992**, *359*, 710-712.
24. V. Alfredsson, M. Keung, A. Monnier, G.D. Stucky, K.K. Unger and F. Schüth, *J. Chem. Soc., Chem. Commun.,* **1994**, 921-922.
25. V. Alfredsson and M.W. Anderson, *Chem. Mater.,* **1996**, *8*(5), 1141-1146.

26. C.-F. Cheng, H. He, W. Zhou and J. Klinowski, *Chem. Phys. Lett.,* **1995**, *244,* 117-120.
27. D.T. On, P.N. Joshi and S. Kaliaguine, *J. Phys. Chem.,* **1996**, *100*(16), 6743-6748.
28. A. Sayari, I. Moudrakovski, C. Danumah, C.I. Ratcliffe, J.A. Ripmeester and K.F. Preston, *J. Phys. Chem.,* **1995**, *99,* 16373-16379.
29. U. Oberhagemann, I. Kinski, I. Dierdorf and M.H. Gies, *J. Non-Crystalline Solids,* **1996**, *197,* 145-153.
30. A. Chenite, Y. Le Page and A. Sayari, *Chem. Mater.,* **1995**, *7,* 1015-1019.
31. C.H. Ko and R. Ryoo, *J. Chem. Soc., Chem. Commun.,* **1996**, 2467-2468.
32. J.S. Beck, J.C. Vartuli, G.J. Kennedy, C.T. Kresge, W.J. Roth and S.E. Schramm, *Chem. Mater.,* **1994**, *6,* 1816-1821.
33. C.Y. Chen, S.L. Burkett, H.-X. Li and M.E. Davis, *Microporous Mater.,* **1993**, *2,* 22.
34. L.-Q. Wang, J. Liu, G.J. Exarhos and B.C. Bunker, *Langmuir,* **1996**, *12*(11), 2663-2669.
35. D. Akporaiye, E.W. Hansen, R. Schmidt and M. Stöcker, *J. Phys. Chem.,* **1994**, *98,* 1926-1928.
36. E.W. Hansen, R. Schmidt, M. Stöcker and D. Akporiaye, *J. Phys. Chem.,* **1995**, *99,* 4148-4154.
37. E.W. Hansen, M. Stöcker and R. Schmidt, *J. Phys. Chem.,* **1996**, *100*(6), 2195-2200.
38. R. Schmidt, E.W. Hansen, M. Stöcker, D. Akporiaye and O.H. Ellestad, *J. Am. Chem. Soc.,* **1995**, *117,* 4049-4056.
39. R. Schmidt, M. Stöcker, E. Hansen, D. Akporiaye and O.H. Ellestad, *Microporous Mater.,* **1995**, *3*(4/5), 443-448.
40. A. Pöppl and L. Kevan, *Langmuir,* **1995**, *11,* 4486-4490.
41. A. Pöppl, P. Baglioni and L. Kevan, *J. Phys. Chem.,* **1995**, *99,* 14156-14160.
42. V. Luca, D.J. MacLachlan, R. Bramley and K. Morgan, *J. Phys. Chem.,* **1996**, *100*(5), 1793-1800.
43. J. Chen, Q. Li, R. Xu and F. Xiao, *Angew. Chem. Int. Ed. Engl.,* **1996**, *34*(No. 23/24), 2694-2696.
44. J. Weglarski, J. Datka, H. He and J. Klinowski, *J. Chem. Soc., Faraday Trans.,* **1996**, *92*(24), 5161-5154.
45. A. Liepold, K. Roos, W. Reschetilowski, A.P. Esculcas, J. Rocha, A. Philippou and M.W. Anderson, *J. Chem. Soc., Faraday Trans.,* **1996**, *92*(22), 4623-4629.
46. S. Komarneni, V.C. Menon, R. Pidugu, J. Goworek and W. Stefaniak, *J. Porous Mater.,* **1996**, *3,* 115-119.
47. A. Firouzi, D. Kumar, L.M. Bull, T. Besier, P. Sieger, Q. Huo, S.A. Walker, J.A. Zasadzinski, C. Glinka, J. Nicol, D. Margolese, G.D. Stucky and B.F. Chmelka, *Science,* **1995**, *267*, 1138-1143.
48. P. Calvert and P. Rieke, *Chem. Mater.,* **1996**, *8*(8), 1715-1727.
49. A. Corma, A. Martínez, V. Martínez-Soria and J.B. Montón, *J. Catal.,* **1995**, *153,* 25-31.
50. A. Corma, M.S. Grande, V. Gonzalez-Alfaro and A.V. Orchilles, *J. Catal.,* **1996**, *159,* 375-382.

51. J.C. Vartuli, C.T. Kresge, M.E. Leonowicz, A.S. Chu, S.B. McCullen, I.D. Johnson and E.W. Sheppard, *Chem. Mater.,* **1994**, *6,* 2070-2077.
52. I. Petrovic, A. Navrotsky, C.-Y. Chen and M.E. Davis in *Zeolites and Related Microporous Materials: State of the Art 1994*; Studies in Surface Science and Catalysis, (Eds. J. Weitkamp, H.G. Karge, H. Pfeifer and W. Hölderich), Elsevier Science B.V., Amsterdam, **1994**, *Vol. 84*, 677-684.
53. C.J. Glinka, J.M. Nicol, G.D. Stucky, E. Ramli, D. Margolese, Q. Huo, J.B. Higgins and M.E. Leonowicz, *J. Porous Materials,* **1996**, *3,* 93-98.
54. S. Schacht, Q. Huo, I.G. Voigt-Martin, G.D. Stucky and F. Schüth, *Science,* **1996**, *273*, 768-771.
55. D.H. Everett, *Pure Appl. Chem.,* **1972**, *31,* 578.
56. H.F. Poulsen, J. Neuefeind, H.-B. Neumann, J.R. Schneider and M.D. Zeidler, *J. Non-Cryst. Solids,* **1995**, *188,* 63-74.
57. A.C. Wright, *J. Non-Cryst. Solids,* **1994**, *179,* 84-115.
58. J. Rathousky, A. Zukal, O. Franke and G. Schulz-Ekloff, *J. Chem. Soc., Faraday Trans.,* **1994**, *90*(18), 282 -2826.
59. N. Coustel, F. Di Renzo and F. Fajula, *J. Chem. Soc., Chem. Commun.,* **1994**, 967-968.
60. G.E. Bacon, *Neutron Diffraction*; 3rd ed., Oxford University Press, Melbourne, **1975**.
61. B. Jacrot, *Rep. Prog. Phys.,* **1976**, *39,* 911-953.
62. O. Glatter and O. Kratky, *Small Angle X-ray Scattering*, Academic Press, London, **1982**.
63. C.G. Windsor, *J. Appl. Cryst.,* **1988**, *21,* 582-588.
64. J. Teixeira in *On Growth and Form - Fractal and Non-Fractal Patterns in Physics*; NATO ASI Series, Series E: Applied Sciences, (Eds. H.E. Stanley and N. Ostrowsky), Martinus Nijhoff Publishers, Dordrecht, **1986**, *Vol. 100*, 145-162.
65. M. Bée, *Quasielastic Neutron Scattering*, Adam Hilger, Bristol, **1988**.
66. J.T. Koberstein, B. Morra and R.S. Stein, *J. Appl. Cryst.,* **1980**, *13,* 34-45.
67. P. Schmidt, *J. Appl. Cryst.,* **1982**, *15,* 567-569.
68. R.-J. Roe, *J. Appl. Cryst.,* **1982**, *15,* 182-189.
69. W. Ruland, *J. Appl. Cryst.,* **1971**, *4,* 70-73.
70. M. Roth, *J. Appl. Cryst.,* **1977**, *10*, 172-176.
71. L.E. Iton, F. Trouw, T.O. Brun, J.E. Epperson, J.W. White and S.J. Henderson, *Langmuir,* **1992**, *8*(4), 1045-1048.
72. *CRC Handbook of Chemistry and Physics*; 75th ed., (D.R. Lide, Ed.), CRC Press, Boca Raton, **1994**.
73. M. Aldissi, S. Henderson, J.W. White and T. Zemb, *Mat. Sci. Forum,* **1988**, *27/28,* 437-444.
74. R. Heenen and S. King in *ISIS User Guide*; (Eds. B. Boland and S. Whapham), ISIS, Rutherford Appleton Laboratory, Didcot, Oxon., U.K., **1992**.
75. R.K. Heenan and S.M. King in *International Seminar on Structural Investigations at Pulsed Neutron Sources Proceedings, 1992*; (Eds. V.L. Aksenov, A.M. Balagurov and Y.V. Taran), Joint Institute for Nuclear Research, Dubna, Russia, **1993**, 176.

76. J.E. Epperson, P. Thiyagarajan, J.M. Carpenter, R.K. Crawford and D.G. Wozniak in *IPNS Progress Report 10th Anniversary Edition*; (Ed. F.J. Rotella), Argonne National Laboratory, Argonne, IL, USA, **1991**, *Vol. 1*, 76.
77. NIST *Cold Neutron Research Facility*; National Institute of Standards and Technology, **1996**, 3.
78. B. Hammouda, S. Krueger and C.J. Glinka, *J. Res. Natl. Inst. Stand. Techol.,* **1993**, *98*(1), 31-46.
79. S.M. King and R.K. Heenan "The LOQ Instrument Handbook, Vol I," RAL-TR-96-036, Rutherford Appleton Laboratory Report, **1996**.
80. C. Glinka, *NG3 and NG7 30-Meter SANS Instruments Data Acquisition Manual*, National Institute of Standards and Technology Cold Neutron Research Facility, **1996**.
81. J. Penfold and S. King in *ISIS 1995 Rutherford Appleton Laboratory Annual Report 1994-1995*; (Ed. C. Wilson), CLRC, **1995**, 78-81.
82. B.E. Warren, *X-Ray Diffraction*, Dover Publications Inc., New York, **1990**.
83. R.F. Garrett, D.J. Cookson, G.J. Foran, D.C. Creagh and S.W. Wilkins, *Rev. Sci. Instrum.,* **1995**, *66,* 1687.
84. D.J. Cookson, R.F. Garrett, G.J. Foran, D.C. Creagh and S.W. Wilkins, *J. Japanese Soc. Synchrotron Radiation Research,* **1993**, *6*(1), 127-129.
85. A.W. Adamson, *Physical Chemistry of Surfaces*; 4th ed., John Wiley & Sons, New York, **1982**.
86. S.J. Gregg and K.S.W. Sing, *Adsorption, Surface Area and Porosity*; 2nd ed., Academic Press, New York, **1982**.
87. S. Brunauer, *The Adsorption of Gases and Vapours*, Princeton University Press, Princeton, New Jersey, **1945**, *Vol. 1*.
88. K.S.W. Sing, D.H. Everett, R.A.W. Haul, R.A. Pierotti, J. Rouquerol and T. Siemieniewska, *Pure & Appl. Chem.,* **1985**, *57*(4), 603-619.
89. K.J. Edler, P.A. Reynolds, P.J. Branton, F. Trouw and J.W. White, *J. Chem. Soc., Faraday Trans.,* **1997**, *93*(8), 1667-1674.
90. P. Dutta, S.K. Sinha and P. Vora in *Ordering in Two Dimensions*; (Eds. S.K. Sinha), North Holland Publishers, **1980**, 169.
91. P.J. Branton, PhD Thesis, University of Exeter, **1994**.
92. Y. Grillet, F. Rouquerol and J. Rouquerol, *J. Colloid Interface Sci.,* **1979**, *70,* 239.
93. C.E. Brown and P.G. Hall, *Trans. Faraday Soc.,* **1971**, *67,* 3558.
94. M. Nielson and W.D. Ellenson, *Annual Report Physics Dept., AEK, Risø,* **1975**, *Report No. 334,* 44.
95. M. Nielsen, *Phys. Rev. B,* **1973**, *7*(4), 1626-1635.
96. W. Langel, D.L. Price, R.O. Simmons and P.E. Sokol, *Phys. Rev. B,* **1988**, *38*(16), 11275-11283.
97. Y.D. Harker and R.M. Brugger, *J. Chem. Phys.,* **1967**, *46*(6), 2201-2208.
98. H. Kapulla and W. Gläser in *Inelastic Scattering of Neutrons in Solids and Liquids*; IAEA, Vienna, **1973**, 841-849.
99. B. Asumussen in *ILL Annual Report*; Grenoble, **1993**, 100-102.
100. W. Press, *Single Particle Rotations in Molecular Crystals*, Springer, Berlin, **1981**.

101. H. Zabel in *Neutron & Synchrotron Radiation for Consensed Matter Studies. Vol. 1 Theory, Instruments and Methods.*; Les Editions de Physique, (Eds. J. Baruchel, J.L. Hodeau, M.S. Lehmann, J.R. Regnard and C. Schlenker), Springer-Verlag, Berlin, **1993**, *Vol. 1*
102. J.A. Young and J.U. Koppel, *Phys. Rev. 3A,* **1964**, *135*, 603-611.
103. G.J. Kellogg, J.W. White, K.W. Herwig and P.E. Sokol, *J. Chem. Phys.,* **1990**, *93*(10), 7153-7162.
104. H. Jobic, M. Bée and G.J. Kearley, *Zeolites,* **1989**, *9,* 312-317.
105. H. Jobic, M. Bée and G.J. Kearley, *J. Phys. Chem.,* **1994**, *98*(17), 4660-4665.
106. A.J. Leadbetter and R.E. Lechner in *The Plastically Crystalline State (Orientationally-Disordered Crystals)*; (Ed. J.N. Sherwood), John Wiley & Sons, Chichester, **1979**.
107. F. Trouw in *IPNS Progress Report 1991-1996 15th Anniversary Edition*; (Ed. B. Marzec), Argonne National Laboratory, **1996**, *Vol. 1*, 50-55.
108. R.K. Crawford, T.G. Worlton and J.M. Carpenter in *IPNS Progress Report 1991-1996 15th Anniversary Edition;* (Ed. B. Marzec), Argonne National Laboratory, **1996**, *Vol. 1*, 100-111.
109. G.L. Gaines Jr., *Insoluble Monolayers at Liquid-Gas Interfaces*; Interscience Monographs on Physical Chemistry, (Ed. I. Prigogine), Interscience Publishers, New York, **1966**, *Vol. 1*.
110. K.S. Birdi, *Lipid and Biopolymer Monolayers at Liquid Interfaces*, Plenum Press, New York, **1989**.
111. P. Martin and M. Szablewski, *Langmuir Blodgett Systems, Tutorial and Operating Manual*; 3rd ed., Nima Technology Ltd., Milton Keynes, **1992**.
112. B.T. Ingram and R.H. Ottewill in *Cationic Surfactants: Physical Chemistry*; Surfactant Science Series, (Eds. D. Rubingh and P.M. Holland), Marcel Dekker Inc., New York, **1991**, *Vol. 37*, 87-140.
113. J.R. Lu, M. Hromadova, E.A. Simister, R.K. Thomas and J. Penfold, *J. Phys. Chem.,* **1994**, *98*(44), 11519-11526.
114. J.R. Lu, M. Hromadova, E. Simister, R.K. Thomas and J. Penfold, *Physica B,* **1994**, *198,* 120-126.
115. J.R. Lu, Z.X. Li, J. Smallwood, R.K. Thomas and J. Penfold, *J. Phys. Chem.,* **1995**, *99*(20), 8233-8243.
116. T. Wolff and G. von Bünau, *Ber., Bunsenges Phys. Chem.,* **1981**, *88,* 1098.
117. L. Sepúlveda and J. Cortes, *J. Phys. Chem.,* **1985**, *89,* 5322.

Chapter 4:

Development of Long Range Order in MCM-41

"I have yet to see any problem, however complicated, which, when you look at it in the right way, did not become still more complicated."

Poul Anderson.

MCM-41 is largely an amorphous silicate. The small angle diffraction peaks arise from the repeat distances between the hexagonally close packed channel system, rather than from regular atomic repeat distances. The silica framework gives no Bragg peaks suggesting shorter-range order. The number of peaks in the diffraction pattern therefore reflects the degree of long-range order - monodispersity and regular arrangement - in the channel packing. The earliest published patterns show up to three peaks,[1-3] however many published patterns show only the first order peak. Such materials have a very broad adsorption step in the nitrogen isotherms and TEM data show areas more reminiscent of Swiss cheese, than ordered honeycomb-like structures. Since the silicate walls of this material are not crystalline, the best strategy for improving the quality of the information from experimental data is to improve the long range order in the channel packing. This more uniform average structure would also make the interpretation of data from techniques which measure 'bulk' properties, such as X-ray and neutron scattering and gas adsorption isotherms, easier since smearing factors like polydispersity in channel dimension play a much smaller role in more ordered materials.

4.1 Introduction

The first synthetic work reported on MCM-41 was that of Beck *et al.*[1,2] Their work investigated the use of various surfactant chain lengths, various silica and alumina sources, and the effects of enlarging the surfactant micelles by swelling them with mesitylene. The materials they synthesised show up to four peaks in the X-ray diffraction patterns with BET surface areas over 1000 $m^2 g^{-1}$, and have crystals with distinct areas of hexagonal channel packing visible in electron micrographs. The peak width for these materials, measured from the published pattern, was 0.3• indicating a coherence length of around 280 Å. Further development of this material has been

centred on distinguishing the possible mechanisms of formation[4-9] as discussed in Chapter 1 and referred to again below. Another focus for development has been the incorporation of catalytically useful atoms, as referred to in Chapters 1 and 2. Synthesis of MCM-41 materials of approximately the same quality as those initially published have been shown to occur at a wide variety of temperatures, initial pH, reaction time and silica sources.[4,5,10-14]

Some further attempts at improving the quality of the MCM-41 material have been made. Stucky *et al.*[14] report X-ray diffraction data containing 5 to 6 peaks, although no details of the preparation are given. Other workers report that the presence of colloidal silica particles in the synthesis promotes the formation of the hexagonal mesophase.[15] The published diffraction patterns in that work, however, show only four peaks at best. Recently an optimisation of the pure silica preparation, using a different silica source to that used in this work, was published by Cheng *et al.*[16] They concluded that the best quality, pure silica MCM-41 was produced from a gel of molar composition 1.0 SiO_2/ 0.19 TMAOH/ 0.27 CTAB/ 40 H_2O aged at 20•C for 24 hours and then heated for 48 hours at 150•C. These materials have high surface areas and a narrow pore size distribution, but again show only five peaks in the diffraction patterns with a full-width-half-maximum of 0.11• indicating a coherence length of 750 Å.

The choice of surfactant template used in the synthesis appears to strongly affect the order of the final product. Materials showing seven peaks in the diffraction pattern have been synthesised from a pure silica preparation using TEOS and cetylpyridinium chloride as the surfactant template. The smaller area per headgroups for the quaternary ammonium ion and the more rigid and smaller micelles of this surfactant compared to those of the cetyltrimethylammonium surfactant were proposed as allowing a stronger interaction between the template and the silica surface, resulting in a more ordered composite.[17] Reforming MCM-41 materials, made in mixed surfactant systems, using a post-synthesis treatment of heating at 100•C at pH values between 7 and 10, also resulted in materials showing between 4 and 8 peaks in the X-ray diffraction patterns.[18]

A synthesis published by Ryoo and Kim,[19] involving the titration of the alkaline MCM-41 synthesis gel with acetic acid during heating, also produced materials with good long range order. Their synthesis resulted in materials showing four to five peaks in X-ray diffraction patterns, with the ordering effect being reversible by addition of NaOH to the gel. This method has been further investigated below and optimised for the reagents used in this work.

The optimisation of the pure silica MCM-41 synthesis, described in Chapter 2, is discussed in detail in this chapter with regard to several variables. The simplest preparations are discussed first -unheated syntheses in which the major variable is aging time in the gel. Experiments using the Langmuir trough and investigating shear on unheated gels are discussed next as they shed some light on processes occurring in this simple system. The effect of pH in unheated syntheses is then discussed in some detail. Secondly, heated preparations are discussed. The investigation of the effects of heating time, and stirring during heating on the initial straightforward preparation is described. This is followed by a discussion of the effects of maintaining a pre-determined pH

during the heating phase of the synthesis, and an investigation of the effects of the various types of acid used in pH adjustments. The stability of materials from each of these four types of preparations; unheated, ordinary, and acid-titrated, and heated, ordinary and acid-titrated, is then reported. A brief description of the exact methods used for preparing each set of samples discussed is given below, to promote clarity in the following discussions. For a detailed preparative description and exact quantities used in each preparation, see Chapter 2 and the Appendix.

4.2 Unheated Syntheses

Unheated MCM-41 syntheses are interesting for a number of reasons. Firstly, at lower temperatures it is possible that the silica-surfactant and silica condensation reactions may occur more slowly, allowing data collection and observation of structure developments on measurable time scales. Secondly, milder reaction conditions may allow the use of more fragile template molecules, or alter the phase diagram of the surfactant used. An unheated synthesis resulting in materials of similar quality to those made from a heated synthesis would also be a considerably cheaper process for industrial applications.

Previously the formation of a templated aluminosilicate MCM-41 at 25•C in an alkali preparation has been reported briefly by Stucky *et al.*[14] who noted a lack of hydrothermal, thermal and mechanical stability for this compound compared to that obtained from a heated preparation. However, considerable retention of structure is found in the present work for molecular sieves prepared using a version of the procedure published by Beck *et al.*[2] The stability of these compounds is probably due to the condensation reactions which occur during aging. The previous work by Stucky *et al.*[14] does not specify the time between the creation of the reaction mixture and sample removal. Other reports have found that silicate phases synthesised at room temperature can be isolated as solids, which are stable to calcination, after synthesis times as short as five minutes.[7] The silicate source used was found to determine the appearance time for the X-ray diffraction pattern, with soluble silicates giving the most condensed products. Samples associated with the very early stages of a preparation showed the characteristics of a salt, including dissolution when placed in distilled water.[7] Hexagonal phase mesoporous silicates can also be obtained from ambient temperature preparations using cationic, neutral or anionic surfactant templates.[20] In the case of anionic and neutral surfactant templating, a more ordered product was found to result from ambient temperature preparations than from heated syntheses, although the reverse was true for cationically templated syntheses.

Formation of a hexagonal mesoporous pure silica product, templated around a primary ammonium ion, dodecylamine, in an acidic preparation at ambient temperature was also reported by Tanev *et al.*[21] and the material was stable to calcination, but no characterisation of the surface properties was reported. Antimony oxide and tin sulphide surfactant templated mesophases have also been synthesised at ambient temperatures,[7] as have mesoporous silicates containing aluminium, gadolinium, iron and boron.[22] Other workers have examined the unheated synthesis gel to obtain mechanistic information,[10,12,13,23-25] but were not concerned with isolating a final,

calcined product from such preparations. Up to 24 hours of aging at room temperature before heating has been found to improve the final long range order in pure silica MCM-41 materials heated during synthesis.[16]

4.2.1 Ordinary Preparations

A brief description of the experimental procedures used to investigate unheated ordinary preparations is given below. This section also contains work carried out on the Langmuir trough, and shear experiments on unheated salted synthesis gels. The preparations in each of the latter cases were based on the ordinary unheated MCM-41 synthesis and so are discussed alongside that section of the work.

A solution of sodium silicate was diluted with Millepore filtered water and slightly acidified. This was stirred for ten minutes. A CTAB in water solution was heated to 80•C for 45 minutes and added to the first solution. This mixture was stirred for 30 minutes before further water was added and the resulting synthesis gel stirred for another five minutes. Some of this solution was loaded into a sealed 1.5 mm diameter X-ray capillary, and the X-ray pattern of this gel collected for two hour intervals for 24 hours to observe the progress of the reaction. From this point, the remaining synthesis gel was sealed and left to age with aliquots being removed at 3, 7, 11, 16 days and 7 months. These samples were filtered, washed with hot water and dried in a desiccator before being calcined under air at 350•C.

Other mechanistic information was obtained by a series of experiments on a Langmuir trough. A monomolecular layer of $(C_{18}H_{37})_2N(CH_3)_3Br$ (25-30 µl of 0.996 mg ml^{-1} solution) was spread from distilled chloroform on a clean water surface on the Langmuir trough. Pressure-Area isotherms of newly spread films of this surfactant were performed at barrier speeds of 50 and 20 cm^2 min^{-1} both continuously, and by raising the pressure to 5 mN, 15 mN and 30 mN, with a 20 minute pause between successive steps. The association of silicate with the surfactant headgroups was then monitored by spreading a new surfactant film, compressing to a pressure of either 5, 15, or 30 mN and injecting various amounts of neat sodium silicate solution under the barriers on the opposite side from the film. Pressure against time information was recorded for these systems, and the compression behaviour of the film which had developed after one hour was investigated.

Similar experiments were done using CTAB solutions at concentrations below the critical micelle concentration, (cmc) (0.8-0.9 mM),[26,27] by looking at the surface excess of the surfactant. The surfactant solutions used were below the cmc, to avoid the instantaneous formation of insoluble MCM-41 particles upon the addition of sodium silicate solution to the system. For these experiments, a 5.94×10^{-4} M solution of CTAB in water was prepared and poured into the trough. Isotherms were run at barrier speeds of 50 and 100 cm^2 min^{-1} at five minute intervals. A second solution was prepared by adding 100 ml of water to 300 ml of the first CTAB solution, and a similar set of isotherms run. The behaviour of the film in the presence of sodium silicate solution was then investigated by adding 0.10 ml of sodium silicate solution in 100 ml water to 300 ml of the first CTAB solution and recording a further set of isotherms with a barrier

speed of 100 cm^2 min^{-1}. Each isotherm required about five minutes to run at that speed and the film was allowed to develop for five minutes between each compression. The pressure sensor was not re-zeroed between these isotherms so that the overall increase in surface pressure could be observed. The solution turned slightly cloudy upon the addition of sodium silicate solution.

In other experiments on unheated synthesis gels, the shear ordering of such gels from an ordinary preparation was investigated. The Couette shear cells available on the small angle neutron scattering machines at the Rutherford Appleton Laboratory, UK and at the National Institute of Standards and Technology, USA were used in these studies. These are shear cells are described in Chapter 3. A number of gels were studied, containing various amounts of CTAB, sodium silicate solution and KBr. The quantities in the gels studied, and whether ordering under shear was observed for that gel, are given in Table A1.2, in the Appendix. The experiment on preparation containing 0.19 M CTAB, despite showing some signs of shear at low temperatures and low shear rates was not continued as the shear cell failed at that point.

4.2.2 Acid Titrated Preparation

From other published work, it has been shown that the addition of dilute acid to an alkaline MCM-41 synthesis during heating to maintain the synthesis gel at a particular pH value during heating results in materials with much greater long range order than those achievable from ordinary synthesis methods.[19,28] These methods were therefore also applied to an unheated synthesis to see if a similar improvement would result.

Table 4.1 *Measured pH for the unheated synthesis gel after various aging times and the amount of 1 M acetic acid titrant required to return the gel to pH = 11.*

Aging Time / days	Initial pH	Acid Added / ml
0	11.42	16.5
7	11.17	2.0
14	11.14	1.0
21	11.02	0.2
35	11.02	0.2
64	11.04	0.2

A MCM-41 synthesis gel of total initial volume *ca.* 250 ml was made up as for an ordinary preparation. After the final period of stirring, the pH of the solution was measured. A titration was performed on the solution with 1 M acetic acid in order to bring the pH to 11. The preparation was then sealed, and allowed to age for seven days, the pH measured again, and a titration performed to return the solution to pH = 11. This was repeated after 14 days, 21 days, 35 days and 64 days. Samples of the wet gel for SAXS pattern determination were taken from the start gel, and before and after every acid addition. The pH before acid addition and the amount of acid added at each

titration are shown in Table 4.1. Samples were also taken after each acid addition, filtered, washed, dried and calcined in order to determine the stability of these materials.

4.3 Results and Discussion of Unheated Syntheses

The discussion which follows is divided into several parts. Firstly, the Langmuir trough work is discussed, since it investigates the association of the silicate anions with the surfactant molecules - an association which is responsible for the initial ordering in the MCM-41 synthesis, and which occurs on time-scales too fast to be accessible to the other methods used. Discussion of the more typical unheated MCM-41 syntheses follows, using the preparation stages as a natural division.

4.3.1 Langmuir Trough Experiments

Pressure-area isotherms run on films of the $(C_{18}H_{37})_2N(CH_3)_3Br$ surfactant spread from chloroform show a continuous, rising trend, typical of a stiff liquid condensed monomolecular film,[29] which compresses uniformly without a sudden phase change or buckling of the film. The limiting area per headgroup of the molecule was 81(5) Å^2 in a freshly spread film compressed at 50 cm^2 min^{-1}, but decreased to 74(2) Å^2 after allowing relaxation for one hour.

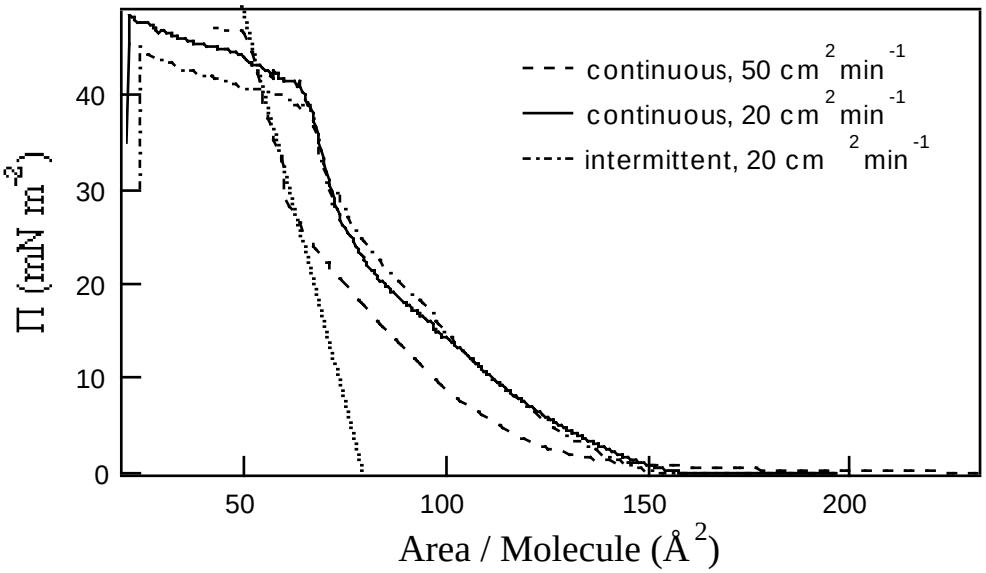

Figure 4.1 *Isotherms of a film of $(C_{18}H_{37})_2N(CH_3)_3Br$ (30 µl of 0.996 mg ml^{-1} solution) run immediately after spreading with two different barrier speeds, both continuously, and with 20 minute pauses at 5, 15,and 30 mN m^{-2}. The dotted line intersecting the Area/Molecule axis indicates the limiting area for the continuous compression carried out at 50 cm^2 min^{-1}.*

The isotherms for continuous compression are shown in Figure 4.1. The dotted line indicates the limiting area per headgroup for the 50 cm^2 min^{-1} compression. The plateau after this steeply sloping region is an area of film collapse where the monolayer is lifting off the surface and collapsing to form multilayer islands or regions of crumpled

film. Since this region is not flat, but is still increasing in pressure with decreasing area, the collapse process is being driven by the continuing compression of the film. Similar behaviour has been seen in films of insoluble short chain polystyrene surfactants.[30] It is not necessarily reproducible between compressions. The dramatic drop in surface pressure after this plateau region is probably due to the meniscus at the barrier interacting with the pressure sensor or the formation of a solid film which pushes the paper pressure sensor away from the vertical position.

Isotherms of this material run at 20 cm^2 min^{-1} with several pauses for 20 minute intervals at various pressures appeared similar to those shown in Figure 4.1. Preliminary isotherms were also run on clean water sub-phases injected with sodium silicate solution and allowed to age for 20 minutes in the absence of surfactant to confirm that no was film formed at the water surface in the absence of surfactant. No pressure increase on compression was observed in those experiments.

To investigate the effects of adding the silicate anions, the $(C_{18}H_{37})_2N(CH_3)_3Br$ film was compressed at 20 cm^2 min^{-1} to a pre-set pressure of 5, 15 or 30 mN m^{-2} and a measured amount of neat sodium silicate solution injected from a syringe under the barrier on the far side from the film. The pressure at constant area was then monitored with time. The pressure increased as the silicate anions reacted with the surfactant headgroups. The increase was greatest for the film at 15 mN m^{-2} initial compression, and for the largest amount of sodium silicate solution injected into the sub-phase. The increases in pressure with time are shown in Figure 4.2. The fact that the increase in pressure is slightly smaller for the film compressed to 30 mN m^{-2} than that at 15 mN m^{-2} may indicate that the distance between surfactant headgroups is less favourable to the silicate condensation reaction at the higher pressure.

The limiting area per headgroup in the film grown at 15 mN m^{-2} is 90(1) $Å^2$ whereas at 30 mN m^{-2} it is 72(1) $Å^2$. For comparison, the area per headgroup in a CTAB micelle is typically 78.1 $Å^2$ for a 0.1 M CTAB solution[31] or, using neutron reflectometry to measure adsorbed molecules at the air/liquid interface, 43±3 $Å^2$ for a solution at the cmc (0.92 mM)[32]. The double chain surfactant, $(C_{18}H_{37})_2N(CH_3)_3Br$ has a larger headgroup surface area due to the extra bulky hydrocarbon chain. In comparison with the bulk silicate/CTAB composite phases, an area per CTAB headgroup of 67.1 $Å^2$ has been reported for hexagonal phase MCM-41, and 59.7 $Å^2$ for the lamellar phase composite.[14] The expansion between the area per headgroup for free CTAB at the air-water interface or a pure CTAB lamellar phase (42.8 $Å^2$)[14] and in a lamellar phase silica/CTAB composite is *ca.* 17 $Å^2$ from the results quoted above. For a CTAB hexagonal phase compared to the silica/surfactant analogue the expansion is 24.1 $Å^2$. From the measurements of the double-chain surfactant film carried out in this work before and after silica addition at 15 mN m^{-2}, the expansion upon the addition of silica is 16 $Å^2$. This may indicate that the film formed under these low concentration conditions is similar to lamellar phase silica/surfactant composites normally found at much higher concentrations and that the silicate anion has considerable effect upon the ordering of the film.

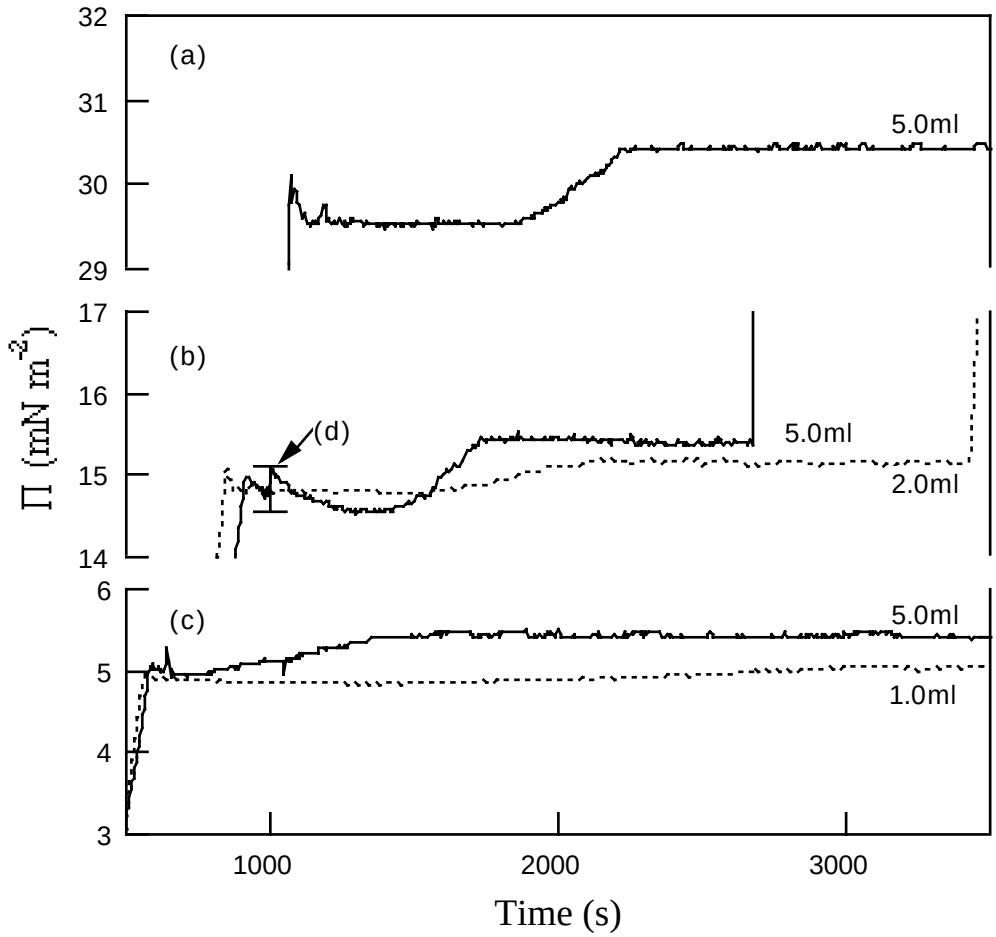

Figure 4.2 *Pressure against time after injection of sodium silicate solution under the $(C_{18}H_{37})_2N(CH_3)_3Br$ film compressed initially to (a) 30, (b) 15 and (c) 5 mN m^{-2}. The solid lines correspond to experiments where 5.0 ml of neat sodium silicate solution was injected into the subphase. The dotted lines indicate other experiments where the amount of sodium silicate solution injected is shown below the line. The point (d) indicates the decrease in pressure between the end of compression and the beginning of the silicate-surfactant reaction.*

The pressure of the film decreases slightly when compression is stopped, (shown at point (d) in Figure 4.2) before the silicate-surfactant reaction causes the pressure increase to begin. Since this initial decrease is largest at highest pressures it would seem to suggest some rearrangement of the film to achieve better packing at that pressure. This indicates that the compression rates used were too high for the film to remain in an equilibrium configuration during compression. There appears to be an induction period of about 1000 seconds between the injection of the silicate solution and the beginning of the pressure rise. This is probably due to the time required for the anions to diffuse under the barrier and towards the film. There will also be a gradient of silicate concentration across the film with areas of the film which are closest to the point of injection reacting with the diffusing species first. Straight lines fitted to the region of increase in pressure give slopes ranging from 0.00012 mN m^{-2} s^{-1} for the film compressed to 5 mN m^{-2} with 1.0 ml of sodium silicate injected into the sub-phase, to a maximum rate of 0.0029 mN m^{-2} s^{-1} for the film compressed to 15 mN m^{-2} with 5.0 ml of sodium silicate injected into the sub-phase.

After the pressure-time curve became constant in each system, the compression was continued at 20 cm^2 min^{-1} to see if the presence of the silicate affected the film behaviour. These pressure-area curves are shown in Figure 4.3. The slight kink in each curve at the pausing pressure (indicated by arrows in Figure 4.3) are artefacts due to the area sensor attempting to reconcile the pressure changes in the film due to the reaction with its last recorded area/pressure reading.

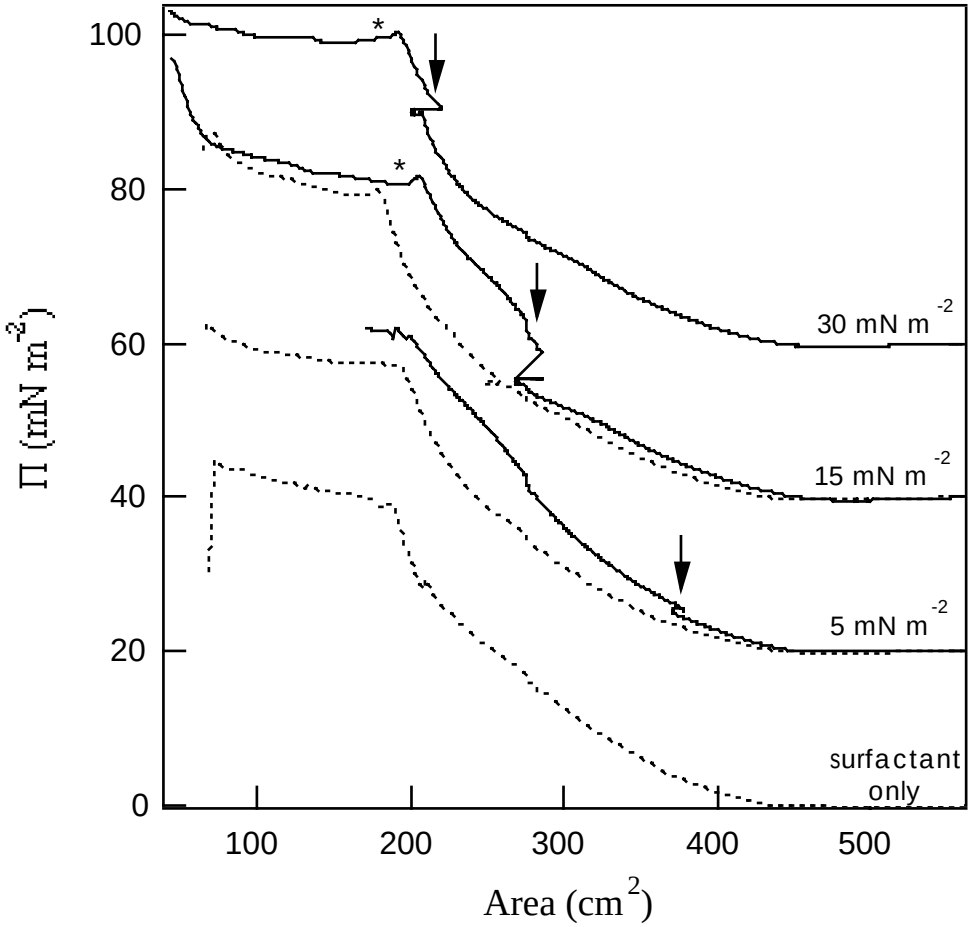

Figure 4.3 *Pressure-area curves for films of $(C_{18}H_{37})_2N(CH_3)_3Br$ compressed to a particular pressure, then held at constant area for the injection of sodium silicate solution into the sub-phase. Compression was continued after the silicate-surfactant reaction appeared to have finished. Solid lines indicate experiments where 5.0 ml of sodium silicate solution was added to the sub-phase. Dotted lines indicate the surfactant only pausing experiment (bottom), and experiments where 1.0 ml of sodium silicate was added to the run paused at 5 mN m^{-2} and 2.0 ml was added to the run paused at 15 mN m^{-2}. The curves sets are offset by 20 mN m^{-2} for clarity. Arrows indicate the pause point on each isotherm, and * indicate the collapse point peaks.*

The shape of the pressure-area curves are similar to those of the pure surfactant, however the film pressure for a given area is higher in those curves where the pressure increased markedly during the addition of silicate than in the surfactant only curve. The small peak at the collapse point (*ca.* 40 mN m^{-2}) becomes more pronounced in these films also. This would appear to indicate the formation of a more rigid film, with a

larger limiting area for the headgroups once the silicate polymerisation has occurred, *eg.* around 99(5) Å^2 for the run where the silicate association occurred with the film at 30 mN m^{-2} during the reaction. Overlaying the curves for 5.0 ml of sodium silicate solution injected under the barrier shows that prior to the addition of silica, the curves follow the surfactant only curve, as expected. After silicate addition at 15 or 5 mN m^{-2} the pressure-area curves increase in pressure, and overlay almost exactly. The curve after silicate addition at 30 mN m^{-2} also increases in pressure but does not reach congruence with the other two curves. This may indicate that the film grown at 30 mN m^{-2} is less stiff than those grown at the other compressions, possibly because the headgroups of the surfactant were too close together for optimum silicate interactions.

A second Langmuir trough experiment was carried out to observe the surface excess in a CTAB solution and the effects of adding silicate anions to this solution. Continuous compression isotherms for the CTAB solutions alone showed a smooth, increasing trend which increased in pressure the longer the solution was left in the trough. Adding sodium silicate solution to the CTAB solution before loading it into the trough caused the solution to become slightly cloudy. The isotherm behaviour changed, becoming more like the liquid expanded isotherms typical of insoluble, long chain surfactants,[29] with an abrupt change of slope at *ca.* 6 mN m^{-2}. Allowing this solution to age on the trough for ten minute intervals caused the pressure of the surface film to rise even when the barriers were fully open. Figure 4.4 shows the increase in the pressure at largest area with time as the silicated CTAB solution was allowed to age in the trough, as well as the changing behaviour of the isotherms from periodically compressing the resultant film.

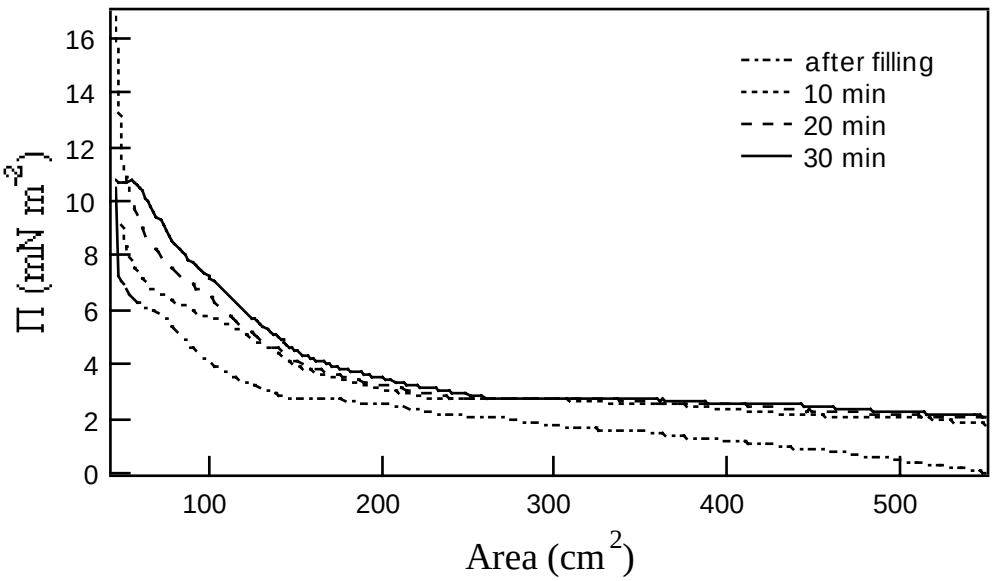

Figure 4.4 *CTAB (0.45 mM) and sodium silicate (1.5 mM SiO_2) solution isotherms run with a barrier speed of 100 cm^2 min^{-1}, run immediately after filling the trough, and then at 10 minute intervals to watch film development.*

The point at which the slope changes appears to move from *ca.* 6 mN m^{-2} in the first two compressions, to about 8 mN m^{-2} in the compressions done after 20 and 30 minutes. Also in the 30 minute isotherm, the limiting behaviour of the film becomes a collapse at around 10.5 mN m^{-2} rather than the sharply increasing trend with pressure shown in the earlier films. These changes in the film compression behaviour indicate the development of a rigid film at the air-water interface, which is probably an array of silicated surfactant micelles.

No other kinetic studies of silica-surfactant films appear in the literature. Previously it has been reported that monolayers of 2- and 4- heptadecyl-pyridine 1-oxide on an under-saturated solution of monosilicic acid form solid films,[33] and monolayers of polyvinylpyrrolidone (PVP) became rigid when spread on water containing 282 ppm SiO_2.[34] In this cases the interaction between the organic molecules and silica was described as hydrogen bonding between the SiOH of silicic acid and the carbonyl group of the PVP. In the former case it was postulated that the monomer was collected at polar groups in the film and possibly polymerised, with the polysilicic acid/silica particles being stabilised by the organic monolayer to prevent re-dissolution.[35]

Other workers have found in a MCM-41 synthesis solutions that silicated surfactant micelles will aggregate in an orientated film at mica surfaces,[36] and at the air-water interface in acidic, heated MCM-41 preparations.[37] It therefore seems plausible that this will also occur at the air-water interface for alkaline silicated surfactant solutions as indicated by the isotherms above. Mesoscopic films grown at mica, graphite and amorphous silica/water interfaces from dilute acidic TEOS solutions with an excess of surfactant have also been reported.[38] These films display distinctly different textures in TEM and AFM images, which were related to the nature of the substrate used. It seems likely that films grown from alkaline solutions at room temperature will have similar textural properties, however, no electron microscopy or AFM work was done on the films in this work. Thin films of hexagonal phase mesoporous materials have also been created by dip or spin coating of synthesis solutions onto various substrates.[39] These will probably have quite different properties to films grown onto substrates from solution.

4.3.2 Unheated Wet Synthesis Gels

The SAXS measurements on the unheated wet synthesis gel from an ordinary MCM-41 preparation show that the characteristic major diffraction peak, at a Bragg *d*-spacing of 42 Å, appeared in the earliest pattern recorded (one hour from the last mixing of the preparation). It persisted at the same *d*-spacing and with almost the same intensity, at room temperature, for the whole of the period covered by the experiment (see Figure 4.5). This major diffraction peak arises from the hexagonal templated surfactant/silica precursor which results in MCM-41 in the standard preparation. This behaviour was also noted by Ortlam *et al.*[40] who report a similarly unchanging diffraction peak in aluminosilicate/cetyltrimethylammonium chloride (CTAC) gels aged for longer than one hour.

One experiment on unheated synthesis gels investigated decreased surfactant concentrations. It was found that the MCM-41 first order diffraction peak was observed even in gels containing only 1.0 wt%* surfactant, although the peak intensity was much reduced from gels with normal CTAB concentrations. This concentration is above the cmc of pure CTAB (0.03 wt% *ie.* 0.8-0.9 mM).[26,27] No peak was observed in a solutions at, or well below the CTAB cmc at 0.03 and 0.015 wt% surfactant. In the Langmuir trough work, no MCM-41 X-ray diffraction peaks were found for solutions containing only 0.45 mM (0.017 wt%) CTAB, even though there was evidence of the silica-surfactant association. This suggests that the presence of CTAB micelles is necessary for formation of MCM-41 in this version of the preparation, although it is clear that the addition of silicate anions alters the phase diagram of the surfactant system.

This agrees with other reports[13,24] which have reported the MCM-41 first order peak in solutions with CTAB concentrations as low as 0.5 wt%, but not at template concentrations below the cmc. Formation of MCM-41 materials at surfactant concentrations below the cmc has been reported, although it is concluded that addition of the silicate drives the phase diagram to lower concentrations in that case (*ie.* the cmc becomes lower for the silicated-surfactant species).[41] The diffraction pattern of the solution at low CTAB concentrations is observed to change upon silica addition, from the broad hump characteristic of an isotropic micellar distribution, to a sharp peak consistent with the formation of the ordered hexagonal silica-surfactant array.[13]

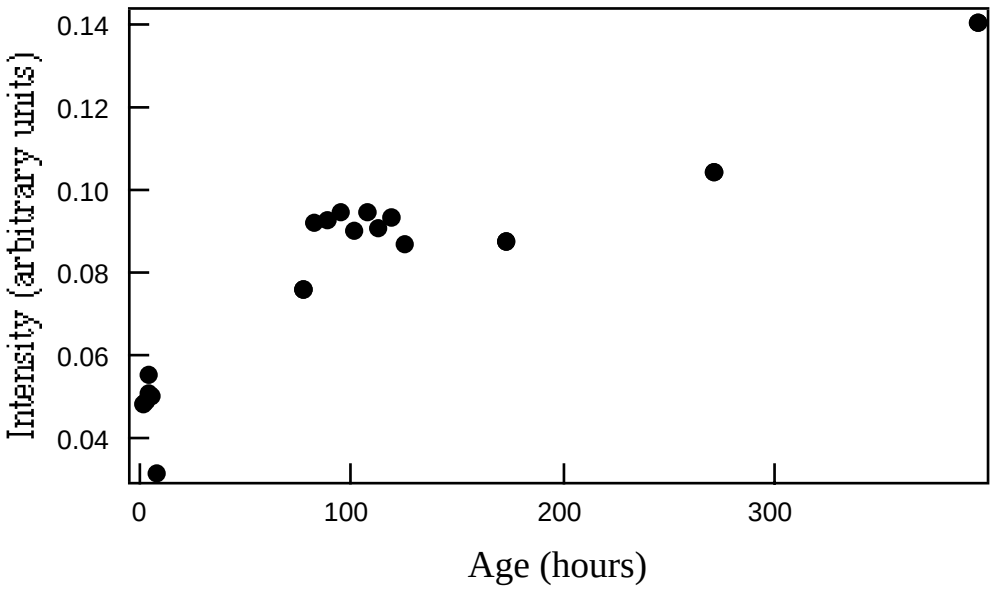

Figure 4.5 *Variation of peak height with aging time in an unheated synthesis gel. SAXS patterns were taken of the same, sealed sample over time to avoid variations in sample packing density.*

The data in Figure 4.5 suggest that this structure is formed almost immediately upon the preparation of the synthesis gel and no further structural changes occur on aging. Peaks at 26 Å and 13 Å were assigned to the lamellar crystalline form of CTAB, which is

* *Concentrations given as wt% refer to weight per weight per cent in all cases.*

present in the synthesis gel. A typical SAXS pattern from an unheated synthesis gel is shown in Figure 4.6. No lamellar silica/surfactant phase was identified at any point in the synthesis gel, unlike that observed by Monnier *et al.*[10] However, the lamellar phase in that case was observed at times between 1 and 20 minutes after the preparation of the synthesis gel, whereas these measurements were taken on time scales of hours.

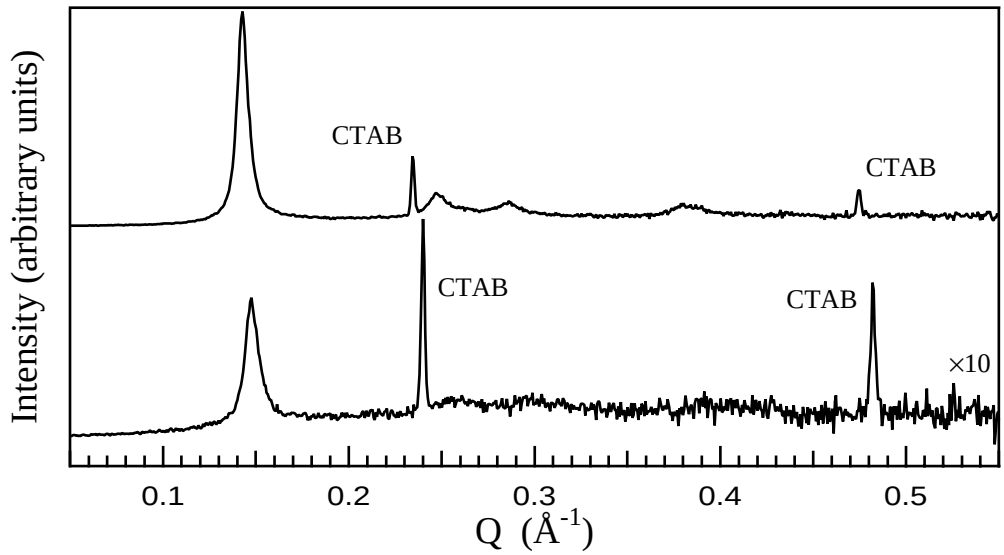

Figure 4.6 *A typical SAXS pattern of a MCM-41 synthesis gel from an unheated ordinary preparation after 16 days (below) and from an unheated acid titrated preparation after 14 days (above). The bottom trace has been multiplied by a factor of 10 to facilitate comparison of the second and third order peak development.*

Figure 4.6 also shows the effects of titration on the development of order in the reaction gel. The gel was titrated with 1 M acetic acid to maintain an approximately constant pH, of 11. The intensity of the first order hexagonal MCM-41 peak is greatly increased, and the second and third order peaks become more intense. The peaks also become slightly narrower, reflecting larger regions of coherent channel structure. The crystallite size calculated from the peak widths via the Scherrer equation is about 1300 Å in the wet gels of the ordinary preparation, and about 1600 Å in the acid titrated gels. The crystallite size in the acid titrated preparations appears roughly constant after the first acid addition, being 1650 Å for both the sample taken after only one acid addition and the sample taken after 64 days aging in the gel and six acid titrations. The peak height increase does not occur immediately upon addition of the acid to the synthesis gel, but develops as the solution is left to age at room temperature. Figure 4.7 shows the peak height as a function of aging time and acid addition. The peak intensity increases with aging time and acid addition up to about 14 days then, levels off. This behaviour reflects the amounts of acid titrant necessary to bring the gels back to the predetermined pH value as the synthesis proceeds - initially larger amounts of acid are necessary, decreasing by a factor of 10 over the first few titrations and then, past 14 days, smaller and roughly constant amounts are required to maintain the required pH (see also Table 4.1). The crystalline CTAB peaks at 13 and 26 Å are also present in the acid titrated gels at all stages of the preparation, indicating the presence of an ‘excess’ of template. Acid titrated, heated gels, discussed below, with an identical stoichiometry, lose these surfactant peaks after about two days heating, indicating a more efficient use of the

template in those systems. Possibly the low solubility of CTAB at room temperature prevents the uptake of the template in these unheated reaction systems. Nevertheless, the crystalline CTAB peaks are less intense in the unheated acid titrated preparations than in the ordinary MCM-41 gels suggesting that more is incorporated into the composite material in these solutions.

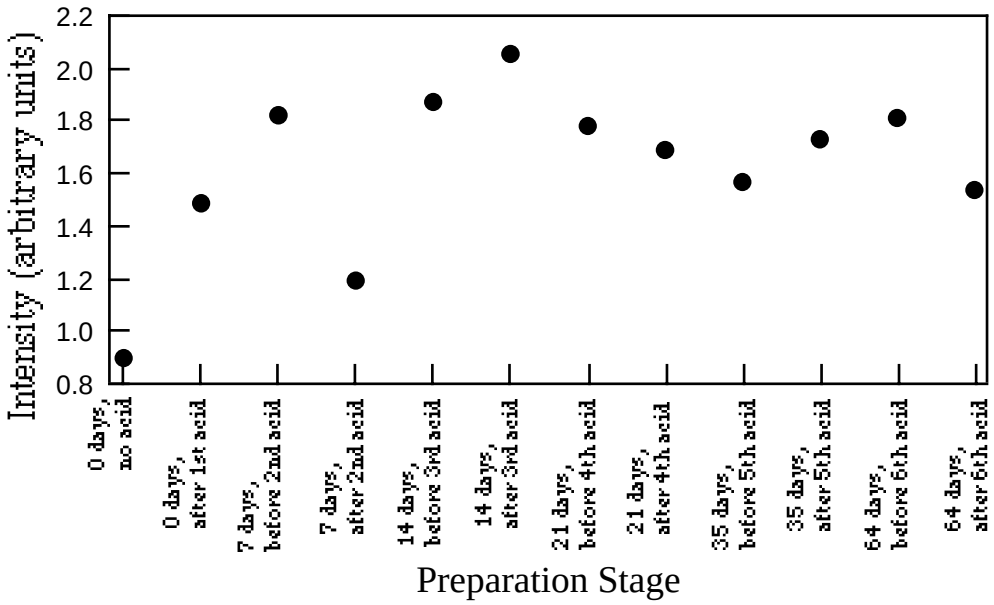

Figure 4.7 *Increase in peak height with acid addition and aging time in an unheated synthesis gel titrated against 1 M acetic acid to maintain a pH of 11.*

4.3.3 Shear Experiments on Wet Synthesis Gels

In heated synthesis experiments concurrent with these unheated experiments, MCM-41 preparations which had been stirred during heating appeared to contain phases other than the usual hexagonal MCM-41 phase, since they showed compound peaks.[42] The effect of controlled shear on the unheated preparations was therefore investigated. Synthesis gels from ordinary MCM-41 preparations were observed under shear using small angle neutron scattering. Gels containing no added salts (*ie.* having the same composition as an ordinary MCM-41 preparation) showed the usual 10 Bragg peak at $Q = 0.15$ Å^{-1} and this peak was remarkably resilient under shear, remaining almost undegraded in fresh and slightly aged gels even up to shear rates of 10,000 s^{-1} and at 7500 s^{-1} over several hours. Figure 4.8 shows the changes in the peak intensity of a five day old synthesis gel during nine hours at 7500 s^{-1}. No further alignment in these gels was observed.

Orientational ordering under shear is observed for pure CTAB solutions only in the presence of added salt. Hayter and Penfold[43] and Cummins *et al.*[44] observed shear ordering in solutions of 0.03 M CTAB/ 0.4 M KBr at 313 K and 1500-7500 s^{-1}. It was therefore decided to add salt to the synthesis gels, starting with a pure CTAB system and gradually increasing concentration of both CTAB and sodium silicate in the system until conditions close to those used in ordinary preparations were reached. The

concentrations of various reagents used, the shear rates, temperature and result for each set of conditions are reported in Table A1.2 in the Appendix.

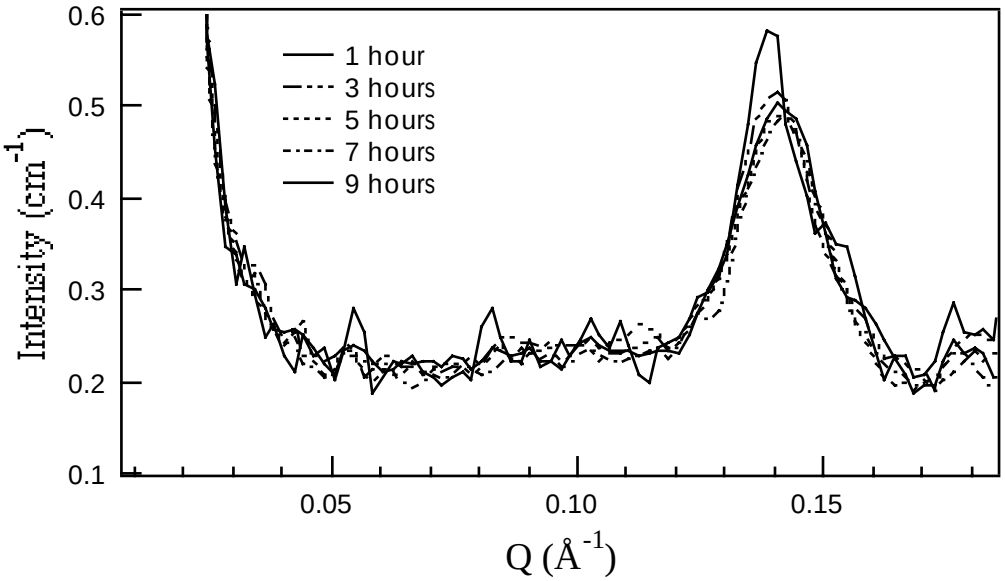

Figure 4.8 *A five day old MCM-41 synthesis gel under shear at 7500 s^{-1} for nine hours showing little decrease in peak intensity during this time.*

Initially alignment was achieved for CTAB/KBr gels using CTAB concentrations as high as 0.12 M. Alignment was also achieved in several silicate-surfactant-salt systems in certain temperature ranges for shear to 5000 s^{-1}. The best alignment was achieved in a 0.12M CTAB/ 0.2M KBr/ 3.81 wt% silicate gel at 5000 s^{-1} at temperatures between 303-323 K, although the best alignment occurred at 313 K. Experiments using this gel are shaded in Table A1.2. Dropping the temperature below 303 K resulted in a loss of orientation, but it returned once the temperature was raised. Lower shear rates at a temperature of 303 K also resulted in a loss of orientation, however at 313 K orientation occurred for shear rates of 1500 and 3000 s^{-1}. This is one third of the usual CTAB concentration in an ordinary MCM-41 preparation (which has 0.36M CTAB) but is the same concentration in silicate.

The most accurate prediction of alignment occurring in the gels was their appearance. If the gel appeared to contain crystals, then it would not align. Preparations that were only slightly cloudy would sometimes align if heated, probably due to the crystals dissolving at the higher temperature. Occasions where the silicate gelled when H^+/D_2O was added to it during preparation of the gel prior to mixing with the CTAB solution also formed solutions which did not align. Experiments using the addition of NaOH and H_2SO_4 to the system to observe the effects of Na_2SO_4 as the added salt did not achieve orientation under shear. Oscillatory shear on a 0.12M CTAB/ 0.2M KBr/ 3.81 wt% silicate gel at 313 K caused considerable bubbling in the solution but did not cause alignment.

At higher CTAB and salt concentrations several gels were prepared that were extremely susceptible to shear ordering - they became aligned merely by loading them with a syringe into a quartz 1.0 mm wide SANS cell and retained that alignment over several days. Further shear in the shear cell did not appear to have any ordering effect, and

destroyed the initial ordering. Some of the salted gels also appeared to undergo shear-thickening, resulting in a loss of containment of the sample. Unfortunately no facilities have been available for a rheological study of these gels. SAXS carried out on the salted synthesis gels showed the development of at least the 10 diffraction peak in all samples, although the peak shape was often distorted compared with ordinary preparations.

The rheological evolution of sols composed of TEOS, water and quaternary ammonium surfactants of various chain lengths prior to the gelation of the silicate have been studied. It was found that the hexagonal mesophase appeared at the point of gelation.[45] Before gelation the solutions were isotropic and fluid. As the reaction progressed the flow behaviour of the sol evolved from Newtonian to thixotropic behaviour. The storage modulus and loss modulus both increased near the gelation point, although a reproducible decrease of the loss modulus before the appearance of the mesophase, for C_{14} surfactant-containing sols, was noted.[46]

Lee *et al*.[47] report a detailed study of the effects of sodium silicate solution (3.98 wt%), with and without extra sodium hydroxide, upon the rheological behaviour of cetyltrimethylammonium chloride (CTAC) solutions. They found that the addition of sodium silicate resulted in the formation of flexible wormlike micelles at all concentrations studied (1.0-25.0 wt% CTAC) whereas pure CTAC solutions contained smaller rigid rod-like micelles at the these concentrations. No precipitation of these micelles was observed, unlike the CTAB/sodium silicate solutions used in the present work. Weak shear thinning as well as the formation of flexible wormlike micelles was noted by the same workers in tetramethylammonium (TMA^+) silicate /CTAC solutions with CTAC concentrations of 4-18 wt%. This shear thinning was explained as being due to greater polymerisation of the silicate at the micelle surface occurring due to the presence of the TMA^+ ion which promotes polymerisation.[47] The presence of unreactive ions from NaCl (3.98 wt%) in CTAC solutions, used as a control solution, did not cause the formation of flexible wormlike micelles, but went formed rigid rod-like micelles in similar concentration regimes. They do not report any X-ray scattering work on these solutions. Other workers[9] have carried out rheological studies on the surfactant solutions in the concentration range used in MCM-41 preparations but did not add silicate anions to the gels. Rheological work has been reported on microemulsion gels containing tetraethylorthosilicate, formamide, CTAB, decanol and decane,[48] but it was concluded that this system had behaviour typical of a gel consisting of clusters and linear polymers of silica.

4.3.4 Washed and Dried Materials from Unheated Gels

The stability of the MCM-41 structure from unheated preparations to washing and drying was investigated by SAXS measurements on the resultant powders. This procedure produced a lattice contraction of approximately 2±1 Å (see Table 4.2 over page). The variation in the degree of contraction observed may be due to different degrees of dehydration caused by slightly different drying times, but generally, the removal of water from the hexagonal network causes a shrinkage and this has been noted elsewhere.[5] That this contraction occurs without significant loss of diffraction

intensity indicates an interesting flexibility of the silica walls of the composite. (A similar contraction is noted when material which has been heated during synthesis is washed and dried (see Table 4.4)).

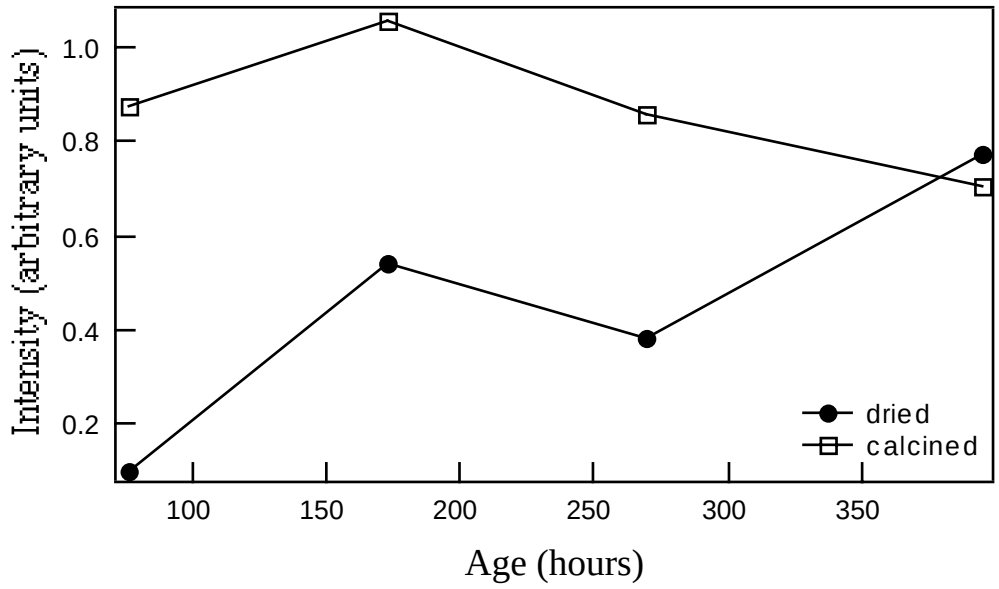

Figure 4.9 *Variation of peak height with aging time in the synthesis gel for washed and dried, and calcined samples from an unheated synthesis gel. The intensity increase between dried and calcined gels is largely due to the removal of the template which causes an increase in contrast between the silica walls and the pore regions.*

Although no effect of aging was noticed on the wet gel diffraction peaks, the intensities of the 40 Å diffraction peak from the dried materials were nearly five times larger for the samples aged for longer than three days when compared to the three day aged sample (see Figure 4.9 above). The increase in intensity between the wet gel and the dried gel samples is due to the removal of water which increases the contrast between the gel particles and the surrounding scattering medium. There was no significant change in the peak width of the dried samples with aging time. The intensity increase in the washed and dried samples suggests that the longer aged samples had higher degrees of condensation of the silica walls and so were more stable to this treatment. The peak intensities of the washed and dried materials reported in Figure 4.9 show a roughly increasing trend with aging time, although the intensity of the 7 day (270 hours) sample is somewhat less than would be expected on the basis of the trend.

Table 4.2 *Diffraction and surface area data on unheated samples from an ordinary and an acid titrated MCM-41 preparation. Before and after in the acid titrated preparation section refer to samples taken before and after acid addition.*

Preparation Type	elapsed time at 25•C	wet spacing / Å	dry spacing / Å	calcined spacing / Å	surface area / m^2 g^{-1}
Ordinary	3 days	41.8±0.5	40.0	32.1	1030
	7	41.9	41.0	33.0	1150
	11	42.3	41.5	32.9	1210
	16	42.7	40.9	34.5	1200
	7 mths	-	42.5	39.3	-
Acid Titrated	0 days	(before) 44.0	40.7	35.2	1090
		(after) 44.0	39.8	35.2	1040
	7	44.0	43.2	39.5	-
		44.0	43.2	39.0	-
	14	44.2	43.5	39.8	-
		44.0	42.9	38.7	-
	21	43.8	43.6	40.2	-
		44.0	43.1	38.7	-
	35	44.0	42.7	37.5	-
		44.0	41.7	37.5	-
	64	44.0	43.8	41.0	-
		43.8	43.8	41.0	-

From Table 4.2 above, it can be seen that the *d*-spacing contraction in the washed and dried materials from the acid titrated preparation is much reduced with aging time and acid addition. There is almost no contraction at all in the materials aged for 64 days both before and after the sixth acid addition. This indicates the development of a much higher quality material with greater silicate condensation in the walls than in the non-acid titrated preparations. It is interesting that the *d*-spacings after acid addition are slightly lower on drying than those before in almost every case, showing a greater lattice contraction in gels which were at a lower pH when they were dried. Possibly the addition of acid initially degrades the structure slightly and it is the reforming during the subsequent aging time which is responsible for the increase in long range order. The intensities in Figure 4.10 follow the same trends as those for the wet gels in this system, increasing up to about 14 days of aging and the third acid addition and then levelling off. The intensities of the materials after each acid addition are slightly altered over those before acid addition, but there is no consistent pattern of increase or decrease upon acid addition.

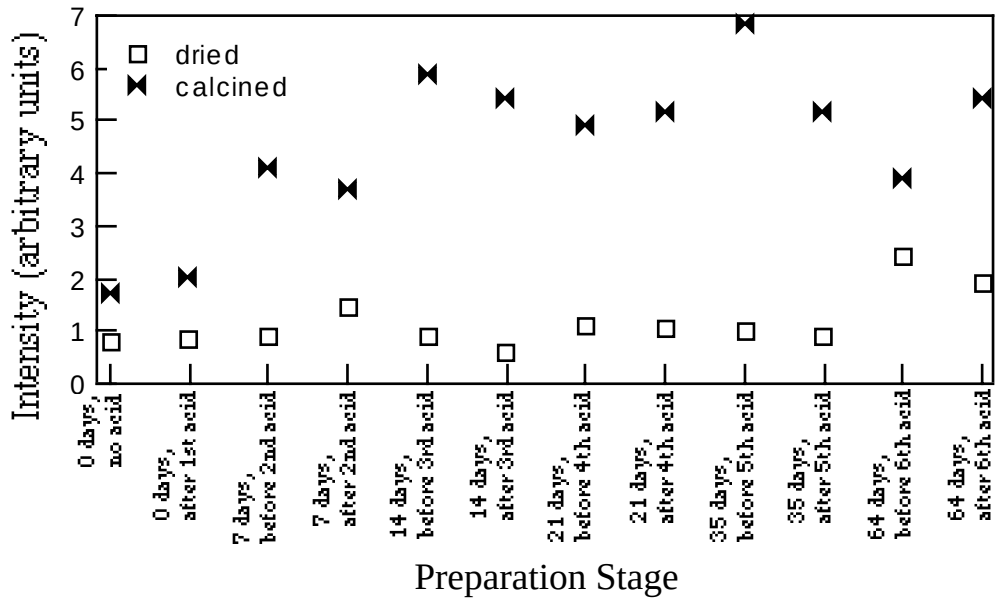

Figure 4.10 *Increase in peak height with acid addition and aging time for washed and dried, and calcined materials from an unheated synthesis gel titrated against 1 M acetic acid to maintain a pH of 11 in the gel during aging. The intensity increase between dried and calcined gels is largely due to the removal of the template which causes an increase in contrast between the silica walls and the pore regions.*

Crystallite sizes calculated from the peak widths for these materials also indicate a much higher retention of coherent structure in the dried acid-titrated materials than in those from the ordinary preparation. In the acid-titrated materials, the wet gels contain particles with a coherent size of around 1600 Å for all aging times and this decreases upon drying to roughly 1400 Å for samples taken up to 14 days aging before the second acid addition. There is a large dip in crystallite size at 14 days after the second acid addition to 800 Å, but this recovers by the 21 day aged samples (1300 Å). After 35 and 64 days aging, the washed and dried crystallite size has improved to around 1600 Å. This behaviour may be an artefact of the sampling procedure, but is also evident in the crystallite size for the calcined materials discussed below. By contrast, for the ordinary preparation the crystallite size in the dried materials peaks at 16 days aging in the gel, at 1350 Å, but, is on average around 1100 Å.

4.3.5 Calcined Materials from Unheated Preparations

Calcination caused further shrinkage of the hexagonal lattice, by 8±1 Å for the unheated materials (see Table 4.2), but the more aged materials shrink less, which again suggests a higher degree of condensation for the silica species in the walls. By comparison, the materials formed in the heated ordinary MCM-41 preparation suffered a shrinkage of 7±1 Å as a result of calcination (see Table 4.4) and thus may be even more condensed before calcination. The amount of shrinkage is not very different and it can be concluded that the product from room temperature synthesis and that made by heating have similar degrees of condensation. The products from the ambient temperature acid-titrated gels, however, undergo much less shrinkage. The amount of contraction of the *d*-spacing with calcination decreases with aging time and acid addition until, at 64 days,

after the sixth acid addition, the lattice shrinks by only 3 Å. This degree of shrinkage is comparable to that observed in heated acid titrated preparations and shows that it is possible to create high quality, well ordered material in an ambient temperature synthesis.

Further condensation of the silanol groups in these materials formed in ambient temperature syntheses to form siloxane bonds during calcination at 350•C is likely, and may contribute to the lattice contraction. Chen *et al.*[5] have carried out ^{29}Si nmr on similar systems and report an increase in the number of Q_4 sites (where one [SiO_4] unit is linked to four others) over Q_3 and Q_2 sites (those linked to three and two other [SiO_4] units) upon calcination, showing that further reactions have occurred. The fact that calcination appears to have a much smaller affect on the materials which were heated in the gel phase and on the acid titrated materials suggests a supplementary role for the calcination in that case.

The diffraction peaks seen in the SAXS from the unheated ordinary MCM-41 preparations are broader upon calcination and have less high angle structure than those for unheated acid titrated preparations. Broad peaks together with diffuse higher order scattering when compared with heated syntheses was also seen in ambient temperature, pure silica ordinary MCM-41 preparations by Tanev and Pinnavaia.[20] Calcination causes an approximately five-fold increase in the intensity of the first order diffraction peak over that of the dried gels, largely due to the change in contrast upon removal of the template. Peak intensities in the calcined materials from the ordinary preparation, also shown in Figure 4.9, are roughly constant with aging time, and are generally much less intense than those of the acid titrated syntheses. In those preparations, the peak intensity rises with aging time and acid addition, as with the uncalcined materials, up to about 14 days, and then also remains roughly constant (see also Figure 4.10). The other obvious difference between the ordinary and acid titrated materials formed in ambient temperature preparations is the development of the second, third and fourth order hexagonal MCM-41 diffraction peaks.

SAXS patterns for calcined materials from both unheated preparations are shown in Figure 4.11. These patterns clearly show that in the ordinary preparation, even after seven months aging in the gel, only the second and third order peaks remain observable after calcination. In the acid titrated materials, however, four orders of diffraction can be clearly seen in the 64 day aged sample. This also indicates a higher degree of long-range order in these titrated materials than in materials from the ordinary preparation. The first order peak can also be seen to be retained at lower Q values in the acid-titrated preparations. The position of the peak moves to lower Q for longer aging time in the gel for the calcined materials from acid-titrated preparations, indicating that progressively less shrinkage is occurring upon calcination in these materials. This effect is also seen in the ordinary preparation calcined materials, but to a lesser extent. The retention of structure upon calcination indicates a greater stability which is probably due to a higher degree of polymerisation of the silicate in the walls of these acid-titrated MCM-41 materials.

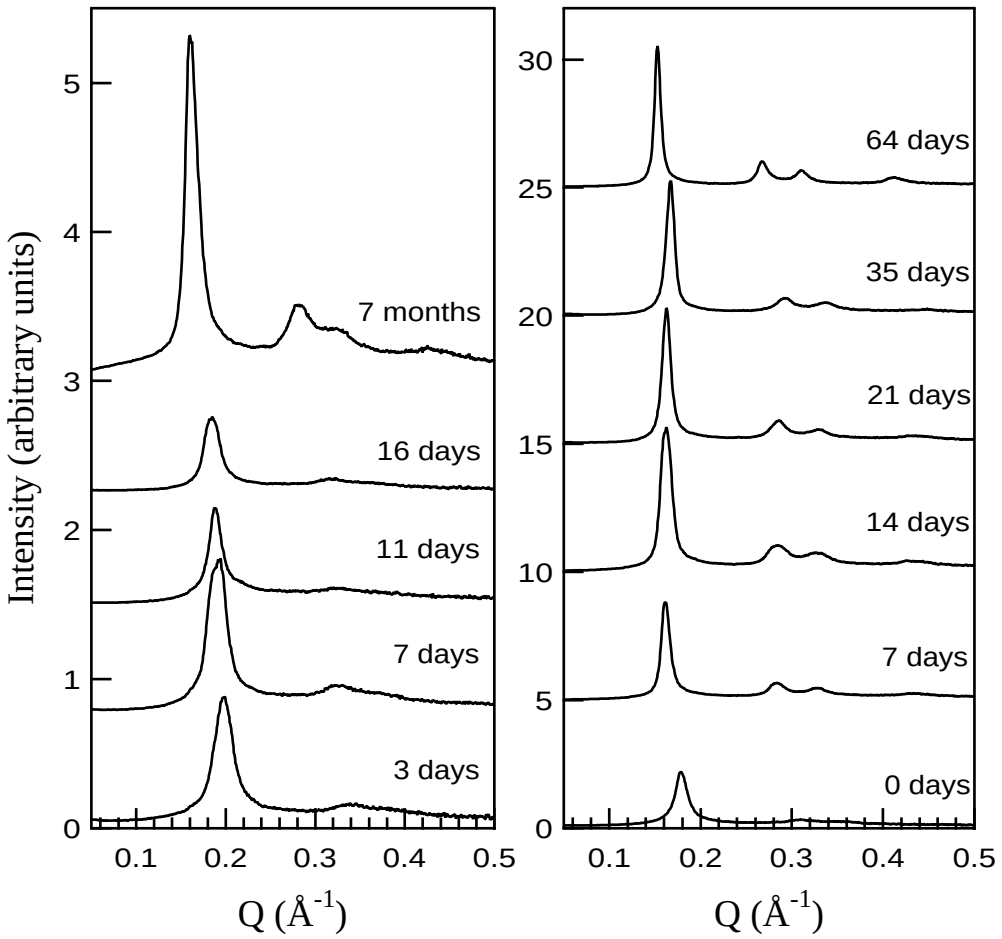

Figure 4.11 *Calcined MCM-41 materials for gels aged for various periods from an unheated ordinary MCM-41 synthesis (left) and from a preparation titrated against 1 M acetic acid to maintain a pH of 11 (right).*

Analysis of crystallite size using the Scherrer equation[49] showed that the coherence length in the ordinary preparation particles went from ~1100 Å in the washed and dried material to ~550 Å in the calcined materials. This suggests that there is partial destruction of the hexagonally close-packed tubes by the escape of water and combustion products from the CTAB during the calcination process. The crystallite size does increase with aging time in the gel for the calcined materials. For materials aged up to 7 days the calcined crystallite size is around 500 Å, increasing to ~600 Å in those aged up to 16 days. After 7 months a coherence length of ~700 Å is retained after calcination. In the acid-titrated materials however, the particle size is ~1500 Å in the washed and dried materials, going to ~1000 Å in the calcined materials after 35 days aging and four titrations, although the dip observed in crystallite size in the uncalcined materials at 7 days after the second acid addition and gradual restoration of order is also seen here. After 64 days in the gel however, the crystallite size after calcination is around 1400 Å. This greater overall retention of coherent structure can be seen in the narrower diffraction peaks shown in Figure 4.11.

Nitrogen adsorption isotherms were measured for each of the calcined samples from the unheated ordinary MCM-41 preparation and on the standard products for comparison. The unheated materials showed reversible isotherms with the characteristic Type IV

shape associated with MCM-41.[50] The BET surface areas were calculated. The resulting surface areas ranged from 1030 $m^2 g^{-1}$ to 1210 $m^2 g^{-1}$, and show a correspondence with aging time up to 11 days, as shown in Table 4.2 above. These surface areas are within the range expected for this mesoporous material and correspond with those measured for materials from the standard alkali heated preparation (typically 1100 $m^2 g^{-1}$). The overall nitrogen capacity for these materials also showed some correspondence with aging time. The three day aged material had the lowest capacity of 12.0 mmol g^{-1} when the pores were full, compared to 23.1 and 21.6 mmol g^{-1} for the 7 and 11 day aged material respectively. The 16 day aged sample had a slightly lower overall nitrogen capacity at 19.2 mmol g^{-1}. Nitrogen adsorption isotherms were only measured for the calcined unaged synthesis gel and the same gel after the first acid addition. There was little change in surface area due to the acid addition with the surface area being around 1050 $m^2 g^{-1}$ for both. The overall nitrogen capacities were 28.0 mmol g^{-1} and 22.2 mmol g^{-1} for the before and after acid samples respectively. This indicates that the addition of acid, which lowers the pH, causes precipitation of silica, infilling some of the voids present in the untitrated material.

4.4 Heated Syntheses

The effect of heating an MCM-41 synthesis is to increase the rate of silicate condensation, so that stable material of higher long range order is achieved in 2-4 days rather than over a week that is necessary to make high quality material from unheated preparations. The synthetic process may also benefit from the higher solubility of the surfactant and the silica at raised temperatures.

In this section of the work, preparation methods used for the heated syntheses, ordinary and acid-titrated, are outlined. The optimisation of the ordinary heated synthesis with respect to heating time and the use of stirring during heating is then discussed. This is followed by a report of the investigation of the effects of various types of acid and the pH used for synthesis in the acid-titrated preparations.

4.4.1 Ordinary Preparation

The synthetic method used followed that of Beck *et al.*[2] Experiments were carried out to determine the optimal heating time and stirring rate for this preparation, given the reagents selected. A more detailed description of the preparation can be found in Chapter 2.

A solution of CTAB in water was made and added hot to an acidified sodium silicate solution. The resulting gel was stirred for a further 15 minutes. After this, further water was added and stirring continued for 30 minutes. Part of this solution was removed to a bomb and heated to 100 •C for six days with aliquots removed after two and three days of heating. This solution was not stirred during heating. The second part of the solution was similarly treated, but was stirred during heating, as has been done in some published syntheses.[14] After heating for the specified periods of time the materials were filtered and washed with Millepore filtered water to remove any unincorporated CTAB.

The product was calcined under a stream of nitrogen in a small tube furnace, at 350 •C, for one day and then under a stream of dry air for four days.

In situ heating experiments were carried out to monitor the progress of the heated reaction by using small angle X-ray scattering. For these experiments the synthesis gel was prepared as outlined above and, after the final stirring, was loaded into a 1.0 mm X-ray capillary which was then sealed with glue. This was mounted in a heated capillary stage (described in Chapter 3) as soon as the glue was sufficiently dry (about an hour after preparation). The capillary was heated to 50, 70 or 90•C and the SAXS pattern monitored for one hour shots over 24 hours. This experiment was also carried out using an unheated synthesis gel which had been aged for over a year to observe the effect of heating on the structure which had developed in that gel.

4.4.2 Acid Titrated Preparation

The synthesis gels were made up as described in Chapter 2. One synthesis mix was carried through to completion without addition of acid, as described above, to provide a control for the acid-titrated preparations. Aliquots from it were taken for small angle X-ray scattering (SAXS) analysis at each step of the process. An acetic acid titrated synthesis gel, directly following the method of Ryoo *et al.*[19] was sampled in the same way. This allowed a direct comparison between structure development at each stage in the two MCM-41 preparations.

In order to compare the effects of different acids on the development of structure, two further syntheses gels were prepared and titrated against various different acids during the heating process. These had typical compositions 1.00 CTAB/ 1.89 SiO_2/ 0.738 Na_2O/ 0.267 H_2SO_4/ 0.123 HX/ 160 H_2O, where HX is the acid used as titre in each case. The initial pH of these synthesis gels was about 11.5 before the first hydrothermal treatment at 100•C. Despite the high pH, no acid was added at this time. In the first series of experiments, the start gel was divided into parts to be heated in separate autoclaves, so that the effects of the addition of various different acids would be compared while avoiding differences in surfactant and silica concentrations. One preparation was titrated with equivalent amounts of sodium acetate to observe the effects of the acetate ion on the synthesis.

For the second series, the start gel was similarly divided to study the effects of conducting the synthesis at pH values between 7 and 11. Sulphuric acid was used as the titre, since the previous experiment showed it to be the most efficacious in increasing the long-range order of the final, calcined product.

The titrations were performed at 24 hour intervals as described in Chapter 2 to maintain the gel system at a pre-determined pH value. At each stage of the titration a small amount of the gel was removed so as to monitor the small angle X-ray scattering from the system. It was found that the acid titre necessary to bring the gel back to a chosen pH value dropped by nearly a factor of 10 over a three day period (*eg.* for a nominally constant pH = 11 preparation). This indicates that the release of alkali into the synthesis gel drops considerably as the synthesis proceeds and is in line with the previous

observation of the most efficacious time for synthesis. Measurements of the pH of a typical synthesis gel titrated with acetic acid after each heating, and the amount of acid required to being it back to pH = 11 are shown in Table 4.3

Table 4.3 *Measured pH for a ca. 250 ml heated synthesis gel after each 24 hour heating at 100•C and the amount of 1 M acetic acid titrant required to return the gel to pH =11.*

Heating Time / days	Initial pH	Acid Added / ml
0	11.48	0
1	11.31	14.8
2	11.24	6.0
3	11.19	2.0

After four days of heating, the synthesis gel was filtered, washed and dried to give a product which was used for physical measurements. The effects of the different mineral acids and the chosen pH value of the synthesis were thus compared. The products were also compared after calcination in a muffle furnace to remove the surfactant template.

4.5 Results and Discussion for Heated Syntheses

A number of variables have been investigated for the heated syntheses. In ordinary preparations the length and effect of heating at 100•C and the effect of stirring were studied using SAXS, SEM, TEM and nitrogen adsorption isotherms. In acid titrated syntheses, the effect of the particular acid used and the pH at which the system was maintained were examined. These variations are discussed first with reference to the SAXS and isotherm work and secondly, the electron microscopy for both systems is considered.

4.5.1 Diffraction from the Heated Synthesis Gels

4.5.1.1 Ordinary MCM-41 Preparation

The effects of heating on the structure in the unheated synthesis gels was investigated by *in situ* heating experiments on the SAXS machine in order to determine whether the initially formed hexagonal array of channels is retained during the heating process. For experiments at temperatures between 50•C and 90•C the diffraction peaks seen in the start gel were retained, with approximately the same intensity and position throughout the heating period observed. This is shown in Figure 4.12 for the highest temperature studied. This behaviour was found for both freshly prepared synthesis gels and one which had been aged unheated in the gel for 18 months. This indicates that the initial structure formed is indeed that which is recovered after the end of the heating period and there is no breakdown of the structure during heating into individual silicated micelles. This means that any improvements in long-range order must occur through

annealing processes in the already-formed structure rather than by repacking of micelles into a more ordered configuration.

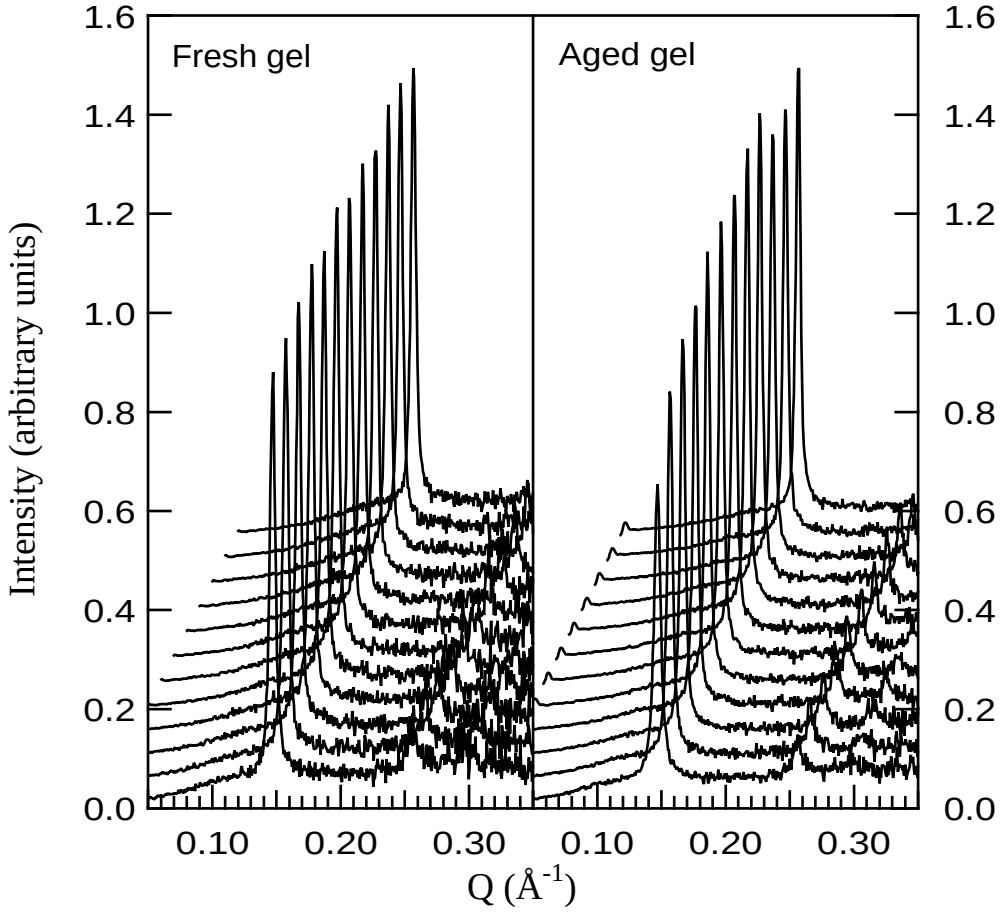

Figure 4.12 *SAXS patterns from an in situ heating experiment at 90•C, a fresh synthesis gel is shown on the left and a synthesis gel aged 18 months before heating on the right.*

For some gels from the ordinary MCM-41 preparation syneresis[51] was observed - the homogeneous, viscous solution separated into a white gel phase at the bottom of the container and a clear fluid phase at the top. The small angle scattering from the clear, viscous supernatant fluid has been examined, Figure 4.13(a). The diffraction was weak had a sharp component at d_{Bragg} = 40 Å and a broad component at d_{Bragg} = *ca* 42 Å. The fluid, though visually clear, must contain small crystallites. In repeated preparations it has been found that this syneresis is rare in the start gels, although similar diffraction patterns were obtained from liquid filtered from the start gel. The supernatant liquor from centrifuged gels did not show any of these diffraction signatures.

The supernatant liquid filtered from heated preparations after cooling also showed some sharp diffraction peaks, often superimposed upon a broad background (Figures 4.13(b),(c)). The sharp first peaks in these solutions occurred at d_{Bragg} = 43.7 Å and d_{Bragg} = *ca* 46.7 Å respectively. The peaks at *ca* 26 Å for both filtered solutions are attributed to CTAB crystallites. These spacings do not correspond to any known CTAB

lamellar phase or any reported CTAB/silica lamellar phase,[14] and are also larger than that of the templated silica peak seen in the SAXS pattern of the bulk start gel.

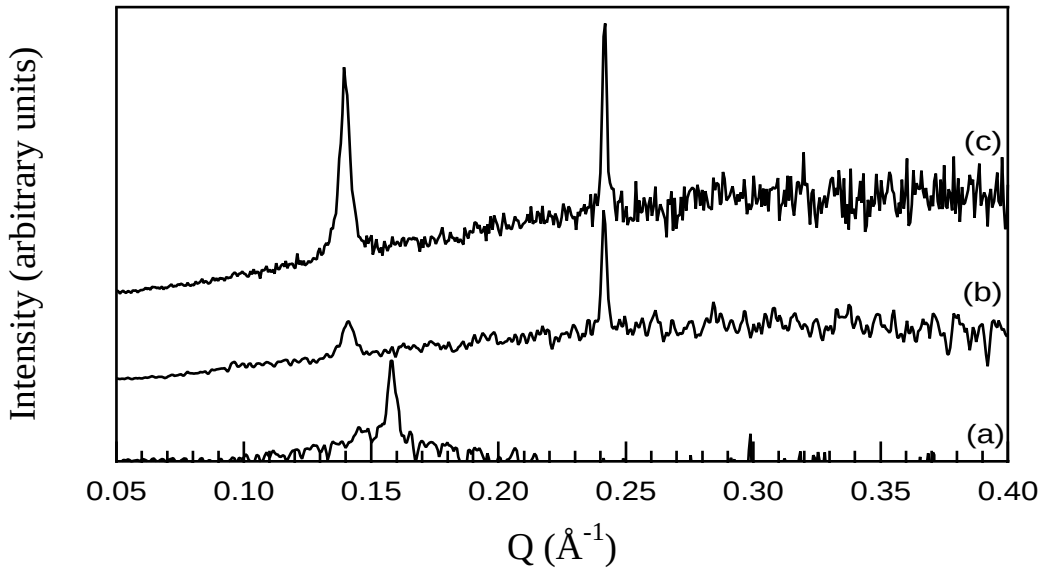

Figure 4.13 *SAXS patterns of (a) syneresis fluid from an unheated ordinary preparation synthesis gel, (b) liquid filtered from a reaction mixture after two days at 100•C, and (c) liquid filtered from a reaction mixture after six days at 100•C.*

The data of Chen *et al.*[4] who carried out ^{14}N nmr on a similar pure silica system go only part of the way to providing an explanation for these observations. They ascribed the single isotropic ^{14}N resonance they observed in a centrifuged unheated synthesis gel to silicated surfactant micelles and saw no sign of the hexagonal phase of the surfactant at any stage during synthesis. The diffraction peaks observed at 40 Å and above must be ascribed to larger aggregations, possibly of such silicated micelles. The variety of *d*-spacings, bigger than those observed in the synthesis gel itself however, suggests different modes of amphiphile-silicate packing.

The dried, templated structure obtained from start gels before heating has a characteristic and relatively sharp diffraction peak at d_{Bragg} = *ca* 42-40 Å but the pattern is sensitive to the gel composition. In an earlier version of the preparation (1.0 mol CTAB/ 2.0 mol SiO_2/ 0.61 mol Na_2O/ 0.267 mol H_2SO_4/ 150 mol H_2O) another broad peak underlay the templated silica peak and a small peak due to free crystalline CTAB was clearly visible. By a slight change in composition (1.0 mol CTAB/ 1.90 mol SiO_2/ 0.74 mol Na_2O/ 0.269 mol H_2SO_4/ 150 mol H_2O) only the peak assigned to templated silica and the small free CTAB peak were present.

A good preliminary indicator, therefore, of the correct stoichiometry for the preparation of a well ordered MCM-41 phase is the sharpness of the major peak in the small angle X-ray diffraction pattern of the start gel. This narrow line structure, as seen in Figure 4.6, is interpreted as pointing to the existence of a single liquid crystal/silicate phase and suggests that compound peaks probably indicate that the wrong stoichiometry has been used. From reports of a number of syntheses,[10,14] it appears that the optimum silica/template ratios might depend on the particular type of silica utilised. For the silica

source used, in ordinary preparations, a ratio of SiO_2/CTAB in the synthesis gel of 1.9:1 was best. Stucky *et al.*[14] report a dependence of the phase formed upon the degree of condensation of the silica source. In that work they found that a lower degree of condensation at a particular pH favours lamellar phases rather than the hexagonal phase. Formation of a second phase co-existing with the hexagonal phase is a possible cause of asymmetric or additional peaks in the SAXS pattern.

4.5.1.2 Acid Titrated MCM-41 Preparation

In an acid-titrated synthesis gel the number and sharpness of MCM-41 peaks increases with the amount of acid added and the heating time. The *d*-spacing in the synthesis gel is however not affected (see Table 4.6 below). A small increase in peak intensity is observed to occur merely with the acid addition, shown in Figure 4.15. This effect is augmented by a factor of two to four by heating. The peaks from the pure CTAB lamellar phase (although present in the initial synthesis gel), decrease rapidly in size with heating and acid addition and are rarely seen after the second titration and heating step. This may indicate that the CTAB present in the synthesis gel has been incorporated into the mesoporous structure rather than remaining as 'excess' unused template in its crystalline form. Figure 4.14 shows the diffraction patterns of the clear, viscous syneresis fluid from a sulphuric acid-titrated preparation which shows a broad peak centred about the first order MCM-41 peak position. This fluid must therefore contain small aggregations of the hexagonal surfactant-silicate phase, not visible to the eye.

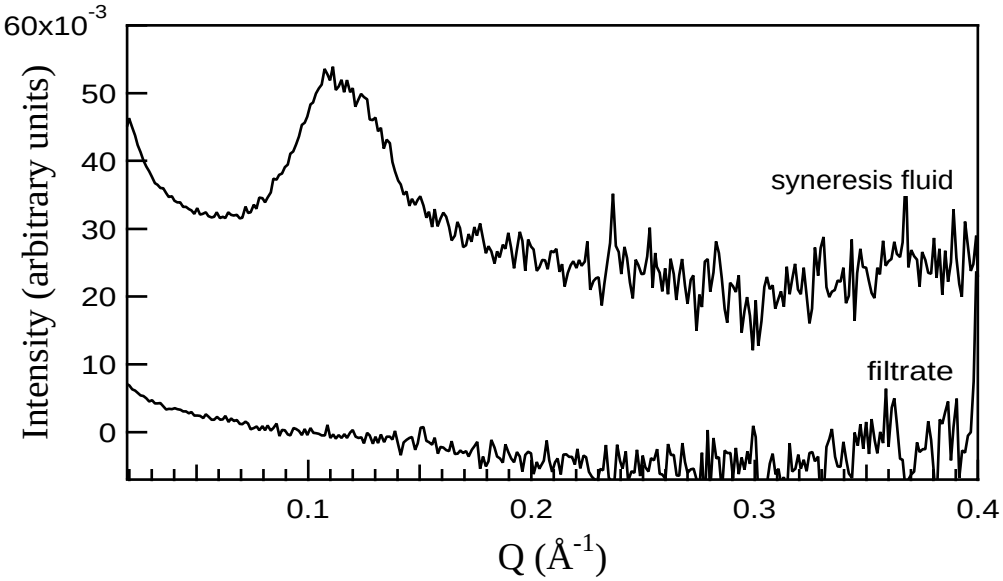

Figure 4.14 *Diffraction patterns of the syneresis fluid (offset by 0.02 in intensity) for a preparation titrated against sulphuric acid to maintain a pH of 11 and the filtrate from the same preparation..*

Fluid filtered from these reaction gels are however, much clearer and contain less particulate matter than those filtered from ordinary MCM-41 preparations. An example of the SAXS pattern from such a filtrate is also shown in Figure 4.14. While it clearly contains scattering higher than the background, it does not show the peaks visible in

filtrate from the ordinary preparation synthesis gels (shown in Figure 4.13). Clearly, the filtration process has been more efficient in isolating particulate matter from the synthesis gel fluids in the acid-titrated case, possibly because the average particle size in the acid-titrated materials is larger.

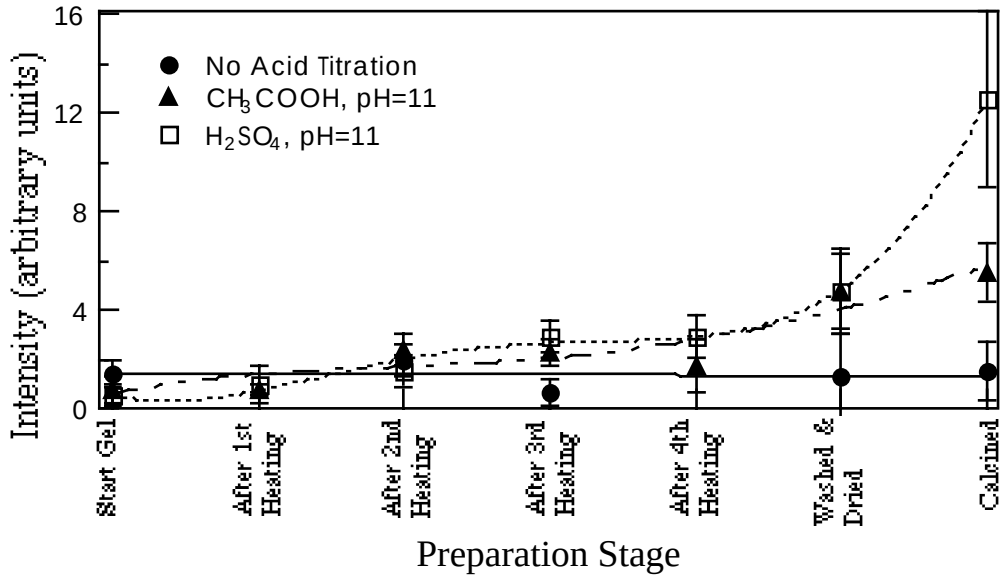

Figure 4.15 *Peak intensity for various preparation stages in some acid titrated preparations and an ordinary MCM-41 synthesis. The lines through the data points are merely guides to the eye. The solid line corresponds to the ordinary preparation, the dotted line to the sulphuric acid titrated preparation, and the dashed-and-dotted line to the acetic acid titrated preparation.*

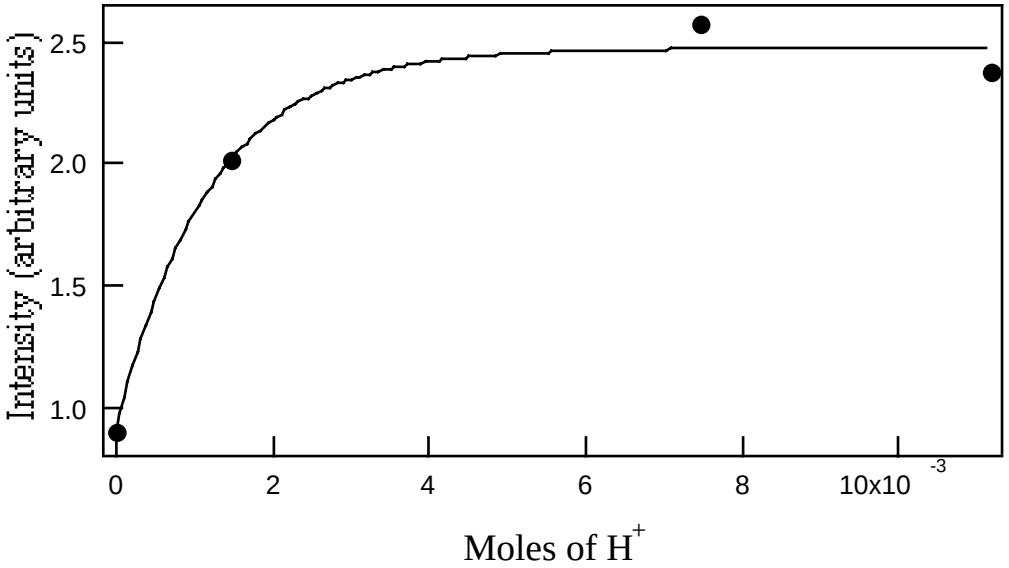

Figure 4.16 *First order peak intensity plotted against acid concentration in the wet synthesis gel for a heated MCM-41 preparation titrated against 1 M acetic acid to maintain a pH of 11.*

A plot of 10 Bragg peak intensity against moles of acid added to the synthesis gel during preparation (Figure 4.16) shows a levelling off of the peak intensity with time. This closely reflects the decreased amount of acid titre needed to bring the pH of the gel back to the desired value as the synthesis proceeds and hence the completeness of

siloxyl condensation. The fact that at each step in the procedure the pH creeps up again during heating after titration shows that the condensation reaction proceeds until an equilibrium is reached between condensing and dissolving silica. Heating under such equilibrium conditions probably aids the observed increase in long range order by allowing a certain degree of annealing of the structure to occur.

4.5.2 Washed & Dried and Calcined Materials from Heated Preparations

Small angle X-ray scattering from washed and dried samples at all stages of an ordinary MCM-41 preparation showed two or three diffraction peaks in the range $15 < d_{Bragg}/Å < 44$ which were assigned as the (10), (11) and (20) reflections of hexagonal phase MCM-41 precursor. Peaks at 26 Å and 13 Å in uncalcined specimens were assigned to the crystalline lamellar phase of CTAB (see Chapter 2). The Bragg spacing and peak widths were found to depend on exact details of the start gel composition, the extent of heating and whether stirred or not. A small decrease in lattice spacing occurs upon the drying out of the synthesis gel. Such shrinkage of the lattice by 1-2 Å upon the removal of water is characteristic of all of the samples from an ordinary MCM-41 synthesis, whether heated or not. The extent of the contraction at this stage of the preparation is probably dependent upon the extent of water removal achieved in each sample investigated. However ,the fact the contraction occurs in these materials obviously points to high flexibility in the silica walls, possibly due to loosely polymerised silica.

4.5.2.1 Unstirred System

Figures 4.15 compares the small angle patterns from calcined, unstirred samples at various stages of heating in an ordinary preparation. Washing the sample with warm water and drying reduced the small CTAB peak at 26 Å but also produced a 2 Å contraction in the main peak *d*-spacing for two day, three day and six day heated samples (see Table 4.4 below). This may be due to a contraction of the molecular sieve lattice upon the removal of at least some of the templating CTAB by washing, similar to the contraction reported by Chen *et al.* after the more vigorous removal of CTAB with HCl/ethanol solution.[5] It has been suggested[52] that the silicate structure in MCM-41 is flexible and under some strain, a point which is supported here by the further contraction by up to about 6 Å (Figure 4.17(b)) after calcining. The behaviour here contrasts with that for the stirred system (see below) where the shift depends upon the extent of heating.

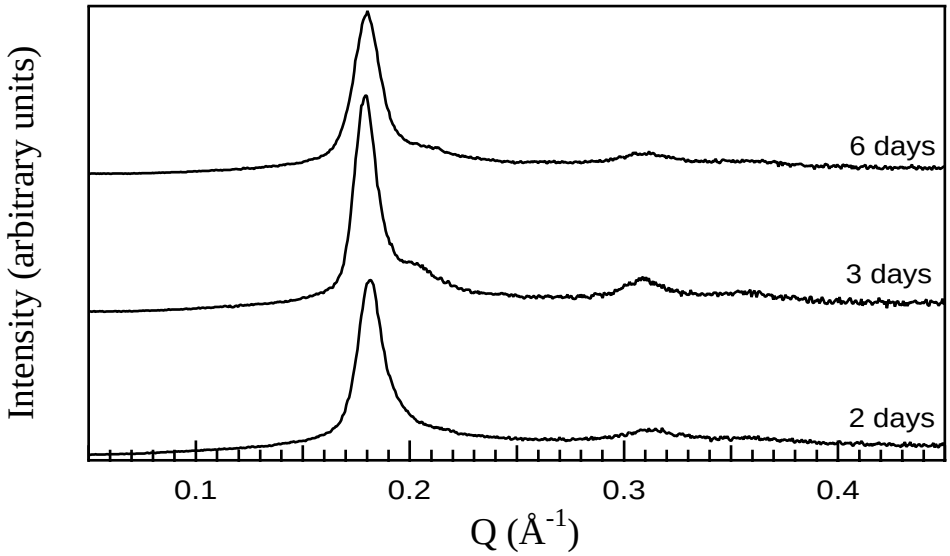

Figure 4.17 *SAXS patterns of calcined materials from an unstirred ordinary MCM-41 preparation after (a) two days, (b) three days and (c) six days of heating at 100•C.*

The main diffraction peak after calcination appears at 34.8 ± 0.3 Å. Judged by its intensity and sharpness, the amount of crystalline MCM-41 appeared to increase with heating up to three days. A second broader peak appears to grow in under the first as heating continues and after six days the main peak was considerably reduced. Further preparations have confirmed this result; samples heated for three days consistently retain the higher reflections in their SAXS patterns after calcination whereas those heated for six days do not.

The nitrogen adsorption isotherms obtained from these samples were Type IV isotherms, similar in shape to those of Branton *et al.*[50] A typical isotherm for nitrogen adsorption at 77 K on ordinary preparation MCM-41 is shown in Figure 4.18. A small amount of hysteresis in the desorption part of the isotherm can be seen at this temperature. This may indicate a degree of polydispersity in the pore size distribution.[53] The broadness of the step, which corresponds to capillary condensation of the gas in the mesopores,[54] also indicates a degree of disorder in the channel system, in comparison with more well ordered MCM-41 samples (see Figure 4.23 below). The amount of nitrogen adsorbed per gram of sample increased with the length of heating up to three days of heating. After six days of heating, however, a considerable loss of total adsorption was observed, although the BET surface area was much the same as for three day heated samples (see Table 4.4 below). Uncalcined samples showed negligible nitrogen uptake, as expected, since the zeolite pores would be already filled by the template molecules.

A BET analysis of these isotherms was carried out.[54] Plots of $p/(x(p-p_0)$ against p/p_0 proved to be linear over the range $0 < P/P_0 < 0.4$. An unstirred two day sample gave a specific surface area of 1950 $m^2\,g^{-1}$ suggesting that even two days heating for this sample was sufficient to produce the desired mesoporous material. This surface area of 1950 $m^2\,g^{-1}$ is extremely high, even for such porous materials. An approximate calculation (discussed in Chapter 3) shows that for pore diameters between 28 and 35 Å,

surface areas of around 900-1000 $m^2 g^{-1}$ are expected (neglecting external surfaces). This would suggest either that the three day heated material is composed of extremely small fragments with a high external surface area, although this is not reflected in the peak widths of the sample, or that there is substantial porous, but completely disordered material in this sample which does not contribute to the diffraction peak.

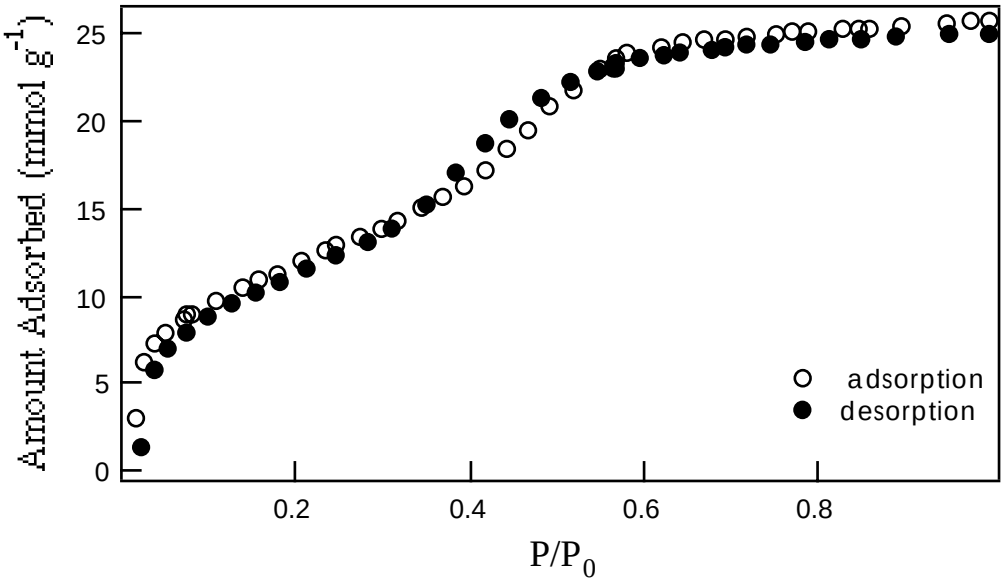

Figure 4.18 *Nitrogen adsorption and desorption isotherm at 77 K for a three days heated, unstirred MCM-41 from an ordinary preparation.*

Some anomaly in the surface area measurement is also possible, although measurements of the other samples were made with the same equipment, in the same manner at roughly the same time, gave reasonable results. Other samples were also analysed in this way giving surface areas ranging from 250 $m^2 g^{-1}$ after two days heating with stirring (see below, Table 4.4) to 1060 $m^2 g^{-1}$ after six days of heating without stirring. The overall capacity of the material for nitrogen decreases with increasing heating time in the static system. For materials from the same synthesis gel, the two day heated sample had a capacity for nitrogen, when full, of 28.9 mmol g^{-1}, the sample heated for three days, a capacity of 25.8 mmol g^{-1} and the six day heated sample, 22.4 mmol g^{-1}.

4.5.2.2 Stirred System

Figure 4.19 shows the diffraction patterns before calcination after two, three and six days of heating with stirring. The very different behaviour from the unstirred system is apparent. Although the samples were washed, some remaining CTAB is evident at d = 26 Å. The main diffraction peak is clearly compound at two days with components at d_{Bragg} = 41 Å (sharp and strong which greatly weakens and shifts to *ca.* 42.3 Å with heating time) and at d_{Bragg} = 38 Å which, though broad, is the main peak after six days of heating at 100•C. The peak at *ca.* 41 Å corresponds to that found in the unheated system after mixing. Its disappearance shows the formation of a new product, whose lattice spacing is still greater than that found above for the calcined unstirred product (which had a *d*-spacing of *ca.* 35 Å).

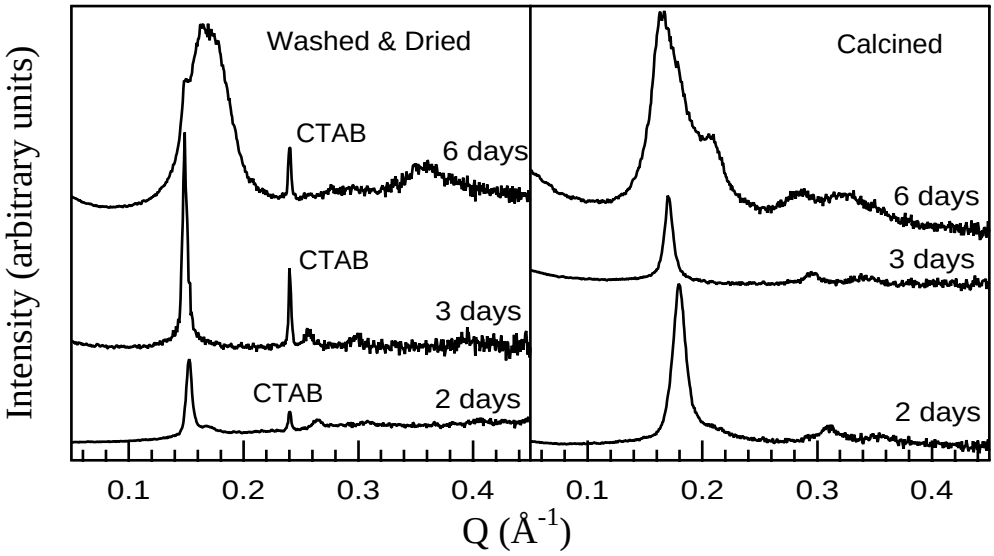

Figure 4.19 *SAXS patterns of washed and dried materials (left) and calcined materials (right) from a stirred ordinary MCM-41 preparation after (a) two days, (b) three days and (c) six days at 100•C.*

The diffraction patterns from the same samples, after calcination, are also shown in Figure 4.19. For two and three days heating respectively, calcination has differentially reduced the d_{Bragg} spacings from 41 Å to 34.8 Å and 42.2 Å to 36.9 Å. The main peak in the calcined data after six days, however, is still at ca 38.3Å although there are noticeable features at *ca.* 30 Å, 22 Å and *ca.* 20 Å. The 22 Å peak is 38 Å divided by •3 and is thus the (11) reflection, but that at 20 Å, though weak suggests that, unlike the unstirred case, other species may have formed. Table 4.4 lists the *d*-spacings and surface areas for some of the ordinary preparation samples studied.

Table 4.4 *Surface areas and d-spacings for samples from an ordinary MCM-41 preparation heated during synthesis.*

sample	*d*-spacing / Å after drying	*d*-spacing / Å after calcination	BET surface area / $m^2\ g^{-1}$
start gel	40.8±0.3	-	-
2 days stirred	41.0	34.8	-
3 days stirred	42.2	36.9	250
6 days stirred	42.3, 38.3	37.6	670
2 days static	-	34.6	1950
3 days static	-	34.9	1070
6 days static	-	35.1	1060

The isotherms measured for these samples showed that there was less gas adsorption than for the unstirred system. The data again fitted the BET equation quite well, giving surface areas of 250 $m^2\ g^{-1}$ and 670 $m^2\ g^{-1}$ for the three day and six day samples respectively. The isotherm data for the sample with two days heating was too noisy to

allow calculation of an accurate surface area. The overall capacity for nitrogen for this material was 11.7 mmol g^{-1} compared with 6.4 mmol g^{-1} for the three days heated, stirred sample and 16.9 mmol g^{-1} for the six days heated, stirred material. These nitrogen capacities are much lower than those found for materials prepared from static ordinary MCM-41 preparations discussed above. There is thus a reduction in surface area and in overall nitrogen capacity of between a factor of ten and a factor of two from stirring. This indicates perhaps, not only the fragility of the intermediate templated species but its susceptibility to mechanical action at raised temperatures.

4.5.2.3 Acid Titrated Preparations

A comparison of the acid-treated and the ordinary, untitrated preparation shows that the beneficial effects of acid treatment on the diffraction pattern from the material are already apparent after the first acid addition (second heating). Figure 4.15, above, shows a comparison between the average peak intensities from SAXS patterns of two acid-treated (CH_3COOH and H_2SO_4) preparations and an ordinary MCM-41 preparation. There is clearly an increase in the peak heights in the wet gels, as a result of the acid titration procedure. Figure 4.20 below, shows the effects of drying and calcining these materials.

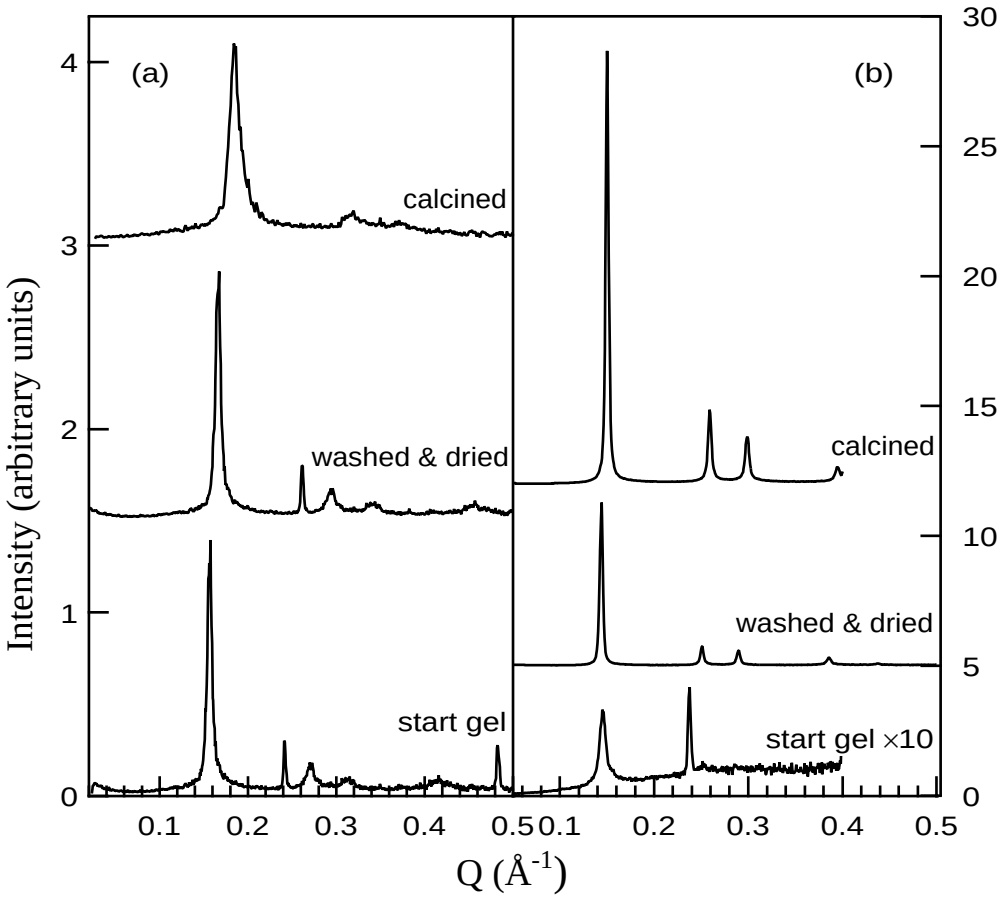

Figure 4.20 *Diffraction patterns for various stages of synthesis for (a) an ordinary MCM-41 synthesis gel and (b) a sulphuric acid titrated preparation.*

The increase in intensity upon washing and drying is probably due to the increase in contrast occurring with the removal of water from the system, and the further increase in intensity upon calcination is due to the removal of template from the pores, which again increases the contrast. This intensity increase due to the increasing difference in contrast upon washing, drying and calcination occurs in all preparations studied. The effect appears to be smaller in the untitrated preparation since the total peak intensities are smaller, however the proportional increase in intensity is much the same as for the acid treated preparations. The sulphuric acid treated systems retain the higher orders of diffraction, to a greater degree than those treated with acetic acid, upon calcination.

Figure 4.20, above, compares diffraction data from non-acid treated (a) and acid-treated (b) preparations at some stages of MCM-41 synthesis. In a non-acid treated MCM-41 preparation up to four hexagonal hk MCM-41 peaks may be seen in the wet synthesis gel at all stages of heating. Often these are accompanied by two sharp peaks from the lamellar phase of crystalline CTAB (*eg.* at Q = 0.24 $Å^{-1}$ and Q = 0.48 $Å^{-1}$ in Figure 4.20(a)). Upon washing and drying this material often still show up to four peaks, and the CTAB peaks are usually also still visible. Calcination removes all signs of the CTAB crystals, but also reduces the number of MCM-41 peaks to three and causes considerable peak broadening, indicating a decrease in crystallite size and, possibly, order. Figure 4.20(a) shows such a progression of diffraction patterns through these preparation stages.

Washing and drying the acid-treated MCM-41 results in a material with up to seven peaks in the synchrotron X-ray diffraction patterns (see also Figure 4.21 and Table 4.5) and usually no visible CTAB peaks. These seven peaks are retained upon calcination and undergo very little broadening. The structure is thus considerably more stable to the calcination process, as well as having greater inherent long range order than materials from the ordinary preparation.

Table 4.5 *Observed X-ray intensities (λ = 1.8963(1) Å) in arbitrary, but consistent units, and indexation after background fitting and subtraction, from template containing and calcined MCM-41, produced from sulphuric acid titrated, controlled pH synthesis conditions.*

Reflection	Calcined		Uncalcined	
	Intensity	2θ /•	Intensity	2θ /•
10	26.683	2.741	10.082	2.573
11	6.576	4.741	1.637	4.463
20	4.465	5.475	1.335	5.146
21	2.436	7.244	1.245	6.804
30	0.124	8.209	0.119	7.729
22	0.030	9.525	0.059	8.935
31	0.141	9.857	0.065	9.277

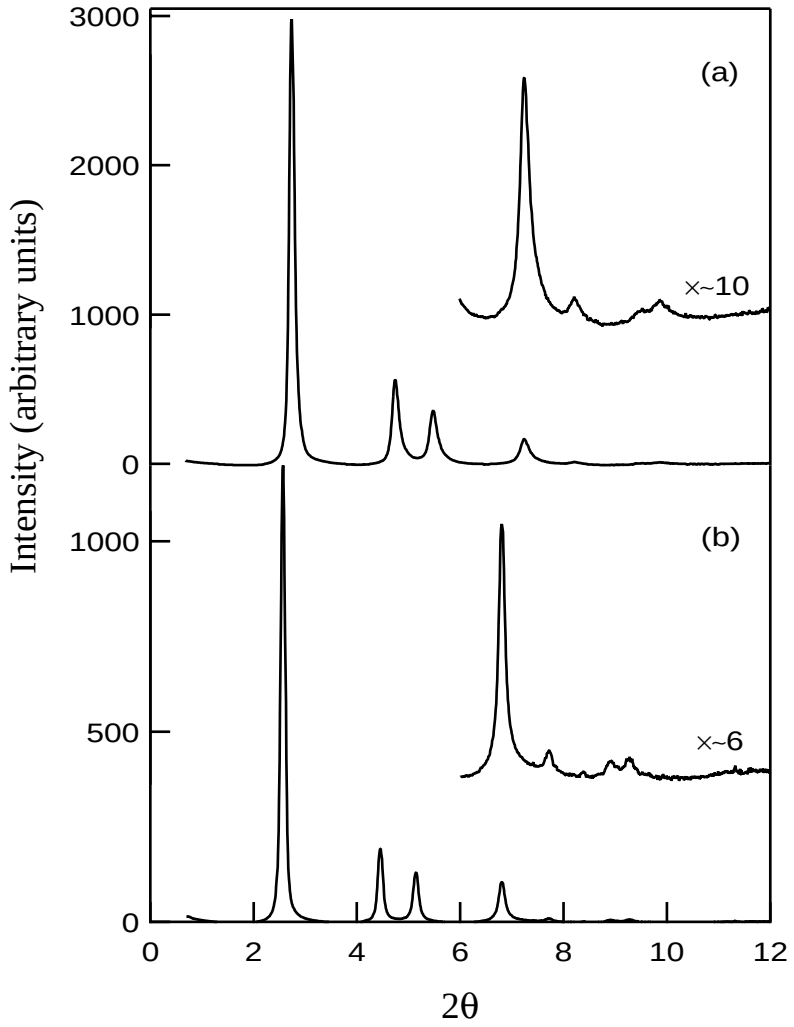

Figure 4.21 *Synchrotron X-ray diffraction pattern from (a) calcined MCM-41 derived from a preparation titrated with sulphuric acid during synthesis and (b) uncalcined MCM-41 derived from the same synthesis.*

All of the acids used were found to be effective in producing an improvement in the X-ray diffraction pattern along the lines reported by Ryoo and Kim.[19] The addition of sodium acetate as a control experiment had no effect on the diffraction pattern. The increase in lonr range order is therefore obviously the result of the acid addition. The relative efficacy of the various acids can be seen by comparison of the small angle diffraction patterns from calcined materials produced from acid-titrated preparations, shown in Figure 4.22. The effect of maintaining the synthesis gel at various approximately constant pH values during synthesis can also be seen in Figure 4.22. Figure 4.21 shows the synchrotron X-ray diffraction patterns from an uncalcined and calcined specimen produced when the titrations were done with sulphuric acid to a constant of pH of 11.0. This material had a total of 4 days heating, with three titrations with the acid to maintain the pH at 11. It is the best result obtained so far. The BET surface area of this material is 990 $m^2 g^{-1}$ compared with 750 $m^2 g^{-1}$ for the material titrated with acetic acid.

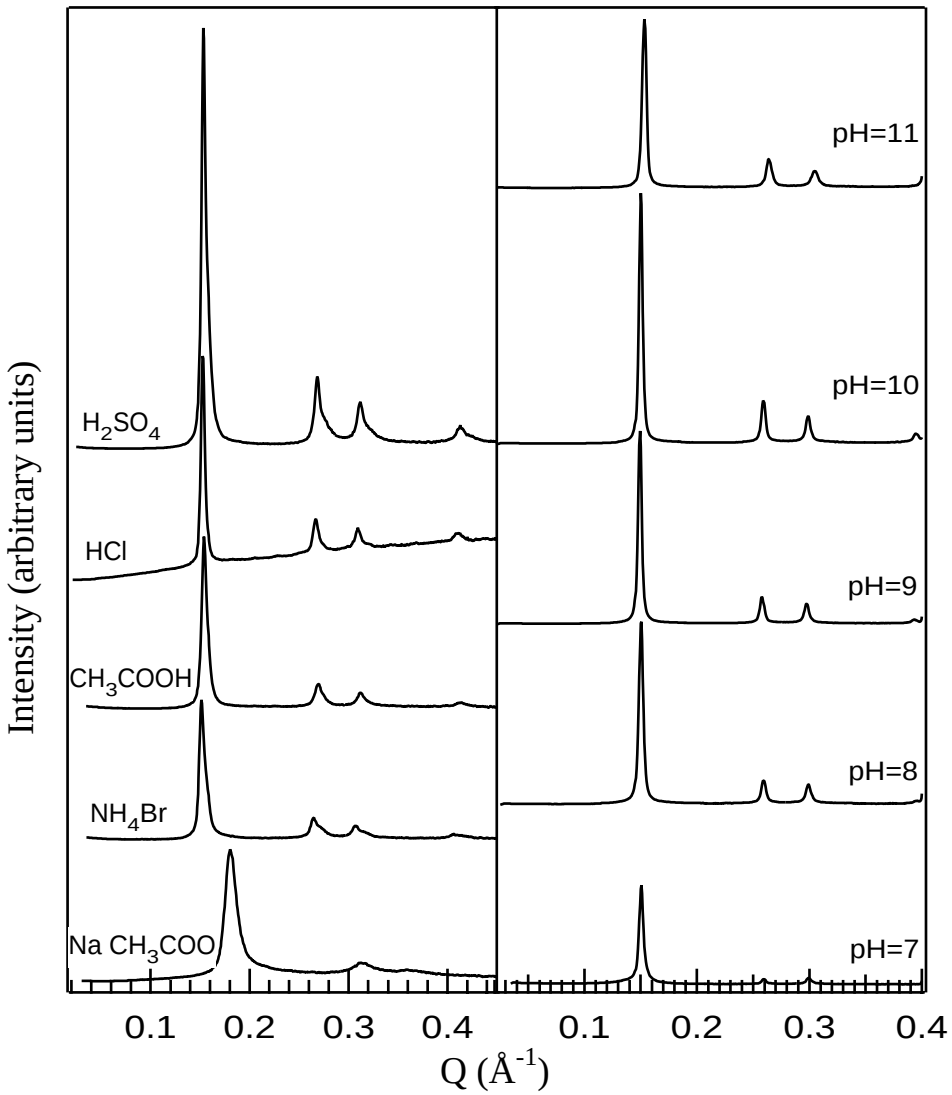

Figure 4.22 *SAXS patterns for calcined MCM-41 materials treated to maintain pH =11 during preparation using a variety of different acids (left) and treated with sulphuric acid to maintain various pH values during synthesis (right).*

The other major difference in behaviour between acid-titrated and ordinary MCM-41 preparations is the degree of shrinkage in the *d*-spacing which occurs during synthesis. In the ordinary preparation, an initial synthesis gel with a *d*-spacing of 44.2(5) Å has a *d*-spacing of 42.7(5) Å by the final stage of heating. This contracts further upon drying and washing to 39.9(5) Å, and again upon calcination to 33.8(5) Å (see also Table 4.4). Other workers observe a similar contraction in *d*-spacing with calcination, by up to 25% for ordinary preparations.[5] However, in the acid-titrated preparations, the initial synthesis gel *d*-spacing (*eg.* of 43.6(5) Å for a preparation titrated with sulphuric acid to maintain a pH of 11) is retained through all of the acid titration and heating steps. There is no decrease in *d*-spacing on drying and washing (43.6(5) Å) and only a small decrease during calcination (to 41.0(5) Å, in this case). The development of this stability is shown for a preparation titrated against acetic acid in Table 4.6. There the wet gel has in all cases a *d*-spacing of around 44 Å, but with successive acid additions and heating periods, the contraction upon drying goes from *ca.* 3 Å to 0.3 Å, and upon calcination the structure shrinks by only 2.5 Å in the final material compared to around 9 Å in the unheated synthesis gel. This stability to calcination was also noted by Ryoo

and Kim[19] in their acetic acid treated materials where there was essentially no contraction in *d*-spacing upon calcination, compared with a 25% contraction for untreated materials.

These differences are attributed to a much higher flexibility in the wall structure of the untreated materials. The increasing, peak width as the ordinary synthesis proceeds, indicates that the shrinkage does some damage to the pre-existing crystallites which is not observed for acid-titrated materials. This again points to a higher degree of siloxyl condensation in the synthesis for the acid-titrated case. In the work of Ryoo and Kim a decrease in the Q_3/Q_4 ratio was observed by ^{29}Si MAS nmr after each acetic acid addition indicating a corresponding increase in the degree of framework condensation.[19]

Table 4.6 *Contraction in d-spacing upon calcination for a preparation titrated against 1 M acetic acid to maintain a pH of 11 during heating. The designations (before) and (after) refer to samples taken before and after acid titration of the synthesis gel.*

Time at 100•C / days	*d*-spacing / Å wet gel	*d*-spacing / Å after drying	*d*-spacing / Å after calcination	BET surface area / m^2g^{-1}	N_2 Capacity / mmol g^{-1}
0	44.0	40.7	35.2	1090	28.0
1	(after) 44.7	41.6	36.2	1120	26.5
2	(before) 43.8 (after) 43.6	42.9 43.2	38.9 38.6	1100 1070	27.9 25.5
3	(before) 44.0 (after) 43.8	43.6	41.4	- -	- -

Nitrogen adsorption isotherms for the acid titrated materials give surface areas which are much the same as for the most ordered materials from the ordinary preparations. Table 4.6 shows that the BET surface area does not change much over the course of the preparation starting from the calcined synthesis gel. The nitrogen isotherm shown in Figure 4.23 however, has a much sharper step at a P/P0 around 0.4 which rises more steeply than was observed for the ordinary preparation materials (see Figure 4.18). This indicates a much lower polydispersity in channel diameters in the acid-titrated materials compared to those from an ordinary preparation.

The overall nitrogen capacities are much the same as for ordinary preparation materials, although they do show a slight decrease after acid titration compared to the capacity of a sample taken immediately before titration. This possibly indicates that silica is precipitated as the pH is reduced, which fills in some of the void space. BET surface areas and overall nitrogen capacities for completely filled pores for all other acid-titrated preparations measured are shown in Table 4.7 below. There does not appear to be any correlation between the acid used for the pH adjustment and the final BET surface area or nitrogen capacity. Comparison plots with non-porous silica[29] carried out for samples X3.6 and X4.6 show no evidence of micropores (see also Chapter 3).

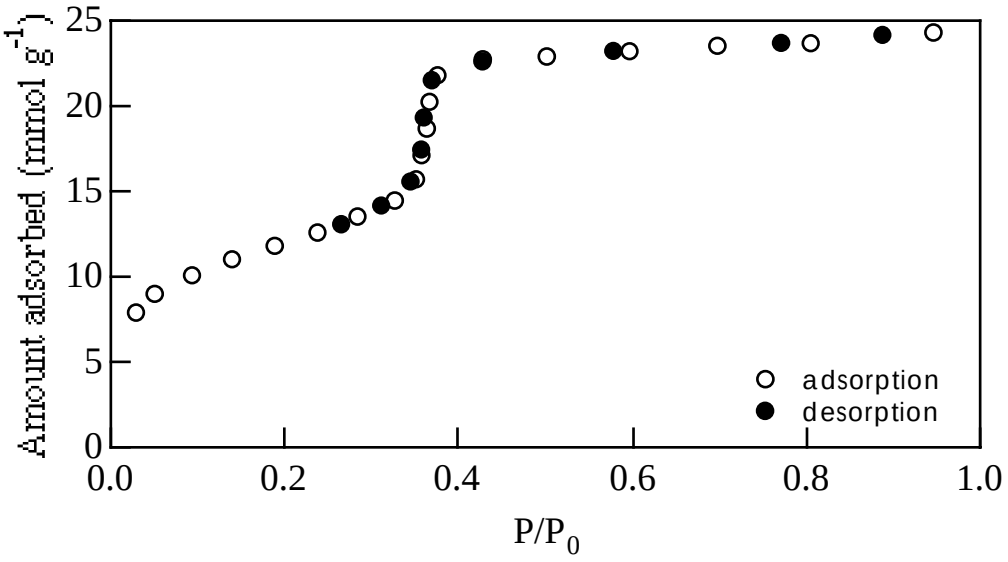

Figure 4.23 *Nitrogen adsorption and desorption isotherm at 77 K for an MCM-41 material from a sulphuric acid-titrated preparation after four days heating at 100•C and three acid titrations.*

Table 4.7 *BET surface areas from nitrogen adsorption isotherms for the final calcined product from all other acid-titrated preparations investigated.*

Sample	Acid	pH	BET Surface Area / $m^2\ g^{-1}$	Nitrogen Capacity / mmol g^{-1}
SAD1.5	CH_3COOH	11	940	26.0
SAD1.6	CH_3COOH	11	920	27.2
X3.6	H_2SO_4	11	990	26.0
X4.6	CH_3COOH	11	750	22.2
QENS calc	H_2SO_4	10	880	24.7
IRIS1.7	H_2SO_4	11	1160	28.4
MARI1 calc	H_2SO_4	10	960	24.3

4.6.2.4 Coherence Length

The resolution functions of the X-ray instruments used are much narrower than the observed peak widths. The peak widths may, therefore, be used to estimate the average crystallite extent in the hexagonal plane. Materials from the ordinary preparation have much broader peaks than those from acid treated preparations and so contain much smaller crystallites in the basal plane directions. Crystallite “sizes” calculated using the Scherrer equation[49] are shown in Figure 4.24 for various stages of untreated preparations and preparations treated with acids to maintain a pH of 11 throughout the synthesis. For untitrated preparations there is a threefold increase in crystallite size following the first heating for 24 hours at 100•C. In this preparation the coherence length continues to slowly increase throughout the heating process up to the third heating but decreases again after the fourth heating - behaviour consistent with the

earlier finding that three days of heating is optimum for this preparation. It then decreases upon washing, and decreases still further on drying and calcination.

Stirring the preparation does not appear to have a great effect upon crystallite size, but may be slightly beneficial to crystal growth. After two days heating, the stirred preparation gave a coherence length of *ca*. 900 Å whereas the unstirred preparation gave 800 Å. Three days heating resulted in a stirred preparation crystallite size of 1690 Å and a static size of 900 Å. After six days however the stirred preparation, as a result of the broad compound peak had only a 460 Å coherence length, whereas the static preparation remained at 800 Å. This indifference to stirring is also suggested by the shear experiments described above where the first order MCM-41 peak was found to be remarkably resilient to shear. In the acid preparations the same sudden increase following the first heating is also observed. After this there is a small further increase in crystallite size over that of the ordinary preparation after the first acid addition and second heating. Coherence length then stays roughly constant until the washing, drying and calcination steps.

Coherence lengths have been reported for calcined mesoporous silicas prepared via various templating methods.[11,20] Those prepared by neutral templating syntheses appear to have scattering domains which are an order of magnitude smaller than those from cationic template syntheses. For a C_{16} carbon chain, the crystallite size from a neutral template preparation is 114 Å, while from a cationic surfactant preparation it is 933 Å.[11] The greatest scattering domain size reported by these authors for a cationic template synthesis is 1020 Å using a C_{14} surfactant.[20] Large coherence lengths are also reported for cationic surfactant/cationic silica preparations which proceed via a counterion mediated intermediate. These are of the same order as have been observed in this work, ranging from 530 Å to 1376 Å.[11] Coherence lengths for silica polymerised between didodecyltrimethylammonium bromide bilayers have been reported to be between 1000 and 2000 Å.[55]

The coherence lengths calculated in this work are consistent with an equilibrium having been reached for the set pH in each synthesis, and with the crystallites dissolving and reforming during the heating process to form the more highly ordered materials. In the ordinary preparation such an equilibrium situation is never reached, and the crystallites once grown, begin to redissolve during the observed period of heating. A similar plateau after 24 hours of heating, followed by a decrease is found for the X-ray diffraction intensities followed over time for an ordinary MCM-41 synthesis by Ortlam *et al*.[40] No explanation for this observation was given.

Reforming of uncalcined MCM-41 materials in solutions of various pH from 7 to 10 at 100•C has been reported by Huo *et al*.[18] In that work, the long-range order and the pore size (dependent upon the surfactant(s) used as template) of the hexagonal phase material is observed to increase during this post-synthesis treatment. The increase in order is probably due to the dissolution and redeposition of silica under these controlled pH conditions, in much the same processes as occur in the reaction mixtures of the pH controlled synthesis gels used in the present work. Reforming of silicate MCM-41 materials under more extreme conditions (150•C for 10 days) in the original synthesis

solution has also been reported.[56] The effectiveness of this treatment was also proposed to be due to the local dissolution and redeposition of silica in areas of high curvature within the pre-existing silica framework.

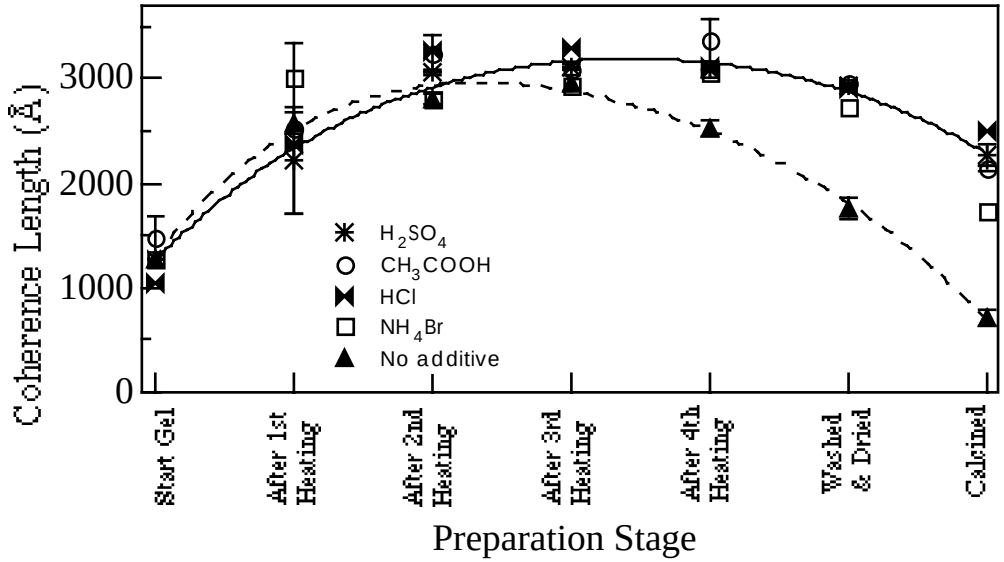

Figure 4.24 *Crystallite size determined from the width of the 10 Bragg reflection for various synthesis stages for preparations titrated with various acids to maintain pH=11. The lines drawn through the points are merely guides to the eye. The solid line indicates trends in the acid titrated preparations, while the dotted line follows the untreated preparation. The error bars correspond to the greatest deviation from the mean in those preparations which were repeated.*

The coherence length in the acid treated materials decreases upon drying and then again upon calcination but this decrease is much less than in the materials from the untreated synthesis. It is concluded, therefore, that the acid treated materials are much more stable to calcination than those from the ordinary preparation. This is consistent with a higher degree of silicate polymerisation having occurred during the synthesis of the acid treated materials. Amongst the acid treated materials, hydrochloric acid produces the largest crystallite sizes in the calcined materials (as it has the narrowest peaks), followed by sulphuric acid, acetic acid and ammonium bromide. The addition of sodium acetate to the preparation has no beneficial effect on the size of the scattering domains and may even have a detrimental effect.

4.5.3 Electron Microscopy

Scanning electron microscope (SEM) pictures of the unstirred, synthesis gel before heating, and after heating for two days at 100•C are shown in Figure 4.25(a) and (b) respectively. Both micrographs show a multitude of curling tubes, with diameters around 0.6-1.0 µm, as well as some more amorphous, fine grained material. In addition, the SEM micrographs of the material heated for two days also contain grainy textured flakes. However, after heating for six days many silicate spheres having diameters of approximately 1-10 µm had formed (Figure 4.26(a)). These spheres were surrounded by the curling tubes, as seen in the earlier material, and by large flakes having a grainy,

porous surface, similar to the smaller flakes observed after two days of heating. In contrast, at the resolution of the SEM, the stirred material heated for six days shows a much finer texture (Figure 4.26(b)), being composed of fibrous agglomerates, with short thin fibres in random orientations and with no visible spheres. This fibrous, mat-like material contains fibres with a diameter of less than half a micron.

Transmission electron micrographs of the unstirred preparation, heated for six days reveal various levels of structure beneath that shown in the SEM pictures. On the scale of *ca*. 0.2 µm (Figure 4.27(a)) worm-like "tactoids" - agglomerations of long, thin structures - are visible components of the larger tube-like structures noted in Figure 4.26. Some of these agglomerations are straight. Most of the images in Figure 4.27(a), however, show highly curved folds as indicated by arrow A. There are also sealed off bundles of tubes (arrow B) such as have been reported elsewhere[57] and the region indicated by arrow C shows some evidence of partially formed material. At the same magnification, Figure 4.27(b) clearly shows the presence (arrow A) of the hexagonal phase in unstirred material heated at 100•C for three days, as well as the striated curved formations (arrow B) and a bicontinuous porous structure reminiscent of Swiss cheese (arrow C) which was also seen by Davis *et al.*[25] The pore packing density of this phase is similar to that in the hexagonal phase. Similar disordered porous structures adjacent to ordered hexagonally packed materials were seen in a static MCM-41 preparation by Kloetstra *et al*.[58]

Figure 4.28(a) shows larger curled tubes, with cross-sections of approximately 0.1 µm. These larger tubes typically occur with the tactoids, and do not have any discernible structure on this scale. At higher magnification (Figure 4.28(b)) the structure of the wormlike agglomerations becomes more obvious. The picture is interpreted as a view of the hexagonal close-packed tubes side on, with the images of the straighter sections of these tactoids closely resembling those of imogolite.[59]

The wormlike agglomerations in Figure 4.28(a) would appear to be bunches of silica coated tubes seen from the side rather than along the axis of the tubes. The micrographs described above argue against these structures belonging to a lamellar phase, despite the suggestion of Alfredsson *et. al.*[57] who submitted that the presence of closed loop structures in the micrographs could not be explained by the hexagonal phase. Other workers have shown how a side-on view of the hexagonally packed tubules would give rise to a set of parallel lines when viewed by transmission electron microscopy.[60] Given the existence of long, rod-like micelles in surfactant solutions which would be expected to be reasonably flexible, the silica coated analogues might plausibly show such curved structures. Similarly, if a surfactant micelle were curved before the silica coating occurred, the coating process would freeze in the curved shape. Long, curved silica coated worm-like micelles have been observed by cryo-TEM in the early stages of an MCM-41 synthesis.[61]

Plates not available in Digital version

Figure 4.25 *SEM micrographs of (a) a static, unheated MCM-41 synthesis gel, (b) a synthesis gel after static heating for 2 days at 100•C. Scale is as marked on the micrographs.*

Plates not available in Digital version

Figure 4.26 *SEM micrographs of an MCM-41 synthesis gel (a) after static heating for 6 days at 100•C and (b) after stirred heating for 6 days at 100•C. Scale is as marked on the micrographs.*

Plates not available in Digital version

Figure 4.27 *TEM micrographs of material from an ordinary static MCM-41 preparation showing (a) curved and folded MCM-41 tubules (scale bar indicates 0.2 µm), and (b) several porous phases (scale bar indicates 0.1 µm).*

Plates not available in Digital version

Figure 4.28 *TEM micrographs of material from an ordinary static MCM-41 preparation showing (a) "tactoid" components of larger tube like structures (scale bar indicates 0.1 µm), (b) the larger tube-like structures (scale bar indicates 0.2 µm),*

Plates not available in Digital version

Figure 4.29 *TEM micrographs material from a static sulphuric acid titrated preparation showing (a) areas of hexagonal packing (scale bar indicates 0.05 µm) and (b) a large finely textured plate (scale bar indicates 0.1 µm).*

Plates not available in Digital version

Figure 4.30 *(a) TEM micrograph of a static, sulphuric acid treated MCM-41 material showing well-defined curved tube (scale bar indicates 0.03 µm) and (b) SEM micrograph of MCM-41 from the same preparation showing smoother texture including long thin crystallites. Scale is as marked on the micrograph.*

Plates not available in Digital version

Figure 4.31 *FESEM images of MCM-41 surfaces from a sulphuric acid titrated preparation at (a) 20,000 times magnification and at (b) 50,000 times magnification. Scale is as marked on the micrographs.*

Transmission electron micrographs of the stirred material show fewer regions of the regular hexagonal lattices found in the static systems and none of the porous bicontinuous phase. Instead they appear to be composed largely of bundles of short fibres with less ordered packing than appears in the static material. In the static material the curved tactoids appear to have lengthwise striations indicating the presence of close-packed tubes or lamellae, and these appear continuous over the length of the structure. In the stirred material however, the order that is seen in the wormlike agglomerations in the static preparation is not apparent. The aggregations here have no uniform orientation although there is some suggestion of crumpled, folded layers in some fragments.

Transmission electron microscope images of materials from the acid titrated syntheses are shown in Figure 4.29 and 4.30(a). There does not appear to be any great textural difference between these materials and those from the ordinary preparations in the hexagonally ordered regions. Figure 4.29(a) shows well defined regions of hexagonal phase material while Figure 4.30(a) contains some more disordered porous structures alongside the large curved tube made up of a bundle of smaller channels seen in cross-section. However, in Figure 4.29(b) a relatively large area of apparently non-porous silica, with a slightly rippled surface can be seen. This thin sheet of silica appears next to some of the ordered hexagonal phase material, and may be amorphous silica which was precipitated by the acid-titration procedure. This precipitation of silica and its subsequent reforming (as observed for colloidal silica used in an MCM-41 preparation[15]) or dissolution and transport, may slow the formation of the hexagonal phase allowing greater micellar ordering to occur before the structure is frozen into place.

Scanning electron micrographs of materials from the acid titrated preparations show similar features to those of the static ordinary MCM-41 materials. The particles appear to have a smooth surface (Figures 4.30 (b), 4.31), which appears to be composed of terraces where rounded layers of material have agglomerated. They are still however, mostly composed of curling tubes and some fibrous sheets, see Figure 4.31(a), although they also have larger coherent surfaces than materials from the ordinary preparation. No silica spheres or crystals were seen in these materials. Attempts were made to image this material using a FESEM (Figure 4.31(a), (b)) however this provided no better resolution than ordinary SEM on these materials, as such smooth curved surfaces do not provide good contrast, making focussing difficult.

4.6 Breakdown of Structure

Little work has been reported on the breakdown of MCM-41 materials under ambient conditions. Some work has been reported on the hydrothermal stability of the pure material under elevated temperatures and humidities,[4,5] and for material which has undergone ion exchange.[62] In the first study it was found that structural collapse of pure silica MCM-41 materials occurred at 850•C in dry conditions and at 800•C under P_{water} = 8 torr.[5] It was also found that the stability of MCM-41 prepared in heated syntheses was dependent upon the reactivity of the ingredients used. Sodium silicate, which is more reactive than fumed silica, gave more stable final products.[4] In the

second study, AlMCM-41 ion exchanged with Y^{3+}, Ca^{2+} and Na^{+} was found to be stable at temperatures over 800•C when heated in water saturated O_2. The incorporation of other elements such as aluminium and titanium into the walls of siliceous MCM-41 materials however, seems to decrease their thermal[63,64] and/or hydrothermal[65,66] stability. It may however merely be dependent upon the synthesis and calcination conditions used in sample preparation.[67]

MCM-41 materials titrated against acetic acid during heating, in a preparation similar to the acid-titrated materials synthesised in this work were found to be stable in humid air, containing 20 torr of water, up to 700•C.[19] It has also been found that the hydrothermal stabilities of MCM-41 materials from acid-titrated preparations, boiled in water for 12 hours, are improved by the addition of salts. Salts such as sodium and potassium chloride, sodium acetate, and sodium and potassium EDTA were added to the synthesis gel after the first pH adjustment. The degree of improvement of thermal and hydrothermal stability was dependent upon the concentration and the nature of the added salt.[68] The improvement in stability was explained as due to interference by the salt anions decreasing the strong electrostatic binding between the surfactant and the silicate which thus allowed a greater degree of silicate polymerisation to occur. Other work on neutrally templated hexagonal mesoporous silicas (HMS), where strong electrostatic binding does not occur, has found that they have thicker (•17 Å), and more condensed walls than cationically templated silicas (12-15 Å) and so are more stable to heating in air at 900•C for 4 hours. The cationically templated silicas collapsed completely, but the HMS retained its long-range order during this treatment.[20]

Other workers,[52] however, make reference to decayed MCM-41 when using it as a reference material for calorimetric measurements. The collapse of the structure after about two months was not investigated, but was suggested to be due to hydrolysis. The collapsed sample contained about 3 kJ mol^{-1} less excess enthalpy than MCM-41 samples which retained their porous structure, but still contained almost 2 kJ mol^{-1} higher than the enthalpy of bulk glass. The excess enthalpy in this system was ascribed to the presence of 3-fold siloxane rings in concentrations which correlated with the concentrations of such rings in the "good" MCM-41 samples and their expected decrease in concentration upon hydrolysis.

The mechanical stability of MCM-41 has also been investigated. The mesoporous structure of this material can be affected by mechanical compression at pressures as low as 86 MPa and essentially destroyed at 224 MPa.[69] This mechanical stability was much lower than had been observed previously for zeolites, alumina, kaolin, and silica gels. Pressures of 235 MPa caused complete loss of structure in X-ray diffraction patterns of the similar mesoporous silicate, FSM-16.[70]

Khushlani *et al*. refer to limited stability of as-synthesised siliceous mesoporous materials.[17] They observed breakdown over periods of days to weeks which caused a gradual loss of intensity and decrease in the *d*-spacing of the first order peak from powder X-ray diffraction. They attribute this to incomplete polymerisation of the siliceous framework which undergoes a degradative process over time. They have since synthesised materials using cetylpyridinium chloride surfactants which do not show

such breakdown over periods of three months.[17] No such decay in as-prepared samples was observed in the present work.

Breakdown of the MCM-41 materials described in this work was discovered when some of the early, unheated, calcined samples were re-run on the SAXS about eight months after they had been prepared. These samples showed a considerable degradation in the intensity of the first order peak, although no increase in peak width, and a complete loss of higher order peaks. Other samples were then investigated, with two samples from heated preparations, described below, being followed by SAXS at regular intervals for 22 months. The MCM-41 samples were stored under ambient conditions, in X-ray capillaries, sealed with high vacuum glue which was not in contact with the dry, powdered materials. Most of the time, the capillaries were stored in a drawer, although no special precautions were taken to exclude light or to control the atmosphere around them. In some of these samples, breakdown of the structure had occurred to such an extent that no sign of the first order peak remained and the SAXS pattern showed only a fall-off in Q resembling amorphous silica. Porod slopes for some broken down materials are compared to those for freshly prepared samples in Table 4.11, below. MCM 41 samples which still contained template were never observed to break down.

Table 4.8 *Surfactant/silica ratios for samples from acid treated and ordinary preparations after washing, calculated by gravimetric calcination.*

Sample	Treatment	Surfactant/Silica wt/wt	Surfactant/Silica mol/mol
Acid Prep 1.1	as prepared	2.68	0.442
1.2	1 wash	1.13	0.186
1.3	2 washes	1.04	0.171
1.4	3 washes	0.93	0.153
1.5	calcined	0	0
Ordinary Prep 2.1	as prepared	2.12	0.349
2.2	1 wash	1.51	0.254
2.3	2 washes	1.35	0.223
2.5	3 washes	1.27	0.209
2.5	calcined	0	0

The breakdown of samples from two preparations, listed in Table 4.8 above, were followed in detail, one from the ordinary MCM-41 preparation, and the other from the more highly ordered acid-titrated variation. The starting gels for these two materials were prepared identically by adding an acidified sodium silicate solution to a cetyltrimethylammonium bromide (CTAB) solution with vigorous stirring as described in Chapter 2. Both gels were heated in an autoclave at 100•C for 3 days, without stirring. One gel was titrated with acetic acid (1M) during the heating process to re-

adjust the pH of the reaction mix to 11, following the method of Ryoo and Kim.[19] The molar compositions of the two gels were as follows; for the preparation titrated with acid (CTAB 1.00/ SiO_2 2.03/ Na_2O 0.79/ H_2SO_4 0.27/ CH_3COOH 0.45/ H_2O 173) and for the ordinary MCM-41 preparation (CTAB 1.00/ SiO_2 1.90/ Na_2O 0.74/ H_2SO_4 0.28/ H_2O 149).

After filtration and washing with water to remove some of the excess CTAB, each preparation was divided into five parts. The first part was left as prepared, and three of the remaining parts were further washed with water by soaking in water overnight in the ratio 3 grams MCM-41 to 40 grams water, with the slurry being heated to roughly 50•C immediately before filtration to remove more CTAB. The final portion in each case was calcined by heating under flowing nitrogen to 350•C overnight and then under compressed air until the powder was white. Small samples of each of the other portions were also calcined gravimetrically to determine the amount of CTAB remaining in each. The surfactant/silica ratios are shown in Table 4.8.

The aging of each of these ten samples was followed by small angle X-ray scattering. The SAXS pattern of each was taken at roughly monthly intervals, and in the intervening periods the samples were at ambient temperatures with no special precautions taken to preserve them. The data for the calcined and three times washed samples from the acid treated preparation and from the ordinary preparation are presented as intensity against Q plots in Figure 4.32 and 4.33.

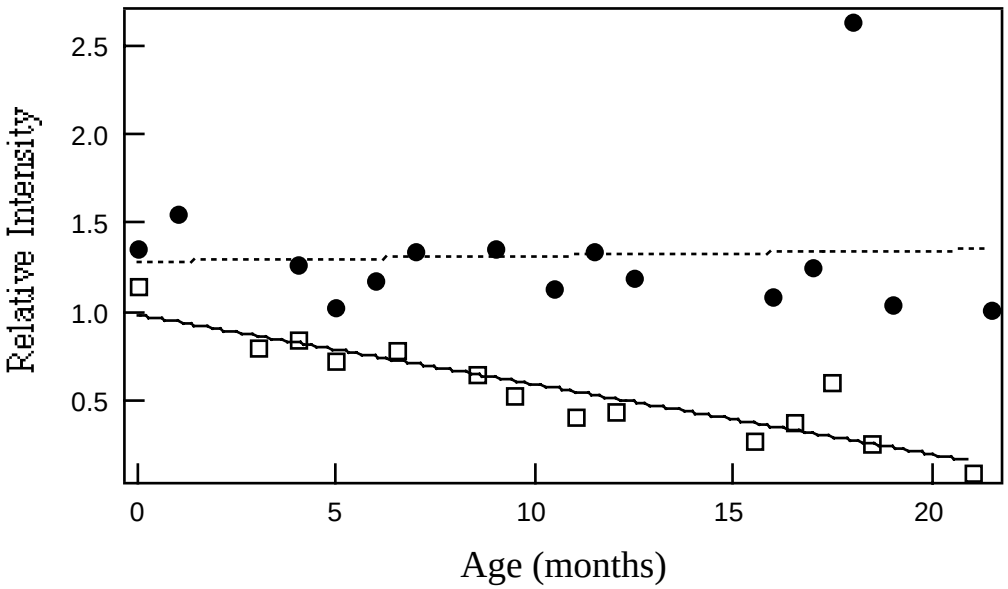

Figure 4.32 *Progression of first order peak intensity normalised against the as-prepared pattern patterns with aging time for calcined (open squares) and three times washed (shaded circles) samples from an ordinary MCM-41 preparation.*

Since MCM-41 samples which still contained template were never observed to break down, the as-prepared samples for each preparation were taken as standards. Peak intensity variations in these materials was ascribed to instrumental vagaries. The intensity data in Figures 4.32 and 4.33 has been normalised against intensities of the first order peak for the as-prepared sample from each preparation. This was done to

correct for a general negative slope apparent in the behaviour of every sample in this series, including those for which the number and relative intensity of all peaks, including those of crystalline CTAB, remained constant. It was therefore assumed that this slope was an instrumental artefact which was corrected for by the division. It can be seen in Figure 4.32 that the calcined sample from the ordinary preparation, which showed greatest signs of degradation at the conclusion of the period investigated, shows a distinct downwards trend in 10 Bragg peak intensity after the normalisation, whereas the three times washed sample from the same preparation undergoes little or no alteration in relative peak intensity. Various stages in the breakdown of the calcined sample are shown in Figure 4.34. In Figure 4.33, both the calcined and the three times washed sample from the acid titrated preparation have a largely constant relative first peak intensity, with the negative slope in the line of best fit caused mostly by the abrupt decrease between the first data point and the rest of the series. This behaviour indicates possibly an initial drop in long-range order from the fresh sample, but then a long period in which most of the original long-range order is retained. It was not observed in the acid titrated samples containing more template. No further breakdown was noted during the period of the experiment, with even the calcined acid-titrated sample retaining all orders of diffraction that were present in the first pattern taken.

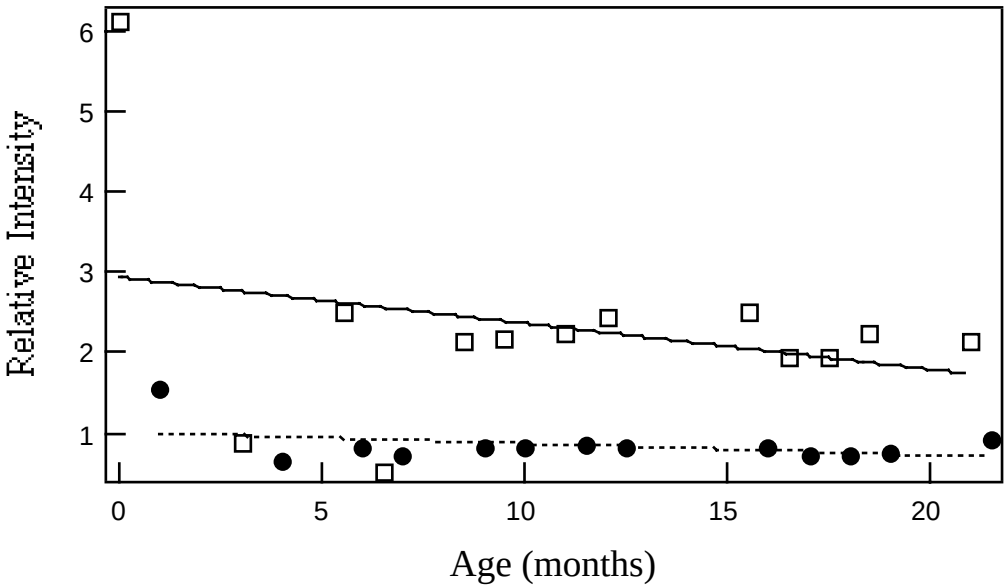

Figure 4.33 *Progression of first order peak intensity normalised against the as-prepared pattern with aging time for calcined (open squares) and three times washed (shaded circles) samples from an acid titrated preparation.*

The breakdown behaviour of every MCM-41 sample prepared for this thesis was also investigated. This overall examination however, took place near the end of the experimental work described in this thesis, so the periods for which the various samples aged are not uniform. The aging periods vary from only two months to 30 months. SAXS patterns were run on all samples immediately after their calcination, and at some later stage. These samples were also in sealed 1 mm Lindemann glass capillaries, and were stored under ambient conditions in a drawer with no precautions taken to preserve them. The breakdown behaviour of all samples from unheated syntheses examined are given in Table 4.9, below. Heated syntheses are shown in Table 4.10 It was also noted

that samples stored under inert gas or under vacuum did not tend to show any breakdown of structure. Breakdown was said to have occurred in samples showing a pattern similar to or worse than, the final pattern shown in Figure 4.34, below.

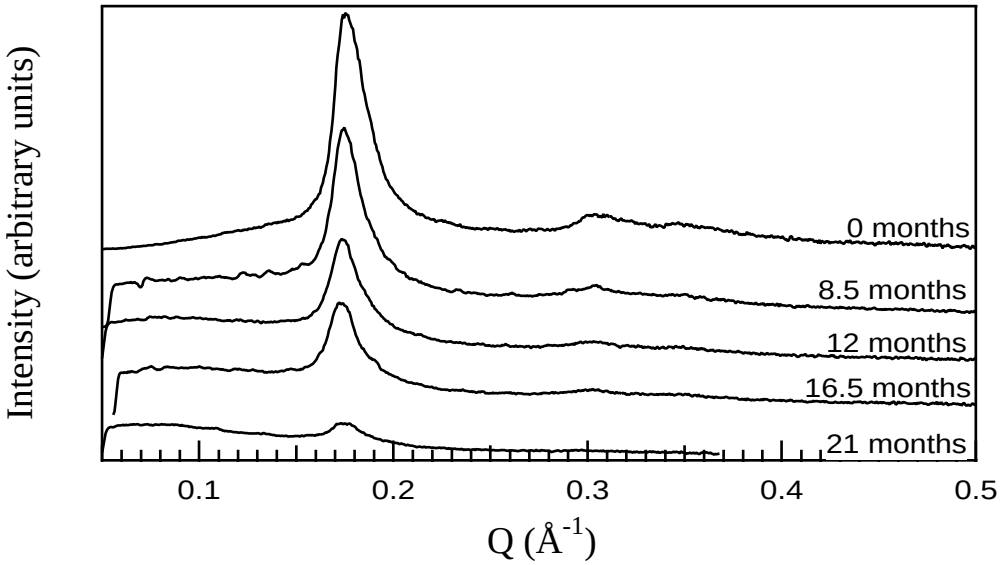

Figure 4.34 *Selected SAXS patterns from the breakdown of the calcined sample from the ordinary MCM-41 preparation.*

4.6.1 Results and Discussion for Breakdown of MCM-41

The intensity of the peaks in the SAXS patterns is due to a number of factors including the X-ray contrast between the surfactant molecules filling the pores and the silica walls, the packing density of a powdered sample in the tube and the degree of order in the sample. Intensities for the same sample with the same packing densities over time should therefore yield useful information about the stability of the structure.

The diffraction patterns from the two preparations followed in detail show distinct differences in crystallinity, as judged by the number and sharpness of the visible peaks. The acid-treated preparation clearly results in patterns with a greater number of narrower peaks, interpreted as resulting from a higher degree of hexagonal ordering in the channel system. However, in both cases the calcined samples underwent at least some degradation of signal over time. The amount of degradation observed in the peaks of the SAXS pattern was dependent upon the amount of surfactant template remaining in the structure. The as-prepared samples with surfactant/silica ratios above 2 (see Table 4.8), the pattern of which include peaks from crystalline free CTAB, show no loss of intensity in the diffraction peaks of the MCM-41 relative to these, within the variation of the technique, on the time scale of the experiment. Samples washed up to three times, although containing no peaks from free CTAB in their diffraction patterns, still show no appreciable decay of intensity over the 10 month aging period. Calcined samples, where the template has been totally removed by heating the material to 350•C under a stream of compressed air, do however show a reduction in the intensity of the peaks in the small angle diffraction pattern after about 9 months in this case. The

breakdown observed was much greater in the material from the ordinary preparation where a least squares fit to the normalised intensity gave a slope of -0.039(5) months^{-1} (see Figure 4.32). By comparison the slope of the least squares fit to the relative intensities of the calcined acid-titrated sample was -0.06(6) months^{-1} (see Figure 4.33) although as discussed above, the negative slope here is largely due to the high intensity of the first order peak in the freshly prepared sample.

Table 4.9 *Breakdown behaviour of materials from static, unheated MCM-41 preparations. A tick indicates that no peak or virtually no peak remained in the SAXS pattern of that material after the time indicated.*

Sample Name	Time in Gel /days	Times Titrated with 1M Acetic Acid	Calcination Method	Age /months	Breakdown
UC1	3	0	small tube	7.5	✓
UC2	7	0	small tube	7.5	✓
UC3	11	0	small tube	7.5	✓
UC4	16	0	small tube	7.5	✓
UC5	7 months	0	muffle	21	✓ (less)
UC5.1	7 months	0	muffle	21	✓ (less)
R30	0	0	muffle	22	✓
R31	0	1	muffle	22	×
R32	7	1	muffle	19.5	×
R33	7	2	muffle	19.5	×
R34	14	2	muffle	19.5	×
R35	14	3	muffle	19.5	×
R36	21	3	muffle	19.5	×
R37	21	4	muffle	19.5	×
R42	35	4	muffle	19.5	×
R43	35	5	muffle	20	×
R48	64	5	muffle	20	×
R49	64	6	muffle	20	×

Note: In this table and the one which follows the calcination methods are those referred to in Chapter 2 where "muffle" is the muffle furnace, and "small tube" and "large tube" were the two tube furnaces used.

Calcined samples from all heated, ordinary preparations (not treated with acid) showed complete loss of the 10 diffraction peak in the SAXS pattern after 6-9 months aging in ambient conditions (see Table 4.10), but the detailed process of aging was not followed in those cases. Materials from ordinary preparations not heated during manufacture appear only slightly less stable than those from heated preparations (see Table 4.9), although breakdown in unheated materials was also not systematically observed. Uncalcined specimens, although not included in the tables, were never observed to undergo significant degradation.

From Table 4.9 above it is immediately obvious that the unheated, acid titrated samples are more stable than those from the ordinary preparation. Despite being prepared later, the acid-titrated samples were aged for longer before the second SAXS pattern was taken, and yet still retained their pore structure, without signs of degradation. The 7 month aged samples from the ordinary preparation do, however, show some slightly higher retention of structure over other ordinary preparation samples aged for shorter times at the point of the second observation. This is consistent with a higher degree of silicate polymerisation due to the longer aging time in the gel for this material. Breakdown occurs for all of the non-acid titrated samples, even R30, the untreated control sample from the same synthesis gel as the other R series samples. The effect of acid on stability is dramatic - even the sample which received only one acid titration and was then immediately washed, dried and calcined with no aging time in the gel before being processes shows a high retention of structure. This sample had a much lower peak intensity, smaller crystallite size and less well developed long-range order than the other acid titrated samples which received more acid, or had a longer aging time in the gel, and yet the structure in this seemingly inferior sample is still retained when untitrated samples have broken down. The acid titration must therefore have immediate effects on silicate condensation.

Table 4.10 *Breakdown behaviour of materials from MCM-41 syntheses heated during preparation. A tick indicates that no peak or virtually no peak remained in the SAXS pattern of that material after the time indicated.*

Sample Name	Stirred	Heating Time /days	Acid	pH	Calcination Method	Age /months	Break-down
A	yes	2	none	NA	small tube	8	✓
B	no	2	none	NA	small tube	8.5	×
C	yes	3	none	NA	small tube	8	✓
D	no	3	none	NA	small tube	9	✓
E	yes	6	none	NA	small tube	9	✓
F	no	6	none	NA	small tube	9	×
GP39	no	2	none	NA	small tube	30	✓
GP40	no	2	none	NA	small tube	30	✓
GP41	no	3	none	NA	small tube	30	✓
GP42	no	3	none	NA	small tube	30	✓
GP43	no	6	none	NA	small tube	30	✓
GP44	no	6	none	NA	small tube	30	✓
Ar1	no	3	none	NA	small tube	8.5	✓
SAD2.5	no	3	none	NA	muffle	21	✓
SAD1.5	no	4	CH_3COOH	11	muffle	21	×
SAD1.6	no	4	CH_3COOH	11	muffle	16	×
R26	no	1	CH_3COOH	11	muffle	22	×
R27	no	2	CH_3COOH	11	muffle	22	×
R28	no	2	CH_3COOH	11	muffle	22	×
R29	no	3	CH_3COOH	11	muffle	22	×

X2.6	no	4	$NaCH_3CO_2$	-	muffle	16	✓
X3.6	no	4	H_2SO_4	11	muffle	7	✓
X4.6	no	4	CH_3COOH	11	muffle	6.5	✓
X5.6	no	4	NH_4Br	-	muffle	6.5	✓
X3.6 recalc	no	4	H_2SO_4	11	muffle	15.5	×
X4.6 recalc	no	4	CH_3COOH	11	muffle	15.5	×
Z1.6	no	4	H_2SO_4	9	muffle	18	✓
Z2.6	no	4	H_2SO_4	11	muffle	18	✓
Z3.6	no	4	H_2SO_4	10	muffle	18	✓
Z4.6	no	4	CH_3COOH	11	muffle	18	✓
Z5.6	no	4	HCl	11	muffle	18	✓
J1.6	no	4	H_2SO_4	11	muffle	13	×
J2.6	no	4	H_2SO_4	10	muffle	13	×
J3.6	no	4	H_2SO_4	9	muffle	13	×
J4.6	no	4	H_2SO_4	8	muffle	13	×
J5.6	no	4	H_2SO_4	7	muffle	13	×
Q calc	no	4	H_2SO_4	10	muffle	13.5	×
IRIS1.7	no	4	H_2SO_4	11	muffle	2.5	✓
IRIS1.7 new	no	4	H_2SO_4	11	muffle	15.5	×
RP calc	no	4	H_2SO_4	10	large tube	4	×
RP calc new	no	4	H_2SO_4	10	large tube	4	×
MARI 1 calc	no	4	H_2SO_4	10	large tube	4	✓
MARI 1 calc new	no	4	H_2SO_4	10	large tube	4	×
MARI2.7	no	4	H_2SO_4	10	large tube	4	✓
MARI2.7 new	no	4	H_2SO_4	10	large tube	4	×

Table 4.10 shows very little pattern to the degradation of the materials investigated. Stirred ordinary preparations appear to result in less stable materials than static ones. Ordinary preparation samples also seem, on the whole, to be less stable than those from acid titrated preparations, although it is notable that in three or four cases, materials from preparations titrated against sulphuric acid to pH values of 10 or 11, showed a complete loss of structure after about 4-6 months, and after only 2.5 months in one case. Ordinary preparation materials usually retained good structure for at least 6 months.

It is also interesting that in these cases of rapid breakdown in acid titrated materials, capillaries filled from the stored bulk of these materials, kept in scintillation vials did not show the same breakdown even after significantly longer aging periods. The samples where a capillary has been newly filled from the bulk sample samples marked "new" in Table 4.10. This would appear to indicate a surface area effect in the

breakdown, or maybe a buffering effect in the bulk. The larger the surface of the powder available, (in capillaries only 1mm thick, most of the powder granules will be at or very near the surface) the faster appears to be the breakdown. This may suggest that moisture diffusing into the structure is responsible for the breakdown, and that a certain concentration of moisture must be reached for breakdown to occur. If this is the case it explains why the bulk, which can disperse water adsorbed at the surface down through the rest of the sample, is more resistant to decay. It is puzzling however that the diffusion of moisture through the walls of sealed glass capillaries is more effective than into scintillation vials sealed only by a screw cap with a foil liner. The samples titrated against acetic acid, may, on the basis of Table 4.10 be slightly more stable than those titrated against the other acids, particularly sulphuric acid, although the evidence is not conclusive.

One interesting feature of the degradation of MCM-41 is the shape of the peaks. The first order peaks do not undergo any broadening indicating firstly, that breakdown does not occur via the formation of larger channels with a disordered distribution of *d*-spacings such that the peak becomes 'smeared' over a range of lattice spacings. Secondly, it shows that the breakdown does not change the size of the coherent particles or crystallites which are responsible for the diffraction. Breakdown must therefore be occurring in such a way that the channels are not widened by just a bit, but must be more than tripled in diameter (and so are out of the range of the SAXS camera) or that the breakdown does not leave any ordered or semi-ordered pattern of channels to cause a diffraction pattern.

Another alternative is that the decay occurs relatively quickly but inhomogeneously so that the MCM-41 particles decay one by one, in a nucleated fashion. That is, once part of a particle begins to decay, the rest of if follows quickly, leaving no intermediate structures which may be observed by SAXS. Such nucleated decay may be enhanced by the location of the crystallites close to a surface which may explain why in small capillaries decay occurs rapidly, but in bulk samples where the surface of the powder is proportionally less, the decay is less observable.

Transmission electron microscopy on uncalcined MCM-41 materials reformed during post synthesis treatments involving heating at 150•C for up to ten days show that the reforming process results in an inhomogeneous size and shape distribution of mesopores. In these materials some adjacent mesopores appear to have missing or broken adjoining walls, while others have pseudo-hexagonal or irregular shapes.[56] The crystals did however retain their original morphology and the peak widths in X-ray diffraction patterns from these materials did not appear to change significantly, indicating that the extent of the diffracting domains remained the same. It was suggested that the restructuring process, therefore, occurred topotactically, without any appreciable solubilization, utilising processes which may have been different from the original mineralisation steps.[56] Similar processes may be involved in the breakdown of the calcined samples observed in the present work.

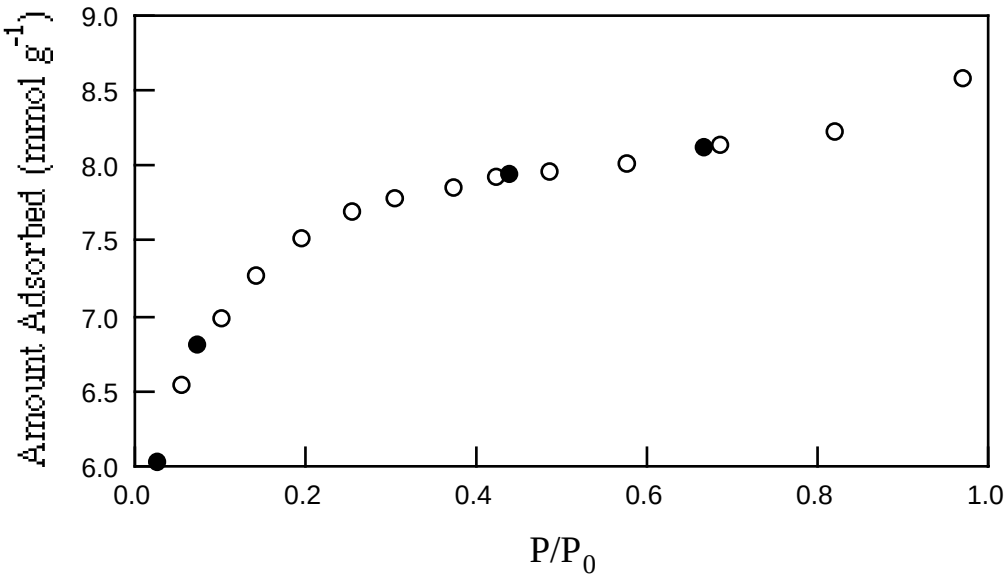

Figure 4.35 *Nitrogen adsorption and desorption isotherm run at 77 K on a decayed MCM-41 sample from an acetic acid titrated preparation (X4.6), synthesised at pH = 11. Open symbols indicate adsorption, shaded ones indicate desorption.*

Nitrogen isotherms on decayed materials are significantly altered from those of ordered MCM-41 samples, as shown in Figure 4.35. This Type II shape[29] suggests the possible development of micropores. There is considerable loss of adsorptive capacity compared to freshly prepared MCM-41 samples. In Figure 4.23 the fresh MCM-41 material adsorbed 24 mmol g^{-1} at complete filling. Here the maximum adsorption is only 8.2 mmol g^{-1}. The isotherm looks very different to the Type I nitrogen isotherms of MCM-41 materials where the pore structure has been destroyed by applied pressure, so that the resulting material is no longer porous.[69] High angle synchrotron diffraction patterns of broken down MCM-41 do not show diffraction peaks at high angles, only a large broad hump characteristic of amorphous silica.

It is also noted that an increase in the intensity of small angle scattering occurs in decayed samples (see Figure 4.34 which shows increasing scattering at low Q with increasing age) which suggests there is a transition to some highly divided form of amorphous silica. It is interesting that, although the intensity of the small angle scattering increases with aging, the Porod slope, from plots of lnI versus lnQ, does not alter very much, indicating that the surface characteristics remain similar (see Figure 4.36 above). Table 4.11 below reports the Porod slopes for a variety of samples, from ordinary and acid-titrated preparations both before and after aging.

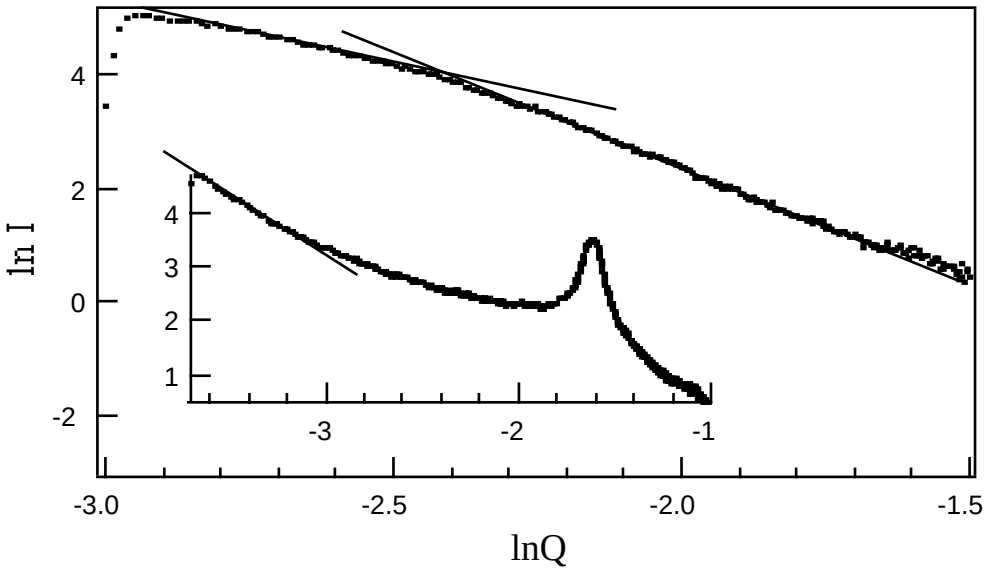

Figure 4.36 *Porod plot for an aged sample from an ordinary preparation (GP40) showing the two regions of different slope. Inset is the Porod plot for the same sample before breakdown of the structure occurred.*

Table 4.11 *Porod slopes from lnI versus lnQ plots for selected new and aged samples. Samples above the thick line are from an ordinary preparation, with one, UC5.1 being from an unheated synthesis, whereas samples below the thick line are from acid-titrated preparations.*

Sample	new slope	aged slope
UC5.1	-2.38(3)	-2.58(1)
SAD2.5	-1.61(2)	-2.37(2)
GP39	-1.77(7)	-1.68(2) -3.82(2)
GP40	-1.88(3)	-2.07(3) -4.06(2)
GP41	-1.78(4)	-2.59(3) -3.85(1)
GP42	-2.00(7)	-2.26(2) -4.15(1)
GP43	-2.39(9)	-2.97(1)
GP44	-2.3(1)	-1.08(1) -2.28(1)
SAD1.5	-2.74(2)	-2.89(2)
Z1.6	-3.03(2)	-2.95(2)
Z2.6	-2.76(2)	-1.85(4) -3.17(2)
Z3.6	-2.02(6)	-2.97(2)
Z4.6	-1.93(3)	-2.05(2) -2.98(2)
Z5.6	-1.69(4)	-2.12(1)

In some of these materials, as shown in Figure 4.36, the patterns of the decayed samples show two regions with different slope. It is difficult to know whether these regions were present in the patterns before decay, as the presence of the peak may mask them in the original SAXS patterns. The region with the second slope may indeed be merely the remnants of the peak, however other studies[71,72] have attributed such regions of different slope as due to surface characteristics on differing length scales. The slopes reported in Table 4.11 are mostly between -2 and -3 which indicate rough, highly divided surfaces. Some of the samples, especially those from ordinary preparations which show two slopes have slopes for the higher Q region which are around -4, indicating development of a much smoother surface upon breakdown.

4.7 Discussion

4.7.1 Ordinary MCM-41 Syntheses

The diffraction patterns of ordinary MCM-41 preparation synthesis gels indicate that mixing the components at room temperature quickly produces a stable templated structure, with *d*-spacing 41-42 Å. The relatively rapid, strong association between the surfactant headgroup and the silicate anions is confirmed by the Langmuir trough experiment. In those experiments, although highly dilute compared to a normal MCM-41 synthesis gel, a rigid film developed over about a 10 minute period which showed quite different compression behaviour to the pure surfactants. Drying out the templated material from the synthesis gels gives a *d*-spacing of *ca.* 41 Å. By adjusting the CTAB concentration, a condition can be reached where little excess CTAB is left in the dried solid. The fact that a peak from templated silica appears in the reaction mixture at ambient temperature demonstrates that the templating reaction occurs at room temperature without further heating, as suggested by Stucky *et al.*[14] This unheated material is stable on drying and calcination, in line with the earlier report of the synthesis of a titanium substituted derivative of MCM-41 under ambient temperature conditions.[21]

Peak intensities and the breakdown behaviour of these unheated ordinary preparation materials point to greatest silicate condensation in those samples which spent the longest time aging in the synthesis gel. *In situ* heating experiments show that the structure formed in the unheated gels is also retained upon heating. It is therefore likely that upon the initial mixing of the template and silica solutions the hexagonal net of MCM-41 is formed and all further heating or aging in the synthesis gel merely increases the extent of silica condensation in the product.

Electron microscopy on the heated products shows that the amount of templated hexagonal phase MCM-41 in the products may be quite small, depending on the hydrothermal conditions. For example, electron diffraction from the "Swiss cheese" morphology (Figure 4.27(b)) showed only diffuse scattering indicating a lack of long range order, perhaps because the tubes have not achieved packing into the hexagonal lattice, but instead have formed a more random aggregate. Such a randomised packing would be possible if the mechanism of Davis *et. al.* were operating.[25] They postulate

the formation of silica encapsulated micelles as discrete species in solution which then aggregate to form the hexagonally packed mesoporous phase before condensation. Under this mechanism, it is clear, that if perfect hexagonal packing were in some way prevented, disordered bunches of tubes could also be frozen into the final silicate material in the same way. Such long silicated micelles have been observed using cryo-TEM on reaction solutions at early stages of the reaction.[61] The charge density matching mechanism of Stucky *et. al.*[14] where a lamellar phase forms first and, under thermodynamic constraints is converted into the lower energy hexagonal phase, is not so consistent with the formation of such disordered arrays.[8]

The evolution of the 42 Å structure with heating differs depending on whether the reaction mixture is stirred. In the unstirred state, extended arrays of templated liquid crystal are able to form and are undisturbed while condensation of water out of the polysilicate counteranion structure of the templated liquid crystal occurs. The data of Figure 4.28(a) suggest some sort of wormlike aggregate formation as a texture forming during this process. Such "tactoids" have known for a long time in anisotropic charged colloidal solutions such as those of tobacco mosaic virus above a critical concentration.[73] The mechanism of their formation is not understood. After calcination an approximately 35 Å structure is made, independent of the heating time, although the product with the greatest degree of long range order appears to be available after only about 2-3 days of heating.

The slight variation in pore sizes observed for the start gels of different preparations could be attributed to the effect of counter-ion concentration effects on the spacing of the silicated liquid crystal precursor phase. Effects related to this have been found when the acid concentration was deliberately varied)[74] and are discussed further with reference to the acid-titrated preparations below, which do not appear to bear this out. In addition, in this work the same start gel was divided to make all of the samples so all concentrations were initially the same. Another source of the variation could be that different amounts of water were lost when the synthesis bomb was opened for sampling. This explanation is doubtful as the bomb was always allowed to cool before opening. The small variation in the decrease of pore size on drying, prior to calcination may, however be explained by differential water loss during storage in the desiccator. The variation after calcination may be due to differing degrees of initial condensation, but other factors must be involved since the sample heated for six days, although suffering the least shrinkage due to calcination, still undergoes the greatest breakdown in long range structure in the process.

In the stirred system, calcination produces material of much lower surface area. Judged by the diffraction line width of the sample heated for six days, the crystals are about half the size of those formed in the unstirred process. However, in systems heated for shorter times, the crystallite sizes in the stirred preparation are slightly larger than those from static preparations. Bragg *d*-spacings range from *ca*. 35 to 38 Å with a strong suggestion of heterogeneity in the six day material. A difference in hexagonal *d*-spacing is therefore detected, as well as texture consequent to stirring. This result might be expected from either of the currently postulated synthesis mechanisms, mechanical stirring disrupting the formation of the initial lamellar phase in the "charge density

matching" mechanism[7,14] or the formation of uniform silicated rod-like micelles in solution which are required by Davis *et al.*[25]

Stirring during heating appears to disrupt the formation of the hexagonal mesoporous MCM-41 phase and allows the freezing in of these disrupted structures with lower surface areas and lower long-range order. The mechanical action of stirring however, does not appear to easily create new, shear-induced phases in the unheated, silicated surfactant system. The hexagonal structure is quite robust and is retained under high shear rates over several hours. Subsequent aging at room temperature did not result in compound peaks as were seen in the stirred, heated preparations. Possibly shear at elevated temperatures has a greater effect on the structure. Some shear alignment of the silicated surfactant micelles was noted in solutions with a high salt content. The hexagonal first order MCM-41 peak was still apparent in such solutions after shear, but had an unusual peak shape with broad wings indicating some effect upon the structure. No higher order peaks were apparent in these solutions, nor in unsheared salted synthesis gels. Overall, then, mechanical shear appears to result in some disruption of the MCM-41 structure, however ionic effects appear to play a much greater role.

As judged by the diffraction patterns shown in Figure 4.19, the stirred, heated preparation gives material containing a number of phases, not purely the desired crystalline molecular sieve phase and these may have different silicate/template/counter-ion stoichiometries. There however, seem to be some "healing" in the calcination process (Figure 4.19) resulting in narrower peaks with less composite nature. This points to the multiple significance of the method of calcination. Not only are physisorbed water and the template molecules eliminated at an early stage of the process, but siloxyl group elimination also occurs, increasing the condensation in the walls. Evidence from ^{29}Si nmr has also pointed to the increase in silica condensation during template removal by various methods.[1,5]

Composite peaks also appear in the SAXS data for static wet gel systems if the stoichiometry is not quite correct and these are attributed to coexisting phases. Pure forms of some of these phases have been synthesised. The cubic analogue to MCM-41 has previously been produced by other researchers in static systems under different reaction conditions.[1] The lamellar phase seen by Monnier *et al.*[10] however, was not observed on the time scale of these experiments. In their work the lamellar phase was seen in freeze-dried samples on reaction times of 1 to 20 minutes whereas here the observations were on gels after reaction times of hours or days. It is suggested that it may be a kinetically favoured phase which precipitates out upon the mixing of the surfactant and the silicate solutions which then redissolves, forming a source of silicate species in a liquid phase ion transportation type process.[75] Such a mechanism is also postulated below to be involved in the process by which acid addition improves long range order. These redissolved species could then interpenetrate the polymerising silica matrix and condense in defects in the structure to form the close packed mesoporous hexagonal phase.

The different nitrogen adsorption behaviour for the unstirred and the stirred systems as a function of gel heating time is noteworthy. The unstirred experiments would appear to

show that the mesoporous structure is in fact destroyed by prolonged heating at the preparation stage but for the stirred system some improvement is clear. For the unstirred system the peaks seen in the small angle X-ray scattering of the washed and dried materials likewise appear to show the destruction of the crystalline phase with heating of the synthesis gel, but calcination, despite the high temperature does not cause significant change in the porosity indicated by the X-ray patterns.

A remarkable feature of the SAXS data for both heated and unheated ordinary preparations (see Tables 4.2 and 4.4) is the contraction of the "hexagonal" net with length of heating time at 100•C, after washing and drying and upon calcination. The elimination of water as the silicate chains condense leads to a densification of *ca* 4% and calcination produces a further densification, from the point of view of lattice spacing, of up to 10%. However, the mere removal of water from the synthesis gel after heating has ended also causes a contraction. The question of how the structure accommodates such changes is unresolved but is probably related to the diffuse nature of the silica walls found in structural studies discussed in the next chapter. Similar contraction on template removal and calcination is reported by Chen *et. al.*[5] who report a lattice contraction with retention of the hexagonal structure during calcining in air at temperatures up to 900•C. There a contraction was also noticed after template removal using HCl/ethanol solution although this was not as severe as for the calcined samples. Calcination in air with P_{water} = 8 torr resulted in a similar degree of contraction to calcination in dry air however the hexagonal structure of MCM-41 broke down at 800•C in the presence of water. An increase in the silica condensation in the walls during template removal by various methods has been observed by ^{29}Si nmr measurements.[1,5,11] The lattice contraction must therefore be due to a combination of factors including degrees of hydration and condensation and the effect of the removal of the surfactant which plays both a physical supporting role and some role in lattice charge neutralisation.

4.7.2 Acid Titrated MCM-41 Syntheses

4.7.2.1 Structure

The addition of acid to the MCM-41 synthesis gels results in an increase in the long-range order which is apparent from the number and intensity of the peaks observed in the diffraction patterns. A similar effect is noted both in unheated and heated preparations, although the same extent of order is not achieved in the unheated syntheses where aging time replaces heating to obtain highly polymerised silicate materials. Materials from the ambient temperature syntheses do however appear more stable once calcined, than materials from some heated preparations. Coherence lengths from these unheated acid-titrated preparations are about half those for similar stages of the heated preparations and are roughly constant in the gel. With drying and washing of aged gels, the crystallite size shows a generally increasing trend with aging time in the gel, which is even more evident in the calcined specimens. A sharp decrease in the size of the scattering domain in the 14 day aged sample after acid addition may indicate that some reforming of the crystallites occurs at this point, as the subsequent samples show a gradual improvement from this point onwards. The retention of coherence length is

greater in these unheated acid titrated materials than in ordinary preparations of the same type, but the heated acid titrated materials show an even better retention of order.

The improved long range order obtained by the acid titration method described above has allowed modelling of the wall structure of MCM-41[76] and this contributes to understanding the mechanism of formation. Structures for MCM-41 derived from acid titrated materials with high long range order are discussed in greater detail in Chapter 5. The major conclusion of that section of the work is that the data requires a three region model for these MCM-41 materials, consisting of a denser continuous wall region, surrounding the hollow parallel channels which are lined with a less dense silica region. The average values obtained for the total wall thicknesses, 15.6(3) Å, for the calcined and 17.5(2) Å for the uncalcined materials are much larger than those estimated from high resolution electron microscopy (8 Å)[57] and combined analysis of nitrogen adsorption isotherms and X-ray diffraction data (12.5 Å).[5,64,77] These earlier methods however, measured only an average wall thickness, since they assume a two region (hole/wall) model. Wall thicknesses measured by these methods of between 4 and 16 Å have been reported for pure silicate MCM-41 syntheses in which the initial pH was controlled.[78] For an optimised ordinary preparation MCM-41 a wall thickness of 17 Å, measured by XRD and nitrogen adsorption, has been reported.[16]

More recently, pure silicate materials from ordinary MCM-41 syntheses have been prepared with wall thicknesses of 13.4-26.8 Å, also measured by these techniques.[79] The *d*-spacing and channel diameters were both also observed to increase in thicker walled samples which required higher synthesis temperatures (165•C) than used for thinner walled materials (70•C). The increase in channel diameter was ascribed to the breakdown of the template surfactant CTAB, into a neutral amine molecule which cannot then stay at the charged interface and moves to the centre of the micelle, swelling the channel. These thick walled materials have BET surface areas which are slightly lower than the thinner walled MCM-41 materials. The BET surface areas measured in that work, around 760 $m^2 g^{-1}$, correspond to those measured for acid-titrated materials above. The thermal stability of the thicker walled materials was also improved over that of thinner walled samples.[79]

The acid-titrated materials appear to be much more hydrothermally stable than those from the ordinary MCM-41 preparation (see discussion of the breakdown of MCM-41 materials in section 4.6 above) and so may well have thicker or more densely polymerised walls than materials from the ordinary preparation to achieve this stability. The completely empty central channel, with a 7 Å radius in the calcined materials, indicated by the structural work in Chapter 5 is also considerably smaller than that observed by others.[2,20,40,58,78,80] Nitrogen isotherms on this material however, indicate pore diameters of 28-35 Å[81] which are equivalent to those measured by other authors. Thus the silicate forming the lining of the channels is possibly itself highly divided and dendritic or that the void space is branched and divergent, a condition that allows adsorbed molecules to penetrate into the walls. Inelastic scattering data,[81] reported in Chapter 6 show that in hydrogen filled MCM-41 at 15 K, about half the adsorbed hydrogen is adsorbed in a reasonably uniform wall site, which also points to highly porous walls.

The form factor data [76] also show that the walls of MCM-41 have very low densities compared to that of colloidal silica. Data from gas adsorption isotherms indicate that the mean density of calcined MCM-41 is about 0.83(5) g cm^{-3}, 0.99 g cm^{-3} for the denser continuous walls and 0.87 g cm^{-3} for the less dense lining of the channels. These values have errors of 4-5% in the absolute values but the difference has an error of less than 1%. These low densities indicate a large amount of void space in the walls. This may be due to counterions binding to the CTAB micelles, as discussed below, causing the silicate polymerisation process to form a loose highly interwoven network rather than dense colloidal silica.

Many factors may influence the density of the silica forming the walls. As the polymerised silica chains are neutral or have low charge, they may be quite hydrophobic and so able to penetrate the CTAB micelle by forcing their way between the surfactant molecules. Work on pure surfactant systems has shown that water molecules may penetrate the micelle surface to distances of 3-6 carbon atoms,[82] so silicate monomers and oligomers could also occupy such regions. Micellar surfaces are known to be rough and, in organic reactions catalysed by cationic micelles, solutes may occupy voids at the surface thereby stabilising the micelle.[83] Neutral polymerised silicate may behave similarly to these hydrophobic organic molecules. As the presence of the surfactant, even in the absence of acid, is known to catalyse silicate polymerisation in MCM-41,[24] an accelerated reaction may also result in looser networks of silica than is typical of the colloidal silicates. Other workers[84] have also noted an increase in the crystallisation rate of a variety of zeolites, including pure silicate structures, templated with quaternary ammonium ions when promoter ions such as PO_4^{3-}, NO_3^-, SO_4^{2-} and CO_3^{2-} were added to the synthesis gel before heating. Liquid state ^{29}Si nmr experiments showed that the promoter ions dramatically accelerated the formation of soluble Q_4 species and their rapid condensation into crystalline silicate units.[84] They conclude that the presence of ionic species with greater polarising ability enhances the process of crystallisation dramatically by speeding up condensation processes between silica-enclathrated template moieties. By analogy, in the formation of mesoporous silicate MCM-41 materials in the presence of acids similar mechanisms may operate and the presence of such ions may also increase the rate of condensation in the synthesis gels of these materials.

Hydrogen adsorption data, also reported in Chapter 6, suggest that all voids in MCM-41 may be connected, or else are extremely uniform. A single, well defined boiling point is observed for all hydrogen contained in the pore system.[81] Small angle neutron scattering from water filled calcined MCM-41 materials discussed in Chapter 5, indicates that all of the void space is accessible to water,[85] and nitrogen adsorption isotherms show no evidence of micropores.[81] The interconnectedness of the pores may be due to the low densities of the walls, however, an alternate model for this material has also been presented,[81] although it is less convincing. MCM-41 may be a defective MCM-48 cubic structure where the smooth-walled channels are largely hexagonally close-packed cylinders, but have interconnections which resemble the infinite periodic minimal surface, which has been postulated as the structure of MCM-48.[86] In projection this would resemble the MCM-41 structure observed in transmission electron

micrographs[57] and diffraction patterns.[19,76] Acid addition during synthesis may in this case, also effect changes on the position of the system within in the silicate/surfactant phase diagram. The initial pH of the silicated surfactant system has previously been shown in a sodium silicate/CTAB gel to determine the formation of lamellar or hexagonal mesophases, with lower pH values favouring hexagonal phase formation.[10] Interchange between MCM-41 and MCM-48 phases during heating hydrothermally under pH controlled conditions at 100•C[18] and between lamellar and MCM-41 phases[23] has also been observed.

4.7.2.2 Counter Ion Effects

The reasonably similar results from the various acids confirm the value of Ryoo's acid-titration method,[19] but the differences, shown in Figure 4.22, do suggest an effect of the counteranion which should be explored further. Phase directing effects of the counteranions of various acids in acidic surfactant templated mesoporous silica have also been reported,[7] as has the beneficial effect on MCM-41 hydrothermal stability of high concentrations of various salts added to the synthesis mixture during preparation.[68] In that case, the addition of sodium acetate in a ratio of NaAc/CTACl = 16 appeared to result in a more stable product than when sodium or potassium chloride, or ETDA was added during the heating process. Addition of such high concentrations of the salts before heating was started resulted in a disordered network of wormlike channels instead of ordered MCM-41 materials. The influence of ionic strength on the surfactant-silica assembly process was also investigated for low (1 M) NaCl concentrations by Monnier *et al*.[10] No salt effect was detected in that work.

The suggestion from these results is that the sulphate ion has had the most beneficial effect in improving the quality of the diffraction pattern in terms of the number and intensity of the diffraction peaks. The order in which the various acids enhance long range order in the calcined material is $SO_4^{2-} > C_2H_3O_2^- > Cl^- > Br^-$. From this it would seem that as well as the direct effect of H^+ on the silicate equilibrium, properties of the anion will also affect the synthesis.

This order appears to be the reverse of the anionic lyotropic series observed for CTAB. The lyotropic series given in Larsen and Magid[87] on the basis of the enthalpy of transfer of the salt from water to solutions of 0.1 M CTABr is: citrate < CO_3^{2-} < SO_4^{2-} < $C_2H_3O_2^-$ < F^- <OH^- < HCO_2^- < Cl^- < NO_3^- < Br^- < $SO_3C_7H_7^-$. It is predicted that titrating the synthesis mix with carbonic or citric acid will promote even greater long range order in the calcined material. Of course, the major ionic component of the solution is the original counterion of the surfactant, in this case, Br^-, as well as the OH^- ion. For a preparation titrated to pH = 11 the total concentration of SO_4^{2-} after addition over the course of the reaction was 8.56×10^{-2} M in an initial solution which contained 0.307 M Br^-. Larsen and Magid[87] observe that although addition of hydroxide decreased the amount of bromide bound to the micelle, no binding of hydroxide was observed in solutions with pH values of 12 to 13. Fluorescence quenching has also shown that OH^- does not directly displace Br^- from the surface of CTAB micelles[83] so, the relative binding strength of bromide and silicate anions will be a more important determinant of structure than the counterions from the titrant, if such effects are

important. Starting with a pure cetyltrimethylammonium chloride, or hydroxide surfactant will thus presumably also enhance the long range order.

Underwood and Anaker,[88] find a similar, although not identical, series for decyltrimethylammonium bromide ranked in order of cmc value. They conclude that the electrostatic headgroup repulsions which hinder assembly of the micellar surface are mitigated most effectively by the least hydrated counterions, which therefore promote the most ordering in the surfactant self-assembly process. It has also been observed for dialkyldimethylammonium surfactants that the properties of their Langmuir films depend greatly on the counterion,[89] with the monolayer being increasingly contracted by anions in the order of increasing hydration (*ie.* $F^- < Cl^- < Br^-$). This means, once again, that the least hydrated ions bind strongest to the surfactant. Large hydrated ions such as fluoride, hydroxide and acetate gave expanded monolayer compression isotherms and did not bind to the surfactant headgroups. The somewhat more hydrated CO_3^{2-} ions showed a lesser degree of binding than SO_4^{2-} ions.[89] This alone could not explain the observed monolayer contractions which indicate that a significant lateral repulsion exists between surfactant headgroups and it was concluded that Stern-layer effects which correlate with the size of the anion are also important. The drop in potential across the Stern layer is proportional to its thickness,[90] and the width of the Stern layer will be related to the counterion size. Presumably, the weaker the binding between the counterions in the reaction mix and the surfactant template, the easier it is for the silicate anion to displace them and so concentrate on the surface of the micelle to polymerise. Tightly bound anions may also become incorporated in the silicate matrix and therefore affect the continuity of the silica polymerisation.

It has also been shown that the aggregation number of a micelle and the fractional micellar charge are affected by the counterion as well as the surfactant concentration.[91] Counterions which promote lower micellar charges may help to slow polymerisation of the silicate and therefore to promote long-range order in the final porous silicate. The size of the micelle may also influence the packing of the silicated species. The observed increase in long-range order dependent on the counterion is small compared to the increase due to the addition of H^+, however it may also improve other properties of the MCM-41 material which have not yet been investigated. Further work using a greater variety of counterions may elucidate this point further.

4.7.2.3 Effect of pH

The effect of the precise pH at which a synthesis is maintained is less strong than the effect of the counteranion. Working with the sulphate ion at a lower pH appears to have been beneficial (Figure 4.22) and the optimum pH for this synthesis appears to be between 9 and 10. This is well below the pH of 10.5-11 at which the neat sodium silicate solution used in this synthesis is found to gel. The gel point of the synthesis mixture also occurs around pH of 11 and can be observed during the acid addition titrations as a distinct viscosity change in the solution and by a slight buffering effect. This buffering effect is probably due to the presence in the solution of dimeric $H_2Si_2O_7$ which has a pK_a of 10.7 and other silicate polyanions with higher pK_a values.[35] Adding further acid once this gel point is passed does not increase the viscosity further and no

further buffering occurs. However, the improvement in the long range order of the product continues in preparations maintained at pH values below this point. It therefore seems unlikely that this crossing of the gel point is directly related to the improvement in order. Some previous work on the effect of the initial pH of the alkaline synthesis gel on wall thickness[78] found that the thickness increased with decreasing pH up to 16 Å, suggesting that a thicker silicate coat is deposited on the micelles as the silica solubility decreases. However, this pH variation did not result in highly ordered material as is the case in the preparations adjusted for pH *during* synthesis.

During the synthesis, heating the titrated reaction gels causes the pH to rise once more. Preparations titrated to maintain a pH of 10 will return to pH values above 11 during the overnight heating following at least the first two acid additions (although not always after the third acid addition). Colloidal silicas have been observed to dissolve just below a pH of 11.[92] Thus by repeatedly returning the synthesis gel to a pH of 10 the reaction is crossing and recrossing this dissolution point during the course of the heating. The potential thus exists for some annealing of the structure to occur through this dissolution and re-precipitation process. Reforming of as-synthesised MCM-41 materials under hydrothermal conditions at pH values of 7-10 has been shown to increase the long-range order of these materials,[18] probably due to a similar dissolution and re-precipitation process. It is also possible that by precipitating a substantial quantity of the silica through lowering the pH, the growth of the MCM-41 crystallites proceeds in a more ordered fashion, with silica drawn as needed from an insoluble form rather than from soluble polyanions.

4.8 Conclusions

The work described above allows a number of conclusions to be drawn. From a mechanistic point of view, the Langmuir trough work shows that it is possible to create a silicated-surfactant species with quite different surface behaviour to that of the pure surfactant. This species is found to occur in solutions with CTAB concentrations below that of the cmc for the pure surfactant, and does not show the X-ray diffraction peaks characteristic of MCM-41. It seems likely then, that the formation of MCM-41 occurs when assemblies of these silicated surfactant species form and further polymerisation of the silicate framework occurs.

The aggregation of these species occurs quickly in solution - too quickly to be directly observed using the methods available - and the composite structure formed at the point of mixing the preparation components is retained in both unheated and heated preparations. Further improvements in the structure appear to occur via densification of the silica network, and possibly through the agglomeration of smaller MCM-41 crystallites to create the larger coherence lengths observed in the acid-titrated structures. Ionic interactions, observed both in the shear experiments and in the variation of order when using different acid titrants obviously play a large role in the ordering of the structure, presumably because of charge screening effects between silicated micelles.

Structurally and from the synthetic point of view, the MCM-41 materials can be synthesised in the simplest case under ambient temperature conditions where silica

condensation occurs during aging time in the synthesis gel. Such materials can be isolated and are stable to calcination, giving surface areas comparable to those from heated preparations.

The initial investigation of the heated preparation settled a number of parameters used in subsequent preparations. The best material, judged by all of the factors studied is concluded to be that heated at 100•C for three days without stirring. Excess heating time destroys the desired crystalline mesoporous structure of MCM-41, leaving amorphous silicate. Similarly the reagent concentrations must be carefully controlled in order to produce material templated from only one liquid crystalline phase.

The acid titration method, first suggested by Ryoo and Kim[19] was extended in this work both to unheated preparations and to a wider range of acid titrants and pH conditions. Titration with 1M acid during the synthesis to maintain a selected pH proved to increase long range order in MCM-41 materials significantly in both heated and unheated preparations, as indicated by the X-ray diffraction data. Up to seven orders of diffraction were observed in synchrotron X-ray studies of material from a heated preparation. Materials prepared at a pH of 9-10 had the sharpest diffraction peaks, indicating larger crystallite sizes, and these remained intact to a greater degree than those in the ordinary preparation throughout the synthetic process. The best results were achieved using sulphuric acid, although the effect of the counterion is small compared to the overall effect of the acid addition. The counterion effect may be due to the strength of the binding between the ion and the surfactant, however the reasons for the greater ordering of the overall structure remain unclear.

4.9 References

1. C.T. Kresge, M.E. Leonowicz, W.J. Roth, J.C. Vartuli and J.S. Beck, *Nature*, **1992**, *359*, 710-712.
2. J.S. Beck, J.C. Vartuli, W.J. Roth, M.E. Leonowicz, C.T. Kresge, K.D. Schmitt, C.T.-W. Chu, D.H. Olson, E.W. Sheppard, S.B. McCullen, J.B. Higgins and J.L. Schlenker, *J. Am. Chem. Soc.*, **1992**, *114*, 10834-10843.
3. J.S. Beck, C.T.-W. Chu, I.D. Johnson, C.T. Kresge, M.E. Leonowicz, W.J. Roth and J.C. Vartuli, *US Patent, No. 5,108, 725*, **1992**.
4. C.Y. Chen, S.L. Burkett, H.-X. Li and M.E. Davis, *Microporous Mater.*, **1993**, *2*, 22.
5. C.-Y. Chen, H.-X. Li and M.E. Davis, *Microporous Mater.*, **1993**, *2*, 17.
6. J.S. Beck, J.C. Vartuli, G.J. Kennedy, C.T. Kresge, W.J. Roth and S.E. Schramm, *Chem. Mater.*, **1994**, *6*, 1816-1821.
7. Q. Huo, D.I. Margolese, U. Ciesla, D.G. Demuth, P. Feng, T.E. Gier, P. Sieger, A. Firouzi, B.F. Chmelka, F. Schüth and G.D. Stucky, *Chem. Mater.*, **1994**, *6*, 1176-1191.
8. J.C. Vartuli, K.D. Schmitt, C.T. Kresge, W.J. Roth, M.E. Leonowicz, S.B. McCullen, S.D. Hellring, J.S. Beck, J.L. Schlenker, D.H. Olson and E.W. Sheppard in *Zeolites and Related Microporous Materials: State of the Art 1994.*; Stud. Surf. Sci. Catal., (Eds. J. Weitkamp, H.G. Karge, H. Pfeifer and W. Hölderich), Elsevier Science B.V., **1994**, *Vol. 84A*, 53-60.

9. J.C. Vartuli, C.T. Kresge, M.E. Leonowicz, A.S. Chu, S.B. McCullen, I.D. Johnson and E.W. Sheppard, *Chem. Mater.*, **1994**, *6*, 2070-2077.
10. A. Monnier, F. Schüth, Q. Huo, D. Kumar, D. Margolese, R.S. Maxwell, G.D. Stucky, M. Krishnamurty, P. Petroff, A. Firouzi, M. Janicke and B.F. Chmelka, *Science*, **1993**, *261*, 1299-1303.
11. P.T. Tanev and T.J. Pinnavaia, *Science*, **1995**, *267*, 865-867.
12. Q. Huo, D.I. Margolese, U. Ciesa, P. Feng, T.E. Gier, P. Sieger, R. Leon, P.M. Petroff, F. Schüth and G.D. Stucky, *Nature*, **1994**, *368*, 317-321.
13. A. Firouzi, D. Kumar, L.M. Bull, T. Besier, P. Sieger, Q. Huo, S.A. Walker, J.A. Zasadzinski, C. Glinka, J. Nicol, D. Margolese, G.D. Stucky and B.F. Chmelka, *Science*, **1995**, *267*, 1138-1143.
14. G.D. Stucky, A. Monnier, F. Schüth, Q. Huo, D. Margolese, D. Kumar, M. Krishnamurty, P. Petroff, A. Firouzi, M. Janicke and B.F. Chmelka, *Mol. Cryst. Liq. Cryst.*, **1994**, *240*, 187-200.
15. J. Liu, A.Y. Kim, J.W. Virden and B.C. Bunker, *Langmuir*, **1995**, *11*(3), 689-692.
16. C.-F. Cheng, D.H. Park and J. Klinowski, *J. Chem. Soc., Faraday Trans.*, **1997**, *93*(1), 193-197.
17. D. Khushalani, A. Kuperman, N. Coombs and G.A. Ozin, *Chem. Mater.*, **1996**, *8*(8), 2188-2193.
18. Q. Huo, D.I. Margolese and G.D. Stucky, *Chem. Mater.*, **1996**, *8*(5), 1147-1160.
19. R. Ryoo and J.M. Kim, *J. Chem. Soc., Chem. Commun.*, **1995**, 711-712.
20. P.T. Tanev and T.J. Pinnavaia, *Chem. Mater.*, **1996**, *8*(8), 2068-2079.
21. P.T. Tanev, M. Chibwe and T.J. Pinnavaia, *Nature*, **1994**, *368*, 321-323.
22. A. Tuel and S. Gontier, *Chem. Mater.*, **1996**, *8*, 114-122.
23. A. Matijasic, A.-C. Voegtlin, J. Patarin, J.L. Guth and L. Huve, *J. Chem. Soc., Chem. Commun.*, **1996**, 1123-1124.
24. C.-F. Cheng, Z. Luan and J. Klinowski, *Langmuir*, **1995**, *11*, 2815-2819.
25. M.E. Davis, C.-Y. Chen, S.L. Burkett and R.F. Lobo in *Mat. Res. Soc. Symp. Proc. "Better Ceramics Through Chemistry VI"*; "Better Ceramics Through Chemistry IV", (Eds. C.J.B. A. K. Cheetham M. L. Mecartney and C. Sanchez), Materials Research Society, Pittsburg, PA, **1994**, *Vol. 346*, 831-842.
26. T. Wolff and G. von Bünau, *Ber., Bunsenges Phys. Chem.*, **1981**, *88*, 1098.
27. L. Sepúlveda and J. Cortes, *J. Phys. Chem.*, **1985**, *89*, 5322.
28. K.J. Edler and J.W. White, *Chem. Mater.*, **1997**, *9*(5), 1226-1233.
29. A.W. Adamson, *Physical Chemistry of Surfaces*; 4th ed., John Wiley & Sons, New York, **1982**.
30. P.M. Saville, I.R. Gentle, J.W. White, J. Penfold and J.P.R. Webster, *J. Phys. Chem.*, **1994**, *98*, 5935-5942.
31. P.S. Goyal, B.A. Dasannacharya, V.K. Kelkar, C. Manohar, K. Srinivasa Rao and B.S. Valaulikar, *Physica B*, **1991**, *174*, 196-199.
32. J.R. Lu, M. Hromadova, E.A. Simister, R.K. Thomas and J. Penfold, *J. Phys. Chem.*, **1994**, *98*(44), 11519-11526.
33. P.F. Holt and E.T. Nasrallah, *J. Chem. Soc. C*, **1969**, (5), 823.
34. J.E. Iribarnegaray, T.J. Minones, S.F. Garcia and P. San Pedrero in *Chem. Phys. Chem. Anwendungstech. Grenzflaechenaktiven Stoffe, Ber, Int. Kong. 6th 1972*; Carl Hauser Verlag, Munich, **1973**.

35. R.K. Iler, *The Chemistry of Silica. Solubility, Polymerization, Colloid and Surface Properties, and Biochemistry*, John Wiley & Sons, New York, **1979**.
36. H. Yang, A. Kuperman, N. Coombs, S. Mamiche-Afara and G.A. Ozin, *Nature*, **1996**, *379*, 703-705.
37. H. Yang, N. Coombs, I. Sokolov and G.A. Ozin, *Nature*, **1996**, *381*, 589-592.
38. I.A. Aksay, M. Trau, S. Manne, I. Honma, N. Yao, L. Zhou, P. Fenter, P.M. Eisenberger and S.M. Gruner, *Science*, **1996**, *273*, 892-898.
39. M.T. Anderson, J.E. Martin, J.G. Odinek and P. Newcomer in *Microporous and Macroporous Materials*; Mat. Res. Soc. Symp. Proc., (Eds. R.F. Lobo, J.S. Beck, S.L. Suib, D.R. Corbin, M.E. Davis, L.E. Iton and S.I. Zones), MRS, Pittsburgh, **1995**, *Vol. 431*, 217-223.
40. A. Ortlam, J. Rathousky, G. Schulz-Ekloff and A. Zukal, *Microporous Mater.*, **1996**, *6*(4), 171-180.
41. N.K. Raman, M.T. Anderson and C.J. Brinker, *Chem. Mater.*, **1996**, *8*(8), 1682-1701.
42. K.J. Edler, J. Dougherty, R. Durand, L. Iton, G. Kirton, G. Lockhart, Z. Wang, R. Withers and J.W. White, *Colloids Surfaces A*, **1995**, *102*, 213-230.
43. J.B. Hayter and J. Penfold, *J. Phys. Chem.*, **1984**, *88*(20), 4589-4593.
44. P.G. Cummins, E. Staples, J.B. Hayter and J. Penfold, *J. Chem. Soc., Faraday Trans. 1*, **1987**, *83*(9), 2773-2786.
45. L. Auvray, A. Ayral, T. Dabadie, L. Cot, C. Guizard and J.D.F. Ramsay, *Faraday Discuss.*, **1995**, *101*, 235-247.
46. T. Dabadie, A. Ayral, C. Guizard, L. Cot and P. Lacan, *J. Mater. Chem.*, **1996**, *6*(11), 1789-1794.
47. Y.S. Lee, D. Surjadi and J.F. Rathman, *Langmuir*, **1996**, *12*(26), 6202-6210.
48. S.E. Friberg, S.M. Jones, A. Motyka and G. Broze, *J. Mater. Sci.*, **1994**, *29*, 1753-1757
49. B.E. Warren, *X-Ray Diffraction*, Dover Publications Inc., New York, **1990**.
50. P.J. Branton, P.G. Hall and K.S.W. Sing, *J. Chem. Soc., Chem Commun.*, **1993**, 1257-1258.
51. C.J. Brinker and G.W. Scherer, *Sol-Gel Science. The Physics and Chemistry of Sol-Gel Processing*, Academic Press, San Diego, **1990**.
52. I. Petrovic, A. Navrotsky, C.-Y. Chen and M.E. Davis in *Zeolites and Related Microporous Materials: State of the Art 1994*; Studies in Surface Science and Catalysis, (Eds. J. Weitkamp, H.G. Karge, H. Pfeifer and W. Hölderich), Elsevier Science B.V., Amsterdam, **1994**, *Vol. 84*, 677-684.
53. P.J. Branton, P.G. Hall, K.S.W. Sing, H. Reichert, F. Schüth and K.K. Unger, *J. Chem. Soc., Faraday Trans.*, **1994**, *90*(19), 2965-2967.
54. S.J. Gregg and K.S.W. Sing, *Adsorption, Surface Area and Porosity*; 2nd ed., Academic Press, New York, **1982**.
55. M. Dubois, T. Gulik-Krzywicki and B. Cabane, *Langmuir*, **1993**, *9*(3), 673-680.
56. D. Khushalani, A. Kuperman, G.A. Ozin, K. Tanaka, J. Garcés, M.M. Olken and N. Coombs, *Adv. Mater.*, **1995**, *7*(10), 842-846.
57. V. Alfredsson, M. Keung, A. Monnier, G.D. Stucky, K.K. Unger and F. Schüth, *J. Chem. Soc., Chem. Commun.*, **1994**, 921-922.
58. K.R. Kloetstra, H.W. Zandbergen, M.A. van Koten and H. van Bekkum, *Catal. Lett.*, **1995**, *33*, 145-156.

59. W.C. Ackerman, D.M. Smith, J.C. Huling, Y.-W. Kim, J.K. Bailey and C.J. Brinker, *Langmuir*, **1993**, *9*, 1051-1057.
60. A. Chenite, Y. Le Page and A. Sayari, *Chem. Mater.*, **1995**, *7*, 1015-1019.
61. O. Regev, *Langmuir*, **1996**, *12*(20), 4940-4944.
62. J.M. Kim, J.H. Kwak, S. Jun and R. Ryoo, *J. Phys. Chem.*, **1995**, *99*, 16742-16747.
63. Z. Luan, C.-F. Cheng, H. He and J. Klinowski, *J. Phys. Chem.*, **1995**, *99*, 10590-10593.
64. Z. Luan, H. He, W. Zhou, C.-F. Cheng and J. Klinowski, *J. Chem. Soc., Faraday Trans.*, **1995**, *91*(17), 2955-2959.
65. A. Corma, M.S. Grande, V. Gonzalez-Alfaro and A.V. Orchilles, *J. Catal.*, **1996**, *159*, 375-382.
66. C.H. Rhee and J.S. Lee, *Catal. Lett.*, **1996**, *40*(3/4), 261-264.
67. A. Corma, V. Fornés, M.T. Navarro and J. Pérez-Pariente, *J. Catal.*, **1994**, *148*, 569-574.
68. R. Ryoo and S. Jun, *J. Phys. Chem. B*, **1997**, *101*(3), 317-320.
69. V.Y. Gusev, X. Feng, Z. Bu, G.L. Haller and J.A. O'Brien, *J. Phys. Chem.*, **1996**, *100*(6), 1985-1988.
70. T. Ishikawa, M. Matsuda, A. Yasukawa, K. Kandori, S. Inagaki, T. Fukushima and S. Kondo, *J. Chem. Soc., Faraday Trans.*, **1996**, *92*(11), 1985-1989.
71. J. Teixeira in *On Growth and Form - Fractal and Non-Fractal Patterns in Physics*; NATO ASI Series, Series E: Applied Sciences, (Eds. H.E. Stanley and N. Ostrowsky), Martinus Nijhoff Publishers, Dordrecht, **1986**, *Vol. 100*, 145-162.
72. O. Glatter and O. Kratky, *Small Angle X-ray Scattering*, Academic Press, London, **1982**.
73. A. Klug and D.L.D. Caspar, *Advan. Virus Res.*, **1950**, *7*, 225.
74. L. Iton, Personal Communication, 2 September 1993.
75. Z. Gabelica, E.G. Derouane and N. Blom in *Catalytic Materials: Relationship Between Structure and Reactivity*; ACS Symp. Ser. 248, (Eds. T.E. Whyte, R.A. Dalla Betta, E.G. Derouane and R.T.K. Baker), ACS, **1984**, 219-252.
76. K.J. Edler, P.A. Reynolds, J.W. White and D. Cookson, *J. Chem. Soc., Faraday Trans.*, **1997**, *93*(1), 199-202.
77. M.D. Alba, A.I. Becerro and J. Klinowski, *J. Chem. Soc., Faraday Trans.*, **1996**, *92*(5), 849-854.
78. N. Coustel, F. Di Renzo and F. Fajula, *J. Chem. Soc., Chem. Commun.*, **1994**, 967-968.
79. C.-F. Cheng, W. Zhou, D.H. Park, J. Klinowski, M. Hargreaves and L.F. Gladden, *J. Chem. Soc., Faraday Trans.*, **1997**, *93*(2), 359-363.
80. E. Terrés, S.S. Ramirez, J.M. Dominguez, A. Montoya, J. Navarrete and M. Gómez-Cisneros in *Microporous and Macroporous Materials*; Mat. Res. Soc. Symp. Proc., (Eds. R.F. Lobo, J.S. Beck, S.L. Suib, D.R. Corbin, M.E. Davis, L.E. Iton and S.I. Zones), MRS, Pittsburgh, **1995**, *Vol. 431*, 111-116.
81. K.J. Edler, P.A. Reynolds, P.J. Branton, F. Trouw and J.W. White, *J. Chem. Soc., Faraday Trans.*, **1997**, *93*(8), 1667-1674.

82. J.H. Fendler and E.J. Fendler, *Catalysis in Micellar and Macromolecular Systems*, Academic Press, New York, **1975**.
83. C.A. Bunton in *Cationic Surfactants: Physical Chemistry*; Surfactant Science Series, (Eds. D.N. Rubingh and P.M. Holland), Marcel Dekker, New York & Basel, **1991**, *Vol. 37*, 323-405.
84. R. Kumar, A. Bhaumik, R.K. Ahedi and S. Ganapathy, *Nature*, **1996**, *381*, 298-300.
85. K.J. Edler, P.A. Reynolds and J.W. White, *J. Phys. Chem.*, **1997**, submitted.
86. V. Alfredsson and M.W. Anderson, *Chem. Mater.*, **1996**, *8*(5), 1141-1146.
87. J.W. Larsen and L.W. Magid, *J. Am. Chem. Soc.*, **1974**, *96*(18), 5774-5782.
88. A.L. Underwood and E.W. Anacker, *J. Colloid & Interface Sci.*, **1987**, *117*(1), 242-250.
89. J. Marra, *J. Phys. Chem.*, **1986**, *90*(10), 2145-2150.
90. R. Hunter, *Zeta Potential in Colloid Science*, Academic Press, London, **1981**.
91. S. Berr, R.M. Jones and J.S. Johnson Jr, *J. Phys. Chem.*, **1992**, *96*(13), 5611-5614.
92. H.E. Bergna in *The Colloid Chemistry of Silica*; Advances in Chemistry Series, (Ed. H.E. Bergna), American Chemical Society, Washington D.C., **1994**, *Vol. 243*, 1-47.

Chapter 5:

Description of MCM-41 Structure

"If it were possible to bore parallel cylindrical holes through solid silica, a series of samples with holes of different sizes could be made while keeping a constant pore volume per gram of silica. . . Since all the pores are the same size, they would all fill at once when a certain vapour pressure is reached. Also, since the pores are of uniform size, no hysteresis should be observed. . . This idealised situation, of course, does not occur in actual silica gels. . . "

Ralph K. Iler, The Chemistry of Silica, p491.

MCM-41 is often proposed as a model mesoporous adsorbent, the perfect material for comparison between experiment and theory in the adsorption field.[1-3] The characteristics of MCM-41 cited as making it a model adsorbent are[4] (1) it consists of an array of uniform hexagonal channels of tuneable size, (2) the pore length is significantly greater than the pore diameter (3) the absence of pore channel intersections guarantees that pore networking effects are negligibly small and (4) X-ray diffraction can provide an independent estimate of pore sizes. The work described in this chapter throws doubt on at least one of the first three characteristics, and suggests that the quality of most published diffraction patterns is insufficient to develop a detailed model for MCM-41. The other significant proposed application of MCM-41, as an inert, high surface area substrate for catalytic applications, which often involves attachment of active molecules to the inner pore surfaces, would also benefit from a more detailed model of the wall structure. This would clarify the mode of attachment and subsequent activity of the guest molecules.

The structure of MCM-41 has for the most part, been assumed to consist of amorphous silica of density similar to that of colloidal silicas,[5,6] pierced by large holes which do not greatly perturb the wall structure. This simple model of the structure has not been verified because of the small number of peaks in the MCM-41 X-ray diffraction patterns. Patterns showing only three or four broad peaks, which are the norm in published literature, do not contain sufficient information about the channel arrangement to allow detailed modelling of the wall structure. The width of these diffraction peaks, and the fact that it has been possible to improve the number and sharpness of visible diffraction peaks from MCM-41 by various preparative methods,

indicate that the channels of these four-peak materials are not very well ordered. Nitrogen isotherm measurements have shown that no micropores are present in the structure,[7] but make no further conclusions concerning the nature of the walls. With the improvements to the preparation reported in Chapter 4, it has been possible to gain more information from the diffraction patterns of the MCM-41 materials and so to propose a structural model which is much more detailed than those previously reported.

5.1 Introduction

As discussed in Chapter 3, the characterisation of MCM-41 in this work is performed using several techniques. Given the mesoscale size range of the structure, small angle scattering and small angle diffraction techniques have been most useful in determining the detailed structure of the material. The model derived from X-ray diffraction is supported by neutron diffraction measurements on adsorbed hydrogen. The results from small angle neutron scattering contrast variation experiments are also compatible with the proposed model.

As mentioned above, the small number of X-ray diffraction peaks from MCM-41 in most published reports has made the determination of a detailed wall structure for this material difficult. Work on MCM-41 wall structure has concentrated on experimental measurements of various types. Most commonly, wall thicknesses are calculated using a combination of nitrogen or argon adsorption isotherms and X-ray data. The thickness is found by subtracting the pore diameter found from the adsorption isotherm from the centre to centre distance of the cylindrical pores found from the X-ray *d*-spacing.[8-15] This method implicitly assumes smooth walled mesopores, since the calculation of pore diameters from adsorption isotherms assumes an absence of micropores.[16]

Pore dimensions have also been calculated using ^{1}H nmr measurements of the phase transitions of water in the MCM-41 channels. These were however, calibrated against nitrogen adsorption isotherms and electron micrograph measurements.[17] In that work a factor is included in the pore radius to achieve agreement with nitrogen isotherm measurements. It is ascribed to a non-freezing layer of water on the pore surface which acts physically as the pore wall reducing the effective, observed pore radius, analogous to the multilayer thickness factor in pore size determination from nitrogen adsorption isotherms. Wall thicknesses are also calculated from through focus high resolution electron microscopy (HREM) photographs with minimum wall thicknesses found to be around 8 Å[18] but higher values also often quoted (10-13 Å).[18,19] The larger values are often explained as being edge or angled views of the wall structure. Some evidence for wall roughness and the presence of amorphous material in the MCM-41 pores has also been found using this technique, and is supported by thermoporimetry on adsorbed water.[20]

Some modelling work has been carried out. A molecular dynamics simulation by Feuston and Higgins[6] used an empirical interaction potential for vitreous silica in a model which contained fixed pores of diameter 39.6 Å, and filled the interstitial spaces with various thicknesses of silica, or kept the lattice constant fixed at 44.6 Å, while

varying the wall thicknesses between 5.9 Å and 10.9 Å. Silica was placed into the structure with a density close to that of vitreous silica and annealed. Atoms were added to ensure most silicon atoms were bound to four oxygens. These simulations resulted in structures with a predominance of 4 and 5-fold siloxane rings whereas experimental results have shown a high proportion of 3-fold[5] and 4-fold[21] siloxane rings. Diffraction patterns calculated from this work show up to four peaks, with the thickest wall structure simulated (11 Å) giving the best correspondence with experiment.

Another theoretical calculation using Monte Carlo methods tried to simulate the nitrogen adsorption isotherms obtained for MCM-41.[22] Again, a smooth pore appears to have been implicitly assumed, with the oxygen atom radius taken from studies of silicalite. The interaction parameter between nitrogen and an MCM-41 oxygen was found by fitting simulated isotherms to experimental results. The results of this simulation suggest that the shape of experimental isotherms indicate the presence of pores which are not monodisperse, and the presence of some micropores (diameter < 2 nm). The situation contrasts with that for buckytubes in which good agreement between experiment and calculations was found. Another study of adsorption isotherms modelled the MCM-41 as smooth cylinders between energetically homogeneous walls 10(3) Å thick.[4] Their predicted isotherms followed the stepwise behaviour of the observed nitrogen adsorption isotherm, but the work showed that a more detailed model of the MCM-41 wall was necessary, to account for the energetic heterogeneity observed in this material.

Beck *et al.*[8] fit X-ray diffraction data containing four peaks using models based both on a hexagonal three-dimensional tetrahedral framework and on hexagonal arrays of cylindrical shells with walls having a continuous distribution of scattering matter. They concluded that any model with a hexagonal array of cylindrical pores and thin walls will exhibit similar patterns, so that diffraction intensities were of limited use in structure determination. Stucky *et al.*[23] report briefly a structure based on fitting of diffraction data containing five to six peaks from the MCM-41 hexagonally packed channel array. They used a model which assumed an amorphous continuous scatterer for the walls, with a periodic array of void tubes. Two parameters were refined, the wall thickness and the pore shape, by using analytically derived functions to describe hexagonal and cylindrical geometries as wall shape functions. They found a best fit for walls 8(1) Å thick for unit cells between 37.5 - 46.9 Å and hexagonal shaped pores. This gave void space fractions of 0.6-0.7 which compared to experimental measurements of 0.62 - 0.74, for argon and nitrogen adsorption measurements.

Other simulations have been performed for the mesoporous silicate FSM-16 using X-ray diffraction (XRD) data containing four peaks, nitrogen adsorption data and transmission electron micrographs.[24] This material has similar pore dimensions to MCM-41 but is synthesised by intercalation of quaternary ammonium surfactants into a layered silicate (kanemite) and there is some debate over whether FSM-16 and MCM-41 are the same material.[18,25] In this study by Inagaki *et al.*[24] the uncalcined materials were found to have pore walls 4 Å thick with a pore diameter of 42 Å, while the calcined materials contained walls 8 - 9 Å thick with pore diameters of 34-37 Å. These were in good agreement with nitrogen isotherm measurements (pore diameters

27-35 Å , wall thickness 16 Å, for the calcined material) and transmission electron micrographs (pore diameter 31 Å, wall thickness 12 Å) for the same materials. The XRD intensity profile was fitted for a hexagonal arrangement of infinitely long cylinders, allowing for hexagonal symmetry by allowing overlap between neighbouring rods. Inagaki and co-workers[24] propose that the walls are made up of a single, or double layer of silica tetrahedra, with the pore shrinkage caused by the degree of wrinkling of the silicate layers. The uncalcined material would have stretched walls, due to the large surfactant cations attached to the walls, while the calcined materials would have strongly wrinkled walls due to the removal of the large cations. This would allow the surface to buckle, and then condense during calcination to form the observed thicker walls. They also acknowledge that this mechanism does not fully account for the observed thickness change.

A study by Ortlam *et al.*[26] calculated pore size by assuming it to be dependent upon the size of the template micelles. This is determined by the packing parameter *v/al* where *v* is the volume of the hydrocarbon chain, *a* the headgroup area and *l* the maximum effective chain length (somewhat less than the fully extended molecular length of the chain). For cylindrical micelles, $1/3<v/al<1/2$. The parameter, *a*, is known to be sensitive to the surfactant counterion, and for silicate species used in that work, was taken to be 0.63 nm^2. The volume and length of the hydrocarbon chain were taken from previous work on surfactants. The mean micelle diameter thus calculated was then assumed to be the pore diameter. A relationship between pore volume, pore diameter, wall density and wall thickness was then derived, wherein a wall density of 2.3 g cm^{-3}, typical of non-porous aluminosilicates was assumed. This relationship was used along with pore diameters from nitrogen adsorption isotherms and unit cell measurements from XRD to calculate experimental wall thicknesses which ranged from 9 to 12 Å. The calculated micelle diameters and pore volumes (assuming wall thicknesses of 8 - 10 Å) gave reasonable agreement with experiment. Calculating back from their experimental results, however, gave a wall density for silica of 1.8 g cm^{-3} and substitution of the density of the MCM-41 walls found in this work (below) resulted in wall thicknesses of around 20 Å, close to those calculated from the X-ray modelling discussed below. This model is, therefore not inconsistent with the structure derived in this work.

5.2 Macroscopic Structure

The morphology of the MCM-41 crystallites has been discussed in Chapter 4 (see the scanning electron micrographs in Figures 4.25, 4.26). No evidence of regular hexagonal crystallites, as seen by other workers,[8,27] was found in this work for either the ordinary preparation materials, or the more highly ordered materials from the acid-titrated preparations. For the materials with greater long range order, scanning electron micrographs show smooth, rounded particles, with frequent, large scale wormlike protrusions, but no evidence of spheres or any other regular shape (see Figures 4.30, 4.31). Transmission electron microscopy (shown in Figures 4.27, 4.28) suggests that the MCM-41 particles consist of bundles of tubes packed in a fairly ordered manner, which then agglomerate with other such bundles, forming the larger particles. Scherrer

analysis of the peak widths from small angle diffraction patterns gives coherence lengths of the order of 1000 - 2000 Å. This corresponds to the size of the large wormlike agglomerations, and curled tubes imaged in the TEM. No further ordering on a macroscopic scale was observed for the materials studied in this work, although other workers have prepared mesoporous spheres with millimetre dimensions,[28] patterned silicate structures resembling diatoms[29] and other very large scale (200 nm--0.5 μm) structures.[30] Monoliths of silica/surfactant composites in the hexagonal, cubic and lamellar phases have also been prepared,[31] with dimensions governed by those of the container in which they were made.

5.3 Mesoscopic Structure

The silicate in MCM-41 surrounds hollow tubes, which are arranged in a relatively regular two dimensional hexagonal array. The material appears otherwise to be amorphous. There is considerable interest in improving the order of the channel array in the final product and in discovering the structure of the walls of the tubes, and their detailed arrangement. Improved X-ray diffraction experiments are one straightforward way to validate more detailed models. Some work on diffraction studies has been reported previously and is described above. The results of the optimised synthetic work described in Chapter 4 allow a more detailed analysis using seven diffraction peaks, and this, combined with data from small angle neutron scattering, and neutron diffraction on hydrogen adsorbed in MCM-41 has resulted in a more detailed model of the wall structure. Quasielastic and inelastic neutron scattering studies of molecules adsorbed in MCM-41, which are described in Chapter 6, provide further support for this model.

5.3.1 Synchrotron X-Ray Study

5.3.1.1 Background

Chapter 4 describes the optimisation of the MCM-41 synthesis. Heating of a CTAB/silicate gel system for periods of about three days at 100˚C, produces a material with X-ray diffraction patterns showing two or three orders of the in-plane (35 Å) *d*-spacing.[32] An improvement to this method was reported by Ryoo and Kim,[33] who took account of the fact that during the synthesis the pH of the system generally rises, and that this might well be inimical to the crystallisation process. Further optimisation of this synthesis by monitoring the observed number of orders of the X-ray diffraction and the intensities of the peaks is reported in Chapter 4 and resulted in materials having in-plane *d*-spacings of around 44 Å. The centre-to-centre distance between the hexagonally arranged channels in the MCM 41 matrix is equal to $2/\sqrt{3}$ times the *d*-spacing from X-ray diffraction patterns for this material.

The synthesis gels for the materials studied using synchrotron X-rays were made up as described in Chapter 4 and were titrated during synthesis with one molar sulphuric or acetic acid to maintain the pH of the reaction mixture at 11, while heating at 100˚C was carried out for 4 days. The molar composition of the synthesis gels were typically 1.00 CTAB/ 1.89 SiO_2/ 0.738 Na_2O/ 0.267 H_2SO_4/ 0.123 HX/ 160 H_2O, where HX is the

acid used as titre in each case. The MCM-41 materials were calcined in a muffle furnace at 500˚C overnight. The sulphuric acid treated samples were from the same preparation, but were calcined at two different times and are labelled (1) and (2), with (2) having been calcined several months later than (1). Nitrogen isotherms at 77 K were obtained from the calcined samples using a Sartorius microbalance, to determine the surface areas. The BET surface areas were 990 $m^2\ g^{-1}$ for material titrated with sulphuric acid, and 750 $m^2\ g^{-1}$ for the material titrated with acetic acid. Nitrogen adsorption isotherms are discussed in more detail in Chapter 6, section 6.8.

5.3.1.2 Results and Discussion

Figure 5.1 shows the patterns obtained from uncalcined and calcined specimens produced by titration with sulphuric acid during synthesis. This is the most highly ordered material obtained so far. Peak areas, on an arbitrary but constant scale, and *d*-spacings, indexed on a two dimensional hexagonal lattice, for calcined and uncalcined samples from preparations titrated with sulphuric and acetic acids are given in Tables 5.1 and 5.2 below.

Table 5.1 *Observed x-ray intensities after background fitting and subtraction, from template containing and calcined MCM-41, produced from sulphuric acid and acetic acid controlled pH synthesis conditions.*

Reflection	Sample				
	H_2SO_4 (1) Calcined	H_2SO_4 (2) Calcined	H_2SO_4 Uncalcined	CH_3COOH Calcined	CH_3COOH Uncalcined
(10)	26.683	*	10.082	*	6.574
(11)	6.576	5.536	1.637	5.536	1.156
(20)	4.465	3.984	1.335	4.317	0.894
(21)	2.436	2.595	1.245	2.249	0.813
(30)	0.124	0.162	0.119	0.171	-
(22)	0.030	0.087	0.059	0.069	-
(31)	0.141	0.187	0.065	0.171	-

Note: * Peaks which had their tops cut off in the process of data extraction.
- Peaks at these positions had no visible intensity.

On removing the template by calcination there is a contraction in the average *d*-spacing from *ca.* 42 Å to 39 Å. This may increase the density of the walls, increasing the X-ray contrast between walls and channels. In addition, removal of the channel contents, template, and perhaps some water, will also increase this contrast. The effect of this change in contrast can be seen in the much higher intensities obtained for calcined specimens in Table 5.1 compared with the uncalcined ones.

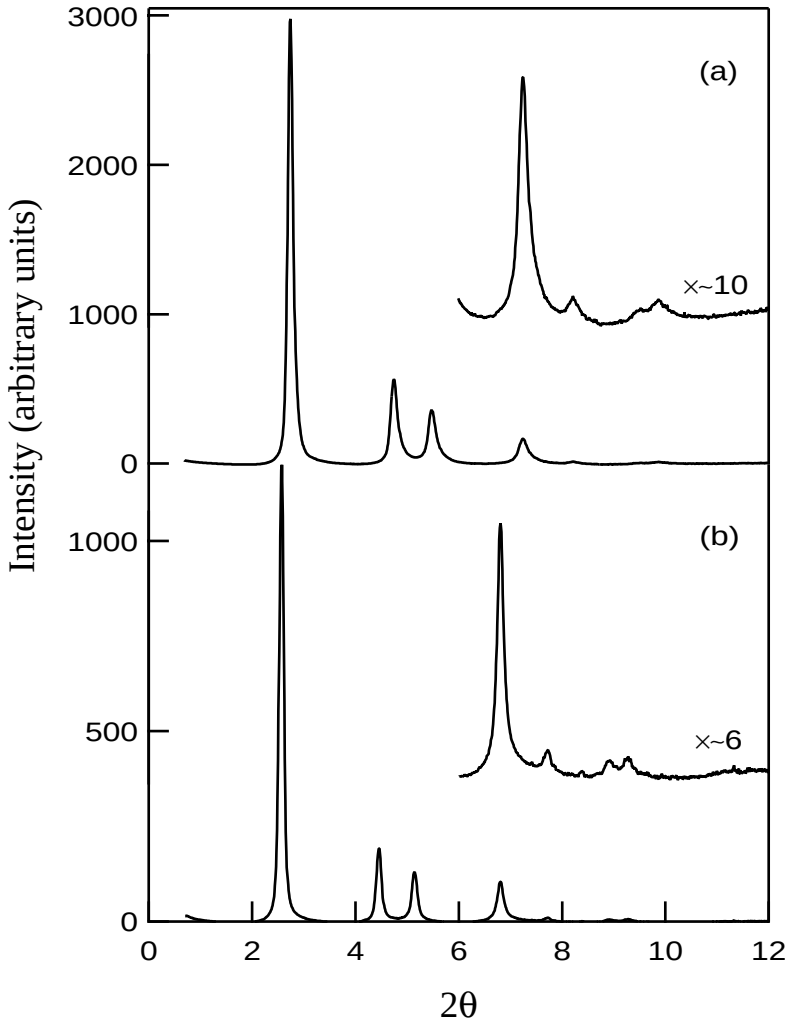

Figure 5.1 *Synchrotron X-ray diffraction patterns for (a) calcined and (b) uncalcined materials titrated against H_2SO_4 to maintain a pH of 11 during synthesis. The last four peaks for each trace, magnified by the factors shown, are inset.*

The data from Figure 5.1 also allow a form factor to be fitted. The natural small angle scattering form factor for such a tubular system is that for a hexagonal array of cylinders.[34] It is reasonable to modify this form factor by a Debye-Waller factor, to take account of thermal motion, and the variability of both tube centre position and tube internal diameter. However, this form factor convoluted with the Debye-Waller factor oscillates strongly in Q space, with sharp decreases to zero, which are not observed. The observed intensities do however change sharply in intensity at Q *ca.* 0.5 $Å^{-1}$ (see for example Figure 5.2), as does the cylinder function for tubes of the expected diameter of *ca.* 20 Å. The data, besides the problem of the zeros, also fit extremely poorly to a single channel model.

To remove these unobserved zeros, a second cylinder of different density to both the walls and the hole, whose form factor 'interferes' with the first, was inserted into the model. Physically this means that the wall structure will be described as concentric cylinders of different contrast density, one of which is slightly smeared by a Gaussian to smooth the interface between them. Thus there is a connected region of denser silica

forming the walls between cylinders, cylindrical regions of less dense silica filling some of the volume within the dense boundary layers, and finally the empty (or surfactant filled, in the case of the uncalcined materials) channels in the centres of the tubes. The equation used to approximate the Bragg intensities is :-

$$A(Q) = \left(\frac{2K_1}{R_1 Q} J_1(Q, R_1) + \frac{2K_2}{R_2 Q} J_1(Q, R_2) e^{-\alpha Q^2}\right)^2 \qquad \textbf{(5.1)}$$

where A is the area under the peak, Q is momentum transfer, R_1 is the radius of the outer cylinder, R_2 is the radius of the inner cylinder, K_1 and K_2 are constants related to the scattering length densities of each region, $J_1(Q,R)$ is the first order Bessel function and α is a Debye-Waller constant. The radii, R_1, R_2, and the constants, K_1, K_2, were parameters in the fit, and α was set to 1.0 Å^2 since varying this parameter did not alter the fit significantly, provided it was kept small.

The fit was carried out using a least squares method, maintaining consistency across the five data sets. This method minimises χ^2, starting from a variety of physically possible values of K_1, K_2, R_1 and R_2. The fit is stable to a wide choice of initial values. In the two cylinder model, introduction of further smearing, via a second α on R_1, does not improve the fit. Figure 5.2 shows a typical fit to a set of data points (for calcined material titrated against sulphuric acid during preparation). Four extra points with zero intensity were added to the data for fitting purposes. These corresponded to Q values where hexagonal peaks for the 32, 33, 41 and 42 reflections would be expected, but which were not observed.

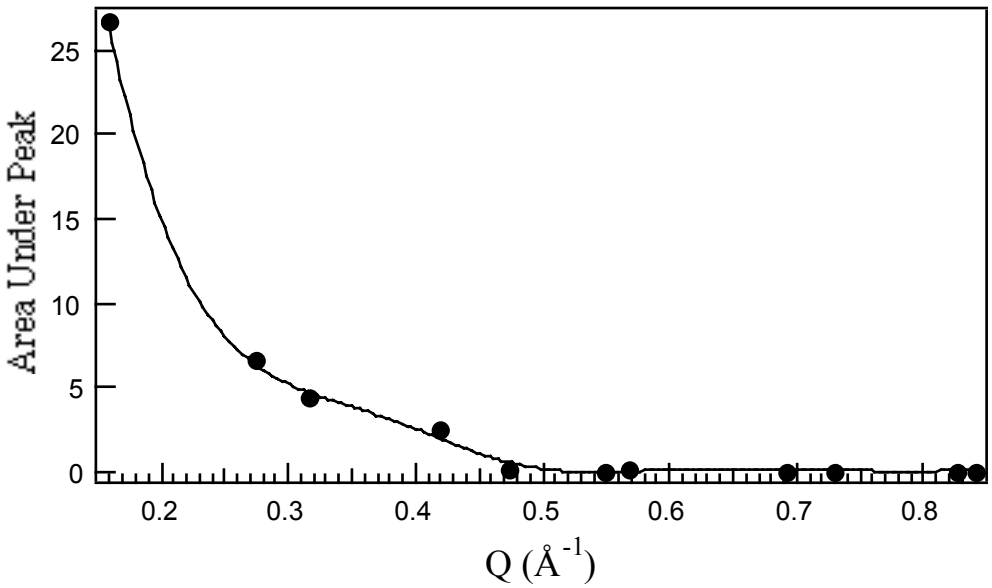

Figure 5.2 *Area under the peak plotted against Q for calcined MCM-41 titrated against sulphuric acid to maintain a pH of 11 during preparation, and the model fit to the data.*

An attempt was made to distinguish between cylindrical and hexagonal shaped large and small pores, following the report of Stucky *et al.* that hexagonal pores were a better fit to their data.[23] Substituting a numerically calculated form factor for a hexagonal

cross-section instead of a circular one, of identical cross-sectional area, resulted in no improvement in the fit and there was no experimental reason to choose one over the other. The change from circular to hexagonal is of the order of ±1 Å in the 20 Å radius. The highest order reflection was observed to be at a *d*-spacing of ~11 Å, giving a resolution of *ca.* 7 Å, which, in itself indicates that such detailed shape information is not available from this data.

Parameter values for the best fit to the data for both the calcined and uncalcined materials are shown in Table 5.2, which also gives the derived minimum wall thicknesses. The features of this model can be summarised as a cylindrical hole of radius R_2, *ca.* 7 Å surrounded by a ring of material of thickness *ca.* 13 Å, of noticeably reduced density from the wall density. The boundary between the hollow core and low density silica region is quite sharp, although the boundary between lower and higher density silicate regions is less so. The requirement for three regions in MCM-41 - hole, intermediate region of significantly reduced density, and wall, is the major conclusion (see Figure 5.3). A two region hole/wall model is not adequate.

Table 5.2 *Lattice parameters measured from SAXS data and fit parameters from iterative fits of the form factors for synchrotron X-ray data from calcined and uncalcined MCM-41 produced from sulphuric acid and acetic acid controlled pH synthesis conditions.*

Fit Parameters	Sample				
	H_2SO_4 (1) Calcined	H_2SO_4 (2) Calcined	H_2SO_4 Uncalcined	CH_3COOH Calcined	CH_3COOH Uncalcined
R_1 / Å	19.69(5)	19.61(5)	21.42(5)	20.18(5)	20.82(5)
R_2 / Å	6.89(5)	7.40(5)	7.02(5)	7.34(5)	6.75(5)
K_1	3.95(5)	7.91(5)	4.18(5)	6.71(5)	3.01(5)
K_2	5.31(5)	6.39(5)	2.92(5)	5.94(5)	2.31(5)
d-spacing / Å	39.64(2)	38.7(1)	42.23(2)	39.9(1)	42.31(2)
centre to centre distance, $2R_3$ / Å	45.77(2)	44.7(1)	48.76(2)	46.1(1)	48.86(2)
dense wall thickness / Å	6.39(5)	5.5(4)	5.92(5)	5.7(4)	7.22(5)
less dense wall thickness / Å	12.80(7)	12.2(7)	14.40(7)	12.8(7)	14.07(7)
total wall thickness per micelle / Å	16.00(5)	15.0(8)	17.36(5)	15.7(8)	17.68(5)

The X-ray data gives a projection of the three dimensional structure onto the hexagonal lattice plane. Thus the radii of the various regions are averages of the structures at various heights in the channels. The radius of the central hole could be somewhat larger than stated, if it had some variation in its centre point. Such a variability of the hole would contribute to the apparently lower density observed in the inner region with reduced silicate density. However the sharpness of the hole boundary, reflected in the low value of α, suggests this is not likely. It should be noted that the three-region model proposed here is the simplest model involving variable silica densities in the wall and lining regions. A model with a small central hole and some smoothly varying continuous silica density in the walls (as shown in Figure 5.3) would also fit the data.

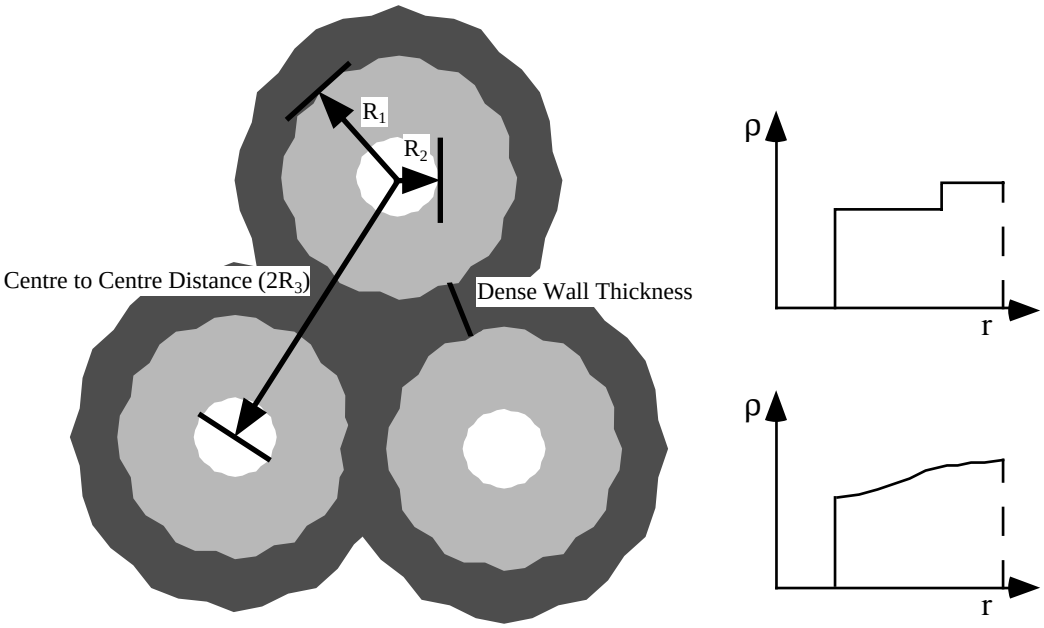

Figure 5.3 *Schematic diagram of the proposed model for MCM-41 (left) with two possible density distributions for the silica in the walls (right). The model discussed in detail here corresponds to the top distribution which is the simplest model for introducing variable silica density into the wall/lining region. The bottom distribution would also fit the data.*

The calcined MCM-41 from the preparation titrated against acetic acid has a slightly thinner dense wall at 5.7(4) Å, than the similarly calcined sulphuric acid sample at 6.4(1) Å, but in the uncalcined materials the trend is reversed, with dense walls of 5.9(1) Å for the sulphuric acid treated, and 7.2(1) Å for the acetic acid treated materials respectively. The minimum thicknesses obtained for the dense parts of the walls for the calcined materials are smaller than those estimated from previous fitting of less extensive X-ray data, (8 Å),[8,23] high resolution electron microscopy (8 - 13 Å)[18,35] and combined analysis of nitrogen adsorption isotherms and X-ray diffraction data (12.5 Å).[10,19,36] The average values obtained for the total wall thicknesses however, 15.6(3) Å, for the calcined and 17.5(2) Å for the uncalcined materials are much larger than those earlier estimates. These earlier methods measured only an average wall thickness, since they assume a simple two region hole/wall model.

In the calcined materials the less dense silicate layer has a thickness of around 12.6(2) Å, whereas in the uncalcined materials it is about 14.2(2) Å. This contraction from uncalcined to calcined materials appears to be the major contribution to the decrease in the *d*-spacing after calcination, since the dense wall thicknesses, and the hole radii appear to remain roughly constant at 6 and 7 Å respectively. As this region has a lower silicate density than the outer walls it is reasonable to assume that upon calcination, as water trapped in the walls and the charged surfactant supporting the first layer of silicates are removed, there will be a further condensation and relaxation of the silicate groups, resulting in a slight increase in density and decrease in thickness of this layer. In FSM-16, a material with a similar hexagonal channel structure, (discussed above in section 5.1) such a contraction with calcination is ascribed to the buckling of the stretched layer of silica tetrahedra forming the walls into a wrinkled configuration upon removal of the large, supporting template ions. The collapse into the wrinkled layer which then condenses is at least partially responsible for the increase in wall thickness.[24] It was also suggested that silicates remaining in solution in the FSM-16 channels even after drying are deposited on the walls during calcination, stabilising and thickening them.[24] Presumably, in MCM-41 materials not titrated with acid during synthesis, where a larger contraction occurs during calcination, this collapse would be more obvious in the X-ray data, although this material does not show enough diffraction peaks to allow useful modelling.

If the thicknesses of the dense and less dense contributions to the walls are summed, then the uncalcined 'walls' are thicker (17.5(2) Å) than those of the calcined materials (15.6(3) Å) by a couple of angstroms. This is largely due to the thicker porous layer discussed above. These overall wall thicknesses are larger than those found in earlier work,[8,10,19,23] for materials prepared using the ordinary alkaline synthesis method. Some work on the effect of the initial pH of the alkaline synthesis gel on wall thickness has found that the thickness increases with decreasing pH up to 16 Å, suggesting a thicker silicate coat is deposited on the micelles as the silica solubility decreases.[37] However none of these earlier results used preparations adjusted for pH *during* synthesis. From the work reported in Chapter 4, these acid titrated materials, appear to be much more hydrothermally stable than those from the ordinary MCM-41 preparation and so may well have thicker or more densely polymerised walls to achieve this stability. Other work using neutral surfactant templates and silicates indicates the existence of thicker walls in those materials[9,11] even though in that case there is a decrease in overall crystallinity. Wall thicknesses of up to 27 Å have been reported for an optimised ordinary MCM-41 synthesis.[14] Those thick walled materials showed greater hydrothermal stability and slightly lower surface areas than thinner walled samples, as are seen for the acid-titrated materials in this work. Thicker walls in these acid titrated materials are therefore not improbable and are possibly reflected in the slightly lower surface BET surface areas found for these materials compared to the less well ordered samples (see Chapter 4).

The constants, K_1 and K_2 in the fits are proportional to the relative scattering length densities in different parts of the structure. Ratios of these numbers, combined with other experimental information can be used to calculate the absolute densities of the walls. In the calcined material, the high surface areas given by the nitrogen isotherms

indicate that there is nothing left in the central hole, and so its density may be set to zero. Also from the nitrogen isotherms of this calcined material, the large volume of nitrogen adsorbed (0.8 $cm^3\ g^{-1}$) allows the mean density of MCM-41 to be calculated at around 0.83(5) g cm^{-3}, assuming a bulk density for silica at 2.5 g cm^{-3}. This is comparable to the particle density of a silica gel formed from a sodium silicate solution at a pH of 9.5, which has been measured to be 0.86 g cm^{-3}.[38] Other workers[39] have measured the mean density of calcined boron-substituted MCM-41 materials to be 0.97(4) g cm^{-3}, in reasonable agreement with the result above. The silicate skeleton in that work was found to have a density of 2.2(1) g cm^{-3}, with the remainder being void space. For the uncalcined materials, the void space will be filled with the template, CTAB, and residual water, so the mean density of the uncalcined material (assuming roughly the same amount of void space as in the calcined material) will be about 1.50(5) g cm^{-3}. These numbers, and the relative volumes of the regions derived from the X-ray model, give the densities of different parts of the structure, by solving simultaneous equations for the relative scattering length densities of various parts of the structure.

In the calcined material, the density of the walls is 0.99 g cm^{-3}, less than half that of amorphous silica, the porous region of the calcined material is 0.87 g cm^{-3}. This corresponds to 60% void space in the dense wall of the calcined materials, and 65% in the less dense wall. While the absolute values given here have errors estimated at 4-5%, the difference has an error of less than 1%. In the uncalcined materials, the denser part of the wall has a density of 1.57 g cm^{-3}, the less dense wall has a density of 1.51 g cm^{-3} and the hole is filled with material having a density of 1.09 g cm^{-3}. This latter value agrees with a theoretical CTAB or water density, and increases confidence in the reality of the model. The wall densities are higher in the uncalcined material since the void space in this material is filled with water and template. The void space in the dense wall of the uncalcined material must therefore be 62%, and in the less dense wall 66%, which is approximately the same as that in the calcined material. There is clearly very little silica in the MCM-41 structure, when compared to the volume enclosed, implying rough, highly-divided “walls”. Attempts to model these density variations by fluctuations in a smooth walled channel diameter required very unlikely distributions. As the difference between the densities of the denser walls and the linings is only about 5%, any fluctuation in a smooth wall would require long stretches of material with the same density as the dense walls, separated by very narrow indentations containing no silica - a "beads on a string" shaped channel space, which was mostly comprised of "string".

Some evidence for roughness in the walls of MCM-41 has been found by through-focus exit wave reconstruction of TEM micrographs of material with a hexagonal morphology.[20] Also observed using this method was the presence of amorphous material inside the pores. Other experimental results on this system , such as small angle neutron scattering and inelastic neutron scattering, discussed below, also point towards this highly porous, three region structure. Other workers have also found evidence for occluded water in the walls of MCM-41.[40] Ion-exchange of Cu(II) ions into Al-MCM-41 has been found to occur on sites which are situated inside the walls of the Al-MCM-41 structure, since they are inaccessible to bulky adsorbate molecules.[41] This is also strongly suggestive of a highly porous wall structure. Low-temperature

phase transitions have been observed in water adsorbed in MCM-41 pores studied using proton nmr.[42] Such transitions have been previously ascribed to the freezing of water in micropores, and one study found that the fraction of water involved in such transitions in MCM-41 implies that more than 60% of the pore volume is related to micropores.[42] In that case, since N_2 adsorption had shown an insignificant amount of microporosity in the samples used in that study, the unfreezing water phase was instead attributed to a layer of thickness 5.4±1.0 Å between the walls and the central channel filled with ice. That work notes that this thickness is of the same order as the dimensions of micropores (0-10 Å), however, observes that the temperature of the phase transition of this interfacial water is significantly higher in mesoporous systems than in solely microporous systems. It is possible that the porous nature of the walls found in this work may be an alternate explanation for their observations, since no evidence of micropores is found from the nitrogen adsorption isotherms for this material either.

5.3.2 Neutron Diffraction Study

5.3.2.1 Background

The behaviour of adsorbed gases on MCM-41 has been studied for many gases. Some of the molecules studied include methane,[43] hydrogen,[44] nitrogen,[2,4,45,46] argon,[7,15] cyclohexane,[18,19] cyclopentane,[47] benzene[8] and water.[42,48-50] As the behaviour of these molecules adsorbed on various substrates has been previously investigated in detail, they may be used as probes of the MCM-41 wall structure. Molecular hydrogen is well characterised both as a bulk solid or liquid[51-54] and as an adsorbate[55-58] and so is used here to probe the channel structure of MCM-41.

The neutron powder diffractometer HIPD at the Intense Pulsed Neutron Source, Argonne National Laboratory (described in Chapter 3) was used for the elastic neutron scattering experiments. A highly ordered MCM-41 sample was used as a substrate. Powder diffraction patterns at 4.2K were measured (with good statistics since subtractions were necessary), at 0, 19.3, 27.2, 34.8 and 50.4 mmol g^{-1}. The latter sample was produced by loading to 50.4 mmol g^{-1} at 21 K and cooling over 30 minutes to 4.2 K. This enabled the excess, unadsorbed hydrogen to first liquefy, and then crystallise, producing a completely loaded sample, with the excess as crystalline solid hydrogen. Although it depends on the temperature, full filling of the space within this MCM-41 was about 40 mmol g^{-1}. Hydrogen and nitrogen isotherms for this MCM-41 material are discussed in Chapter 6, section 6.8. Neutron diffraction patterns at 1.9 K from bare MCM-41 and at various hydrogen loadings are shown in Figure 5.4 below.

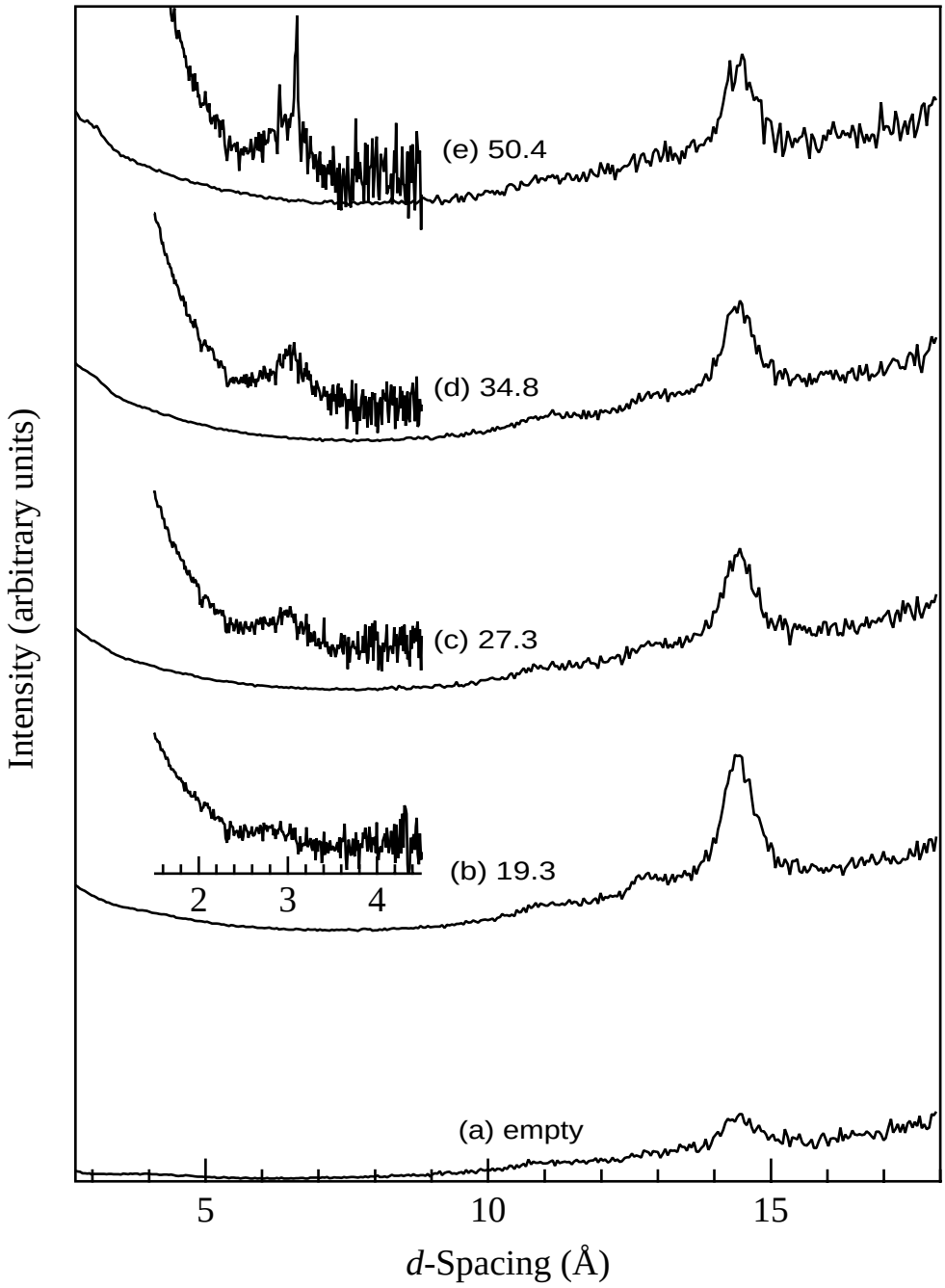

Figure 5.4 *Neutron diffraction pattern from MCM-41, 30˚ counter bank at 1.9 K and various H_2 loadings (mmol g^{-1}) showing the MCM-41 (21) peak. The loadings correspond to 0, 48%, 68%, 87%, and 1.26% of the pore volume filled with hydrogen. The hydrogen peak at ca. 3.1 Å for the same loading is inset.*

5.3.2.2 Unloaded MCM-41

The diffraction pattern from bare, unloaded MCM-41, (Figure 5.4(a)) in both 90˚ and 30˚ counter banks shows the strong scattering from the aluminium can, and weaker scattering from the MCM-41. At lower *d*-spacings the latter is relatively featureless, with only a broad peak stretching from 3 to 5 Å peaking at 4 Å, characteristic of disordered silica materials.[59,60] However at longer *d*-spacings a distinct (21) peak from the hexagonal pore arrangement in the MCM-41 is seen at 14.38(3) Å, with a weaker

peak at 12.8(1) Å from the (30), and at 11.0(2) Å from the unresolved (22) and (31) peaks. The latter are more clearly seen in the 19.3 mmol g^{-1} H_2 loading pattern. These correspond in spacing and intensity to those observed in the X-ray diffraction experiment. The (10), (11) and (20) peaks observed in addition in the X-ray experiment at longer *d*-spacings are out of the wavevector range of HIPD. The observed hexagonal spacing of 38.0 Å is comparable to that observed in the X-ray experiment on freshly prepared calcined samples.

5.3.2.3 Hydrogen Loaded MCM-41

When hydrogen is adsorbed onto the sample three changes to the scattering patterns occur:
(1) Dominating the scattering, a smooth incoherent elastic scattering background from the hydrogen molecules appears, together with, as *d*-spacings decrease, an increasing inelastic intensity in the background, due to the neutron energies becoming sufficient to cause *ortho* to *para* conversion.

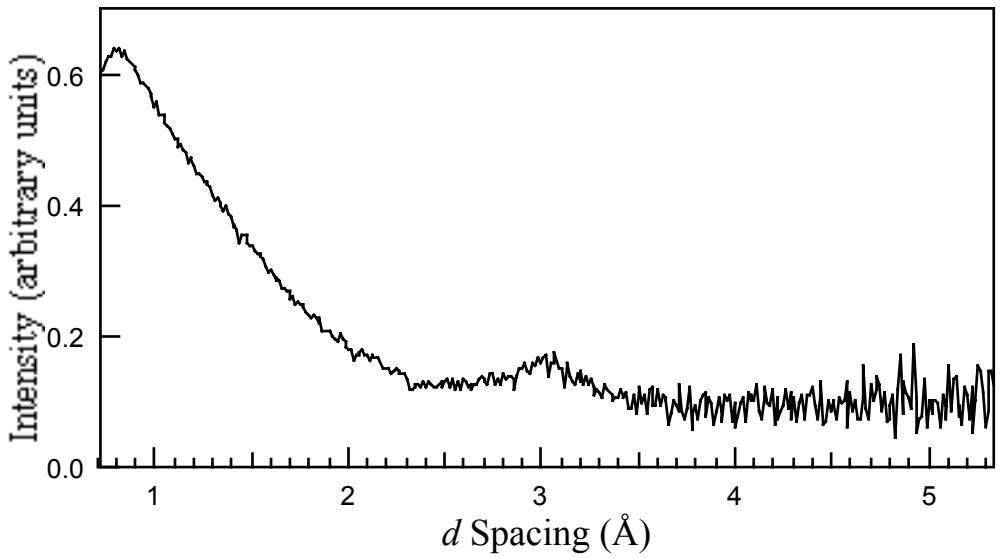

Figure 5.5 *Neutron diffraction pattern from the 90˚ counter bank from 34.8 mmol g^{-1} H_2 on MCM-41 with normalised background from MCM-41 alone subtracted.*

(2) For higher hydrogen loadings a peak at 3.1(1) Å appears. The total scattering, including the peak at 3.1 Å are shown in Figure 5.5. Here, the MCM-41 plus sample container background scattering have been subtracted from a 34.8 mmol g^{-1} H_2 loaded sample at 1.9 K. At the very highest hydrogen loading (50.4 mmol g^{-1}), which is about 20% in excess of the adsorption capacity of the MCM-41 sample, an extra sharp peak at 3.09(1) Å appears in both banks. This is the expected (002) peak from the HCP crystalline phase of H_2 with a unit cell of a= 3.76, c= 6.11 Å previously determined by X-ray diffraction.[51] No other significant crystalline H_2 peaks are observed, again as expected from the X-ray diffraction pattern, where only (002) is strong. This was also the case for hydrogen adsorbed in the pores of vycor glass where higher order peaks were suppressed.[55]

(3) The MCM-41 diffraction peaks, most noticeably the (21), change in intensity, but not in *d*-spacing.

The peak at 3.1 Å for higher hydrogen loadings is relatively broad with a FWHM of about 0.5(1) Å (not as sharp as the H_2 HCP crystalline (002) peak with FWHM of 0.025(5) Å). The position of the peak corresponds to the expected diffraction from H_2-H_2 correlations. In the HCP crystal, the strong peak is observed at 3.09 Å.[51] In a less ordered solid, where a hydrogen molecule is similarly surrounded by hydrogen neighbours, a peak might be expected at a similar position. In an earlier study using methane (discussed in Chapter 6), it was found that the methane within the MCM-41 channels was amorphous as interactions with the silicate walls had prevented crystalline packing. The FWHM of the hydrogen peak observed here (0.5 Å) is that expected from a crystal of size *ca.* 20 Å, which is consistent with possible internal tube diameters in MCM-41. It is thus not possible to distinguish crystalline from amorphous solid hydrogen, especially as local ordering is likely to be similar, and a clear distinction can only be made at longer correlation ranges than 20 Å.

Estimates of the intensity of the 3.1(1) Å peak from both the 30˚ and 90˚ counter banks have been made by subtraction of a linear background. This procedure was also followed for the 50.4 mmol g^{-1} loading where the sharp (002) crystal peak is easily separable from an underlying broader peak. The intensities are shown in Table 5.3, and are normalised to the broad component of the H_2 diffraction for the sample containing 50.4 mmol g^{-1} loading (*ie.* where the MCM-41 pores are saturated). The two counter banks show comparable variation with H_2 loading, though at different Q's, and have been averaged.

Table 5.3 *Relative intensities of the 3.1 Å peak. Note the 50.4 mmol g^{-1} loading includes ca. 20% crystalline H_2 material which is external to the MCM-41 pores.*

Loading	Experiment	Theory
19.3	0.12(6)	0.12
27.2	0.49(5)	0.44
34.8	0.83(5)	0.77
50.4	1	1

Also included in Table 5.3 is a theoretical estimate of the 3.1 Å peak intensity. This is derived by accepting the QENS result (discussed in Chapter 6, section 6.7.1), that there are two distinct types of hydrogen within the MCM-41 pores; a surface adsorbed species whose sites are saturated at a filling of 20 mmol g^{-1}, and a subsequently adsorbed bulk-like species produced by adsorption of a further 20 mmol g^{-1}. It is assumed that the 3.1 Å peak arises only from the two species within the MCM-41 pores (*ie.* not from any external bulk hydrogen), but that the surface adsorbed species has fewer H_2 neighbours. If 1.1 H_2 neighbours for each surface absorbed species is assumed (and 8 for the bulk), the theoretical estimate of intensity shown in Table 5.3 is obtained. This theoretical prediction of the peak intensity agrees well with observation. The estimate of *ca.* one H_2 neighbour for each surface adsorbed dihydrogen molecule is

probably too low because of a greater variability of H_2-H_2 distances at the surface, and should not be taken quantitatively.

The adsorption of H_2 on MCM-41 changes the intensity of the diffraction pattern from the hexagonal patterns of pores in the silica. The (21) peak changes strongly with H_2 loading, increasing in intensity by a factor of three, from zero loading to 19.3 mmol g^{-1}, compared to the unloaded material. Addition of a further 20 mmol g^{-1} then reduces the peak intensity (Table 5.4). The other MCM-41 peaks, although much weaker, go through the same qualitative sequence of intensity change. This pattern of intensity change is not just monotonic and will thus provide a good test of the structural models.

The intensity change of the (21) peak between empty and fully loaded MCM-41 is independent of the detailed structure, and, assuming that all voids are filled with H_2, the relative scattering length densities of crystalline silica and solid hydrogen may be used to predict the intensity ratio of full to empty as 2.3. This is in good agreement with the experiment, indicating that all void space is accessible to H_2. It is at intermediate loadings that differences appear between various possible structural models.

Even though it is at variance with the previously discussed X-ray diffraction results, a fit was attempted to a simple model of a cylindrical, smooth walled tube, in a matrix of relatively dense vacancy-free silica. The relative intensities in two extreme models of hydrogen distribution have been calculated; firstly where the hydrogen is uniformly distributed within the micropore; secondly where the hydrogen sticks to the wall as a skin of density 0.095 g cm^{-3}. Neither model fits the experimental data well, particularly the 19.3 mmol g^{-1} result (Table 5.4). A realistic hydrogen distribution in such a pore may be intermediate, with a density of hydrogen at a minimum in the pore centre, and increasing to the wall. This distribution will give (21) Bragg intensity changes intermediate between the two models. It can be concluded that any reasonable hydrogen distribution in this pore does not fit the neutron diffraction data. Thus the initial assumption about the silica framework is incorrect.

Table 5.4 *Relative intensity of (21) MCM-41 diffraction peak at various H_2 loadings, compared with three models for the system.*

Loading	Experiment	Present Model	Simple Pore Model	
			uniform	skin
0	1	1	1	1
19.3	2.9(3)	2.9	1.57	2.39
27.2	1.9(3)	1.7	1.81	2.84
34.8	2.0(3)	2.1	2.09	1.94
50.4	1.8(4)	2.3	2.3	2.3

When the model proposed from the synchrotron X-ray data from highly ordered MCM-41 (section 5.3.1.2) is used, the neutron results can be reproduced naturally. The silica framework is an inner small diameter cylinder, a larger, void-filled silica framework inside walls which themselves contain voids, though of lesser amount. The adsorbed hydrogen and voids must be partitioned at each loading between the three regions. At lower loadings it is assumed that the central hole is all void, with no hydrogen, in agreement with the isotherm results concerning capillary condensation. The relative Bragg intensities are quite sensitive to the distribution of hydrogen between wall and lining. The observed ratios for 19.3 and 27.2 mmol g^{-1} can be reproduced. In particular the ratio of 2.9 for 19.3 mmol g^{-1} emerges uniquely for a quite reasonable distribution, and the decrease to 2 naturally occurs when a change in loading is made. The model does not even allow that *any* loadings could duplicate both results. The 34.8 mmol g^{-1} data cannot be produced with an empty central core, *all* distributions between wall and lining give ratios of 1 or less. However a 50% loading of the central hole produces a satisfactory fit. At such high overall loadings this loading of the central hole is to be expected, and it is gratifying that the data require it.

Overall the results listed in Table 5.5 suggest a model in which the lining preferentially adsorbs hydrogen and is preferentially saturated. The walls fill at higher loadings and less completely, while the central hole fills last. That is, the lining has a higher surface area and smaller voids (per gram of silica), than the wall.

Table 5.5 *Distribution of volumes ($m^3 \times 10^8$) per gram of MCM-41 under various loadings (mmol g^{-1}) of H_2.*

H_2 Loading	0		19.3	27.2	34.8
Species	silica	void	H_2	H_2	H_2
Central 7 Å Hole	0	11	0	0	6
12.7 Å Lining	25	48	30	38	45
Wall	15	23	10	16	20

5.3.3 SANS Contrast Matching Study

5.3.3.1 Background

Small angle neutron scattering (SANS) provides another test of the proposed model. The contrast match points determined by the contrast variation method are extremely sensitive to the variations in density and template distribution in the silica-organic composite. The SANS contrast variation technique has previously been used for studies of crystallisation and nucleation of zeolites from organic/inorganic composite gels.[61-63] SANS measurements were carried out on MCM-41 synthesis gels at various stages of preparation, as well as on the final calcined products, and the results of these experiments were shown to be are consistent with the model of template and silica distribution described above.

Only a few other SANS studies on MCM-41 and related systems have been published. Firouzi *et al.*[21] report one pattern taken in D_2O of a 1 wt% CTAB solution, with and without dissolved silica, showing the development of a sharp peak due to a hexagonal array of rods from the broad peak characteristic of spherical micelles. Auvray *et al.*[64] published a brief report of a SANS study on the formation of silica gels from TEOS in the presence of n-alkyl ammonium bromide surfactants with different chain lengths. They also show that prior to silicate addition the SANS pattern is typical of disordered isotropic phases containing rod-like micelles. In short chain surfactant systems (C_8 and C_{12}) upon silica gel formation, SANS developed corresponding to a fractal aggregate structure with dimension 1.9. The scattering however, remained dominated by micelle interference peaks indicating a system with short-range order, but no liquid crystal structure. For C_{14}, the development of the hexagonal mesophase during gelation was noted. Finally, a more extensive study has been reported by Glinka *et al.*[65] which also focuses on the synthetic mechanism. They also found that the scattering from calcined samples can be masked by a solution containing 60% D_2O, having the same scattering length density as amorphous silica, and that the calcined samples are fully accessible to water. The power-law scattering for dry calcined materials is reported to have a $Q^{-4.3}$ dependence, characteristic of a rough surface. They found that the masking solutions were not able to penetrate the structure of uncalcined samples, but no further comment on the detailed structure of these materials was made.

A SANS study of the polymerisation of silica in a lamellar mesophase prepared from didodecyldimethylammonium bromide surfactant (DDAB) was carried out by Dubois *et al*.[66] They observed a change in contrast match point between that of a surfactant system containing unpolymerised silica oligomers in the water layers, which scattered in the same way as pure surfactant (contrast match point 4.3 vol% D_2O), and a polymerised silica-surfactant bilayer system, which had a contrast match point of 14 wt% D_2O for a TMOS/water ratio of 10%. From calculations of the contrast match point they showed that most of the silica in the system had condensed onto the DDAB bilayers. From modelling the X-ray diffraction pattern they showed that the polymerisation of silica in the bilayer caused some disruption to the structure which caused a roughening of the bilayer surfaces. This was also observed in electron microscopy. The scale of the disorder was a few times larger than the period of the bilayer, and was attributed to the mechanical tension applied to the silicate polymer by the attraction to the surfactant headgroups. In regions of high silica concentration, surfactant headgroups would be pulled together and cause a curvature of the bilayer surface.

In this work the MCM-41 preparations were made up as described in Chapter 2. Various amounts of purified H_2O and D_2O were used in making up the acidified sodium silicate solutions, and the surfactant template solutions, in order to achieve solutions ranging in D_2O content from 0 mol% to 90 mol% D_2O. Contrast series were prepared for unheated synthesis gels containing 11.5 wt%, 5 wt% and 2 wt% CTAB (as weight percent of the total preparation mass) as well as for a gel containing 4.3 wt% CTAB and 0.2M KBr.

The two different synthesis conditions for MCM-41 were investigated. The first synthesis followed the optimised ordinary synthesis referred to in Chapter 4, based on the initial paper by Beck *et al*.[8] A contrast series of five solutions, having D_2O concentrations of 0, 30, 50, 70, 90 mol% were heated in autoclaves at 100˚C for 3 days, without stirring. The unfiltered wet synthesis gel was run on the SANS machine LOQ, and is hereafter referred to as the "ordinary preparation heated synthesis gel" series. A second ordinary preparation was also made up using this synthesis method. This wet gel was filtered after heating and three dried MCM-41 samples were obtained from it. These were, a filtered sample which still contained excess template (as-prepared), a filtered sample which had been washed three times in hot water to remove excess template, and a calcined sample. These ordinary MCM-41 preparations typically had molar compositions (CTAB 1.00:SiO_2 1.90:Na_2O 0.74:H_2SO_4 0.28:H_2O/D_2O 149). Contrast series on the dried MCM-41 materials were obtained by suspending them in solutions containing D_2O concentrations of 10, 30, 50, 70 and 90 mol%. A dry sample was also run to provide another contrast point, as air has a scattering length density corresponding to 8.9 mol% D_2O. To ensure no air was trapped in the MCM-41 channels, the samples were evacuated before the aqueous solutions were added to the powders. Scattering patterns from these samples at air contrast are shown in Figure 5.6.

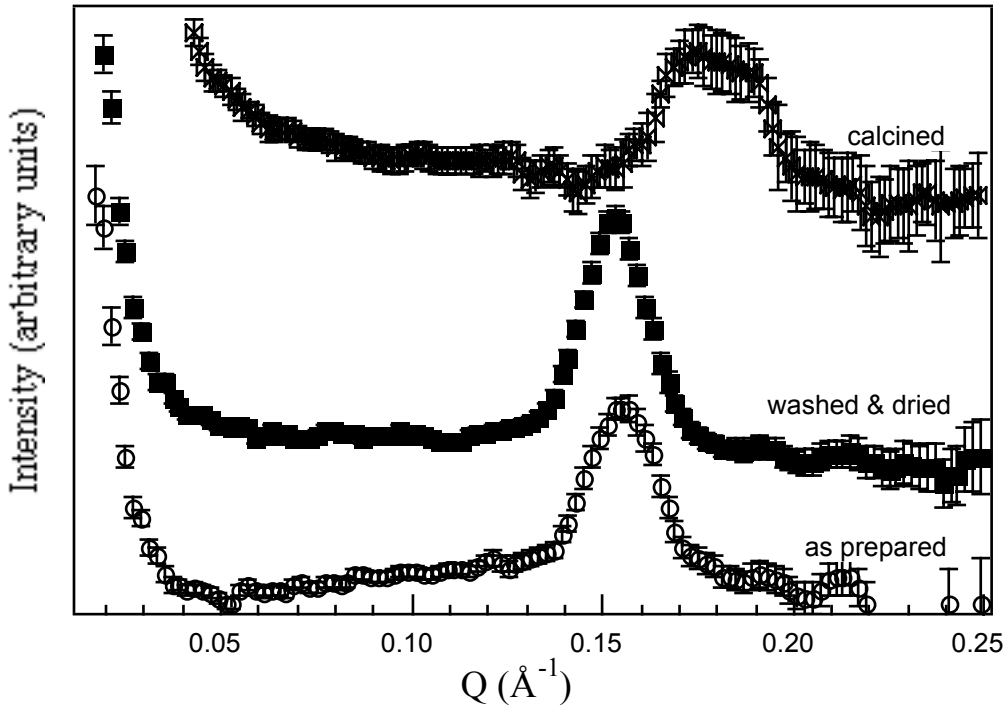

Figure 5.6 *Small angle scattering patterns at air contrast for the as-prepared, washed and calcined samples from the ordinary MCM-41 synthesis.*

The second synthetic method investigated followed the optimised acid-titrated preparation,[67] based on the method published by Ryoo and Kim[33] which results in MCM-41 having a much higher degree of long range order. Using this method a heated synthesis gel contrast series of 0, 30, 50, 70, 90 mol% D_2O was also prepared. In this synthesis, after 24 hours heating of the start gels at 100˚C, each autoclave was cooled to a comfortable handling temperature, opened and a titration performed with one molar acetic acid so as to bring the pH of the whole gel system back to a pH of 11**.** The

autoclaves were then resealed and heated for a further 24 hours and the sequence repeated until 4 days of heating had elapsed. The molar composition of the preparations titrated with acid was typically (CTAB 1.00:SiO_2 2.03:Na_2O 0.79:H_2SO_4 0.27:CH_3COOH 0.45:H_2O/D_2O 173).

As with the ordinary preparation, a second acid-titrated preparation was made up. After filtration and washing with water to remove some of the excess CTAB, this preparation was also divided into several parts. One part was washed with hot water to remove excess CTAB. A second portion was calcined. Small samples of each of the portions of this preparation, and the dried MCM-41 materials from the ordinary preparation were calcined gravimetrically to determine the amount of CTAB remaining in each. The surfactant/silica ratios are shown in Table 5.6. Contrast series of 10, 30, 50, 70, 90 mol% D_2O were run on these materials, with the air contrast used to provide another contrast point. A contrast series was also run, for comparison, on a second washed, dried MCM-41 sample prepared by the acid-titration method, but which used H_2SO_4 as the titrant to maintain a constant pH of 10 during the synthesis, as this had been found to produce material with the greatest degree of long range order. The molar composition of this preparation was (CTAB 1.00:SiO_2 2.08:Na_2O 0.81:H_2SO_4 0.57:H_2O 166).

Table 5.6 *Surfactant/silica ratios for as-prepared, washed and calcined samples from ordinary and acid titrated MCM-41 preparations.*

Sample	Acid Titrated Preparation	Ordinary Preparation
As Prepared	2.68	2.12
Washed	0.93	1.27
Calcined	0	0

5.3.3.2 Particle Surface Structure

Electron microscopy[68] shows that calcined MCM-41 materials contain tactoid-like structures on the scale of microns (see Figure 4.28). Bundles of templated tubes tens of microns long and about a micron across are partially aligned. The origin of the small angle scattering signal is thus an interesting question. One possibility is that only the smallest sizes of the total particle size distribution are sampled in the Q range of the instrument. Another is that the observed scattering comes in part from the scattering length discontinuities at the edges of the tactoids and resembles the "crack scattering" observable for highly crazed solids. To examine these possibilities the power law in the scattering function has been determined for the various gels. Porod's law states that:

$$\ln I \propto -n \ln Q \qquad \textbf{(5.2)}$$

where I is the scattered intensity, Q is momentum transfer and n is the Porod slope, which is related to the nature of the surface of the particles in the scattering medium (see Chapter 3).[34] Porod slopes of 4 indicate that the particles have a smooth surface

with a constant curvature, whereas lesser slopes indicate rougher surfaces. Analysis of Porod plots of the scattering function for the acid titrated, more highly ordered MCM-41 samples at various contrasts shows a set of linear functions with slopes of around 4, (see Table 5.7). This corresponds with that the value of -4.3 found by Glinka *et al.*[65] for a calcined sample at air contrast. The slopes are largely independent of the stage in the synthesis at which the samples were taken. These MCM-41 particles must therefore have a smooth surface at length scales between Q = 0.01 $Å^{-1}$ and Q = 0.06 $Å^{-1}$, over which the power law is obeyed.

At mol% of D_2O close to the contrast match points for these samples, the Porod slopes become lower, around 2.5 to 3. This may indicate a roughness in the surface or an internal structure[69] which is only apparent when the mean density of the particle is matched to the surrounding solution. MCM-41 samples synthesised from the ordinary preparation have lower Porod slopes of around 3 to 3.5 at all contrasts, indicating more inhomogeneity in these samples. Again, close to the contrast match points the slope is lower. In all samples at contrasts close to the match points, as the intensity is close to zero, the effect of noise in the scattering patterns is more apparent, leading to a greater error in estimating the Porod slopes. A set of Porod plots for various contrasts of an ordinary preparation synthesis gel containing 11.5 wt% CTAB is shown in Figure 5.7.

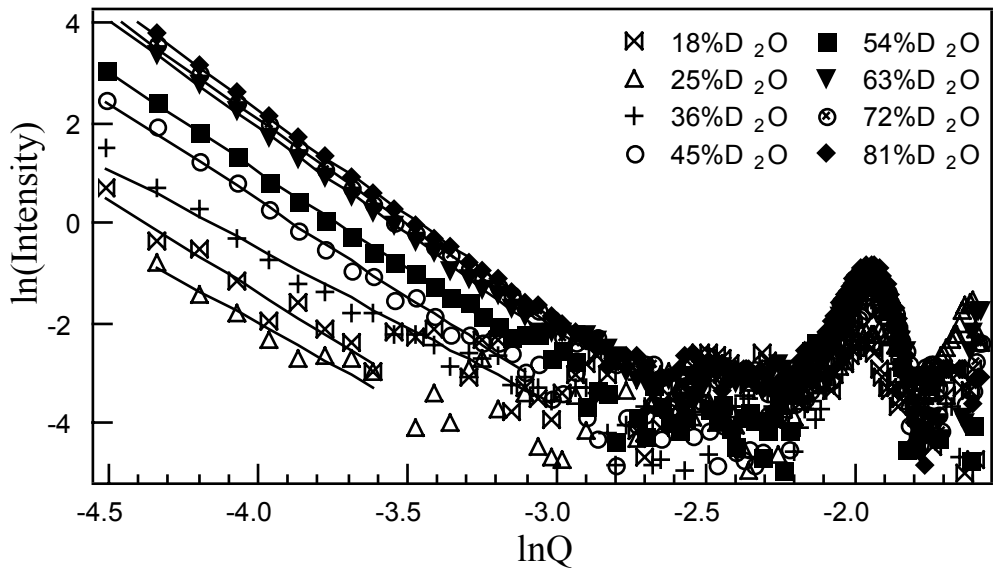

Figure 5.7 *Porod plots of lnI versus lnQ for the contrast series on an unheated MCM-41 synthesis gel containing 11.5 wt% CTAB.*

An estimation of the radii of gyration of particles of all samples by Guinier analysis was attempted but was not successful as the resulting large radii (for instance, 260 Å for a washed, acid titrated sample), indicated that the Guinier approximation (which requires $R_gQ < 1$) was not valid for the minimum Q available, *ca*. 0.006 $Å^{-1}$. This is consistent with evidence from SEM,[68] and from a Scherrer analysis of the peak widths of X-ray diffraction data,[67] which indicate coherence lengths for the hexagonal MCM-41 lattice of the order of 2000 Å.

Table 5.7 *Porod slopes from plots of lnI versus lnQ for MCM-41 samples at various preparation stages.*

Sample	Contrast / mol%D_2O	Acid Preparation	Ordinary Preparation
Heated Synthesis Gel	0	3.9(2)	3.1(2)
	20	3.9(5)	3.7(2)
	40	4.05(6)	4.1(1)
	60	4.08(4)	4.07(4)
	80	3.91(2)	4.08(3)
Washed & Dried	0	4.07(5)	3.13(2)
	10	3.94(4)	2.47(9)
	30	2.5(2)	3.2(2)
	50	3.98(3)	3.21(4)
	70	4.00(4)	3.23(5)
Calcined	8.9	3.72(3)	3.29(3)
	10	3.78(4)	-
	30	3.67(3)	3.11(4)
	50	3.4(1)	2.99(6)
	70	2.9(1)	-
	90	3.56(5)	3.20(4)

Note: - these contrasts were not measured due to restrictions on experimental time.

5.3.3.3 Particle Contrast Match Points

The Porod plots discussed above show that the MCM-41 materials, prepared by the methods described above, obey power law scattering function at low Q. All points on the power law scattering contrast in the same way. Thus it is possible to obtain the scattering length density difference at the interface between particle and solution, through contrast variation plots by selecting a particular Q value, and plotting the square root of the intensity at that value against the concentration of D_2O. A typical example (for the ordinary, unheated synthesis gel containing 11.5 wt% CTAB) is shown in Figure 5.8.

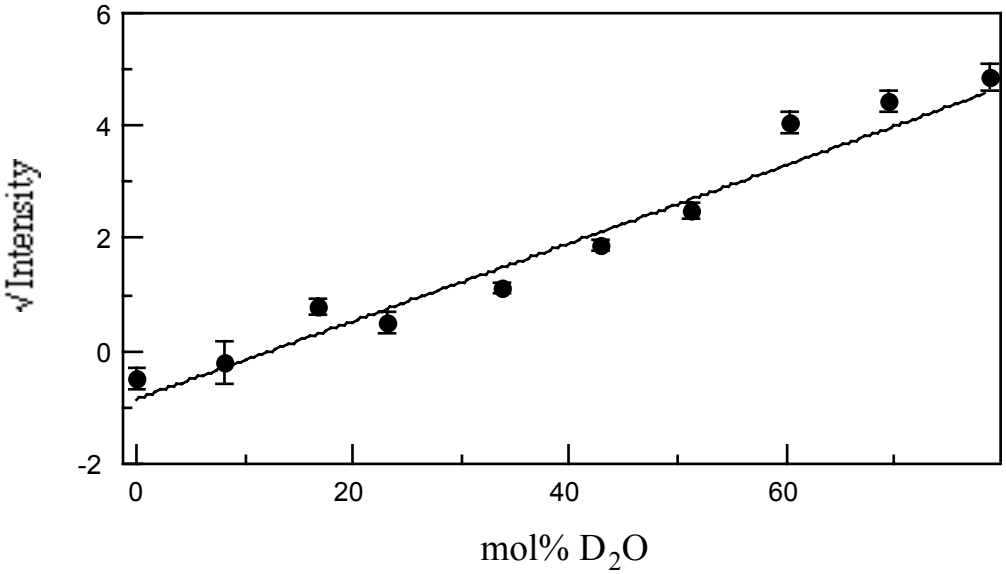

Figure 5.8 *A contrast plot of √I from Porod plots at Q = 0.015 Å^{-1} against mol% D_2O in the solvent mixture of H_2O/D_2O for the synthesis gel sample containing 11.5 wt% CTAB.*

The intensity of the (10) neutron diffraction peak from the hexagonal arrangement of channels was also found to be sensitive to the H_2O/D_2O concentration of the preparation, and for re-wetted, dried samples, also to the composition of the surrounding medium. This indicates some degree of water penetration into the structure, unlike that noted by Glinka *et al.*[65]

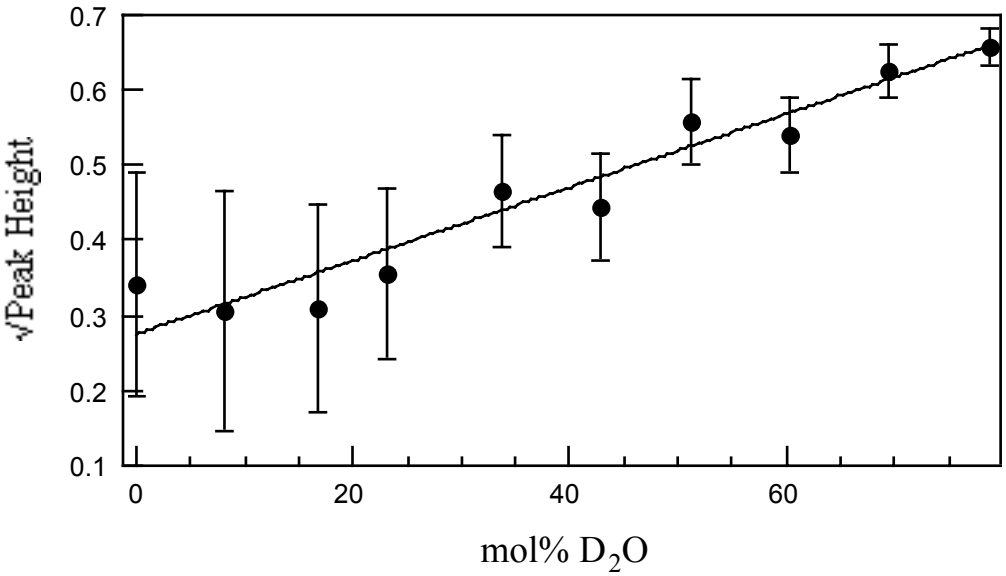

Figure 5.9 *A contrast plot of √Peak Height against mol% D_2O in the solvent mixture of H_2O/D_2O for the synthesis gel containing 11.5 wt% CTAB.*

Contrast match points for the (10) diffraction peak from the hexagonal arrangement of channels were also obtained for all samples. These contrast match points were determined from plots of √(Peak Height) versus mol% D_2O for samples in which a peak was observed. They generally occurred at a different contrast match points to those for

the low Q scattering. A (10) peak height contrast plot is shown in Figure 5.9. The contrast match points for all of the unheated synthesis gels are given in Table 5.8. Those for other heated samples, using both the ordinary and acid titrated MCM-41 synthesis methods, are listed in Table 5.9 below.

The contrast match points at low Q values for all of the ordinary preparation, unheated synthesis gels are low, between 10 and 18 mol% D_2O, indicating the relatively high levels of CTAB in these samples. The trend in the low Q contrast match points measured here, seems to be opposite to that expected. As the CTAB content, with its negative scattering length density, decreases, the low Q contrast match point, considered merely as the sum of components in the system, would be expected to increase, because the remaining components all have positive scattering length densities. This observation is however, probably not significant as the error bars on the low Q contrast match points are large. At present therefore, it is concluded that the synthesis gels have much the same contrast match point with the limits of the experiment.

As the contribution of the CTAB in solution to the scattering length density is also relatively small (-0.244×10^{10} cm^{-2}), while that of the silica is high (3.48×10^{10} cm^{-2}) large changes in CTAB concentration do not much alter the low Q contrast match points. In addition, at 25˚C CTAB is not very soluble in water and is observed to crystallise out of solution, forming large needle-like crystals. These crystals would be too large to contribute to the small angle scattering studied here, and so the scattering from the proportion of CTAB incorporated in such crystals should be ignored, when calculating the expected contrast match points of these solutions. Unfortunately it was impossible to measure the relative amounts of CTAB in the crystals and in the MCM-41 structure.

Table 5.8 *Experimental values for the contrast match points for intensity values at low Q and peak intensities of initial synthesis gels containing various amounts of CTAB. The contrast match points are given as mol% D_2O and the errors given are carried through from the errors from least squares fitting to the data.*

CTAB /wt%	Low Q	(10) Peak
11.5	12(2)	-56(28)
5	10(4)	-52(39)
2	14(5)	-180(47)
4.3+0.2M KBr	18(1)	-

Note: - No peak was observed in this experiment as it was beyond the Q range of the SANS camera.

The structural model proposed in this Chapter for a highly ordered, washed and dried MCM-41 specimen, from an acid titrated preparation, has overall 33 vol% silica and

67 vol% void space. Thus, when the void space in such a sample is completely filled with CTAB, a contrast match point of 22 mol% D_2O is expected, slightly higher than those observed in the synthesis gels. This is probably due to the presence of excess CTAB and the lower degree of silica polymerisation in the walls of these unheated synthesis gels.

In a similar silica-surfactant system containing freshly polymerised silica and DDAB bilayers (10 wt% in water)[66] the peak contrast match point was 12.8 wt% D_2O in a 10% TMOS/water system, in good agreement with the low Q contrast match points found for the MCM-41 synthesis gels, although not with the peak match points found for this hexagonal system. In a 2% TMOS/water - DDAB system, the peak contrast match point was found to be 5.6 wt% D_2O. In that case, calculations showed the contrast match points to correspond to layer of silica condensed next to the surfactant headgroups, or within the bilayers, with the former being regarded as more likely, although the resolution was insufficient to distinguish these. A rise in the scattering at small Q as polymerisation proceeded, which did not contrast at the same point as the diffraction peak, was attributed to the formation of lumps of segregated silica of the order of 1000 Å. The space between bilayers in this lamellar system was 200 Å. Such a large distance between bilayers probably allows the silicate layer to grow from the headgroups into solution, in a manner more akin to ordinary amorphous silica than in MCM-41, where the headgroups of adjacent micelles are close enough to affect the polymerisation of silica polymers on a single micelle.

The synthesis gel containing 4.3 wt% CTAB and 0.2M KBr showed highly unusual behaviour. The small angle X-ray scattering pattern showed a single MCM-41 diffraction peak with broad wings at Q = 0.1394 $Å^{-1}$ which did not change much with aging. The SAXS pattern for the corresponding 5 wt% CTAB synthesis gels, without KBr, always contained several sharp peaks, indicating more long range order. There is clearly some disruption to the formation of an ordered structure caused by the salt. A sample with 11.5 wt% CTAB and 0.4M KBr never developed any hexagonal MCM-41 peaks at all, showing only the lamellar crystalline CTAB peaks.

It is hypothesised that, analogous to the effect of salt on surfactant solutions,[70] the KBr disrupts the formation of a hexagonal structure. The silicated rod-like micelles of CTAB therefore agglomerate into the hexagonal phase in a less ordered fashion than is usual in the unheated synthesis gels. The effect of the added salt is not apparent in the low Q contrast match point. This is much the same as those for the ordinary synthesis gels even though the added salt, with a positive scattering length density, should have pushed the low Q contrast match point higher. The (10) diffraction peak was not, in this case, within the range of the SANS experiment.

The heated synthesis gel samples also have lower contrast match points than expected, perhaps due to the excess CTAB coating the particles. The contrast match point for the ordinary preparation MCM-41 heated synthesis gel is lower than that of the acid-titrated synthesis gel. This may be because it is less crystalline. It shows fewer diffraction peaks in the small angle X-ray scattering (SAXS) pattern, which measures a larger Q range than the SANS machines. Thus heated gels from the ordinary preparation may

contain less polymerised silica in the MCM-41 structure. Also amorphous silica, which precipitates in large particles with sizes beyond the range of the SANS camera, can be neglected for considerations of contrast. SEM micrographs of materials from similar ordinary MCM-41 preparations, included in Chapter 4, show evidence of large silica spheres, which co-exist with the more fibrous material which is believed to be the porous MCM-41.[68] SEM micrographs of the acid titrated preparations, which have much greater long range order (up to 7 peaks visible in the SAXS patterns), show no silica spheres. The effect of removing some of the silica from structures within the range of the SANS camera would be to reduce the low Q contrast match point slightly.

Table 5.9 *Contrast match points for ordinary and acid titrated MCM-41 preparations at various stages of the synthesis. Contrast match points for both intensity values at low Q and peak height are given. Errors are carried through from least squares fitting of the experimental data.*

Preparation Stage	Acid Preparation		Ordinary Preparation	
	Low Q	10 Peak	Low Q	10 Peak
Heated Synthesis Gel	13(1)	-36(20)	9(2)	-120(13)
Filtered & Dried	*	*	19(1)	-90(10)
Washed	22(1)† 28(1)‡	-160(20)† -390(28)‡	19(1)	-100(6)
Calcined	58(2)	61(4)	61(4)	62(6)

Note: * this specimen was not run due to constraints on experimental time.
† from the acetic acid titrated preparation.
‡ from the sulfuric acid titrated preparation.

The low Q contrast match points for the filtered, dried and washed samples, shown in Table 5.9 above, are slightly higher than those of the wet synthesis gels. This is probably due to the removal of a large part of the excess CTAB during the filtration and subsequent washings, and the slight contraction and silica densification of the MCM-41 channel lattice upon drying. X-ray diffraction shows a lattice spacing change from *ca.* 43.5 Å for an ordinary preparation synthesis gel, to 41.4 Å for the dried, uncalcined material from the ordinary preparation, and then to 35.8 Å for calcined materials from the same preparation. This contraction is probably at least partially due to further silica condensation, and physical relaxation as the water is removed and is also observed upon calcination, although to a greater degree. The samples from the acid titrated preparations contract least upon calcination (from *ca.* 43.7 Å wet, to 43.5 Å dried, to 41.6 Å calcined), indicating that the silica lattice is already fairly densely polymerised in the as-synthesised samples. This higher silica density is the likely explanation for the higher contrast match points than for the corresponding ordinary preparation MCM-41 materials at the same preparation stage.

In the calcined materials, for both the ordinary preparation and the acid titrated preparation, the observed contrast match points for both the diffraction peak and low Q scattering are close to those observed and calculated for amorphous colloidal silica, 61-66 wt% D_2O.[61,63] This indicates that the whole framework is permeable to water, as has been found for molecular hydrogen,[44] and that the silica network throughout this framework has approximately the same density as ordinary amorphous colloidal silica. There are very few completely enclosed void spaces in the walls, since this would give lower contrast match points than those observed. Other workers have published helium pycnometry results showing that the skeletal density of the oxide network is equal to that of amorphous silica, 2.2 g cm^{-3},[71] which also indicates the absence of enclosed voids in the walls. Likewise, measurements of the volumes of various liquids adsorbed into boron substituted MCM-41 channels[39] indicated a silica skeletal density of 2.2(1) g cm^{-3}, while the overall density was measured to be 0.97(4) g cm^{-3}, pointing to a low density but completely permeable structure.

5.3.3.4 Particle Internal Structure

The diffraction peak is much more sensitive to the CTAB concentration than the low Q scattering intensity. This can be seen from difference between the absolute intensities of the peak for the calcined and uncalcined samples from the same initial preparation (Figure 5.6). The negative values for the contrast match point of the peak, observed in all uncalcined MCM-41 samples studied, simply means that the contrast match point is never reached (*ie.* it is never possible to add enough H_2O to the silica matrix to match the -0.244×10^{10} cm^{-2} scattering length density of the included CTAB) and is a hypothetical, and unphysical, extrapolation. The trend to more negative values as CTAB is removed however, is of considerable importance in distinguishing possible structures for MCM-41.

The low values of the low Q contrast match points for the unheated synthesis gels, discussed previously, are one indication that a simple model of MCM-41 is not correct. The contrast match points of between 10 and 18 mol% D_2O correspond to volume fractions of between 75% and 90% of holes filled with CTAB of normal density, whereas the simplest model of MCM-41 - CTAB filled tubes of *ca.* 40 Å diameter in a silica matrix with 8 Å walls between tubes - gives a hole volume fraction of only 41%. This simple calculation points to the need for a lower density silica in the walls, thinner walls, high penetrability of the walls by water, or some combination of all three.

From the work discussed above on synchrotron X-ray data[72] on the (h,k) in-plane diffraction from acid titrated samples, a minimum model of MCM-41 was proposed. It required a three region structure; a denser continuous wall region between pores, a shell of less dense silica lining the cylindrical channels and a narrow pore with no silica content. To explain the SANS data, the same three component structural model as proposed in the X-ray work is used. The observed scattering intensities are described in terms of an equation, modified slightly for the neutron case at I(0):

$$I(Q) = ((\Delta\rho_1)A_1 \frac{2J_1(Q,R_1)}{R_1Q} + (\Delta\rho_2)A_2 \frac{2J_1(Q,R_2)}{R_2Q} e^{-\alpha Q^2} + (\Delta\rho_3)A_3 \frac{2J_1(Q,R_3)}{R_3Q})^2 \quad \textbf{(5.3)}$$

where I is the measured intensity, R_1 is the radius of the outer cylinder, R_2 is the radius of the inner cylinder, R_3 is half of the centre to centre distance between the channels (see Figure 5.3) A_1, A_2 and A_3 are the relative areas of each component, $J_1(Q,R_n)$ is the first order Bessel function and α is a Debye-Waller constant. The relative areas, A_1, A_2 and A_3 were taken from the X-ray model, and α was likewise set to 1.0 Å^2. The contrasts, $\Delta\rho_1$, $\Delta\rho_2$, $\Delta\rho_3$ are the differences in scattering length density between the wall and the shell, the shell and the hole, and the wall and the solvent respectively. These were calculated for the empty dry lattice from the silica densities of the X-ray model, and then, given the experimental contrast match points, both for the peak and at low Q values, the amounts of solvent and surfactant in each part of the structure could be calculated.

The extra term of identical form to the first term in equation 5.1 (in the X-ray model above) is necessary at low Q values, in the neutron case, to account for the solvent-wall contrast. This term is required because at, or near I(0) the volume average of the scattering length densities of the various components in the particles (which is the conventional way of determining theoretical contrast match points) must give the same result as the model from the X-ray data. The X-ray equation (5.1) as given is for diffraction. However, at or near I(0) there is also a significant contribution to the scattering from solvent-particle interactions which must be included. The extra term is not necessary in the consideration of the diffraction peak, since it is only the internal density fluctuations which contribute to the intensity of the peak. Because the X-ray model was fitted to data from acid titrated MCM-41 materials only, the calculations were restricted to these materials. As the contrast match points for the ordinary preparation MCM-41 materials are generally similar, the conclusions also hold for these materials. For convenience it is assumed that the partitioning of water into the three components of the structure is isotope independent.

This model worked well for those samples which had been removed from their synthesis liquor, *ie.* those which had been filtered, and/or washed and dried, or calcined. Modelling the calcined sample gave water concentrations filling 100% of all void space in the structure, indicating that the solvent had uniformly penetrated all of the non-silica volume. Attempts in the modelling to fill this void space with any surfactant gave unphysical results.

A fit of the model to data for the washed and dried samples indicated high concentrations of CTAB still present in the void spaces. The washed, acid preparation sample with a contrast match point for the power law region of 22(1) mol% D_2O gave physical values of surfactant and water concentration only when 100% of the central hole was occupied by CTAB, but the wall was *ca.* 8 vol% water/ 52 vol% CTAB/ 40 vol% silica and the lining contained about 1% solvent, being around 64 vol% CTAB/ 35 vol% silica. The sample with a higher power law contrast match point of 28(1) mol% D_2O, indicating less total CTAB present, gave physical values for the full

range of possible concentrations of water and CTAB in the central hole (*ie.* 0-100 vol% water) and between, *ca.* 19-50 vol% water/ 41-10 vol% CTAB/ 40 vol% silica in the denser walls, while the shell contained *ca.* 4-30 vol% water/ 61-35 vol% CTAB/ 35 vol% silica. For water concentrations in the central hole higher than 19%, the walls fill with water preferentially to the lining, so that if the central hole is 100% water, then the void space in the walls are filled with 50 vol% water, and the void spaces in the lining contain only 4 vol% water. Some intermediate situation for example 50 vol% water/ 50 vol% CTAB in the central hole, 35 vol% water/ 25 vol% CTAB/ 40 vol% silica in the walls, and 15 vol% water/ 50 vol% CTAB/ 35 vol% silica in the lining, seems intuitively more realistic.

These values are largely what would be intuitively expected for solvent penetration as the CTAB template is removed from the structure, however it is perhaps surprising that the outer silica wall fills with solvent preferentially to the lining. Possibly this indicates the void spaces present in the wall are smaller, and are positions of higher energy than those of the lining so that as CTAB is washed out of the structure, protruding CTAB molecules retract into a more uniform micellar configuration. That the hole should fill with solvent preferentially to the lining possibly indicates however, that the lining sites are of lower energy to the formation of a self-stabilised micelle within the tube structure. It is likely also, that the surfactant in the walls is, for the most part, comprised of the headgroups with the hydrocarbon tails being more concentrated in the central parts of the micelle. Unfortunately the contrast of the surfactant headgroup (-0.45×10^{10} cm^{-2}) is very similar to that of the tail (-0.46×10^{10} cm^{-2}), so they could not be distinguished in the modelling, given the accuracy of the collected data. Overall, the surprising highly negative extrapolated contrast match points for the diffraction peaks arise quite naturally for differentiated CTAB occupancy of void spaces within the model of MCM-41.

The X-ray model cannot be manipulated by variation of any of the parameters to give results for any of the synthesis gel samples, even the acid titrated heated synthesis gel, which would be expected to be the closest in structure to the dried and calcined materials for which the X-ray model was developed. The presence of unpolymerised silica, and excess CTAB partitioned between the MCM-41 phase, solution, the lamellar CTAB crystalline phase and even large particles of precipitated, amorphous silica create too many variables to allow modelling. The fact that the MCM-41 structure itself may only be partially polymerised in the unheated start gels, and thus has a much lower density than in the heated products, could also contribute.

5.4 Discussion

In the three region model suggested in this Chapter, it is postulated that the denser walls in MCM-41 occur where two cylindrical surfactant micelles, partially covered with silica, have touched and interpenetrated during synthesis. The porous nature of the silicate, however, suggests a significant impact of the surfactant template on the local structure of the silicate, when compared with that of the amorphous silica which forms in this system in the absence of CTAB. In the inner cylinder, closer to the surfactant

headgroups of the micelle template the silicate density is lower, suggesting condensation of the silicate is even less continuous. Previous work has shown the surfactant to have a significant catalytic effect on the silicate polymerisation.[73] Possibly the increase in the reaction rate near the surfactant headgroups is responsible for the growth of an extended, open, kinetically formed network which interpenetrates, as silica coated micelles pack together to form the hexagonal phase crystals. The presence of other anions (*eg.* Br^-, OH^-) in the double layer surrounding the surfactant micelle may also affect the structure of the silicate in this region through steric effects when the anions become trapped by the polymerising silica, interrupting the continuity of the silicate polymerisation.

The surfaces of the micelles may also not be smooth, with some silicate species extending into the interior of the micelle where the hydrocarbon tails of the surfactant are concentrated. Work on pure surfactant systems has shown that water molecules may penetrate the micelle surface to distances of 3-6 carbon atoms,[74] so silicate monomers could also occupy such regions. As long chain silicate polymers form, the neutral silica 'tail' on a growing polymer chain may also be able to preferentially enter the CTAB micelle, as it will be less hydrophilic than the charged silica monomers. However, given the *ca.* 60% reduction in density from pure silica, some type of microstructure in the walls must be inferred, since a purely random creation of voids to this extent would be unlikely to form a stable silica structural framework.

Some form of clathrate structure may be involved in the wall network. Such structures are often proposed as precursors to silicate condensation in zeolites formed with single molecule templates,[75-78] and have even been suggested as MCM-41 precursors.[79] In those cases, the charged silica polyanions cluster around the template molecules, creating a loosely organised silica-organic species. A similar mechanism may operate here, although the supramolecular micelle structure formed by the association of the enclathrated template species obviously disrupts the silica crystallisation into atomically ordered arrays. The low densities indicated by this work may explain why other methods have not shown such small mesopores - in gas adsorption experiments the large amount of void space indicated by the experiments discussed above would merely appear to contribute to the mesopore volume. Previous workers[5,6,26] have implicitly assumed wall densities appropriate for bulk silica giving a much greater mesopore radius.

5.4.1 Other Possible Models for the MCM-41 Structure

Some structural facts about MCM-41 are reviewed:

- There is a hexagonal array of tubes at a spacing of *ca.* 40 Å which are capable of absorbing molecules to at least the size of benzene,[8,80-86] but not much larger (in three dimensions).
- The tubes may be interconnected by pathways capable of supporting bulk hydrogen, so that the void space may be a single space (see Chapter 6, section 6.8).
- Silica densities are everywhere low, less than 50% of cristobalite, even in the so-called walls.

- The projection of the electron density on the hexagonal plane gives a complex pore structure, with a 7 Å radius hole, surrounded by a 12 Å silica lining (of density 35% of bulk silica), with the separating wall 40% of bulk silica density.
- The void space is separated from silica in such a way that when filled with hydrogen, 50% of the hydrogen does not touch silica (see Chapter 6, section 6.7.1).
- When filling with hydrogen the central 7 Å projected void begins filling when the lining and wall are not totally filled, implying that there are voids with radii of *ca.* 7 Å in the lining and wall.
- When sheared, the MCM-41 forming gel, at the CTAB concentrations used here, does *not* decompose into parallel rod-like micelles, but maintains its structure (as discussed in Chapter 4) implying three-dimensional connections between the walls of the pores, and the micelles forming these.

To explain these observations two extreme models may be proposed - if the usual model of an array of large diameter, smooth-walled, non-connected tubes is discounted as not fitting the data listed above at all.

Firstly a model in which the tube is essentially straight and the walls are highly dissected into fibrils and tendrils of silica, with random interconnections between the tubes. That is to say, a model whose structure is random with a short coherence length - the essential structure describable in only ten or twenty Ångstroms of tube length. This model assumes straight, parallel tubes which are not intertwined on length scales of less than hundreds of Ångstroms. Transmission electron micrographs show bends and twists in the channels of MCM-41, but these are on too long a length scale to register in this analysis.[35] In this model, the wall is more massive, while the silica in the linings is more finely divided. This is an entirely reasonable result considering the preparation from the gel.[67] Such a model explains all of the observations, but leaves open the question of what microscopic architecture can stably support the tube network with more than 60% void space, and no micropores.

An alternative is a model in which the free volume is essentially smooth walled, but meanders in some way through the structure. This naturally implies a structural description requiring tens of Ångstroms in size to properly describe the major features. A natural trial model is a defective version of the MCM-48 structure. Intermediate structures between lamellar and hexagonal are commonly discussed,[87] but those between hexagonal and cubic MCM-48 have not been, mainly because the MCM-48 structure itself has only recently been firmly established[88] to be related to that conjectured earlier for corresponding surfactant systems.[70,89-95] A transition of hexagonal phase material to the cubic MCM-48 structure has been recently observed, although the intermediate structure is not discussed.[96] This model of MCM-41 has relatively smooth walled channels, which are largely hexagonally close-packed cylinders, but which have interconnections which resemble pieces of the infinite periodic minimal surface, although much less well ordered than in the material which is normally characterised as MCM-48. Although, considering the method of MCM-41 preparation, this model is considered less likely, it should be considered in more detail.

MCM-48 is a three-dimensionally ordered material of cubic Ia3d symmetry. Although, at the experimental resolutions, a structural description in terms of a network-of-rods model may well be possible, the discussion will concern the infinite periodic minimal surface model. The gyroid minimal surface is of symmetry Ia3d, and such a double sided silica surface of thickness 3-13 Å fits both the available X-ray and TEM data from MCM-48.[88] This structure has infinite helical tubes along {111} and {100} forming two interconnected single voids separated by the minimal surface.

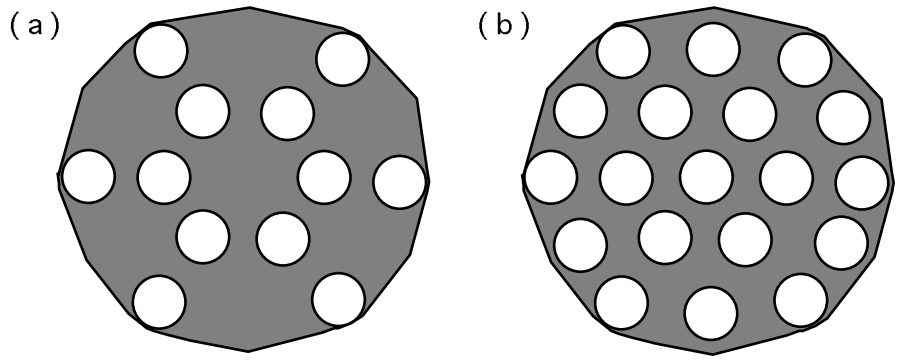

Figure 5.10 *The [111] projections of (a) MCM-48 and (b) MCM-41, showing similarities between these materials - the arrangement of channels is similar, there are merely "missing" channels in the [111] projection of MCM-48.*

To discuss the possible relation to MCM-41, the [111] projection of MCM-48 is considered,[93] the important features of which are shown in Figure 5.10. In this projection it is clear that MCM-41 and MCM-48 may be structurally related. This is already clear from the gross similarity of the X-ray diffraction pattern envelopes of lamellar, hexagonal and cubic phases. MCM-48 has a hexagonal arrangement of tubes along [111] in which one third of the simple hexagonally packed tubes of MCM-41 have been removed. The tube spacing in both MCM-41 and MCM-48 is 45 Å, if typical observed values for unit cells of 45 and 95 Å respectively, are assumed. If a surface thickness of 12 Å in the MCM-48 minimal surface is assumed, then a tube diameter of *ca.* 9 Å along [111] is predicted, surrounded by a lining of thickness 6 Å, at which point the density increases due to the presence of the projection of the minimal surface on the (111) plane. That is, the "wall" region in MCM-41 corresponds to those regions of MCM-48 where the projection of the minimal surface exists. Furthermore, if a mechanism is invoked by which the [111] tubes in MCM-48 can move sideways in (111) by ±[1/3, -1/3, 0], ±[1/3, 0, -1/3] and ±[0, 1/3,-1/3] only, perhaps by some type of stacking fault, then a structure will result in which there is a simple hexagonal lattice of tubes along [111], with no continuous tubes or ordering along the other three body diagonals ([1-11], [-111] and [11-1]). In addition there is a narrow pore in projection, surrounded by a lining, with strong (unshearable) wide pore interconnections between the tubes, a low overall silica density, and smooth walled pores throughout. This seems a reasonable model for MCM-41 consistent with the observations listed above.

It should also be noted that a model proposed for the structure of the related mesoporous silicate, FSM-16, suggests that it may be composed not of long straight channels, but instead contains pores which are likely to be interconnected in a three dimensional network.[18] In that work, this observation is used to distinguish MCM-41

and FSM-16. It may be, however, that the interconnectedness of the pore system is merely a matter of degree, which is dependent upon the synthesis used, and that MCM-41 may therefore also contain connections between channels.

The concentrations of the reagents in the reaction gel used in this work are firmly within the hexagonal, MCM-41 region of the synthesis space.[23] If the MCM-41 and MCM-48 structures are closely related, as proposed above, this suggests a large degree of fuzziness in the definitions of these mesophase surfactant/silica composite structures. Two extreme interpretations of the data are presented here, although many variants and intermediates are equally possible. However, all models *must* satisfy, in particular the detailed data on the projection of the structure on the basal plane presented in this chapter.

5.5 Conclusions

The modelling of the envelope of synchrotron X-ray data from highly crystalline MCM-41 samples shows that these materials have walls made up of silica with variable density regions, not previously suspected. This is modelled as a continuous wall with density much reduced from that of ordinary amorphous silica, and cylinders of less dense material lining the channels created by the dense phase. The completely empty pore space has smaller dimensions than has previously been measured for MCM-41, being only 7 Å in radius, however the 13 Å wide, low density inner lining of the channels will also contain much void space. Even the denser continuous wall structures in this material have been shown to contain void space, which may be responsible for the collective behaviour of gases in MCM-41 (see Chapter 6), since they allow a high degree of connectivity between the pores.

Neutron diffraction patterns show two interesting coherent elastic diffraction features associated with the MCM-41, besides the expected inelastic and incoherent elastic scattering from hydrogen alone (discussed in Chapter 6). There is a peak at 3.1 Å due to H_2-H_2 scattering from bulk hydrogen. The filling dependence of its intensity confirms the inelastic result that the ratio of surface to bulk hydrogen at full filling is 1:1. The second features are MCM-41 diffraction peaks observed at long *d*-spacings (10.7-14.4 Å). The most intense of these, the (21) hexagonal peak, shows dramatic change in intensity of up to a factor of three, as the hydrogen filling is changed. A simple model of MCM-41 of a uniform large mesopore in dense silica does not predict these changes - whether uniform hydrogen filling is assumed, or filling localised to a skin on the mesopore surface, or any intermediate situation. However the more complex “three region” structural model used to fit the synchrotron X-ray data provides an excellent fit. This model has a small empty cylindrical pore, surrounded by a thicker cylindrical lining of silica with some 65 vol% void space. This is in turn surrounded by silica walls which contain 60 vol% void space. This highly porous model fits the (21) diffraction data if hydrogen adsorption is modelled as occurring in three overlapping stages. Initially hydrogen is surface adsorbed in the lining region and fractionally less so in the wall region. Later, the lining pores start to fill up and then the wall pores. Lastly, as the filling of lining and wall becomes almost complete the empty small central pore fills.

The contrast match points from small angle neutron scattering experiments give detailed information about the structure of MCM-41. They indicate that the calcined material is completely penetrable to water, all voids completely filling. Those parts of the structure which are not penetrable, contain silica with the same scattering length density as for amorphous colloidal silica, indicating that the silica structure has much the same density as normal amorphous silica. The contrast match points also indicate that in the uncalcined materials a large part of the wall and shell volume contain CTAB molecules and solvent, and so must be highly porous to account for this. The contrast match points for the synthesis gels reflect the high CTAB concentrations and low degrees of silica polymerisation present in these samples.

These detailed results - bulk properties plus structural data concerning projections onto the MCM-41 basal plane - can be rationalised in two extreme ways. A locally uniform three-dimensional structure can be postulated in which the silica is relatively finely divided into tendrils and sheets with that in the walls being relatively more massive, while the silica in the lining is more finely divided. This means that, proportionately to the total volume in each region, the lining has more surface and the walls more large voids. Thus, considering gas absorption, initially a gas will be adsorbed on the surfaces, and thus be concentrated in the lining. Later the voids will fill, with the largest, the central pore, filling last. Alternatively, at another extreme, a smoother walled mesopore can be imagined which, over longer distances, snakes between hexagonal sites in a way which locally resembles the pore structure of the three-dimensionally ordered structure of MCM-48.

5.6 References

1. O. Franke, G. Schulz-Ekloff, J. Rathousky, J. Stárek and A. Zukal, *J. Chem. Soc., Chem. Commun.,* **1993**, 724-725.
2. P.J. Branton, P.G. Hall and K.S.W. Sing, *J. Chem. Soc., Chem Commun.,* **1993**, 1257-1258.
3. R. Schmidt, M. Stöcker, E. Hansen, D. Akporiaye and O.H. Ellestad, *Microporous Mater.,* **1995**, *3*(4/5), 443-448.
4. P.I. Ravikovitch, S.C.O. Domhnaill, A.V. Neimark, F. Schüth and K.K. Unger, *Langmuir,* **1995**, *11,* 4765-4772.
5. I. Petrovic, A. Navrotsky, C.-Y. Chen and M.E. Davis in *Zeolites and Related Microporous Materials: State of the Art 1994*; Studies in Surface Science and Catalysis, (Eds. J. Weitkamp, H.G. Karge, H. Pfeifer and W. Hölderich), Elsevier Science B.V., Amsterdam, **1994**, *Vol. 84*, 677-684.
6. B.P. Feuston and J.B. Higgins, *J. Phys. Chem.,* **1994**, *98,* 4459-4462.
7. P.J. Branton, P.G. Hall, K.S.W. Sing, H. Reichert, F. Schüth and K.K. Unger, *J. Chem. Soc., Faraday Trans.,* **1994**, *90*(19), 2965-2967.
8. J.S. Beck, J.C. Vartuli, W.J. Roth, M.E. Leonowicz, C.T. Kresge, K.D. Schmitt, C.T.-W. Chu, D.H. Olson, E.W. Sheppard, S.B. McCullen, J.B. Higgins and J.L. Schlenker, *J. Am. Chem. Soc.,* **1992**, *114,* 10834-10843.
9. P.T. Tanev and T.J. Pinnavaia, *Science,* **1995**, *267,* 865-867.

10. Z. Luan, H. He, W. Zhou, C.-F. Cheng and J. Klinowski, *J. Chem. Soc., Faraday Trans.,* **1995**, *91*(17), 2955-2959.
11. S.A. Bagshaw, E. Prouzet and T.J. Pinnavaia, *Science,* **1995**, *269*, 1242-1244.
12. C.Y. Chen, S.L. Burkett, H.-X. Li and M.E. Davis, *Microporous Mater.,* **1993**, *2,* 22.
13. C.-F. Cheng, D.H. Park and J. Klinowski, *J. Chem. Soc., Faraday Trans.,* **1997**, *93*(1), 193-197.
14. C.-F. Cheng, W. Zhou, D.H. Park, J. Klinowski, M. Hargreaves and L.F. Gladden, *J. Chem. Soc., Faraday Trans.,* **1997**, *93*(2), 359-363.
15. P.I. Ravikovitch, D. Wei, W.T. Chueh, G.L. Haller and A.V. Neimark, *J. Phys. Chem. B,* **1997**, *101*(19), 3671-3679.
16. R.K. Iler, *The Chemistry of Silica. Solubility, Polymerization, Colloid and Surface Properties, and Biochemistry*, John Wiley & Sons, New York, **1979**.
17. R. Schmidt, E.W. Hansen, M. Stöcker, D. Akporiaye and O.H. Ellestad, *J. Am. Chem. Soc.,* **1995**, *117,* 4049-4056.
18. C.-Y. Chen, S.-Q. Xiao and M.E. Davis, *Microporous Mater.,* **1995**, *4*(1), 1-20.
19. C.-Y. Chen, H.-X. Li and M.E. Davis, *Microporous Mater.,* **1993**, *2,* 17.
20. K.R. Kloetstra, H.W. Zandbergen, M.A. van Koten and H. van Bekkum, *Catal. Lett.,* **1995**, *33,* 145-156.
21. A. Firouzi, D. Kumar, L.M. Bull, T. Besier, P. Sieger, Q. Huo, S.A. Walker, J.A. Zasadzinski, C. Glinka, J. Nicol, D. Margolese, G.D. Stucky and B.F. Chmelka, *Science,* **1995**, *267*, 1138-1143.
22. M.W. Maddox and K.E. Gubbins, *Int. J. Thermophys.,* **1994**, *15*(6), 1115-1123.
23. G.D. Stucky, A. Monnier, F. Schüth, Q. Huo, D. Margolese, D. Kumar, M. Krishnamurty, P. Petroff, A. Firouzi, M. Janicke and B.F. Chmelka, *Mol. Cryst. Liq. Cryst.,* **1994**, *240,* 187-200.
24. S. Inagaki, Y. Sakamoto, Y. Fukushima and O. Terasaki, *Chem. Mater.,* **1996**, *8*(8), 2089-2095.
25. S. Inagaki, Y. Fukushima, K. Kuroda and K. Kuroda, *J. Colloid Interface Sci.,* **1996**, *180,* 623-624.
26. A. Ortlam, J. Rathousky, G. Schulz-Ekloff and A. Zukal, *Microporous Mater.,* **1996**, *6*(4), 171-180.
27. C.-F. Cheng, H. He, W. Zhou and J. Klinowski, *Chem. Phys. Lett.,* **1995**, *244,* 117-120.
28. Q. Huo, J. Feng, F. Schüth and G.D. Stucky, *Chem. Mater.,* **1997**, *9*(1), 14-17.
29. S. Schacht, Q. Huo, I.G. Voigt-Martin, G.D. Stucky and F. Schüth, *Science,* **1996**, *273*, 768-771.
30. S.A. Davis, S.L. Burkett, N.H. Mendelson and S. Mann, *Nature,* **1997**, *385,* 420-423.
31. G.S. Attard, J.C. Glyde and C.G. Göltner, *Nature,* **1995**, *378*, 366-368.
32. D. Zhao and D. Goldfarb, *J. Chem. Soc., Chem. Commun.,* **1995**, 875-876.
33. R. Ryoo and J.M. Kim, *J. Chem. Soc., Chem. Commun.,* **1995**, *7*, 711-712.
34. O. Glatter and O. Kratky, *Small Angle X-ray Scattering*, Academic Press, London, **1982**, 32-35.
35. V. Alfredsson, M. Keung, A. Monnier, G.D. Stucky, K.K. Unger and F. Schüth, *J. Chem. Soc., Chem. Commun.,* **1994**, 921-922.

36. M.D. Alba, A.I. Becerro and J. Klinowski, *J. Chem. Soc., Faraday Trans.,* **1996**, *92*(5), 849-854.
37. N. Coustel, F. Di Renzo and F. Fajula, *J. Chem. Soc., Chem. Commun.,* **1994**, 967-968.
38. C.J. Plank and L.C. Drake, *J. Colloid Sci.,* **1947**, *2,* 399-412.
39. B. Marler, U. Oberhagemann, S. Vortmann and H. Gies, *Microporous Mater.,* **1996**, *6,* 375-383.
40. D. Khushalani, A. Kuperman, G.A. Ozin, K. Tanaka, J. Garcés, M.M. Olken and N. Coombs, *Adv. Mater.,* **1995**, *7*(10), 842-846.
41. A. Pöppl, M. Hartmann and L. Kevan, *J. Phys. Chem.,* **1995**, *99*(47), 17251-17258.
42. E.W. Hansen, M. Stöcker and R. Schmidt, *J. Phys. Chem.,* **1996**, *100*(6), 2195-2200.
43. K.J. Edler, P.A. Reynolds, F. Trouw and J.W. White, *Chem. Phys. Letters,* **1996**, *249,* 438-443.
44. K.J. Edler, P.A. Reynolds, P.J. Branton, F. Trouw and J.W. White, *J. Chem. Soc., Faraday Trans.,* **1997**, *93*(8), 1667-1674.
45. V.Y. Gusev, X. Feng, Z. Bu, G.L. Haller and J.A. O'Brien, *J. Phys. Chem.,* **1996**, *100*(6), 1985-1988.
46. J. Rathousky, A. Zukal, O. Franke and G. Schulz-Ekloff, *J. Chem. Soc., Faraday Trans.,* **1994**, *90*(18), 2821-2826.
47. J. Rathousky, A. Zukal, O. Franke and G. Schulz-Ekloff, *J. Chem. Soc., Faraday Trans.,* **1995**, *91*(5), 937-940.
48. P.L. Llewellyn, F. Schüth, Y. Grillet, F. Rouquerol and K.K. Unger, *Langmuir,* **1995**, *11,* 574-577.
49. D. Akporaiye, E.W. Hansen, R. Schmidt and M. Stöcker, *J. Phys. Chem.,* **1994**, *98* 1926-1928.
50. S. Komarneni, R. Pidugu and V.C. Menon, *J. Porous Mater.,* **1996**, *3,* 99-106.
51. R.L. Mills and A.F. Schuch, *Phys. Rev. Lett.,* **1965**, *15,* 722-.
52. J.A. Young and J.U. Koppel, *Phys. Rev. 3A,* **1964**, *135*, 603-611.
53. M. Nielsen, *Phys. Rev. B,* **1973**, *7*(4), 1626-1635.
54. W. Langel, D.L. Price, R.O. Simmons and P.E. Sokol, *Phys. Rev. B,* **1988**, *38*(16), 11275-11283.
55. P.E. Sokol, R.T. Azuah, M.R. Gibbs and S.M. Bennington, *J. Low Temp. Phys.,* **1996**, *103*(1/2), 23-33.
56. G.J. Kellogg, J.W. White, K.W. Herwig and P.E. Sokol, *J. Chem. Phys.,* **1990**, *93*(10), 7153-7162.
57. W.J. Stead, P. Meehan and J.W. White, *J. Chem. Soc., Faraday Trans. II,* **1988**, *84*(10), 1655-1668.
58. G.J. Kellogg, P.E. Sokol and J.W. White in *Momentum Distributions*; (Eds. R.N. Silver and P.E. Sokol), Plenum Press, New York & London, **1990**, 351-354
59. H.F. Poulsen, J. Neuefeind, H.-B. Neumann, J.R. Schneider and M.D. Zeidler, *J. Non-Cryst. Solids,* **1995**, *188,* 63-74.
60. A.C. Wright, *J. Non-Cryst. Solids,* **1994**, *179,* 84-115.
61. J. Dougherty, L.E. Iton and J.W. White, *Zeolites,* **1995**, *15,* 640-649.
62. S.L. Suib, *Chem. Rev.,* **1993**, *93*(2), 803-826.

63. L.E. Iton, F. Trouw, T.O. Brun, J.E. Epperson, J.W. White and S.J. Henderson, *Langmuir,* **1992**, *8*(4), 1045-1048.
64. L. Auvray, A. Ayral, T. Dabadie, L. Cot, C. Guizard and J.D.F. Ramsay, *Faraday Discuss.,* **1995**, *101,* 235-247.
65. C.J. Glinka, J.M. Nicol, G.D. Stucky, E. Ramli, D. Margolese, Q. Huo, J.B. Higgins and M.E. Leonowicz, *J. Porous Materials,* **1996**, *3,* 93-98.
66. M. Dubois, T. Gulik-Krzywicki and B. Cabane, *Langmuir,* **1993**, *9*(3), 673-680.
67. K.J. Edler and J.W. White, *Chem. Mater.,* **1997**, *9*(5), 1226-1233.
68. K.J. Edler, J. Dougherty, R. Durand, L. Iton, G. Kirton, G. Lockhart, Z. Wang, R. Withers and J.W. White, *Colloids Surfaces A,* **1995**, *102,* 213-230.
69. B. Jacrot, *Rep. Prog. Phys.,* **1976**, *39,* 911-953.
70. G.J.T. Tiddy, *Physics Reports,* **1980**, *57*(1), 1-46.
71. T. Dabadie, A. Ayral, C. Guizard, L. Cot and P. Lacan, *J. Mater. Chem.,* **1996**, *6*(11), 1789-1794.
72. K.J. Edler, P.A. Reynolds, J.W. White and D. Cookson, *J. Chem. Soc., Faraday Trans.,* **1997**, *93*(1), 199-202.
73. C.-F. Cheng, Z. Luan and J. Klinowski, *Langmuir,* **1995**, *11,* 2815-2819.
74. J.H. Fendler and E.J. Fendler, *Catalysis in Micellar and Macromolecular Systems*, Academic Press, New York, **1975**.
75. S.L. Burkett and M.E. Davis, *J. Phys. Chem.,* **1994**, *98*(17), 4647-4653.
76. W.M. Hendricks, A.T. Bell and C.J. Radke, *J. Phys. Chem.,* **1991**, *95*(23), 9513-9518.
77. C.T.G. Knight, *Zeolites,* **1990**, *10,* 140-144.
78. S.L. Burkett and M.E. Davis, *Chem. Mater.,* **1995**, *7*(5), 920-928.
79. J. Emmer and M. Wiebcke, *J. Chem. Soc., Chem. Commun.,* **1994**, 2079-2080.
80. E. Armengol, M.L. Cano, A. Corma, H. Garcia and M.T. Navarro, *J. Chem. Soc., Chem. Commun.,* **1995**, 519-520.
81. K.M. Reddy, I. Moudrakovski and A. Sayari, *J. Chem. Soc., Chem. Commun.,* **1994**, 1059-1060.
82. K.R. Kloetstra and H. van Bekkum, *J. Chem. Soc., Chem. Commun.,* **1995**, 1005-1006.
83. A. Corma, V. Fornés, H. García, M.A. Miranda and M.J. Sabater, *J. Am. Chem. Soc.,* **1994**, *116*(21), 9767-9768.
84. J. Aguado, D.P. Serrano, M.D. Romero and J.M. Escola, *J. Chem. Soc., Chem. Commun.,* **1996**, 725-726.
85. T. Blasco, A. Corma, M.T. Navarro and J. Pérez Pariente, *J. Catal.,* **1995**, *156,* 65-74.
86. R. Netrabukkana, K. Lourvanij and G.L. Rorrer, *Ind. Eng. Chem. Res.,* **1996**, *35*(2), 458-464.
87. A. Monnier, F. Schüth, Q. Huo, D. Kumar, D. Margolese, R.S. Maxwell, G.D. Stucky, M. Krishnamurty, P. Petroff, A. Firouzi, M. Janicke and B.F. Chmelka, *Science,* **1993**, *261*, 1299-1303.
88. V. Alfredsson and M.W. Anderson, *Chem. Mater.,* **1996**, *8*(5), 1141-1146.
89. V. Luzzati, A. Tardieu, T. Gulik-Krzywicki, E. Rivas and F. Reiss-Husson, *Nature,* **1968**, *220,* 485.
90. K. Fontell, *Colloid and Polymer Sci.,* **1972**, *43,* 156.
91. K. Fontell, *Colloid and Polymer. Sci.,* **1990**, *268,* 264.

92. K. Fontell, *Adv. Colloid and Inter. Sci.,* **1992**, *41,* 127.
93. L. Larsson, *J. Phys. Chem.,* **1989**, *93,* 7304.
94. P. Ekwall, L. Mandell and K. Fontell, *J. Colloid and Inter. Sci.,* **1969**, *29,* 639.
95. J. Charvolin and J.F. Sadoc, *Colloid and Polymer Sci.,* **1990**, *268,* 190.
96. Q. Huo, D.I. Margolese and G.D. Stucky, *Chem. Mater.,* **1996**, *8*(5), 1147-1160.

Chapter 6:

Characterisation of Molecules in MCM-41 Channels

"Under the most rigorously controlled conditions of pressure, temperature, humidity, and other variables, the organism will do as it damn well pleases."

Anon.

The observation of molecular clusters has been of interest for some time. Molecular clusters can show quite different dynamic and static phase behaviour from bulk systems, and, because of their limited size, are accessible to computational molecular dynamics techniques.[1-3] Experimentally, molecular clusters are made using several methods, including supersonic jets, vapours, confinement of phases in emulsion droplets, condensation on surfaces and condensation in pores.[1]

The pore system of MCM-41 has previously been used to produce nanophase particles of platinum[4,5] cobalt,[6] binary caesium-lanthanum oxide clusters[7] and manganese-oxo species,[8] for catalysis purposes, and as a substrate for the creation of molecular wires.[9,10] The effects of confinement in the mesopores were studied only in relation to the molecular wires. It was found that polyaniline chains polymerised in MCM-41 channels were more conductive than similar chains polymerised in smaller, zeolite channels where inter-chain interactions were inhibited.[11] Some investigation of the properties of confined particles was carried out for semiconducting iron oxide particles.[12] The effect of confinement in uniform mesopores in that case was to produce a much wider bandgap, due to the quantum size effect, than had been previously seen for such materials. It has also been shown that the properties of polymers confined in the pores of MCM-41 differ from those in the bulk. The molecular weight has been observed to increase for poly(methyl methacrylate)[13] polymerised within the mesopores, and the glass transition temperatures of poly(vinyl acetate)[13] and polystyrene[14] has been shown to decrease with increasing confinement in MCM-41 materials.

Here the condensation of methane and hydrogen in the pores of MCM-41 results in mesoscale molecular structures which can be characterised by the use of gas isotherms, quasielastic neutron scattering and inelastic neutron scattering, and which show phase

behaviour which differs from that of bulk samples. Gases adsorbed in MCM-41 which have been studied by other workers include nitrogen,[15-17] argon,[18] cyclohexane,[19,20] benzene[21] and water.[22] In these cases the gas adsorption was used to characterise the MCM-41 pore system, not to observe changes in the behaviour of the adsorbate.

6.1 Methane in MCM-41

The experiments investigating the behaviour of methane in MCM-41 studied the capillary melting[23,24] of the methane and the phase transitions of a molecular solid and liquid absorbed in these narrow pores. This allowed some examination of the effect of small particle size in two dimensions upon the phase behaviour of methane. These experiments were done using early MCM-41 samples with low long range order.

The mesopores can be conveniently loaded to monolayer or multilayer coverage by equilibrating the outgassed silicate with appropriate doses of methane. When methane is present its scattering completely dominates that from the host lattice, owing to the large neutron-scattering incoherent cross-section of hydrogen compared to that of the other atoms present (see Table 3.1). The rotational dynamics of adsorbed methane in both tunnelling and librational energy ranges have provided much information on two dimensional phases and phase melting in other systems.[25-27]

6.2 Quasielastic Neutron Scattering from Methane

6.2.1 Background

The sample of MCM-41 used was prepared by the method of Beck *et al.*[28] The BET surface area from nitrogen adsorption was about 1,000 $m^2\ g^{-1}$. For the neutron scattering experiments the sample was outgassed at 250˚C with pumping to 10^{-5} torr for about 12 hours. It was then heated for three hours at 350˚C at 10^{-5} torr before being transferred into the aluminium sample container under an atmosphere of pure helium. The sample was filled with methane at 760 torr, sample temperature 140 K, that is, well above the condensation temperature of liquid methane and 6.68 mmol g^{-1} of methane were taken up.

The MCM-41 sample would have been extensively dehydrated by the vacuum and high temperature treatment applied before the filling with methane. It, nevertheless, contained surface hydroxyl groups arising from incomplete condensation of the polysilicate anions involved in the synthesis process. No attempt was made in this experiment to remove these either by deuterium exchange or ammoniation. These residual hydroxyl groups were responsible for a temperature dependent intensity variation in the quasielastic scattering from the empty MCM-41 sample shown in Figure 6.1. This background was taken into account in the analysis of the methane scattering data.

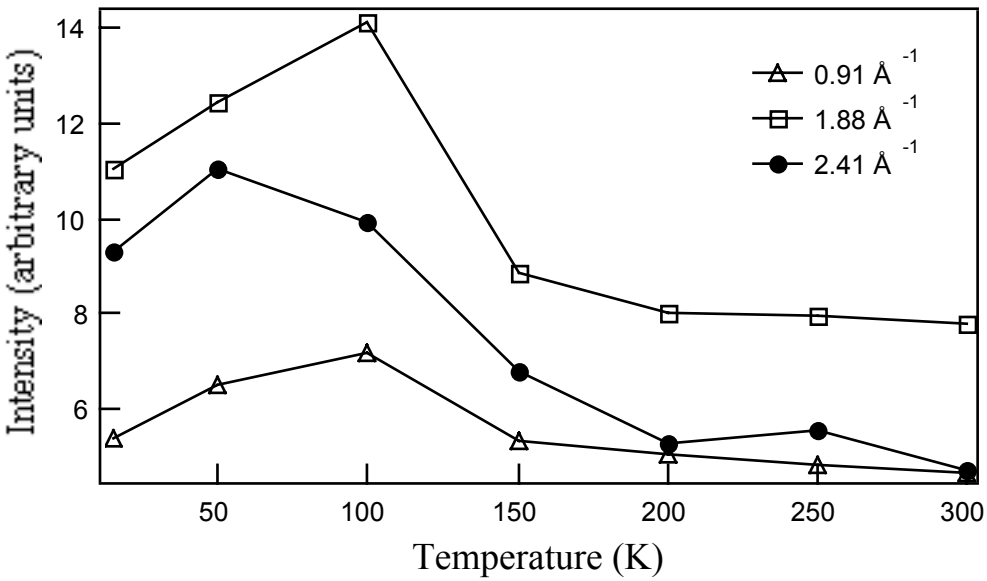

Figure 6.1 *Temperature dependence of the quasielastic scattering from the empty MCM-41 sample at several scattering angles.*

The quasielastic scattering was measured on the QENS instrument at the Intense Pulsed Neutron Source described in Chapter 3. There were clear changes in the elastic scattering intensity and the momentum transfer (Q) dependence of the quasielastic broadening with temperature between 15 and 180 K. These show that a modified phase behaviour for the adsorbed methane has arisen from the confinement in the channel system. Neutron scattering experiments on the outgassed MCM-41 from 15 to 300 K, were also carried out to ensure that any inelastic scattering from the siloxyl groups was accounted for, and also to define the elastic resolution function of the instrument. The resolution was found to be about 80 microelectron volts* over a momentum transfer, Q, range of $0.3 < Q < 2.6$ Å^{-1}. The resolution of the instrument did not allow clear observation of excitations below *ca* 100 microelectron volts (μeV) and no definite conclusions could be made on the existence of tunnelling. Data from bulk methane were taken with the same apparatus in a subsequent experiment as a control.

The quasielastic scattering functions from methane-filled MCM-41 such as that shown in Figure 6.2, were fitted with a delta function and the minimum number of Lorentzian components by a least squares method. Usually only one Lorentzian was required. The intensities of the Lorentzian and delta function components of the quasielastic peak were used to determine the elastic incoherent structure factors, EISF.[29] In addition, the energy widths of the Lorentzian components were determined.

* *Note: 1eV = 8068 cm^{-1}.*

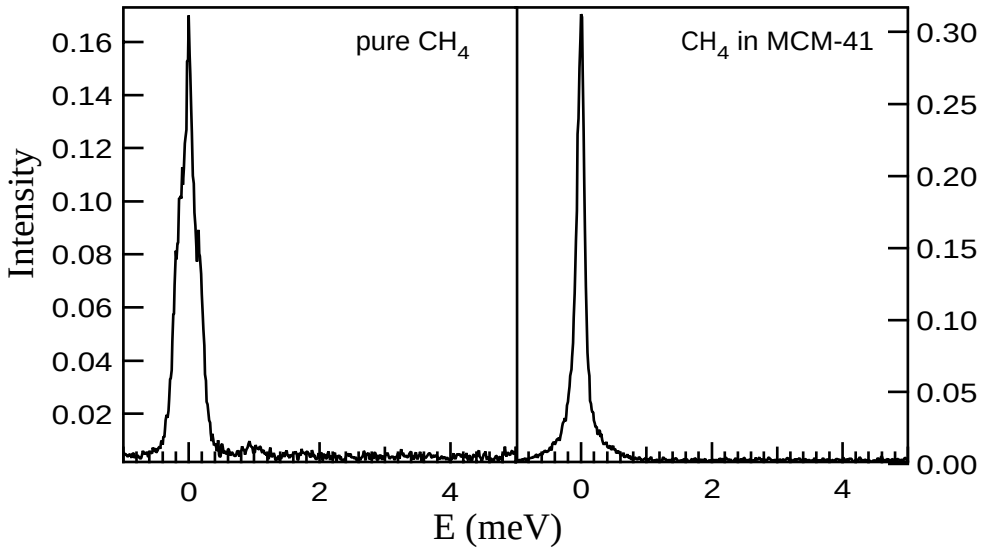

Figure 6.2 *Quasielastic scattering spectra for bulk methane at 15 K, Q = 2.41 Å^{-1} and for MCM-41 filled with 6.68 mmol g^{-1} of methane at the same temperature and scattering angle.*

In bulk methane, the face centred cubic solid structure is in an orientationally disordered plastic phase in the region below its melting point, down to T_c=20.4 K, where it undergoes a transition into the partially ordered structure of CH_4-II.[30,31] In this phase 75% of the molecules are orientationally ordered and librate about the minima of a strong anisotropic potential, while the other 25% are orientationally disordered. In the spectra of CH_4-II tunnelling peaks are expected at 75 μeV and 145 μeV, while a higher energy excitation, due to the almost free rotation of the disordered methane molecules, occurs at 1.07 meV.[31-33] In Figure 6.2 above the spectra collected for pure CH_4 at 15 K and Q = 2.41 Å^{-1} is shown. The peak at 1.07 meV can be seen, but the tunnelling lines are visible only as a distortion of the quasielastic peak centred around zero energy transfer, since the resolution is not sufficient to distinguish them at this temperature.

6.2.2 Results

The "window method" in quasielastic neutron scattering is a sensitive method of detecting transitions involving distinct changes in hydrogen motion, such as from rigid to rotator phase solids, as well as liquefaction. Figure 6.3 shows the temperature dependence of the quasielastic scattering intensity within the 80 μeV resolution "window" of the spectrometer for three different angles of scattering. The intensity drops each time the energy breadth of a newly activated dynamical process extends outside the "window". Here, it falls strongly between 60 and 120 K, indicating the onset of some new dynamic process in that temperature range. This phase transition might be relatively broad, but more experiments with higher resolution and a finer grid of temperatures would be needed to ascertain the degree to which the transition in this system has become continuous.

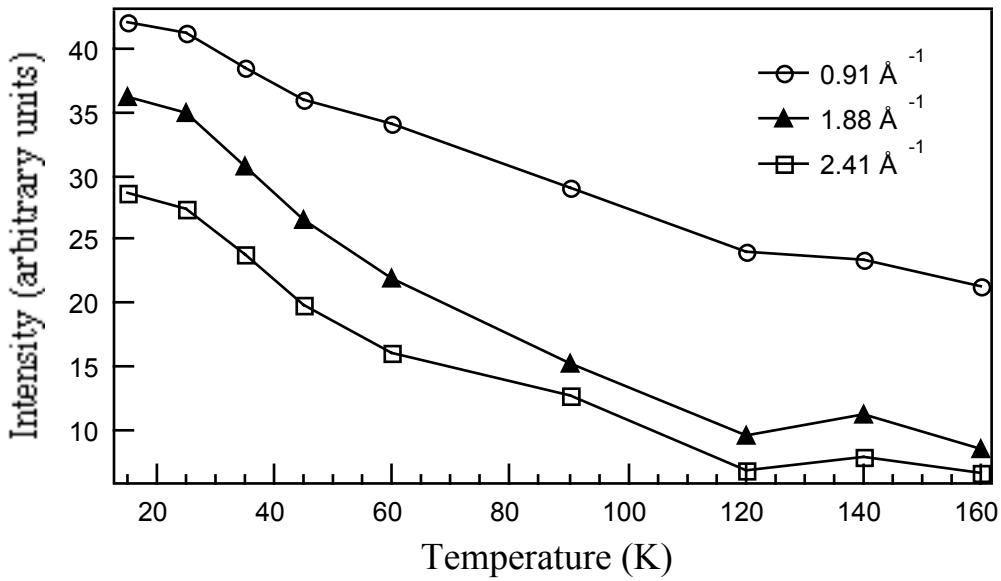

Figure 6.3 *Temperature dependence of the quasielastic scattering intensity at zero energy transfer for 6.68 mmol g^{-1} of methane in MCM-41, observed at various Q values.*

Figure 6.3 also shows that there is also a strong dependence of the total intensity on momentum transfer. This suggests that diffusion is associated with the transition observed in the intensity changes shown there. Vibration alone is unlikely to involve the large amplitude hydrogen motion that such a strong Q dependence implies. The momentum transfer dependence of the quasielastic broadening at various temperatures allows the transition seen by the "window method" to be assigned to diffusion. The melting point for bulk methane has been measured to be 91 K.[34] A reasonable inference, is therefore that the transition observed between 60 and 120 K is from rotational to translational diffusion. The elastic incoherent structure factors as a function of temperature, a more revealing observable, have been analysed and are shown in Figure 6.4.

From Figure 6.4 it is clear that the behaviour of the methane molecules in the MCM-41 channels is much the same for temperatures between 15 and 60 K. The slight increase in the EISF with increasing temperature is opposite to that observed in other systems. In those cases, a decrease in the EISF with increasing temperature was ascribed to jump rotational diffusion between inequivalent sites.[35,36] The small change seen here may be within the error of the measurements. However, there is also clearly a larger change in the methane behaviour which occurs between 60 and 90 K. The EISF decreases as the temperature increases, and the slope of the plot become much less. Large decreases in the EISF with temperature for water adsorbed in anionic clays have been assigned to the onset of haphazard large-scale movement of the water molecules.[36] Similar motions may be occurring here. The change in shape indicates a change from rotational diffusion to translational diffusion, for at least some of the molecules. By 160 K it can be seen that the shape of the EISF has completely changed. By this temperature, 50 K above the melting point of bulk methane at 112 K, most of the molecules in the MCM-41 channels would be undergoing translational diffusion.

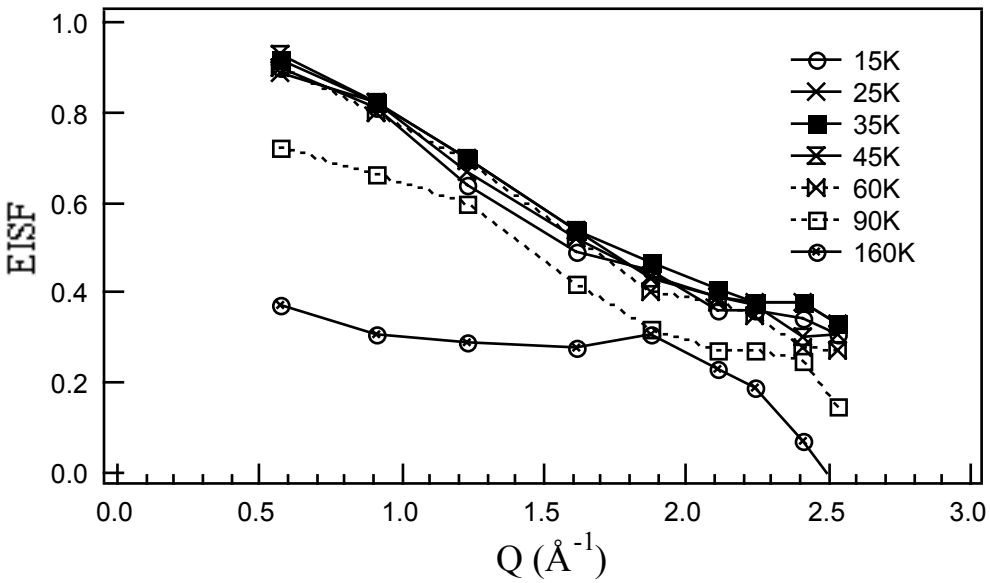

Figure 6.4 *Elastic incoherent structure factors for 6.68 mmol g^{-1} methane in MCM-41 at various temperatures.*

The EISF may also give further information concerning the type of rotational motion occurring at the lower temperatures through modelling of the fall-off with Q. Figure 6.5 below shows several models from the literature compared with the data taken at 15 K. The first model, isotropic rotation of the methane hydrogens on the surface of a sphere, has been found previously to describe the motion of methane in silicalite at 300 K.[37] The radius of the sphere was taken to be the C-H bond length in methane, 1.09 Å. The expected value of the EISF for such motion is then:

$$EISF = j_0^2 (Q.r) \qquad \textbf{(6.1)}$$

where $j_0^2(Qr)$ is the zeroth order spherical Bessel function, and r is the radius of the sphere. This curve is shown in Figure 6.5 labelled as "isotropic."

The second model corresponds to jump diffusion of the methane hydrogens between two sites on a circle, 180° apart, in a powder sample with no favoured orientations.[38] It has been used to describe cases where a nucleus flips from side to side. The equation for this motion is:

$$EISF = \tfrac{1}{2} + \tfrac{1}{2}\frac{\sin(2Qr)}{2Qr} \qquad \textbf{(6.2)}$$

In this case 2r is the distance between the two sites is taken to have the same value as for equation 6.1 above. The resulting curve is plotted in Figure 6.5 as "2 sites."

The final model assumes a situation where some (65%) of the methane molecules are fixed, undergoing no rotational diffusion, but 35% are rotating isotropically. The EISF for this case is given by:

$$EISF = 0.39 + 0.65 j_0^2(Qr) \qquad \textbf{(6.3)}$$

The curve is plotted in Figure 6.5 as "39% static, 61% mobile."

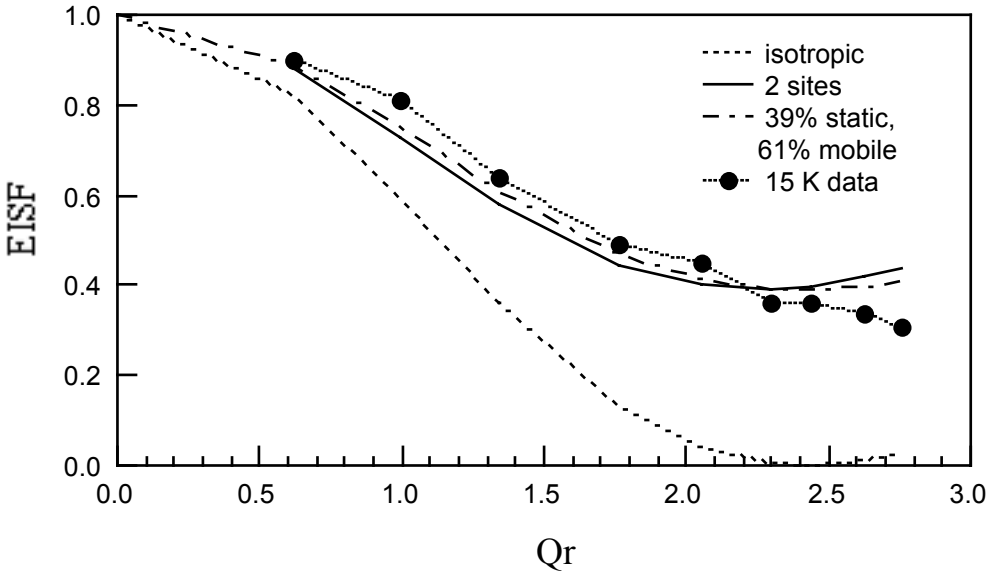

Figure 6.5 *The EISF for various models of rotational diffusion - isotropic motion on the surface of a sphere, jump diffusion between two sites 180˚ apart and a combination of static and rotationally active molecules. The experimental EISF measured at 15 K is shown for comparison.*

From Figure 6.5 it can be seen that the isotropic rotation model does not compare well with the data. The jump model over two sites is a reasonable fit to the observed EISF at 15 K, but the combination of static and rotationally active molecules is a slightly better fit. It is difficult to imaging why a rotating methane molecule might have two preferential sites for jump transitions. A three-site jump rotation model falls between the two-site model and the unhindered isotropic rotation model and so is clearly not a good description of the data. A combination of some molecules which are strongly hindered near the walls of the mesopore, together with isotropically rotating molecules located further from the walls seems more likely. This is similar to the case in crystalline Phase II methane, where one molecule per unit cell rotates freely while the others are fixed.[33] The greater disorder in the present system is likely to allow a greater proportion of "free" molecules on one hand, although strong interactions with the walls are likely to cause static molecules to be present in this system to much higher temperatures than in bulk methane. Much more complex modelling would be required in order to determine the exact nature of the rotational diffusion in this system and it is not pursued further in this work. The models for rotational diffusion are all temperature independent, and so do not give any further information concerning the experimentally observed temperature dependence of the EISF.

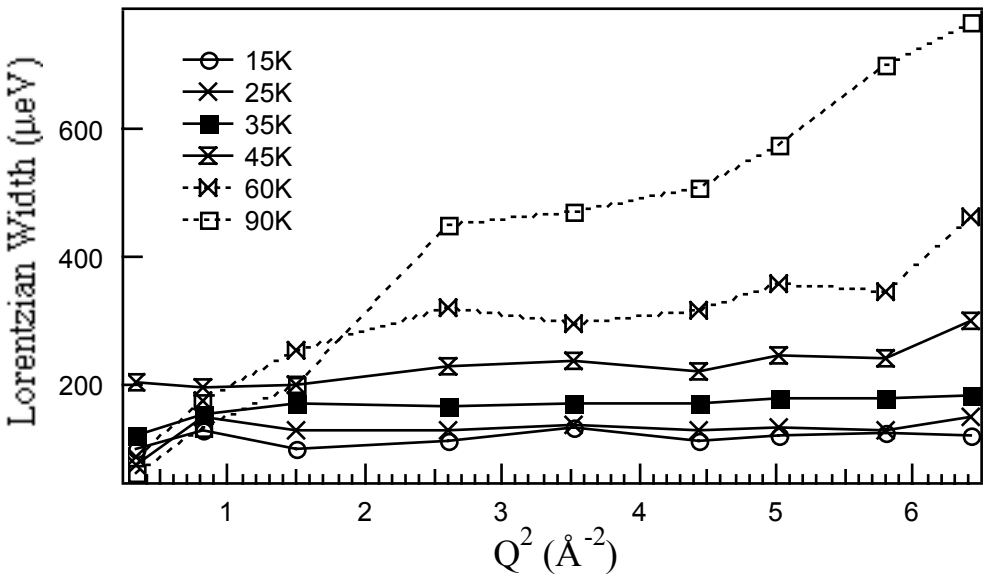

Figure 6.6 *Momentum transfer dependence of the Lorentzian width of the quasielastic scattering from 6.68 mmol g^{-1} of methane adsorbed in MCM-41 at different temperatures.*

Figure 6.6 shows the Q-dependence of the width of the Lorentzian component as a function of temperature. At low temperatures ($15 < T < 45$ K) the Lorentzian width increases slowly with temperature but is essentially independent of Q. These almost Q-independent Lorentzian widths, or more strictly, bounded hydrogen diffusive motions, at low temperatures are characteristic of rotational diffusion of the molecule. An Arrhenius plot, shown in Figure 6.7, of the temperature dependence of these widths gives an Arrhenius law for the correlation time for isotropic rotational diffusion for the temperature region $15 < T < 45$ K of $\tau = 1.5(3)\times10^{-11}$ exp(0.13(4)/RT) sec. The activation energy of 0.13(4) kJ mol^{-1} is, of course, smaller than normally seen for larger molecules.

The rotational activation energy for methane on a graphite caesium intercalate compound ($C_{28}Cs(CH_4)$) was found to be 1.1 kJ mol^{-1} for data in the range 50-160 K[39] which is somewhat higher than observed here. This indicates a greater interaction between the methane and the substrate than exists in the methane-MCM-41 system. Rotational diffusion coefficients for methane in NaY zeolite at 100 K[40] and for methane in ZSM-5 at 200 K[41] have been found to be 4.5×10^{10} s^{-1} and $2.5\text{-}4.2\times10^{10}$ s^{-1} (dependent upon methane loading in the pores) respectively. The values of the rotational diffusion constant in these silicate and aluminosilicate systems are lower than the values obtained for methane adsorbed on graphite (6×10^{11} s^{-1} at 55 K)[42] or in bulk solid methane (10^{12} s^{-1} at 21 K)[43] indicating slower rotation due to interactions of the molecule with the framework. The value of the rotational diffusion constant for methane on MCM-41 of 7×10^{10} s^{-1}, indicates somewhat less hindering of the methane rotation than is observed in the other zeolites.

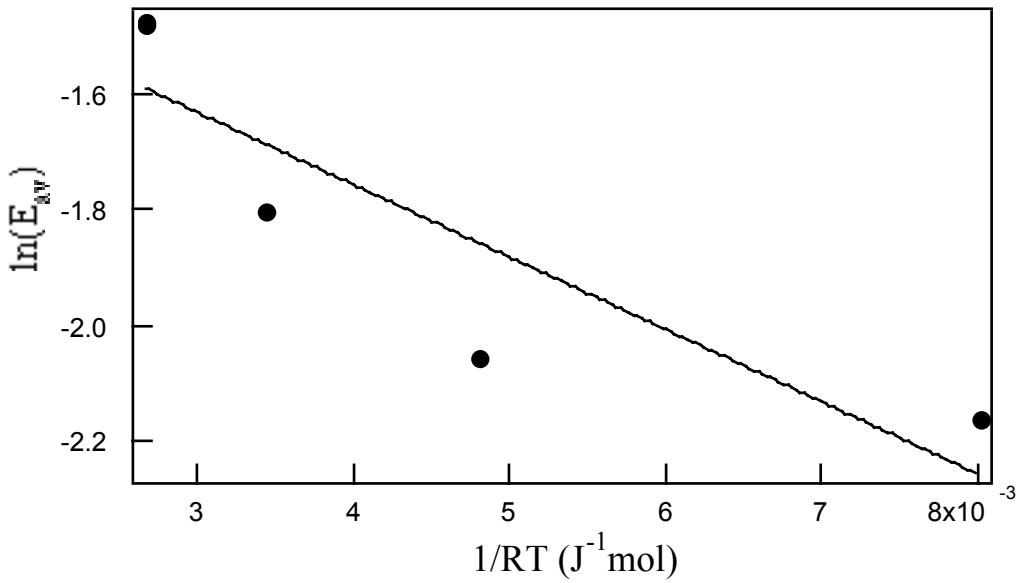

Figure 6.7 *Arrhenius plot of the temperature dependence of the width of the quasielastic scattering for temperatures between 15 and 45 K.*

Above 45 K a strong Q dependence with an approximately Q^2 dependence is observed for the energy widths of the Lorentzian component. This is characteristic of unconfined translational diffusion. Although the statistics are relatively poor this behaviour persists at higher temperatures and there appears to be a component behaving according to this scattering law up to 180 K. The slope of the curves at 60 K and 6.68 mmol g^{-1} in Figure 6.6 imply diffusion constants for long-range translational motion of $4.5(8)\times10^{-6}$ cm^2 s^{-1} and $11.1(8)\times10^{-6}$ cm^2 s^{-1} compared with that of 2.7×10^{-6} cm^2 s^{-1} at the triple point of pure methane at 191 K.[44]

The diffusion constants for all temperatures above 45 K are plotted as a function of inverse temperature in Figure 6.8. For comparison the diffusion constants for methane in various other porous systems at a range of temperatures are also plotted in Figure 6.8. The values were taken from a number of sources, and were measured by QENS,[40,41,45,46] pulsed field gradient nmr[45-48] and through molecular dynamics simulations.[48-50] The translational diffusion constants for MCM-41 appear to be comparable to those for diffusion of methane in silicalite and NaY zeolite for temperatures where the measurements coincide with those for MCM-41.

Given the values at higher temperatures for methane diffusion in the silicalite and NaY systems shown in Figure 6.8, the slope of a plot of diffusion constants with inverse temperature will be quite different from that found for MCM-41. They have a greater slope and thus will have a higher activation energy. From Figure 6.8 the Arrhenius law for the long-range translational diffusion of methane in MCM-41 channels can be derived: $D = 4(2)\times10^{-5} \exp(-1.2(3)/RT)$ cm^2 s^{-1}. The activation energy observed here, 1.2(3) kJ mol^{-1}, is smaller those observed in the other zeolitic systems for which diffusion constants were plotted in Figure 6.7. For methane in ZSM-5, activation energies of 4-5 kJ mol^{-1} were found in the temperature range 200-250 K using both QENS and pulsed field gradient nmr.[46] In silicalite the activation energy for methane translational motions calculated from similar experimental data was 3.9 kJ mol^{-1}.[45] For

methane in NaY zeolite between 100 and 250 K an activation energy of 6.3 kJ mol^{-1} was also found using QENS and pulsed field gradient nmr results.[40] The slightly lower activation energy for translation in MCM-41 may be due to the large amount of empty channel space in the structure, and lack of restrictive cage sites as well as low methane-wall interactions.

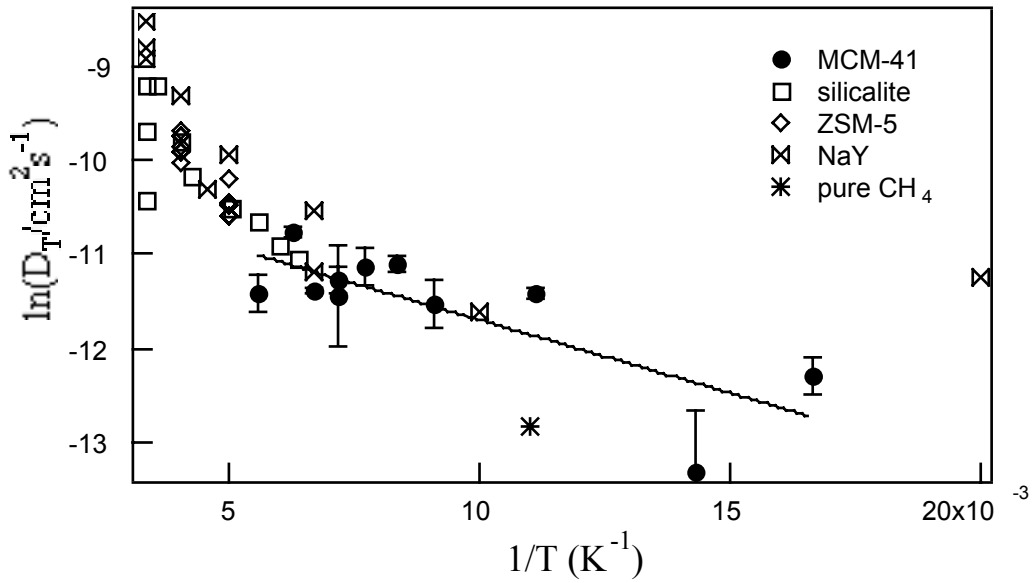

Figure 6.8 *Diffusion constants of methane in MCM-41 pores for temperatures above 45 K compared to values for the diffusion constant of methane in another pure silica system, silicalite,*[45,48] *in aluminosilicate zeolites, ZSM-5*[41,46] *and NaY*[40,47,49,50] *and in bulk methane at 191 K.*[44] *The solid line is a least squares fit to the MCM-41 data.*

It can be concluded that methane diffusion in MCM-41 has a slightly larger rotational diffusion constant and a smaller activation energy for translation than in other, more restrictive zeolite cage materials. The diffusion constants and activation energies are, however, in the expected range, which is quite different to that of pure methane.

6.3 Inelastic Scattering from Methane

The experiment using the machine QENS described above also collected data for methane on MCM-41 in the inelastic scattering region which can be compared to inelastic scattering measurements on bulk methane.

Solid methane II at low temperatures has well developed rotational tunnelling excitations and at 15 K a clear librational excitation at *ca.* 1 millielectron volt.[51] This was verified in the control series of experiments on QENS with bulk methane, but no trace of it was found in the near inelastic region for methane in MCM-41. Figure 6.9 shows the energy transfer region $0 < \delta E < 120$ millielectron volts from MCM-41 containing methane at temperatures between 15 K and 140 K. The inelastic scattering signal is about 100 times weaker than the scattering from the quasielastic region but is persistent. Even at 180 K, where the adsorption isotherm shows there is still plenty of methane present, there is a strong scattering signal of approximately the same intensity as at lower temperatures. For comparison the very weak scattering from empty MCM-

41 is shown. The inelastic scattering is likely to be due to the recoil spectrum for methane within the MCM-41 channels.

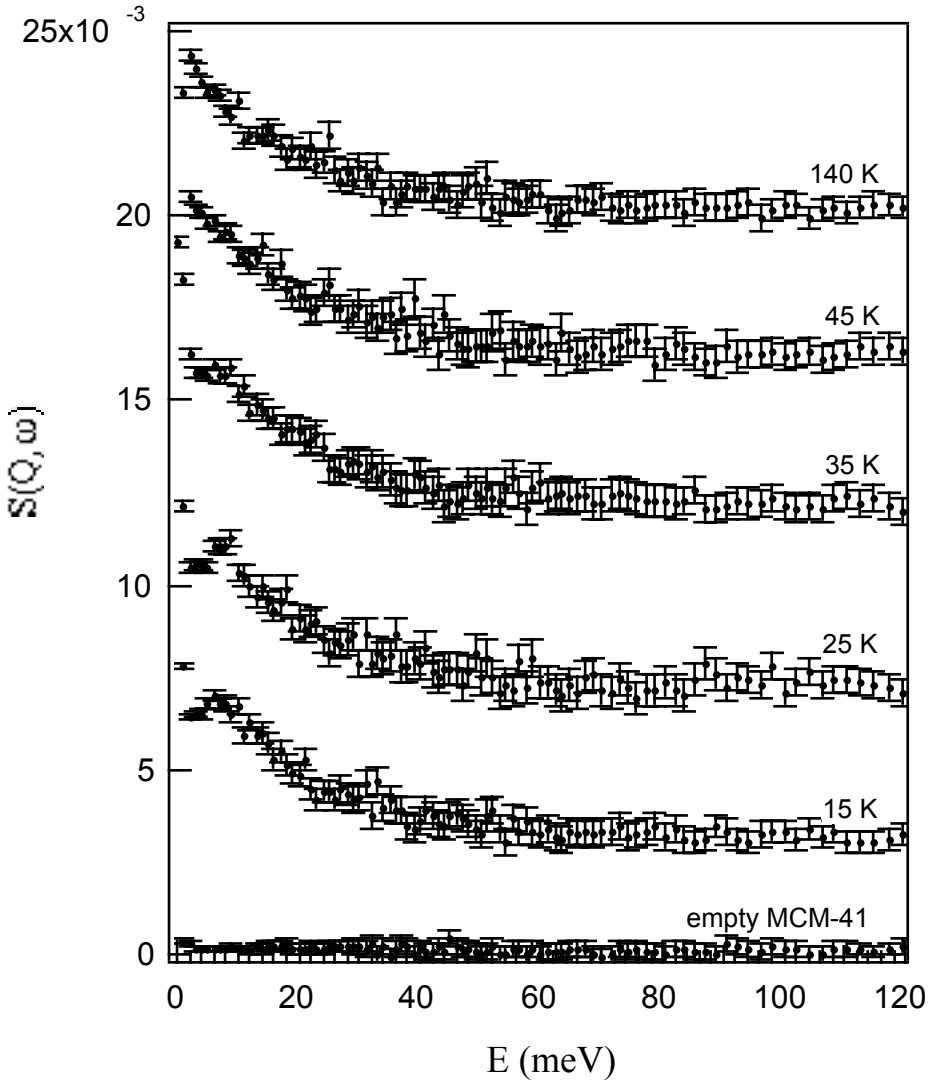

Figure 6.9 *Inelastic scattering from 6.68 mmol g^{-1} of methane adsorbed on MCM-41 at various temperatures, compared to an empty MCM-41 sample at 15 K.*

6.4 Methane Adsorption Isotherms

The adsorption isotherm of methane at 77 K on MCM-41 closely resembles that for nitrogen.[17] Figure 6.10 shows typical comparable isotherms, in this case for material of much improved long range order,[52] following the method of Ryoo and Kim.[53] Surface areas were calculated using molecular areas of 16 Å^2 per molecule for nitrogen[54] and 14.2 Å^2 for methane.[55] The BET surface area available to methane for this material was 760 m^2 g^{-1} while the nitrogen BET surface area was 1160 m^2 g^{-1}.

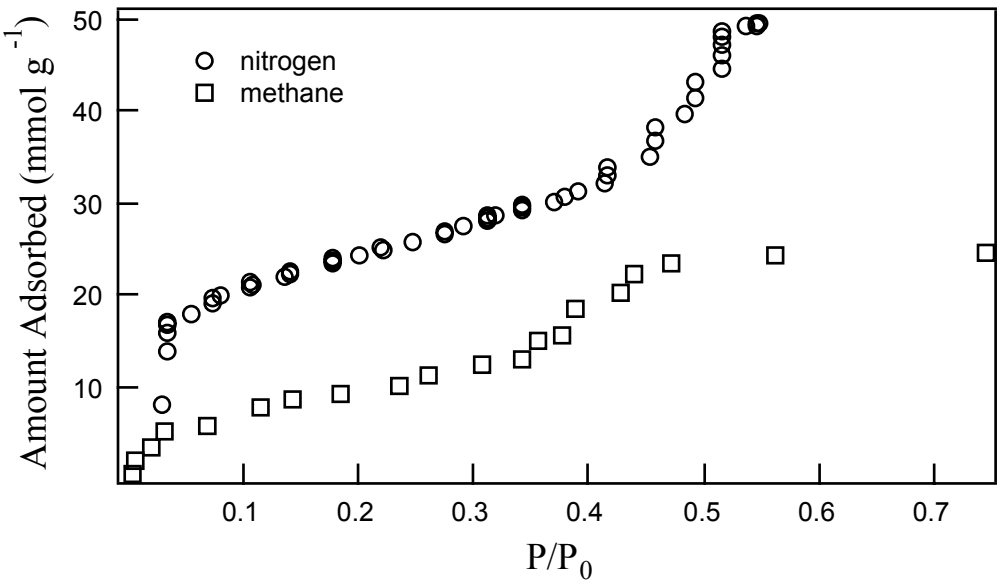

Figure 6.10 *Adsorption isotherms for methane and nitrogen on an MCM-41 sample with high long range order.*

6.5 Discussion

The absence of librational or rotational excitations in methane-filled MCM 41 at energy transfers between about 200 microelectron volts and 10 millielectron volts would not be surprising for temperatures above 25 K, since they are strongly damped in this range of temperature even for solid methane II. The spectra for bulk methane shown in Figure 6.1 at 15 K shows at least the first rotational transition at 1.07 meV although it is not very intense, and although the tunnelling lines cannot be distinguished from the quasielastic peak at this temperature, the peak is broadened and distorted by them. Similar features were, however, not apparent in the methane-filled MCM-41 at the same temperature.

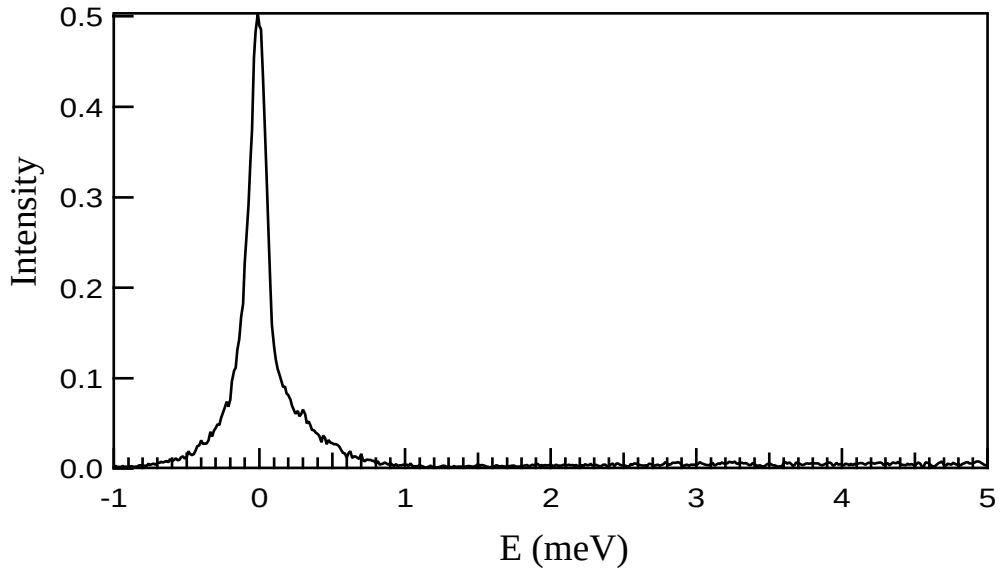

Figure 6.11 *MCM-41 filled with 12.5 mmol g^{-1} of methane at 1.5 K and Q = 2.41 $Å^{-1}$.*

That no clear librations were seen in the experiments for methane adsorbed on MCM-41 even at 1.5 K suggests a distribution of librational and tunnelling states rather than a single well defined set of such excitations. The spectrum for methane filled MCM-41 at 1.5 K is shown in Figure 6.11 below. This points to the incorporated methane being in a glassy or partly ordered state at low temperatures. One explanation is that there is a distribution of packing density from the walls to the core of the tubes, if indeed the tubes are as relatively uniform as the isotherms and other workers have suggested. It may also be explained by having methane adsorbed on a multiplicity of wall sites with different potentials in a highly divided silica matrix.

With these hypotheses in mind the changes seen in the neutron quasielastic peak intensity with temperature between $60 < T < 120$ K (Figure 6.3) can be associated with a melting transition. Some degree of rotational freedom for at least some of the molecules is allowed at lower temperatures. Between 15 and 60 K it appears that around 40% of the methane molecules are stationary, while 60% are undergoing isotropic rotation. It seems logical to conclude that the stationary molecules occupy wall sites, while the mobile ones are contained in the pore region. The proportion of static to mobile molecules is about 1:2. This is similar to the proportions of hindered and unhindered hydrogen adsorbed in MCM-41, which were observed in the experiments described below. A similar situation also exists in crystalline Phase II methane where only one molecule per unit cell is allowed to rotate but here, due to the lack of translational symmetry, the description is less precise. In a model having low density, porous silica walls, an increasing degree of rotational freedom, observed in the increasing Lorentzian widths, with increasing temperature is consistent with molecules in the free pore region becoming active while those nearer the walls experience more hindrance to motion. The drop in intensity between 60 and 120 K would occur where the molecules in wall sites begin to desorb. This model is complex as three types of methane could potentially be present at a single temperature - highly restricted or stationary methane on wall sites, methane with some rotational freedom in pores in the walls, and freely translating methane in the central, empty channel.

As the temperature dependence of the EISF shows, there is a solid to liquid phase transition for at least part of the sample between 60 and 90 K. That it is only some of the methane molecules is suggested by the further evolution of the EISF. Between these temperatures, the EISF shown in Figure 6.4 changes shape, at the higher temperature decreasing continuously but less sharply in the experimental Q region, starting from 0.7 at 0.57 $Å^{-1}$ reaching 0.2 at 2.53 $Å^{-1}$. This suggests that there is still some solid, rotationally active methane present, but that the remainder is now translationally diffusing. As the temperature increases further, the EISF continues to become flatter. Although the interpretation of the EISF when the quasielastic scattering contains both translational and rotational diffusion components in the Lorentzians is more difficult, it is only safe to conclude that above approximately 60 K there is a form of fluid methane present in the MCM-41 cylindrical tubes. This represents a depression of the melting point for this component of nearly 30 K from the bulk value of 91 K. The Lorentzian width data also suggest that at 120 K there is still a well defined fluid component, and so there may also be an elevation of the boiling point from the bulk value of 112 K.[34]

Lastly the results show persistent scattering between 0 and approximately 40 millielectron volts for all samples containing methane at temperatures between 15 K and 140 K. This scattering, shown in Figure 6.9, is probably due to the recoil spectrum of methane within the pores. Even at 140 K there is almost no diminution of the extrapolated limiting intensity at zero energy transfer compared to the data at 15 K or 25 K. The scattering is unlikely to contain enhancement of the empty MCM-41 lattice modes but may involve some interaction between highly dendritic silica and the methane molecules. A more detailed interpretation would require further work over a wide range of momentum transfers.

6.6 Hydrogen in MCM-41

The work on hydrogen adsorbed in MCM-41 covers both inelastic neutron scattering and a detailed analysis of hydrogen adsorption isotherms, compared to those of nitrogen in the same MCM-41 sample. Adsorbed hydrogen is a probe of the tube structure, and, in the fine state of division produced by the tubes, is itself currently of interest.[1,56,57] Hydrogen doped into MCM-41 was examined and data on the dynamics of the adsorbed molecule from inelastic neutron scattering measurements on hydrogen adsorbed into MCM-41 at various temperatures and dopings is reported below.

6.7 Quasielastic & Inelastic Neutron Scattering From Hydrogen

A highly ordered form of MCM-41[52] showing seven orders of the in-plane hexagonal synchrotron X-ray diffraction pattern was used as the substrate (see Figure 5.1 in the previous Chapter). Prior to any experiments, the material was outgassed at 250˚C under a pressure of 10^{-4} torr at 350˚C for two days to remove any residual water in the mesopores. A small quantity of residual hydroxyl groups arising from incomplete siloxyl condensations in the synthesis remained as the only hydrogenous material in the substrate. To remove these, the calcined MCM-41 material was soaked in D_2O to exchange the hydrogen for deuterium. Although the experiment involved doping this deuterium-exchanged material with hydrogen gas, further exchange of the deuterium was unlikely because the low temperature experimental conditions and lack of catalytic material ensured stability of the dihydrogen molecules to both spin conversion (so that spin equilibrium was never reached) and exchange. The sample, weighing 1.10(5) g, was transferred to an aluminium sample can mounted in a cryostat capable of reaching 1.5 K. Hydrogen gas was admitted to the sample in volumetrically determined amounts with an accuracy of *ca.* 2% in volumes, and 2 torr in pressure, which is 0.2% of the highest pressures used.

The quasielastic neutron scattering spectrometer, QENS, at the Intense Pulsed Neutron Source, Argonne National Laboratory (described in Chapter 3) was used for the inelastic neutron scattering experiments. A series of spectra at 1.9 K were taken with hydrogen loadings of 0, 9.5, 12.1, 21.5, 34.5 and 40.3 mmol g^{-1}. Higher temperature spectra were also obtained at 9.8 K (34.5 mmol g^{-1}), 13.3 K (37.7 mmol g^{-1}), 14.7 K (33.1, 40.3 mmol g^{-1}), and 21 K (23.1 mmol g^{-1}). A spectrum is shown in Figure 6.12.

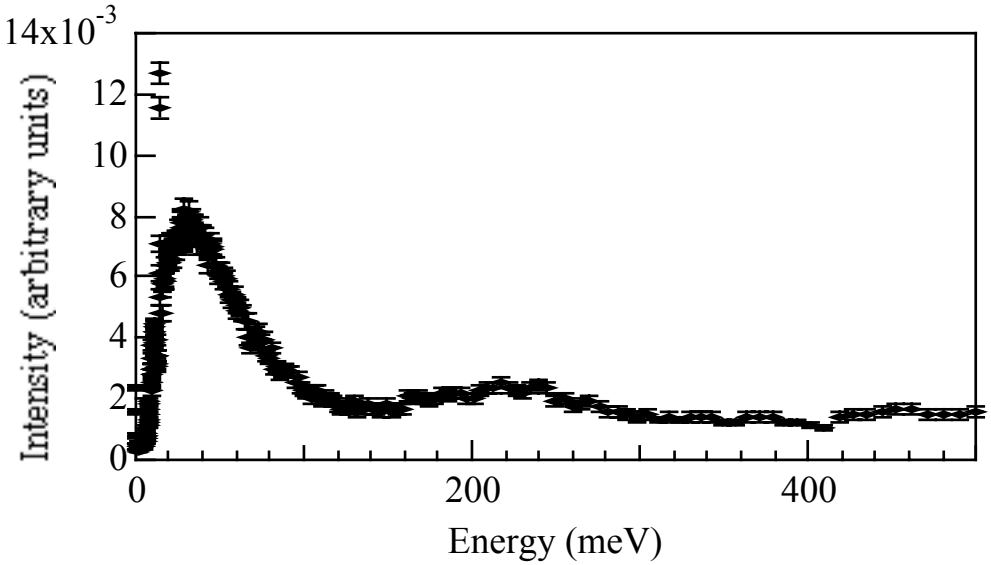

Figure 6.12 *Inelastic neutron scattering from 40.3 mmol g^{-1} hydrogen adsorbed on highly ordered MCM-41 at 1.9 K.*

6.7.1 Results and Discussion

In the experiment discussed in above, the dynamics of methane between 1.5 K and 200 K in filled pores was studied. It was found that this confinement of methane strongly suppresses the normally observable librational excitations of free methane II. It is plausible that the hydrogen case may be the opposite to that of methane. For hydrogen, the high rotational constant and weak interactions may allow observation of molecular rotational dynamics which are modified by the confinement, rather than suppressed. The molecular rotational constant for hydrogen, B = 85.25 K or 7.35 millielectronvolts (meV), is very much greater than the intermolecular potential from the interactions between the molecules in the solid state.

Previous work has shown that hydrogen molecules adsorbed by intercalation compounds[58,59] have rotational tunnelling excitations between about 0.2 and 2 meV while hydrogen at the graphite surface has only weakly hindered rotations at about 12 meV[60] which is comparable to the $J = 0 \rightarrow 1$ transition between free rotor states, at an energy of 14.7 meV. For the intercalates, well defined librational excitations have been observed at energies between 10 meV and 40meV and, even at low temperatures, there is a broad underlying continuum from the molecular recoil scattering.[56] Porous vycor glass (96% SiO_2, 3% B_2O_3[34]) having a nominal pore radius 35 Å filled with *para*-dihydrogen has a strong peak in the inelastic scattering at 14.7 meV and a broad spectrum of scattering present from 15 to 25 meV in measurements taken at 2 and 14 K.[61] The strong peak indicates that the hydrogen is freely rotating within the pores at these temperatures, while the broad band of scattering represents the collective excitations of the liquid or solid phase shifted by the rotational transition. Liquid hydrogen, causing broadening of the quasielastic scattering peak, is present in the vycor pores at 14 K, although not at 2 K. The hydrogen was observed to freeze at 10 K into a solid, unlike bulk solid hydrogen, which freezes around 14 K.

There is no measurable energy broadening of the elastic peak for hydrogen on MCM-41, at any of the observed fillings and temperatures. An upper limit to the broadening is 0.1 meV at a Q of 2.41 $Å^{-1}$, even for the data at 21 K on partially filled samples, or at 14.7 K on fully filled (see section 6.8 for discussion of hydrogen isotherm data). This is far smaller than arises from diffusion in fluid hydrogen,[62] or in vycor pores,[61] indicating that the hydrogen in MCM-41 is much more translationally confined than that in the free fluid or in vycor pores of similar dimensions.

The major feature of the inelastic scattering in the spectrum is a broadly structured continuum to the highest energy transfers measured (Figure 6.12). The first features are relatively sharp peaks at 11.8(2) and 14.7(3) meV (see Figure 6.13 for detail) which can be assigned to $J = 0 \rightarrow 1$ rotational transitions of two types of hydrogen molecules. Above the sharp $J = 0 \rightarrow 1$ peaks the spectrum has a broad peak at 20-30 meV, and further broader, weaker peaks at 180-220 and 400-500 meV. The quoted range reflects not uncertainty in the peak positions, but their variation with scattering angle. The intensity of this continuous spectrum is proportional to the total loading, and thus all hydrogen, both unhindered and weakly hindered contributes to it. Such continuous spectra have been observed in other systems containing hydrogen molecules and hydrogen atoms.[57,58,61,63] They arise from the molecular form factor and the recoil of the hydrogen molecule in the scattering collision which broadens the rotational transitions and allow the effective mass of the scatterer and its mean kinetic energy to be determined. The theoretical result for liquid hydrogen predicts just such a spectrum, with peaks in the observed positions, which, as observed are slightly Q dependent.[64] However a more extensive net of parameters in energy-momentum space would be required to extract reliable values for the dynamical parameters.[56,57]

The $J = 0 \rightarrow 1$ transitions can be used as a probe of the environments of the hydrogen molecules, independent of a calculation of the whole inelastic spectrum. Figure 6.13a(ii) shows the neutron inelastic scattering from the hydrogen in the 21.5 mmol g^{-1} loaded system (where the pores are roughly half filled) at 1.9 K for energy transfers between 0 and 20 meV. The distribution peaks at about 11.8(2) meV which suggests, as with H_2 on graphite, that some of the adsorbed hydrogen is weakly hindered in its rotation. In addition there is a weak peak at 14.7(3) meV characteristic of rotationally unhindered H_2 molecules.[61,65] At higher loadings the intensity of this unhindered peak grows rapidly (Figure 6.13a(i) 40.3 mmol g^{-1} loading). A plot of the intensity of the 14.7 meV peak is linear with loading, but intercepts the zero intensity at a finite loading of 19.7 mmol g^{-1}. The 11.8(2) meV peak is distinctly broader than that at 14.7(3) meV indicating more dispersion in the former sites.

It can be concluded that there are two types of hydrogen present, a weakly rotationally hindered type, in a variety of sites, whose amount can reach 20 mmol g^{-1}; and up to a further 20 mmol g^{-1} of an unhindered species which is adsorbed subsequently. It is natural to assign these to a surface adsorbed species and a bulk-like species. The linearity of the plot of the 14.7 meV peak intensity versus filling indicates that this division into two species is a good model. If there were a continuum of species types then curvature in this plot would be expected.

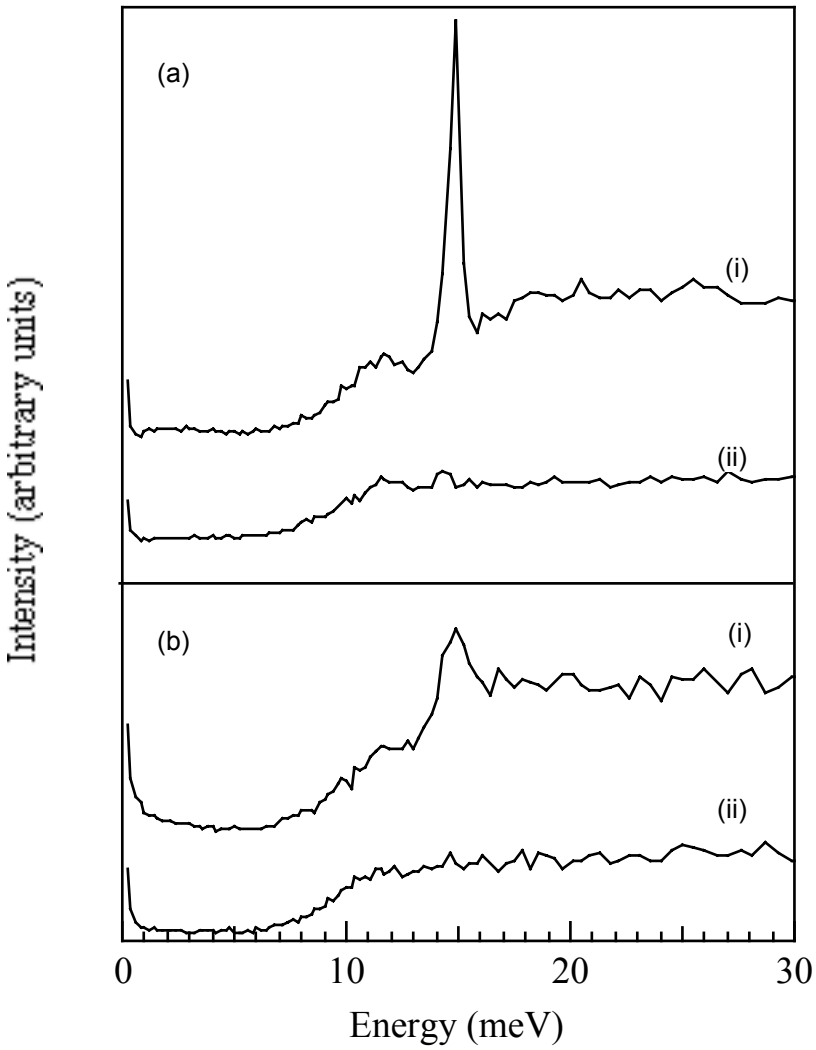

Figure 6.13 *Inelastic neutron scattering from H_2 adsorbed onto MCM-41, 0-30 meV. (a)(i) 40.3 and (ii) 21.5 mmol g^{-1} at 1.9 K; (b)(i) 37.7 mmol g^{-1} at 13.3 K and (ii) 23.1 mmol g^{-1} at 21 K.*

Two species of molecules adsorbed in MCM-41 channels are also seen in ^{1}H NMR experiments on water adsorbed on MCM-41.[22,66] There, three "water phases" were observed. A residual "non-freezing" water is seen at 183 K and is ascribed to silanol groups on the walls of the pores, as well as two phases described respectively as free water within the pores and water bound on the walls. It is likely that the sites so occupied correspond to those occupied by the hydrogen species in this work.

The 14.7 meV peak shows distinct momentum transfer and temperature dependence. Data at three scattering angles was taken, at Q = 2.14, 3.26 and 3.96 Å^{-1}. The highly loaded samples (> 33 mmol g^{-1}) at 1.9 K show a peak width of 0.45(5) meV which is independent of Q, after correction for experimental resolution. Quadrupole-quadrupole interactions, which are very sensitive to the number and distance of nearest neighbours are calculated to give a width of 0.58 meV, independent of Q, in solid, 25% *ortho*-hydrogen, molecular hydrogen.[67] Thus the width observed indicates a nearest neighbour packing of the bulk hydrogen in the pores that is very close to that observed

in the crystal, and much denser than in liquid hydrogen, in which $<1/r^5>$ is 60% of the crystal value. The intensities are given by:

$$I(Q) \propto j_1^2 \left| \frac{Qd}{2} \right| e^{-2W} \qquad \textbf{(6.4)}$$

where $j_1(Qd/2)$ is the spherical Bessel function, d is the distance between the nuclei in a molecule, and e^{-2W} is the Debye-Waller factor. After adjustment for scale factors and the form factor of a proton freely moving on a sphere of radius 0.3707 Å, the intensities therefore show a decrease with Q fitted well by a mean square translational displacement factor ($<U^2>$) of 0.55(5) Å^2. This value is marginally larger than that observed for crystalline hydrogen at 5.4 K of 0.48(3) Å^2, which is attributable to the large zero-point motion in this quantum crystal.[58,68]

This amplitude again indicates a local environment close in density to that of the solid material. At 13.3 K for the 37.7 mmol g^{-1} loading the amplitude increases to 0.7(1) Å^2, and the FWHM of the peak has increased, being 0.9(1), 1.0(1), and 1.2(1) meV at the three scattering angles (Figure 5.5b(i)). At 21 K the 14.7 meV peak is no longer apparent (Figure 5.5b(ii)). The main features are as expected - increase in temperature increases translational thermal motion from values typical of zero-point hydrogen motion, and decreases the lifetime of the rotational states.

6.8 Nitrogen and Hydrogen Adsorption Isotherms

The measurements and analysis in this section were done by Dr. Peter Branton and Dr Philip A. Reynolds. They are included here for completeness, to show the thermodynamic behaviour of the highly ordered MCM-41 materials used.

Considerable thermodynamic data can be derived from adsorption isotherm measurements on MCM-41. Hydrogen adsorption isotherms complement the neutron scattering work reported in the preceding sections, and nitrogen adsorption isotherms were investigated as a control and for comparison with published nitrogen adsorption data on less well ordered MCM-41 materials.[15,17,18,69,70]

Both adsorption and desorption isotherms with hydrogen were performed at low temperature, although, because of the thermal inertia and uncertainty about gas volumes in the sample area they are not of the highest accuracy. They are, however, valuable since they are not easily obtainable with the usual experimental equipment. A complete adsorption isotherm was measured at 21.5 K. The desorption isotherm at 21.5 K was less detailed (Figure 6.14). At 15 K an initial large dose of hydrogen was adsorbed on the MCM-41, and desorption measured in detail at this temperature. Adsorption up to *ca.* 100 torr pressure was also measured at temperatures between 31 and 61 K. Besides their intrinsic interest, these isotherms were used to verify hydrogen loadings at various stages of the neutron experiments. Errors in the temperature readings were of the order of a few tenths of a Kelvin.

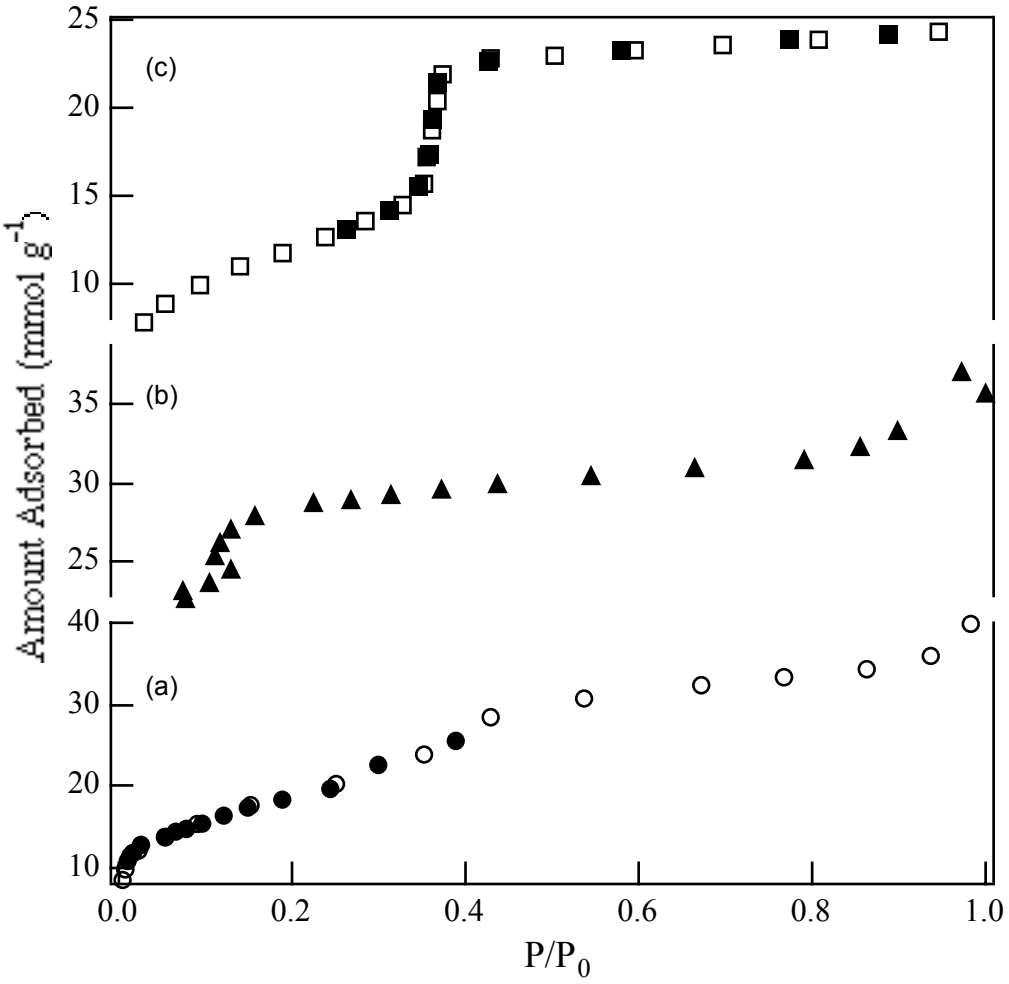

Figure 6.14 *Isotherms of H_2 on MCM-41 (a) at 21.5 K (circles) and (b) at 15.2 K (triangles), and (c) adsorption isotherm of N_2 on MCM-41 at 77K (squares), open symbols denote adsorption, filled symbols denote desorption.*

In the course of adsorption and neutron measurements some interesting thermal behaviour was noticed. For example, at a loading of 34.8 mmol g^{-1}, about 90% of fully filled, upon allowing the sample to warm to 21 K from 2 K, the H_2 vapour pressure increased smoothly and slowly, at *ca* 2 torr min^{-1}, to 48.8 torr. At this pressure, in less than a minute the pressure increased to 318 torr, and then remained relatively stable. However for 27.2 mmol g^{-1} loading, the pressure increase was slow and steady to the final equilibrium pressure at 21 K. This behaviour was observed several times - an apparently first order transition for higher loadings, but for lower loadings (at and below about 50%) this behaviour was suppressed.

6.8.1 Results and Discussion

Adsorption and desorption isotherms of hydrogen on MCM-41 at 21.5 K are shown in Figure 6.14(a), (b). Similar to the nitrogen isotherm (also measured using a volumetric technique) at 77 K and shown in Figure 6.14(c), these are of Type IV in the IUPAC classification.[71] The nitrogen isotherm is completely reversible at 77 K. For the hydrogen isotherm at 21.5 K an insufficient number of desorption points makes it

unclear whether there is small hysteresis or completely reversible capillary condensation-evaporation from the mesopores. The desorption branch at 15 K (Figure 6.14(b)) showed a point of inflection where evaporation occurs at a relative pressure, $P/P_0 = 0.12$, while the same point of inflection occurs on the 21.5 K desorption branch at *ca*. $P/P_0 = 0.4$. Hysteresis is known to be dependent on the temperature; as the critical temperature is approached, theory predicts that any hysteresis will diminish in size and shift towards higher relative pressures.[72,73] Nitrogen adsorption on MCM-41 is a good example of this phenomenon; Ravikovitch *et al*.[15] determined that for a pore spacing of 45 Å, hysteresis was observed at 70.6 K over the pressure range *ca.* 0.34-0.45, but at 77 K no hysteresis was evident and the reversible capillary condensation/evaporation occurred over the range *ca.* 0.38-0.45.

The pore diameter range in Table 6.1 has been estimated by the application of the Kelvin equation (with the usual drastic assumptions such as hemispherical meniscus, zero contact angle and bulk surface tensions) with allowance made for multilayer adsorption on the pore walls.[71,74] The derived values of 13 to 26 Å are smaller than the values derived from the nitrogen isotherm in the same way (28-35 Å), which may reflect the questionable validity of the Kelvin equation when applied to small mesopores.

Values of the BET monolayer capacity, n_m(BET) and the corresponding BET constant, c(BET) in Table 6.1 have been derived from the isotherm data in the usual manner.[71,74] The BET plot was linear over the approximate range, $0.05 < P/P_0 < 0.3$. A surface area, A(BET) of 980 $m^2\ g^{-1}$ was calculated from the BET equation on the nitrogen isotherm over the range $0.05<P/P_0<0.32$ and by assuming the molecular area, a_m, to be 16.2 $Å^2$ in the completed monolayer.[71] If this area is assumed to be the area available for the adsorption of hydrogen, the apparent molecular area, $a_m(1)$, can be calculated from the hydrogen n_m(BET) value. This value of 10.3 $Å^2$ is smaller than the corresponding value, $a_m(2)$=14.4 $Å^2$, calculated from the liquid density[34,54] (*ie*. assuming close-packing, as in the free liquid). The neutron scattering experiments, described above and in Chapter 5, support hydrogen in a solid-like state. By calculating $a_m(2)$ using the density of solid hydrogen, a value of 11.7 $Å^2$ is obtained, in much better agreement with the $a_m(1)$ value of 10.3 $Å^2$. It can thus be deduced that the hydrogen in the pores is more densely packed than in the free liquid and approaches the solid hydrogen density.

Table 6.1 *Pore characteristics from isotherm data.*

Adsorbate	T /K	n_m(BET) /mmol g^{-1}	c(BET)	$a_m(1)$ /Å^2	$a_m(2)$ /Å^2	P/P_0	d_p /Å	V_p /m^3Mg^{-1}
Nitrogen	77	10.0	118	(16.2)	16.2	0.33-0.37	28-35	0.84
Hydrogen	21.5	15.8	94	10.3	$14.4^{(l)}$ $11.7^{(s)}$	0.33-0.44	19-26	$1.02^{(l)}$ $0.75^{(s)}$

$a_m(1)$ is the cross-sectional area calculated from the nitrogen area and the individual value of n_m. $a_m(2)$ is the cross-sectional area calculated from the adsorbate density ($^{(l)}$ refers to liquid and $^{(s)}$ refers to solid hydrogen density). P/P_0 refers to the range of mesopore filling/emptying. d_p is the effective pore diameter obtained by application of the Kelvin equation with allowance made for multilayer adsorption on the pore walls. V_p is the total mesopore volume ($^{(l)}$ assuming adsorbed liquid hydrogen and $^{(s)}$ assuming adsorbed solid hydrogen).

The total mesopore volume, V_p, in Table 6.1, was obtained from the volume adsorbed at $P/P_0 = 0.95$ and assumed that the pores have been filled with condensed liquid adsorptive.[54] It was larger than the value calculated from the nitrogen isotherm. The pore volume was calculated again, assuming that the adsorbed hydrogen was in a solid-like state and, as above, gives clear evidence that the hydrogen in the mesopores has solid-like properties, again supporting the neutron scattering evidence.

Confirmation that chemisorption is not occurring is provided by calculations of the isosteric enthalpy of adsorption, q^{st}. A value significantly greater than the enthalpy of vaporisation of hydrogen, ΔH_l, (0.898 kJ mol^{-1} at 20.3 K),[54] is an indication of chemisorption. Using temperatures between 15 and 50 K, and assuming a monolayer capacity, n_m(BET) of 15.8 mmol g^{-1}, q^{st} varied from *ca*. 3.4 kJ mol^{-1} at $\theta = 0.2$, to *ca*. 1.7 kJ mol^{-1} at $\theta = 0.8$, to *ca*. 1.2 kJ mol^{-1} at $\theta = 2$ (where θ is the surface coverage). The higher q^{st} values below a monolayer surface coverage are consistent with a heterogeneous surface, which has been noted for MCM-41 by other authors.[75] The approximately constant value of q^{st} above a monolayer is only slightly above ΔH_l and thus physisorption only can be inferred.

The fact that all the void space is filled, and that at higher loadings upon warming, a first order transition, assignable to a boiling transition, is observed, suggests the possibility that the hydrogen is filling a single connected void volume. This agrees with the contrast variation SANS results from water in calcined MCM-41, discussed in Chapter 5 which show all voids filled. If different mesopores vary in properties, it might be expected that the hydrogen within them would boil, if it does, at slightly different temperatures, so that the phase transition would occur over time-scales of minutes rather than seconds. The observation suggests either that *all* the mesopores are coupled and behave collectively or the mesopores are remarkably uniform, considering the amorphous nature of the silica. By implication this suggests that there are significant void connections through the walls between different mesopores. At lower

loadings the hydrogen aggregations become disconnected and there is no single boiling point, indicating, at a minimum, that different mesopores are no longer influencing each other.

6.9 Conclusions

Methane in completely filled MCM-41 channels does not behave like bulk methane. The major component of the sample shows isotropic rotational diffusion of some of the methane between 15 and 60 K, although around 40% of the molecules are stationary at these temperatures. This is followed by a liquefaction transition above 60 K. The extent of melting has not been determined but it seems that liquid is present at 120 K and a persistent fluid up to 180 K. This indicates a smearing in temperature of both melting and boiling of the methane in the mesoporous tubes compared to bulk methane.

The inelastic neutron scattering from hydrogen in MCM-41 shows the spectrum characteristic of the hydrogen molecule recoil spectrum. However at low energy transfers, because the momentum transfer is low enough, discrete H_2 molecule rotational J = 0 -> 1 transitions are observed. At lower fillings a somewhat broadened peak at 11.8(2) meV is seen, corresponding to physisorbed molecules on a range of surface sites. At higher coverages a sharp 14.7(3) meV peak is observed, corresponding to H_2 molecules surrounded by others. These two types are sharply differentiated, with little intermediate, and in the fully filled MCM-41 are in the molar ratio 1:1. The translational thermal motion observed in the intensity of the 14.7 meV peaks, the small value of diffusion indicated by lack of quasielastic scattering, and the peak width, indicate that the bulk-like molecules are solid rather than liquid-like in density and packing up to 14 K.

Agreement of hydrogen adsorption isotherms with nitrogen adsorption data is obtained if it is assumed that the hydrogen in the pores is 20% denser than the free liquid, more like that of the free solid, giving surface area and pore volume of 0.75 $cm^3\ g^{-1}$ and 1110 $m^2\ g^{-1}$ respectively. The observed isosteric heats of adsorption show an initially very heterogeneous surface, varying from 3.4-1.7 kJ mol^{-1} at low surface coverages between 0.2 and 0.8. As the hydrogen coverage increases above a monolayer amount, the heat, as expected, decreases towards the enthalpy of vaporisation of liquid hydrogen (0.9 kJ mol^{-1}) being 1.2 kJ mol^{-1} just before free liquid condenses. At higher fillings, on warming the sample, a first order transition apparently due to all the sample hydrogen simultaneously boiling indicates that the array of hexagonally packed MCM-41 tubes may be a single interconnected void. This implies significant voids penetrating the walls between the tubes. This collective behaviour is suppressed at lower fillings.

6.10 References

1. L.S. Bartell, *J. Phys. Chem.,* **1995**, *99*(4), 1080-1089.
2. E.M. Piotrovskaya and E.N. Brodskaya, *Langmuir,* **1995**, *11*(6), 2121-2124.
3. D. Nicholson, *J. Chem. Soc., Faraday Trans.,* **1996**, *92*(1), 1-9.
4. R. Ryoo, C.H. Ko, J.M. Kim and R. Howe, *Catal. Lett.,* **1996**, *37,* 29-33.
5. U. Junges, W. Jacobs, I. Voigt-Martin, B. Krutzsch and F. Schüth, *J. Chem. Soc., Chem. Commum.,* **1995**, 2283-2284.
6. A. Jentys, N.H. Pham, H. Vinek, M. Englisch and J.A. Lercher, *Microporous Mater.,* **1996**, *6*(1), 13-17.
7. K.R. Kloetstra, M. van Laren and H. van Bekkum, *J. Chem. Soc., Faraday Trans.,* **1997**, *93*(6), 1211-1220.
8. R. Burch, N. Cruise, D. Gleeson and S.C. Tsang, *J. Chem. Soc., Chem. Commun.,* **1996**, 951-952.
9. C.-G. Wu and T. Bein in *Zeolites and Related Microporous Materials: State of the Art 1994.*; Stud. Surf. Sci. Catal., (Eds. J. Weitkamp, H.G. Karge, H. Pfeifer and W. Hölderich), Elsevier Science B.V., **1994**, *Vol. 84A*, 243-250.
10. C.-G. Wu and T. Bein, *Science,* **1994**, *266*, 1013-1015.
11. C.-G. Wu and T. Bein, *Science,* **1994**, *264*, 1757-1759.
12. T. Abe, Y. Tachibana, T. Uematsu and M. Iwamoto, *J. Chem. Soc., Chem. Commun.,* **1995**, 1617-1618.
13. P.L. Llewellyn, U. Ciesla, R. Stadler, F. Schüth and K.K. Unger in *Zeolites and Related Microporous Materials: State of the Art 1994.*; Stud. Surf. Sci. Catal., (Eds. J. Weitkamp, H.G. Karge, H. Pfeifer and W. Hölderich), Elsevier Science B.V., **1994**, *Vol. 84A*, 2013-2020.
14. H.L. Frisch and J.E. Mark, *Chem. Mater.,* **1996**, *8*(8), 1735-1738.
15. P.I. Ravikovitch, S.C.O. Domhnaill, A.V. Neimark, F. Schüth and K.K. Unger, *Langmuir,* **1995**, *11,* 4765-4772.
16. V.Y. Gusev, X. Feng, Z. Bu, G.L. Haller and J.A. O'Brien, *J. Phys. Chem.,* **1996**, *100*(6), 1985-1988.
17. P.J. Branton, P.G. Hall and K.S.W. Sing, *J. Chem. Soc., Chem Commun.,* **1993**, 1257-1258.
18. P.J. Branton, P.G. Hall, K.S.W. Sing, H. Reichert, F. Schüth and K.K. Unger, *J. Chem. Soc., Faraday Trans.,* **1994**, *90*(19), 2965-2967.
19. C.-Y. Chen, S.-Q. Xiao and M.E. Davis, *Microporous Mater.,* **1995**, *4*(1), 1-20.
20. C.-Y. Chen, H.-X. Li and M.E. Davis, *Microporous Mater.,* **1993**, *2,* 17.
21. J.S. Beck, J.C. Vartuli, W.J. Roth, M.E. Leonowicz, C.T. Kresge, K.D. Schmitt, C.T.-W. Chu, D.H. Olson, E.W. Sheppard, S.B. McCullen, J.B. Higgins and J.L. Schlenker, *J. Am. Chem. Soc.,* **1992**, *114,* 10834-10843.
22. E.W. Hansen, M. Stöcker and R. Schmidt, *J. Phys. Chem.,* **1996**, *100*(6), 2195-2200.
23. A. Hüller, M.V. Smalley, R.K. Thomas and J.W. White, *Mol. Phys.,* **1981**, *44,* 533.
24. Z. Tan and K.E. Gubbins, *J. Phys. Chem.,* **1992**, *96,* 845.
25. J.Z. Larese and Q.M. Zhang, *Phys. Rev. B,* **1995**, *51,* 17023.
26. A. Inaba, J. Skarbek, J.R. Lu, R.K. Thomas, C.J. Carlile and D.S. Sivia, *J. Chem. Phys.,* **1995**, *103,* 1627.

27. R.P. Humes, M.V. Smalley, T. Rayment and R.K. Thomas, *Can. J. Chem.,* **1988**, *66,* 557.
28. J.S. Beck, C.T.-W. Chu, I.D. Johnson, C.T. Kresge, M.E. Leonowicz, W.J. Roth and J.C. Vartuli, *US Patent, No. 5,108, 725,* **1992**.
29. M. Bée, *Quasielastic Neutron Scattering*, Adam Hilger, Bristol, **1988**.
30. Y.D. Harker and R.M. Brugger, *J. Chem. Phys.,* **1967**, *46*(6), 2201-2208.
31. H. Kapulla and W. Gläser in *Inelastic Scattering of Neutrons in Solids and Liquids*; IAEA, Vienna, **1973**, 841-849.
32. W. Press and A. Kollmar, *Solid State Commun.,* **1975**, *17*(4), 405-408.
33. B. Asumussen in *ILL Annual Report*; Grenoble, **1993**, 100-102.
34. *CRC Handbook of Chemistry and Physics*; 75th ed., (D.R. Lide, Ed.), CRC Press, Boca Raton, **1994**.
35. F. Guillaume, J. Doucet, C. Sourisseau and A.J. Dianoux, *J. Chem. Phys.,* **1989**, *91*(4), 2555-2567.
36. W.W. Kagunya, *J. Phys. Chem.,* **1996**, *100*(1), 327-330.
37. F.R. Trouw, *Spectrochimica Acta,* **1992**, *48A*(3), 455-476.
38. A.J. Leadbetter and R.E. Lechner in *The Plastically Crystalline State (Orientationally-Disordered Crystals)*; (Ed. J.N. Sherwood), John Wiley & Sons, Chichester, **1979**, 285-320.
39. F.R. Trouw and J.W. White, *J. Chem. Soc., Faraday Trans.,* **1988**, *84*(7), 861-884.
40. H. Jobic, M. Bée and G.J. Kearley, *J. Phys. Chem.,* **1994**, *98*(17), 4660-4665.
41. H. Jobic, M. Bée and G.J. Kearley, *Zeolites,* **1989**, *9,* 312-317.
42. P. Thorel, J.P. Coulomb and M. Bienfait, *Surf. Sci.,* **1982**, *114,* L43.
43. T. Springer, *Springer Tracts in Modern Physics*, Springer, Berlin, **1972**, *Vol. 64*.
44. P.A. Egelstaff, *An Introduction to the Liquid State*; 2nd ed., Clarendon Press, Oxford, **1992**, 263.
45. P. Demontis, G.B. Suffritti, E.S. Fois and S. Quartieri, *J. Phys. Chem.,* **1992**, *96*(3), 1482-1490.
46. H. Jobic, M. Bée, J. Caro, M. Bülow and J. Kärger, *J. Chem. Soc., Faraday Trans. 1,* **1989**, *85*(2), 4201-4209.
47. J. Kärger and H. Pfiefer, *Zeolites,* **1987**, *7,* 90.
48. A.K. Nowak, C.J.J. den Ouden, S.D. Pickett, B. Smit, A.K. Cheetham, M.F.M. Post and J.M. Thomas, *J. Phys. Chem.,* **1991**, *95*(2), 848-854.
49. S. Yashonath, P. Demontis and M. Klein, *Chem. Phys. Lett.,* **1988**, *153*(6), 551-556.
50. S. Yashonath, P. Demontis and M.L. Klein, *J. Phys. Chem.,* **1991**, *95*(15), 5881-5889.
51. W. Press, *Single Particle Rotations in Molecular Crystals*, Springer, Berlin, **1981**.
52. K.J. Edler and J.W. White, *Chem. Mater.,* **1997**, *9*(5), 1226-1233.
53. R. Ryoo and J.M. Kim, *J. Chem. Soc., Chem. Commun.,* **1995**, 711-712.
54. S.J. Gregg and K.S.W. Sing, *Adsorption, Surface Area and Porosity*; 2nd ed., Academic Press, New York, **1982**.
55. P. Dutta, S.K. Sinha and P. Vora in *Ordering in Two Dimensions*; (Ed. S.K. Sinha), North Holland Publishers, **1980**, 169.

56. G.J. Kellogg, P.E. Sokol and J.W. White in *Momentum Distributions*; (Eds. R.N. Silver and P.E. Sokol), Plenum Press, New York & London, **1990**, 351-354.
57. G.J. Kellogg, J.W. White, K.W. Herwig and P.E. Sokol, *J. Chem. Phys.,* **1990**, *93*(10), 7153-7162.
58. W.J. Stead, P. Meehan and J.W. White, *J. Chem. Soc., Faraday Trans. II,* **1988**, *84*(10), 1655-1668.
59. I.P. Jackson, J. McCaffrey, W.J. Stead and J.W. White, *J. Chem. Soc., Faraday Trans. II,* **1988**, *84*(10), 1669-1682.
60. M. Nielson and W.D. Ellenson, *Annual Report Physics Dept., AEK, Risø,* **1975**, *Report No. 334,* 44.
61. P.E. Sokol, R.T. Azuah, M.R. Gibbs and S.M. Bennington, *J. Low Temp. Phys.,* **1996**, *103*(1/2), 23-33.
62. P.A. Egelstaff, *Proc. Phys. Soc.,* **1966**, *90,* 681.
63. F. Fillaux, R. Papoular, A. Lautie, S.M. Bennington and J. Tomkinson, *International Conference on Neutron Scattering, Sendai,* **1994**.
64. J.A. Young and J.U. Koppel, *Phys. Rev. 3A,* **1964**, *135*, 603-611.
65. W. Langel, D.L. Price, R.O. Simmons and P.E. Sokol, *Phys. Rev. B,* **1988**, *38*(16), 11275-11283.
66. E.W. Hansen, R. Schmidt, M. Stöcker and D. Akporiaye, *J. Phys. Chem.,* **1995**, *99,* 4148-4154.
67. R.J. Elliott and W.M. Hartmann, *Proc. Phys. Soc.,* **1967**, *90.* 671.
68. M. Nielsen, *Phys. Rev. B,* **1973**, *7*(4), 1626-1635.
69. O. Franke, G. Schulz-Ekloff, J. Rathousky, J. Stárek and A. Zukal, *J. Chem. Soc., Chem. Commun.,* **1993**, 724-725.
70. J. Rathousky, A. Zukal, O. Franke and G. Schulz-Ekloff, *J. Chem. Soc., Faraday Trans.,* **1994**, *90*(18), 2821-2826.
71. K.S.W. Sing, D.H. Everett, R.A.W. Haul, R.A. Pierotti, J. Rouquerol and T. Siemieniewska, *Pure & Appl. Chem.,* **1985**, *57*(4), 603-619.
72. A. Keizer, T. Michalski and G. Findenegg, *Pure & Appl. Chem.,* **1991**, *63,* 1495.
73. W.D. Machin, *Langmuir,* **1994**, *10,* 1235.
74. S. Brunauer, P.H. Emmet and E. Teller, *J. Am. Chem. Soc.,* **1938**, *60,* 309.
75. P.J. Branton, P.G. Hall, M. Treguer and K.S.W. Sing, *J. Chem. Soc., Faraday Trans.,* **1995**, *91,* 2041.

Chapter 7:

Conclusion

"A conclusion is simply the place where you got tired of thinking."

Martin H. Fischer

The two major foci of this thesis have been the synthesis of MCM-41 hexagonal phase, pure silicate materials, showing high long range order and the determination of a detailed structural model for these materials. A simplified preparation containing only sodium silicate solution, CTAB and some acid was chosen, with the aim of reducing the number of variables in the system with the attendant possibility of investigating the formation mechanism for this material.

The synthetic work, reported in Chapters 2 and 4 concerned four major variations on the preparation. The first two were the heated and unheated ordinary MCM-41 preparations, which were optimised in relation to heating or aging time in the gel, and the use of stirring during the synthesis. The other two were the heated and unheated acid titrated preparations. These were optimised in relation to the type of acid used for the titration and the pH level maintained during the heating or aging in the gel. The syntheses were followed experimentally through all stages of preparation - wet synthesis gels, washed and dried MCM-41 materials which still contained template, and the calcined materials in which the CTAB had been removed by burning out at high temperatures.

Of these preparations, the acid titrated materials prepared using four days of heating, with three acid titrations, using 1M sulphuric acid to maintain a pH of 10, had the highest degree of long-range order, as revealed by the number and intensities of the observable X-ray diffraction peaks. The pH at which the system was maintained during heating was shown to have an important effect upon the long-range order of the MCM-41 formed. The order appeared greatest for pH values around 10, with diffraction peak intensity decreasing with deviations from this value.

Other acids proved to have a similar, though less marked effect upon the long-range order of the product. The order in which the acid counterions were effective in

increasing the order was shown to be the reverse of the lyotropic series for CTAB, the surfactant template. The lyotropic series measures binding strengths of a counterion with the surfactant headgroup. The result here therefore indicate that more ordered materials are produced in systems where the other anions in solution bind least strongly to the surfactant headgroups, enabling enhanced ion-exchange with the silicate polyanions during synthesis. Unheated materials were shown to be stable to isolation from the synthesis gel, and retained their structure on calcination, although their stability appears to be proportional to the length of aging time in the gel. The long range order of these materials also benefited from the acid titration method used for the heated materials.

Despite the formation and observation, in Langmuir trough experiments, of a silicated surfactant species, under conditions where no micelles had formed, no final conclusions could be drawn on formation mechanisms. The templated structures in the preparation under study formed too quickly to be directly observed using the methods available, and showed no further gross structural evolution with time. Shear experiments on freshly prepared, unheated synthesis gels showed that the initial structure formed in the reaction mixture retained its neutron diffraction signature at shear rates up to 10 000 s^{-1}. These gels must therefore contain hexagonal phase material with a high degree of connectivity between individual cylindrical silicated micelles from an early stage of the preparation.

The manufacture of MCM-41 materials with high-long range order enabled X-ray diffraction patterns showing up to seven orders of diffraction to be obtained. The data from these patterns was fitted by a model for the scattering from cylinders. These calculations showed that the MCM-41 material contained two distinct density regions in the walls. These were identified as a denser, continuous wall region, and a less dense material lining the inside of each channel. The central empty hole in these materials appears to be smaller than has previously been reported for other MCM-41 materials which have been characterised using gas adsorption isotherms. The wall density of MCM-41 was also shown from these calculations to be very low, being about 40% silica by volume, even in the dense, continuous part of the structure.

Data from neutron diffraction, small angle neutron scattering, and inelastic and quasielastic neutron scattering experiments have been shown to be consistent with the three region model which contains highly porous walls. Since the X-ray data only gives structural information projected onto two dimensions, a second possible model for the MCM-41 material, consistent with the X-ray data has also been proposed. In this case the material could contain smooth-walled channels with high degree of tortuosity and connectivity, which give the two dimensional projection of differing density regions. This may approach a highly defective MCM-48 structure, however the resources available were not able to model this possible structure.

Finally, the MCM-41 material prepared in this work was used in a study of the behaviour of methane and hydrogen condensed into the channel system. The confinement in the silicate channels resulted in a raised temperature for the onset of rotational diffusion in methane, but a decreased temperature for the melting point transition compared to that of bulk methane. A persistent fluid in the pores at

temperatures up to 180 K shows also a smearing in the boiling point of the confined methane. Hydrogen was shown to exist in two sites within the MCM-41 channels. The proportion of molecules in each site was dependent upon filling. The more hindered site, which filled first was identified as a site adjacent to the silica wall, while the less hindered site, which filled at higher gas loadings corresponded to a site within the pore region.

The final conclusion for this work therefore, is that it is possible to create more highly ordered MCM-41 materials by means of pH control during synthesis. These materials show up to seven peaks in the X-ray diffraction pattern, enabling the construction of a detailed structural model. The two-dimensional projection of the wall structure contains two density regions in the silica, as well as a small central pore. The low overall wall densities indicate highly porous silica frameworks within these walls.

Appendix: Compositions of Preparations

Table A1.1 *Reagent quantities for most synthesis gels studied in this work.*

Sample Name	CTAB /g	Water 1† /g	Sodium Silicate Solution /g	Water 2† /g	Conc. H_2SO_4 /g	Water 3† /g	Additive	Total Additives /g
A	3.2279	9.6749	3.7480	7.9351	0.2379	3.9438	-	-
B	2.2441	6.7263	2.6058	5.5166	0.1654	2.7418	-	-
C	3.2279	9.6749	3.7480	7.9351	0.2379	3.9438	-	-
D	2.2441	6.7263	2.6058	5.5166	0.1654	2.7418	-	-
E	3.2279	9.6749	3.7480	7.9351	0.2379	3.9438	-	-
F	2.2441	6.7263	2.6058	5.5166	0.1654	2.7418	-	-
UC Prep (AR1)	16.4031	49.2298	19.0688	40.7028	1.2268	20.1174	-	-
AR2	8.2839	24.6198	9.6000	20.2710	0.6246	10.0243	-	-
GP Prep	16.3866	49.50	19.0634	40.59	1.2015	20.05	-	-
Argonne Prep 1	32.758	98.3399	38.14	81.02	2.407	40.10	-	-
Argonne Prep 2	8.1963	24.5953	9.5378	20.2713	0.6009	10.023	-	-
R Prep heated	20.4772	61.4865	23.8121	50.6878	1.5689	25.3343	CH_3CO_2H	22.50
R Prep unheated	20.4772	61.4865	23.8121	50.6878	1.5689	25.3343	CH_3CO_2H	20.10
SAD1	16.7798	50.2503	20.795	40.2360	1.2421	20.4063	CH_3CO_2H	20.90
SAD2	16.6291	50.1304	19.304	40.1973	1.2799	20.5345	-	-
X2	3.3471	10.0314	3.8720	8.0717	0.2451	4.0229	$NaCH_3CO_2$	2.9896
X3	3.3471	10.0314	3.8720	8.0717	0.2451	4.0229	H_2SO_4	1.4332
X4	3.3471	10.0314	3.8720	8.0717	0.2451	4.0229	CH_3CO_2H	2.98
X5	3.3471	10.0314	3.8720	8.0717	0.2451	4.0229	NH_4Br	4.1170
LOQ1	0.0010	5.0039	4.6564	1.5273	-	-	-	-
LOQ2	0.0018	5.0004	4.6349	1.5135	-	-	-	-
LOQ3	0.0494	4.9764	4.6500	1.5584	-	-	-	-
LOQ4	0.2519	4.7679	4.6558	1.5353	-	-	-	-
LOQ5	0.5078	4.4964	4.6739	1.5285	-	-	-	-
LOQ6	0.7550	4.2653	4.6397	1.5260	-	-	-	-
LOQ‡A-D,I-K, O,P	1.1592	3.3273	1.421	2.6409	0.0806	1.3666	-	-
LOQ‡S-W	0.2568	1.6817	0.6985	1.2953	0.0325	0.6841	-	-

LOQ‡X-BB	0.1027	1.6703	0.7195	1.3343	0.0335	0.6947	-	-
LOQ shear	8.7726	25.3722	10.8933	20.2642	0.6212	10.3093	-	-
Z1	3.3187	10.0422	4.0722	8.0859	0.2500	4.0328	H_2SO_4	3.1157
Z2	3.3187	10.0422	4.0722	8.0859	0.2500	4.0328	H_2SO_4	1.9577
Z3	3.3187	10.0422	4.0722	8.0859	0.2500	4.0328	H_2SO_4	2.8812
Z4	3.3187	10.0422	4.0722	8.0859	0.2500	4.0328	CH_3CO_2H	3.70
Z5	3.3187	10.0422	4.0722	8.0859	0.2500	4.0328	HCl	3.8936
IRIS	16.5127	50.0483	20.4422	40.6708	1.2264	20.0620	H_2SO_4	8.15
J1	3.2765	10.1754	3.8082	8.0117	0.2410	4.0003	H_2SO_4	1.70
J2	3.2765	10.1754	3.8082	8.0117	0.2410	4.0003	H_2SO_4	3.15
J3	3.2765	10.1754	3.8082	8.0117	0.2410	4.0003	H_2SO_4	3.15
J4	3.2765	10.1754	3.8082	8.0117	0.2410	4.0003	H_2SO_4	3.47
J5	3.2765	10.1754	3.8082	8.0117	0.2410	4.0003	H_2SO_4	5.00
LOQ‡ Heated Ordinary 1-5	2.2962	6.6844	2.858	5.316	0.162	2.7232	-	-
LOQ‡ Heated Acid 1-5	2.3087	6.6500	2.8423	5.3389	0.1688	2.704	H_2SO_4	0.9
QENS	24.4447	75.1470	31.0325	60.1452	1.8367	30.1445	H_2SO_4	19.63
KBr Prep	0.4392	5.2016	1.4680	2.7371	0.0901	-	KBr	0.2425
RP Prep	24.6134	75.1350	31.3480	60.0160	1.8266	30.0140	H_2SO_4	22.62
MARI1	24.3818	75.2116	31.840	60.364	1.8136	30.1656	H_2SO_4	24.11
MARI2	32.8036	100.175	40.997	80.365	2.4038	40.4300	H_2SO_4	23.22
In situ 1	1.1592	3.6997	1.4290	3.7160	0.0869	-	-	-
In situ 2	1.1519	3.3618	1.4249	4.0418	0.1032	-	-	-

Note: † Water 1, 2 and 3 refer to (1) the water added to the solid CTAB to form the surfactant solution, (2) the water added to the acidified sodium silicate solution and (3) the water added after the first two solutions have been mixed during the stirring. Water 3 was also usually used to rinse out the container which formerly contained the surfactant solution.

‡ These solutions were made up with different H_2O/D_2O proportions for the purposes of small angle neutron scattering contrast variation experiments. The quantities given are for the 0% D_2O preparations, but in preparations containing D_2O, the amounts of CTAB, H_2SO_4, and sodium silicate solution would be within ±0.005 g of the amounts shown. The D_2O was evenly distributed into the various water fractions to create synthesis gels ranging in concentration from 10-90 mol% D_2O.

The preparations are listed in approximately chronological order. Syntheses named with different numbers, but the same letter, correspond to a group of samples which

contain exactly the same amounts of all reagents, except additives. These are cases where a single synthesis gel was made up and then split between the various solutions to observe the effect of the different additives while otherwise maintaining constant reagent proportions.

Table A1.2 *Composition of unheated synthesis gels used in shear experiments and a summary of their behaviour under various shear conditions.*

CTAB /M	KBr /M	Other Salt	silicate /%	shear rate /s^{-1}	Temp /K	alignment
0.366	-	0.3042g NaOH 0.1375g H_2SO_4	-	2	298	no
0.366	-	0.3042g NaOH 0.1375g H_2SO_4	-	5	298	no
0.366	-	0.3042g NaOH 0.1375g H_2SO_4	-	500	298	no
0.0336	-	0.0227g NaOH 0.0795g H_2SO_4	-	0	298	no
0.0336	-	0.0227g NaOH 0.0795g H_2SO_4	-	5000	298	no
0.0336	-	1.6227g NaOH 3.4095g H_2SO_4	-	5000	298	no
0.03	0.4	-	-	5000	298	no
0.03	0.4	-	-	5000	313	yes
0.16	0.4	-	-	5000	300-303	no
0.03	0.4	-	1.75	5000	313	yes
0.03	0.4	-	3.86	5000	313	yes
0.06	0.2	-	3.81	5000	313	yes
0.36	-	some NaOH, H_2SO_4	3.86	5000	313	no
0.36	-	some NaOH, H_2SO_4	3.86	5000	323	no
0.06	-	-	3.86	5000	313	no
0.06	-	-	3.86	5000	323	no
0.06	-	0.2M Na_2SO_4	-	5000	313	no
0.03	-	0.4M Na_2SO_4	-	5000	313	no
0.12	0.1	-	-	5000	313	no
0.12	0.2	-	-	5000	313	yes
0.12	0.2	-	-	5000	323	yes
0.12	0.2	-	-	5000	303	yes
0.12	0.2	-	-	5000	293	no
0.12	0.2	-	-	500	303	no
0.12	0.2	-	-	1500	303	no
0.12	0.2	-	-	3000	303	no
0.12	0.2	-	-	5000	303	no
0.12	0.2	-	-	5000	313	yes
0.12	0.2	-	-	5000	303	yes
0.12	0.2	-	-	5000 after stopped 5min	303	yes
0.12	0.2	-	-	1500 after stopped, T inc.	313	yes
0.12	0.2	-	-	3000	313	yes
0.12	0.2	-	-	5000	313	yes
0.12	0.2	-	3.81	5000	313	no

0.12	0.2	-	3.81	5000	323	yes (slight)
0.12	0.2	-	3.81	5000	303	yes
0.12	0.2	-	3.81	5000	293	no
0.12	0.2	-	3.81	5000	313	yes
0.12	0.2	-	3.81	5000 after stopped 5 min	303	yes
0.12	0.2	-	3.81	0	303	no
0.12	0.2	-	3.81	5000	303	no
0.12	0.2	-	3.81	1500 after stopped, T inc.	313	yes (slight)
0.12	0.2	-	3.81	3000	313	yes
0.12	0.2	-	3.81	5000	313	yes
0.12	0.2	-	1.5	5000	313	no
0.12	0.2	-	1.5	5000	323	no
0.12	0.2	-	1.5	5000	303	no
0.12	0.2	-	1.5	5000	313	no
0.12	0.2	-	1.5	5000	323	no
0.12	0.2	-	1.5	5000	333	no
0.12	0.2	-	1.5	5000	323	no
0.12	0.2	-	1.5	5000	313	no
0.12	0.2	-	1.5	5000	303	no
0.36	0.4	-	3.81	0 SANS cell	298	yes
0.36	0.2	-	3.81	0 SANS cell	298	yes
0.36	0.2	-	3.81	0	298	yes (slight)
0.36	0.2	-	3.81	78-3112	298	no
0.36	0.2	-	3.81	39-3112	303	no
0.36	0.2	-	3.81	39-195	313	no
0.36	0.2	-	3.81	389	313	yes
0.36	0.2	-	3.81	778	313	yes
0.36	0.2	-	3.81	1945-3112	313	no
0.19	0.2	-	3.81	0	298	no
0.19	0.2	-	3.81	39	298	yes (slight)
0.19	0.2	-	3.81	79-778	298	no
0.12	0.2	-	3.81	0-389	303	no
0.12	0.2	-	3.81	778	303	yes (slight)
0.12	0.2	-	3.81	1945	303	yes (slight)
0.12	0.2	-	3.81	3112	303	yes
0.12	0.2	-	3.81	0-3112	313	no but IvQ changes noticeably

Note: The shaded region corresponds to the experiments done using the gel which showed the greatest degree of ordering under shear. This is discussed in Chapter 4, section 4.3.3.

The experiment on preparation containing 0.19 M CTAB, despite showing some signs of shear at low temperatures and low shear rates was not continued as the shear cell failed at that point.